Developing New Ligand Platforms for MRI Contrast Agents

by

Kevin John Harvey Allen
B.Sc., University of Victoria, 2008

A Dissertation Submitted in Partial Fulfillment
of the Requirements for the Degree of

DOCTOR OF PHILOSOPHY

in the Department of Chemistry

Supervisory Committee

Developing New Ligand Platforms for MRI Contrast Agents

by

Kevin John Harvey Allen
B.Sc., University of Victoria, 2008

Supervisory Committee

Dr. David Berg, Department of Chemistry
Supervisor

Dr. Fraser Hof, Department of Chemistry
Co-Supervisor

Dr. Lisa Rosenberg, Department of Chemistry
Departmental Member

Dr. Stan Dosso, School of Earth and Ocean Sciences
Outside Member

Abstract

Supervisory Committee
Dr. David Berg, Department of Chemistry
Supervisor
Dr. Fraser Hof, Department of Chemistry
Co-Supervisor
Dr. Lisa Rosenberg, Department of Chemistry
Departmental Member
Dr. Stan Dosso, School of Earth and Ocean Sciences
Outside Member

A series of lanthanide complexes, $\{[CpCo(P{=}O(OR)_2)_3]_2Ln(H_2O)_x\}^+Cl^-$ (Ln = Nd, Eu, Tb, Yb; R = Et, Ph), $(Kläui)_2Ln$, were prepared. The related complex $\{[CpCo(P{=}O(OPh)_2)_3]_2Yb\}^+$ $[CoCl_3(THF)]^-$ was crystallographically characterized and the cation in this case was confirmed to be 6-coordinate and solvent free. To determine the Kläui complexes potential as magnetic resonance (MR) imaging agents, ligand exchange rates between the d_0- and d_{60}-isotopomers of the Kläui lanthanide complexes were determined in acetonitrile by electrospray mass spectrometry. The ligand exchange rate was found to increase by almost 4-orders of magnitude from the smallest (Yb) to largest ion (Nd) in acetonitrile. Additionally, the ligand exchange rate increased rapidly for the Tb complex with increasing water concentration. Changing the phosphite substituent had no significant impact on the rate of ligand exchange for R = Ph relative to R = Et. Modification to the phosphite substituents to decrease ligand exchange was unsuccessful indicating that these ligands were not suitable as MR imaging agents.

Oxazoline based ligands are known to complex lanthanide ions, however, most of these complexes undergo rapid ligand exchange when not in water solution. Several novel oxazoline based ligands with increased chelation to stop ligand exchange were designed. During the course of their synthesis it was discovered that these ligands were too unstable to be used in vivo and this ligand set was abandoned for a more stable alternative.

A series of ligands based on a calix[4]arene scaffold were developed. Through modifications to the upper rim of the calix[4]arene scaffold a mono, di, and tri substituted catechol calix[4]arene were designed. After the mono-catechol tri-sulfonated calix[4]arene was found to decompose in solution the catechol substituent was determined to be too reactive for use as a contrast agent. An upper rim tetra substituted iminodiacetic acid calix[4]arene was synthesized. Upon addition of the lanthanide a coordination polymer was likely forming. Using a dye displacement assay it was found that this ligand was not able to out-compete the dye for metal chelation and would not be suitable for MR use. Using established Suzuki chemistry, DO3A functionality was incorporated onto a tri-sulfonated calix[4]arene scaffold. Using a dye displacement assay it was found that the stability constant K_{ML} of this complex was similar to DO3A at pH 8.35. At pH 3.99 it was found that no displacement occurred, most likely due to intramolecular hydrogen bonding.

Table of Contents

List of Tables

List of Figures

List of Schemes

List of Abbreviations

^{1}H	Proton
^{13}C	Carbon 13
ACN	Acetonitrile
AN-DVB	Acrylonitrile-divinylbenzene copolymer
BnBr	Benzyl bromide
BNP	Binaphthyl phosphoric acid
BnPyBOx	2,6-Bis[(4R)-4-(4-(benzyloxy)benzyl)-2-oxazolinyl]pyridine
Boc	*Tert*-butyl carbonate
Boc_2O	Di-*tert*-butyl dicarbonate
BzCl	Benzoyl chloride
C.I. MS	Chemical Ionization Mass Spectrometry
CEST	Chemical Exchange Saturation Transfer
Cp	Cyclopentadienyl
Cyclen	1,4,7,10-tetraazacyclododecane
D	Dye
DMSO	Dimethyl Sulfoxide
DO3A	1,4,7,10-tetraazacyclododecane-1,4,7-tris(acetic acid)
DOTA	1,4,7,10-tetraazacyclododecane-1,4,7,10-tetraacetic acid
EDTA	Ethylenediaminetetraacetic acid
EPR	Enhanced permeability and retention
ESI	Electrospray Ionization
ESI-MS	Electrospray Ionization Mass Spectrometry
Et	Ethyl
ET3N	Triethyl amine
ETOH	Ethanol
GMA	Glycidyl methacrylate
H2Bpz	dihydrobis(pyrazol-1-yl)borato
HMBC	Heteronuclear multiple-bond correlation spectroscopy

HPLC	High Pressure Liquid Chromatography
HPLC/MS	High Pressure Liquid Chromatography/Mass spectrometry
HR-ESI-MS	High resolution Electrospray Ionization Mass Spectrometry
IDA	Iminodiacetic acid
K_{11}^{c}	Conditional stability constant 1:1 species
K_{12}^{c}	Conditional stability constant 1:2 species
K_{MD}^{c}	Metal-dye conditional stability constant
K_{ML}^{c}	Metal-ligand conditional stability constant
K_{ML}	Stability constant of M-L complex
K_n	Stepwise protonation constant
Kläui lanthanide	Bis[(h^5-cyclopentadienyl)tris(diR-phosphito)-k^3-P,P',P"-cobaltate(III)-k3-O,O',O"]lanthanide(III)
Kläui Ligand	$Na[CpCo\{P(O)(OR)_2\}_3]$
Kläui Stack	Bis[(h^5-cyclopentadienyl)tris(diR-phosphito)-k^3-P,P',P"-cobaltate(III)-k3-O,O',O"]cobalt(II)
L	Ligand
LD_{50}	Lethal dose, 50%
Ln	Lanthanide
LR-ESI-MS	Low resolution Electrospray Ionization Mass Spectrometry
M	Metal
MCC	5-(1,4,7,10-tetraazacyclododecane-1,4,7-tris(acetic acid)-10-(methylphenyl-3-boronic acid pinacol ester))-25, 26, 27, 28-tetrahydroxy-11-17-23-trisulfonatocalix[4]arene
Me_5Ph	Pentamethyl benzene
MR	Magnetic Resonance
MRI	Magnetic Resonance Imaging
NBS	N-Bromosuccinimide
NIR	Near infrared
NMR	Nuclear Magnetic Resonance
NSF	Nephrogenic systemic fibrosis
o-BnTyPyBOx	2,6-Bis[(4R)-4-(2-(benzyloxy)benzyl)-2-oxazolinyl]pyridine

o-TyPyBOx	2,6-Bis[(4R)-4-(2-hydroxybenzyl)-2-oxazolinyl]pyridine
ParaCEST	Paramagnetic Chemical Exchange Saturation Transfer
PCC	5-(1,4,7,10-tetraazacyclododecane-1,4,7-tris(acetic acid)-10-(methylphenyl-4-boronic acid pinacol ester))-25, 26, 27, 28-tetrahydroxy-11-17-23-trisulfonatocalix[4]arene,
Pd/C	Palladium on carbon
Ph	Phenyl
PhME	Toluene
PhOH	Phenol
Phth	Phthalimide
PNNL	Pacific Northwest National Labs
por	porphyrin derivatives
PPh3	Triphenyl phosphine
PSC	*p*-sulfonatocalix[4]arene
py	Pyridine
PyBOx	2,6-Bis[(4R)-4-phenyl-2-oxazolinyl]pyridine
q	Hydration number
r_1	Relaxivity due to T_1 effects
r_2	Relaxivity due to T_2 effects
r_1^{IS}	T_1 Relaxivity enhancement due to inner sphere water
r_1^{OS}	T_1 Relaxivity enhancement due to outer sphere water
Red-Al®	Sodium bis(2-methoxyethoxy)aluminum hydride
RF	Radio Frequency
Rochelle Salt	Potassium sodium tartrate
RT	Room temperature
S	Spin quantum number
T_1	Longitudinal relaxation
T_{1m}	Relaxation time of agent bound water
τ_{1m}	Lifetime of inner sphere water
T_2	Transverse relaxation

TBAB	Tetrabutylammonium bromide
^{t}BuPbxa	2,6-bis[(4S)-tert-butyl-carbamoyl-2-oxazolin-2-yl]pyridine
TETRA	5-11-17-23-tetramethyl(iminodiacetic acid)-25, 26, 27, 28-tetrahydroxy-calix[4]arene
TGA	Thermogravimetric analysis
THF	Tetrahydrofuran
TROX	Tri{[2-(4s)-(4-phenyl-1,3-oxazolinyl)]methyl}amine
TsCl	p-toluenesulfonyl chloride
TsOH	p-toluenesulfonic acid
TyPyBOx	2,6-Bis[(4R)-4-(4-hydroxybenzyl)-2-oxazolinyl]pyridine
UV-VIS	Ultraviolet-Visible
μW	Microwaves
VT	Variable temperature

List of Compounds

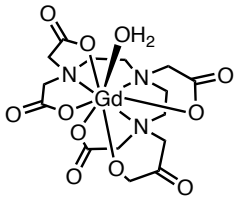

1.1

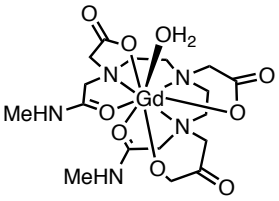

1.2

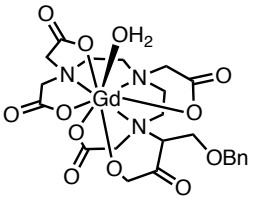

1.3

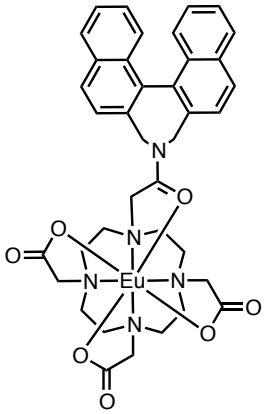

1.4

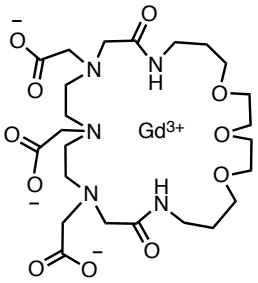

1.5

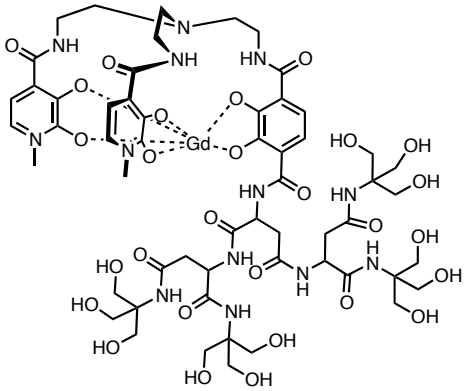

1.6

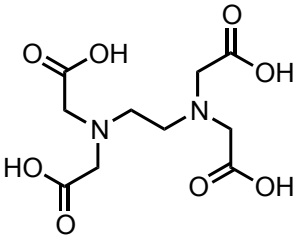

1.7

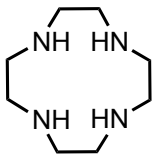

1.8

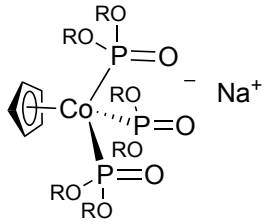

2.1a R = Et
2.1b R = Ph

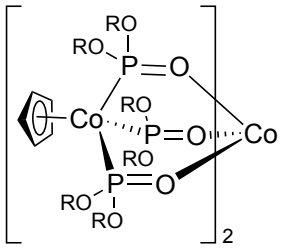

2.2a R = Et
2.2b R = Ph

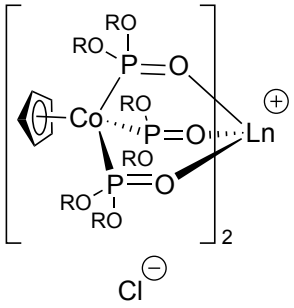

2.3a Ln = Nd, R = Et
2.3b Ln = Nd, R = Ph
2.4a Ln = Eu, R = Et
2.5a Ln = Tb, R = Et
2.5b Ln = Tb, R = Ph
2.6a Ln = Yb, R = Et
2.6b Ln = Yb, R = Ph

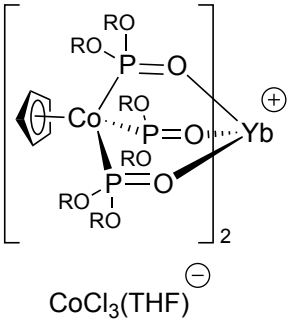

2.7

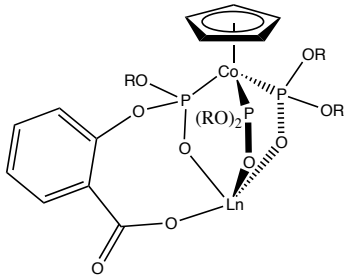

2.8

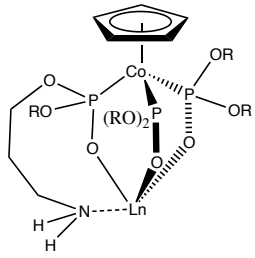

2.9

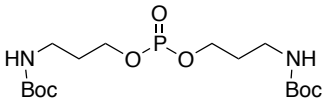

2.10

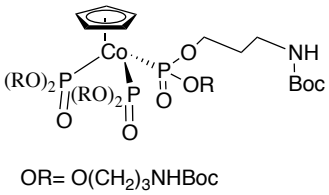

OR= $O(CH_2)_3NHBoc$

2.11

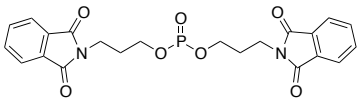

2.12

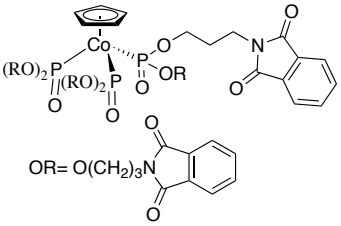

OR= $O(CH_2)_3N$

2.13

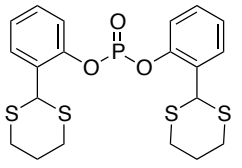

2.14

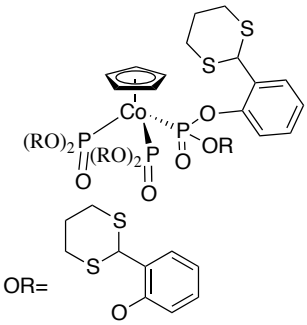

OR=

2.15

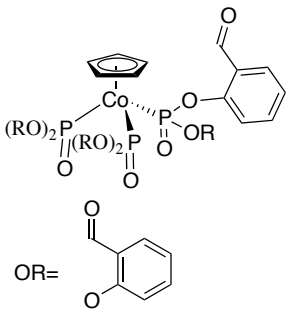

OR=

2.16

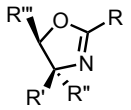

3.1

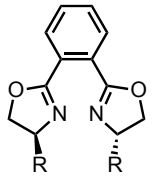

3.2

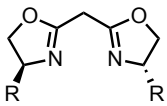

3.3

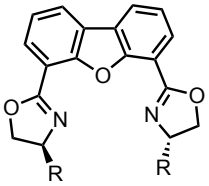

3.4

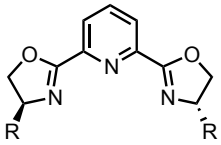

3.5

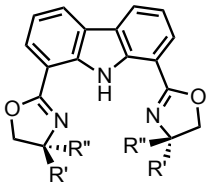

3.6

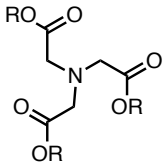

3.7 R = H
3.7b R = Me

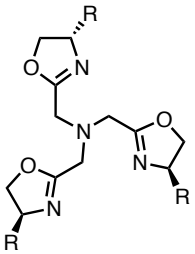

3.8a R = 2-MeOPh
3.8b R = Ph
3.8c R = 2-(OH)Ph

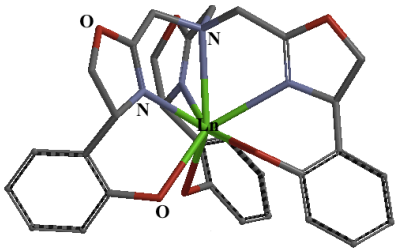

3.9

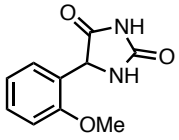

3.11

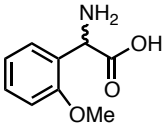

3.12

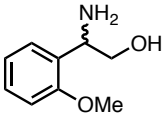

3.13

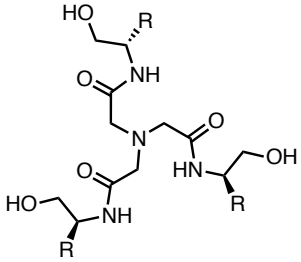

3.14a R = 2-MeOPh
3.14b R = Ph

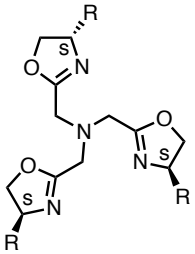

3.15a R = 2-MeOPh
3.15b R = Ph

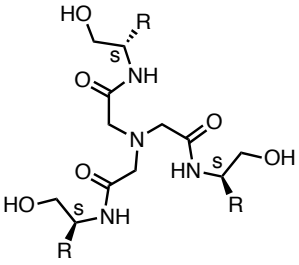

3.16a R = 2-MeOPh
3.16b R = Ph

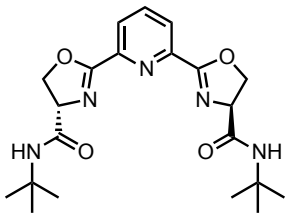

3.17

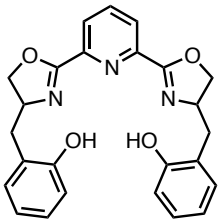

3.19

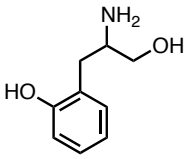

3.21

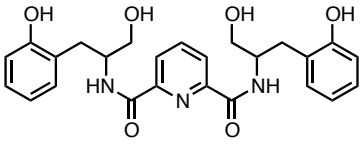

3.22

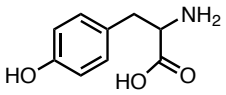

3.23

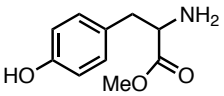

3.24

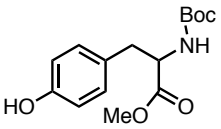

3.25

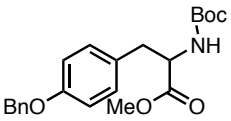

3.36

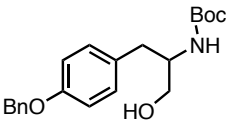

3.27

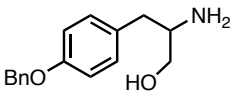

3.28

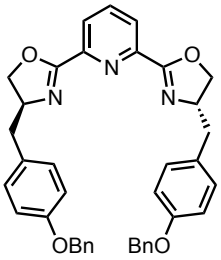

3.29

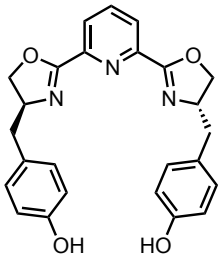

3.30

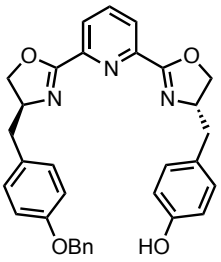

3.31

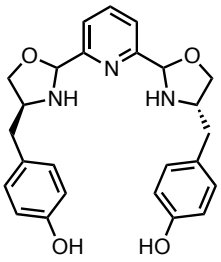

3.32

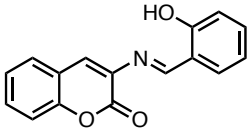

3.33

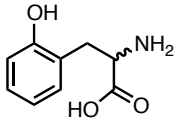

3.34

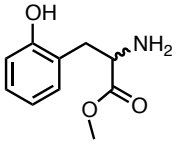

3.35

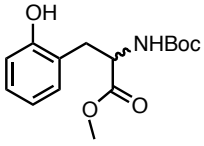

3.36

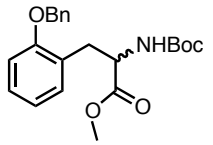

3.37

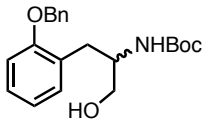

3.38

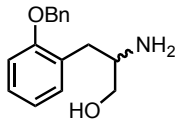

3.39

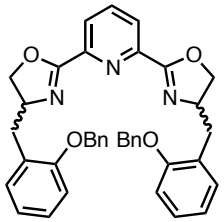

3.40

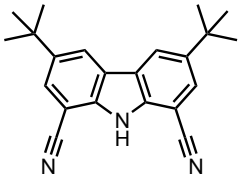

3.41

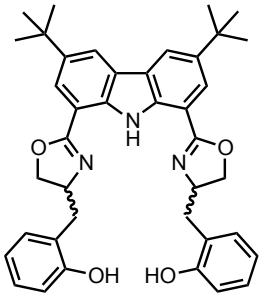

3.42

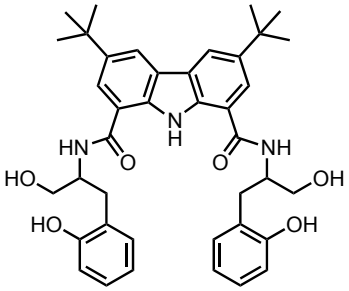

3.43

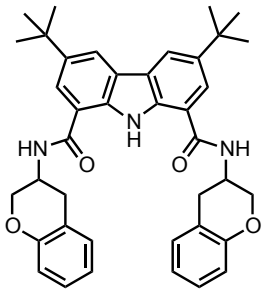

3.44

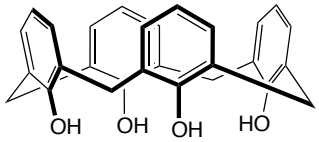

4.1

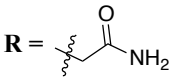

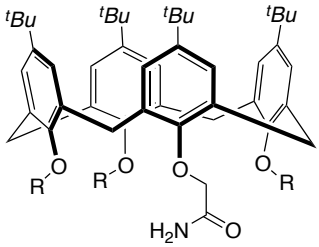

4.3

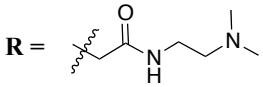

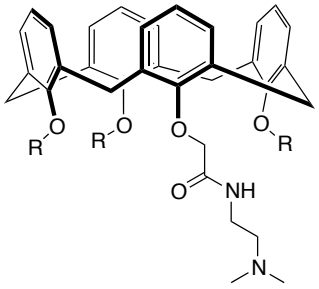

4.4

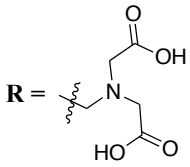

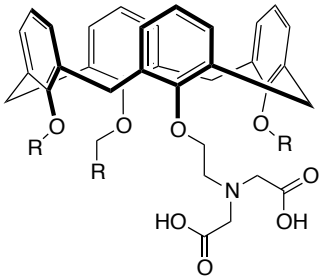

4.5

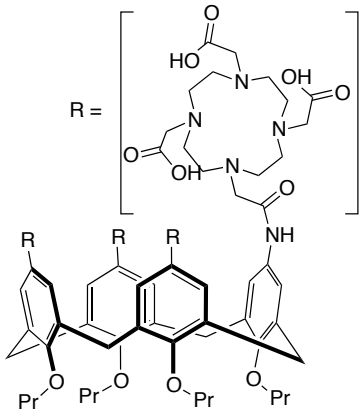

4.6

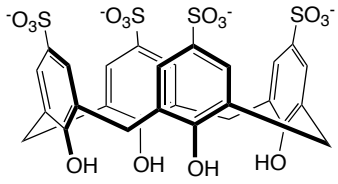

4.7

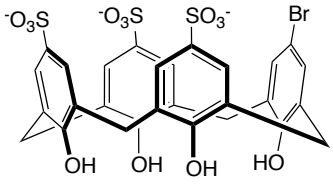

4.8

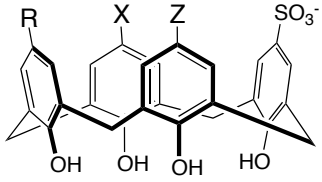

4.9 X = Z = Br, R = SO_3^-
4.10 X = R = Br, Z = SO_3^-

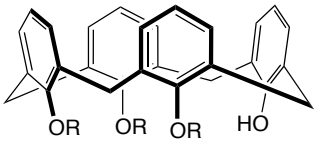

4.23 R =

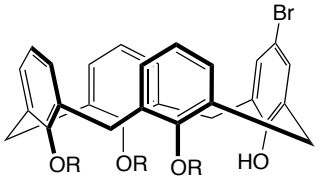

4.24 R =

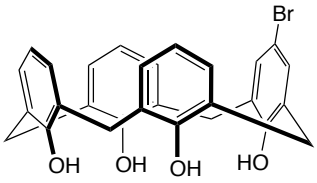

4.25

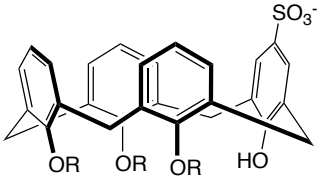

4.26 R =

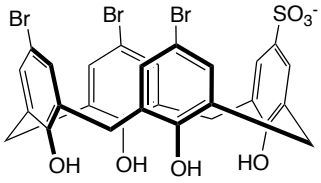

4.28

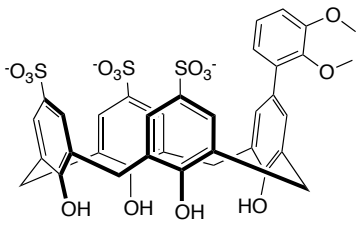

4.33

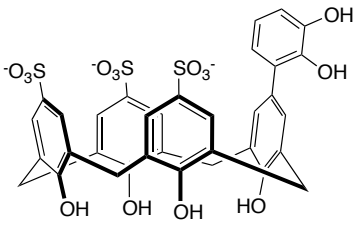

4.34

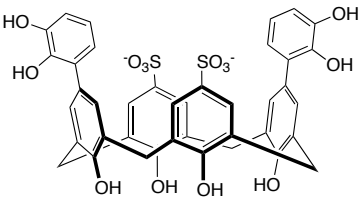

4.35

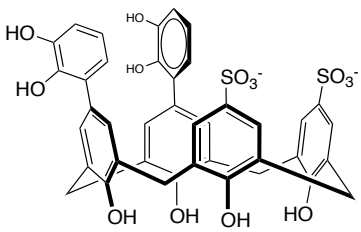

4.36

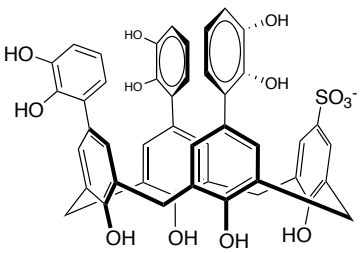

4.37

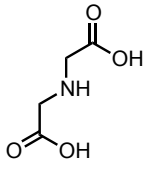

4.38

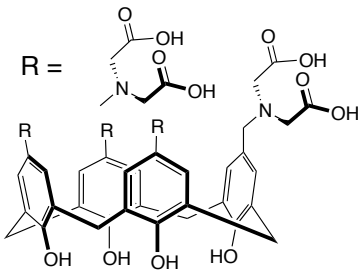

4.39

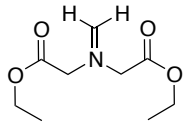

4.40

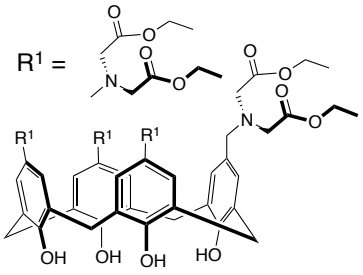

4.41

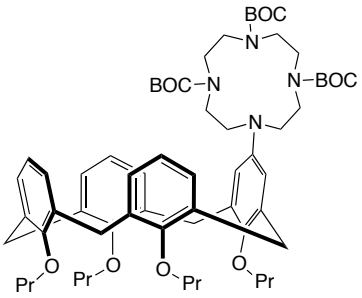

4.49

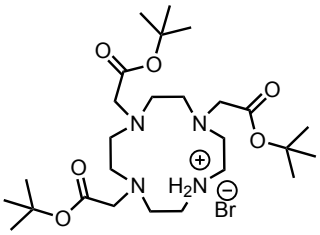

4.54

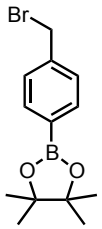

4.55

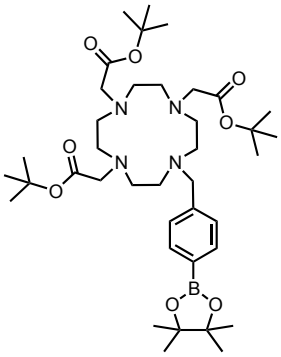

4.56

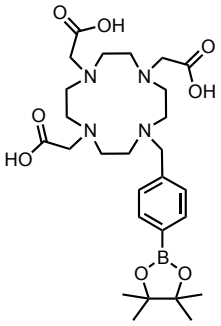

4.57

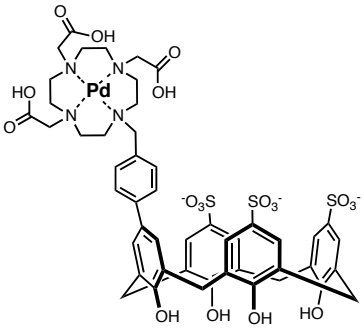

4.58

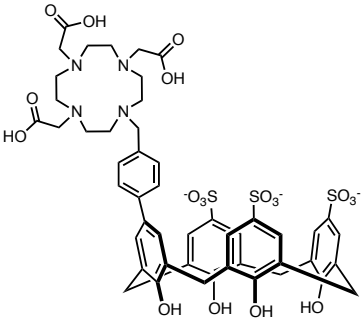

4.59

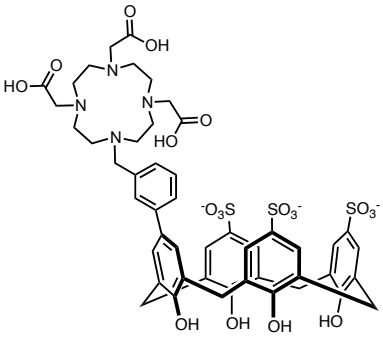

4.60

Acknowledgments

First, I would like to take this opportunity to thank my supervisors Dr. David Berg and Dr. Fraser Hof. Dave, thank you for always providing me with support, encouragement, and being the voice of positivity when my pessimism would take over. Fraser, thank you for giving me a place when I was in need. Your support and advice were always appreciated, no matter how they were delivered. I truly do appreciate everything you two have done for me, thank you.

Next, I would like to thank the technical staff at the University of Victoria. Thank you to Chris Greenwood, and Chris Barr for all their assistance with the NMR. Your work at keeping the machines operational, as well as all the training provided was greatly appreciated. Thank you to Dr. Ori Granot and Dr. Tyler Trefz for their assistance with the mass spec and for always keeping them up and running. Thank you to Sean Adams for bringing my drawings (in the loosest form of the word) to life. Thank you to Jean-Paul Gogniat and Andrew Macdonald for your willingness to get your hands dirty and help out with any problem I brought to you.

I would like to thank the teaching staff, Dr. Dave Berry, Dr. Jane Browning, and Kelli Fawkes. I can't put into words how much you all have done for me. From my time in undergrad, to my Ph.D., learning from you has been truly inspiring. You have helped shape who I have become and I am grateful for everything.

I must thank all my peers who I have worked with over the course of my graduate degree. The past Berg group members Pengrong Zhang and Jin Zou, who took a wide-eyed new graduate student and taught him how to function in a lab. The Hof group for all their help, especially Kevin Daze for his friendship and for having the patience to listen to my every rant and hyperbole and Sara Tabet for providing me with nourishment that kept me growing. The Wulff group for their chemicals when ours had expired (Natasha O'Rourke for her good hearted nature and constant help with ideas).

Lastly, I would like to thank my family who have given me nothing but support and love in all my decisions over the course of my degree. Most importantly, my mother who has never stopped encouraging and believing in me, thank you.

Dedication

To my mother, sister, Matt, and Wyatt,
for your unconditional support, love, and smiles

Chapter 1 – Introduction

1.1 Introduction to MRI

Magnetic resonance (MR) was first presented as a tool to gather basic *in vivo* images in 1973 by Paul Christian Lauterbur.[1] Only eight years after this discovery the first magnetic resonance imaging (MRI) machines were developed and brought into clinical use. Since then it has become an essential tool in the medical community as a non-invasive technique to diagnose a variety of medical ailments such as cancer, cardiovascular disease, and organ or tissue damage.[2] As with any new technology, the first pictures gathered were limited to grainy images where the differences between healthy and diseased tissue was difficult to elucidate. Two key areas were focused on to improve the image quality: specially designed hardware and software capable of more advanced algorithms (pulse sequences), and development of internal contrast agents to improve the sensitivity and resolution of the images.

MR imaging works by creating a 3D contrast map of the human body and highlighting abnormalities in the water/tissue ratio. These differences may be indicative of tumours and tissue death. MR imaging operates on the same principles as nuclear magnetic resonance spectroscopy (NMR), a technique widely utilized as a method to characterize the molecular structure of compounds in modern day chemistry. NMR spectroscopy makes use of the fact that nuclei of certain atoms have a non-zero nuclear spin that give rise to spin states that differ in energy in an external magnetic field. The population of the ground state (lower energy) and excited state (higher energy) differ by a Boltzmann distribution. The lower energy state can be excited by a radiofrequency (RF) wave causing the population to equalize (saturate). In order to generate a NMR spectrum this saturation must be reversible when the RF wave is halted; the mechanism by which the higher energy state returns to the lower energy state is known as relaxation.[3] The most studied nuclei are those with a nuclear spin of ½, called dipolar nuclei, and the most studied of these is the ^{1}H nucleus (proton). MR imaging exploits the abundance of water

(~45 M)[4], and thus hydrogen atoms, in the human body. By exciting these nuclei with bursts of RF waves of a specific pulse sequence a detectable signal can be measured. By using gradient coils in the x, y, and z plane detection is focused on a specific 3D volume (voxel). As the proton signal intensity (of water) varies so does the shading of the voxel (higher intensity generates a brighter voxel). By scanning the body and combining all the voxels, a contrast map is generated which is dependent on the water/tissue ratio. Examining the contrast map, doctors are able to diagnose problem areas and determine the best course of action using data from a completely harmless, non-invasive procedure.

MR imaging is inherently an insensitive technique due to the small differences in the tissue/water ratio between healthy and diseased tissue; however, changing the RF pulse sequence or administering contrast agents can address this. Due to the large amount of water present and the small relative difference in water concentration between healthy and diseased tissue, it is often difficult to locate small abnormalities. Altering the RF pulse sequence will change the relaxation of the protons providing enhancement to different tissue types as required.[5] Another method of image improvement is to administer contrast agents that rely on the paramagnetic properties of their lanthanide core to alter relaxation time, **Figure 1**.[6]

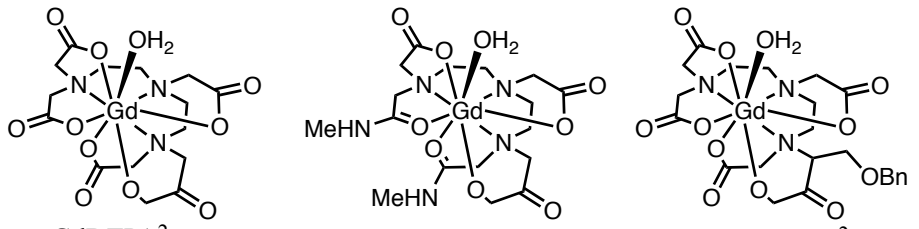

Figure 1.1: Examples of first generation T_1 contrast agents

1.2 T_1 Contrast Agents

Commercial T_1 contrast agents are by far the most frequently used with over 10 million Gd contrast-enhanced MRI scans run each year.[7] They utilize a paramagnetic gadolinium metal centre to increase the relaxation rate of bound water, which increases the signal

intensity of surrounding water and creates a *positive contrast.* MR imaging, like NMR, takes advantage of the fact that when a spin active nucleus is placed in a magnetic field the number of spins aligned with the magnetic field (α, lower energy) and the number of spins opposing the magnetic field (β, higher energy) are slightly different based on a Boltzmann distribution. When irradiated at the resonance frequency, the energy is absorbed by the nucleus causing the α state to flip to the β state, giving rise to a detectable signal. The greater the difference in the population of the α and β states, the more energy that can be absorbed, and the more intense the signal will be. When the pulse is stopped, the spins will relax to their natural state (equilibrate) leaving no detectable change, allowing for them to be excited again. The method by which they return to this equilibrium is termed relaxation.[3] Relaxation is split into two categories, longitudinal (T_1) and transverse (T_2) relaxation. As the excited spins return to their equilibrium position they must discard the excess energy they have acquired from the RF pulse, this is accomplished by either interactions with the surrounding lattice (T_1) or by transmitting the energy to other spins (T_2). As the longitudinal relaxation rate T_1 of the water protons surrounding the contrast agent is increased, the rate at which the spectrum is acquired can also be increased. The protons which are not in close proximity to the contrast agent retain their original longitudinal relaxation rate and therefore will not have fully relaxed to their equilibrium position between acquisition times. This will cause their signal to become less intense due to signal saturation, creating a *positive contrast* between areas where the T_1 contrast agent is present in higher and lower concentrations. As T_2 is affected less than T_1 by lanthanide-based contrast agents, this type of relaxation is usually neglected.[5]

Currently, a large dose of contrast agent (0.5 mmol/kg)[8] must be delivered in order to see any appreciable signal enhancement. By increasing the rate of longitudinal relaxation, the effectiveness of the T_1 agents can be improved allowing for a smaller dosage of contrast agent while still providing adequate *positive contrast*. Changes in the rate of relaxation ($1/T_1$) can be influenced by many different mechanisms such as dipole-dipole or electronic interactions, and rotational diffusion, these all contribute to the relaxivity of a contrast agent. The term relaxivity, **Equation 1.1**, is defined as how much the

relaxation rates are changed with respect to the concentration of contrast agent. Where $1/T_1$ is the relaxation rate before contrast agent is administered, $1/T_{1CA}$ is the rate after contrast agent is present, and [CA] is the concentration of contrast agent added.[4] This equation can be further expanded where the total relaxivity is a sum of the relaxivity enhancement caused by inner sphere water, r_1^{IS}, (water bound to the metal centre) and outer sphere water, r_1^{OS}, (bulk water), **Equation 1.2**.[5]

$$r_1 = \frac{\left[\left(\frac{1}{T_{1CA}}\right) - \left(\frac{1}{T_1}\right)\right]}{[CA]} \quad (\mathbf{1.1})$$

$$r_1 = r_1^{IS} + r_1^{OS} \quad (\mathbf{1.2})$$

As the outer sphere relaxivity contributions cannot be directly altered, changes in r_1 are effected by ligand modification to alter the inner sphere relaxivity. Inner sphere relaxivity (r_1^{IS}) is defined by **Equation 1.3**, where q is the hydration number (number of inner sphere water), T_{1m} is the relaxation time of agent-bound water, and τ_{1m} is the lifetime of an inner sphere water.[4]

$$r_1^{IS} = \frac{q/[H_2O]}{(T_{1m} + \tau_{1m})} \quad (\mathbf{1.3})$$

In order for the shortened relaxation time of contrast agent bound water to affect the relaxation rate of bulk water there must be rapid water exchange between the sites. From **Equation 1.3**, it can be seen that an increasing hydration number, q, would increase the relaxivity linearly. To increase the hydration number a coordination site of the chelating ligand on the metal must be "sacrificed", reducing the thermodynamic stability constant of the metal-ligand complex. The thermodynamic stability of a contrast agent is very important as any ligand dissociation would release the lanthanide ion which is known to be toxic *in vivo*.[8, 9]

Each contrast agent exists in equilibrium between the ligand-bound metal complex and the free species, **Equation 1.4**. This is represented by the thermodynamic stability

constant (K_{ML}), which is derived from **Equation 1.5,** where $[ML(OH_2)_n]$ is the concentration of metal bound ligand, $[M(OH_2)_x]$ and [L] is the concentration of free metal aqua complex and ligand respectively.

$$\{M(OH_2)_x\}^{3+} + \{L\}^{z-} \rightleftharpoons \{ML(OH_2)_n\}^{3-z} + (x\text{-}n)H_2O \quad \textbf{(1.4)}$$

$$K_{ML} = \frac{[ML(OH_2)_n]}{[M(OH_2)_x][L]} \quad \textbf{(1.5)}$$

It can be seen that K_{ML} is inversely related to the concentration of free metal ion so the larger the value for K_{ML} the less likely that the lanthanide ion will be released *in vivo*. Thermodynamic stability constants, reported as the log of K_{ML}, vary substantially (8 orders of magnitude) between commercially available contrast agents, **Table 1.1**.[5] Reports from European health authorities have linked contrast agents Omniscan®, and Optimark® to nephrogenic systemic fibrosis (NSF). This risk was attributed to their lower K_{ML} value. These same reports also placed Magnevist in the same high-risk group, while placing MultiHance in a low-risk group even though they have almost identical log K_{ML} values.[10] It can be seen that while log K_{ML} values are important there is much more that must be understood to assess the suitability of a metal complex as a contrast agent.

Table 1.1: Stability constants of commercially available contrast agents

Commercial name	Short name	Log K_{ML}	Ligand structure
Dotarem®	Gd-DOTA	24.78	macrocyclic
ProHance®	Gd-HP-DO3A	23.8	macrocyclic
Primovist®	Gd-EOB-DTPA	23.46	linear
MultiHance®	Gd-BOPTA	22.59	linear
Magnevist®	Gd-DTPA	22.46	linear
Gadovist®	Gd-DO3A-butrol	20.8	macrocyclic
Omniscan®	Gd-DTPA-BMA	16.85	linear
Optimark®	Gd-DTPA-BMEA	16.84	linear

The thermodynamic stability constant of the gadolinium complex is not the only factor that affects how the contrast agents react *in vivo*; how strongly it binds other ions like calcium, zinc, and copper also affects *in vivo* reactivity. Omniscan® and Optimark® have significantly lower K_{ML} values than the other agents but were still considered safe enough for FDA approval. The reason for their low toxicity profile is that the K_{ML} for other biologically relevant ions (Ca^{2+}, Zn^{2+}, and Cu^{2+}) is also significantly lower, **Table 1.2,** meaning that transmetallation effects are minimized.

Table 1.2: Stability constants of commercial contrast agent derivatives

Ligand	**Log K_{ML}**			
	M = Gd^{3+}	**M = Ca^{2+}**	**M = Zn^{2+}**	**M = Cu^{2+}**
DTPA (Magnevist)	22.46	10.75	18.29	21.38
DTPA-BMA (Omniscan)	16.85	7.17	12.04	13.03

Gadolinium is the only metal centre used in commercial T_1 contrast agents. The reason for this is that Gd has 7 unpaired electrons. Dipole-dipole relaxation has a very large effect on the longitudinal relaxation rate and is directly proportional to the spin quantum number, S, **Equation 6**.[11]

$$\frac{1}{T_1^{DD}} \propto S(S+1) \qquad (\mathbf{1.6})$$

Gd^{3+} has the maximum possible value of S at 3.5; Eu^{2+} and Tb^{4+} also have S = 3.5 however, they risk being oxidized or reduced, respectively, to return to their most stable 3+ oxidation state and destabilizing the complex. Manganese has also been suggested as an alternative due to its lower toxicology profile (the intravenous LD_{50} has not calculated but the oral LD_{50} is very high > 500mg/g Mn, vs. ~2.5mg/kg Gd)[9], however, as it has only 5 unpaired electrons (S = 2.5) the dipole-dipole longitudinal relaxation rate would be reduced by 55% requiring a much larger dose of contrast agent.

Slowing the tumbling rate of a molecule increases the relaxivity. Electronic relaxation and rotational diffusion both affect the relaxivity, however, at the typical MRI 1.5 tesla magnetic field (^{1}H resonant frequency = 63.8 MHz) electronic relaxation is much less significant than tumbling effects and can be neglected.[4] By increasing the size of the contrast agent the tumbling rate can be significantly slowed down (**Figure 1.2**).[12-14]. This has been accomplished by adding bulky groups to Ln chelates (**1.4)**, using large macrocycles to encapsulate a gadolinium ion (**1.5**), or attaching a Gd ion to large macromolecule like proteins or polymers (**1.6**). By attaching a Gd chelate to Albumin the relaxivity was found to be 14.9 mM^{-1} s^{-1} compared to commercial contrast agents that have a relaxivity of 3.5-3.8 mM^{-1} s^{-1}.[7]

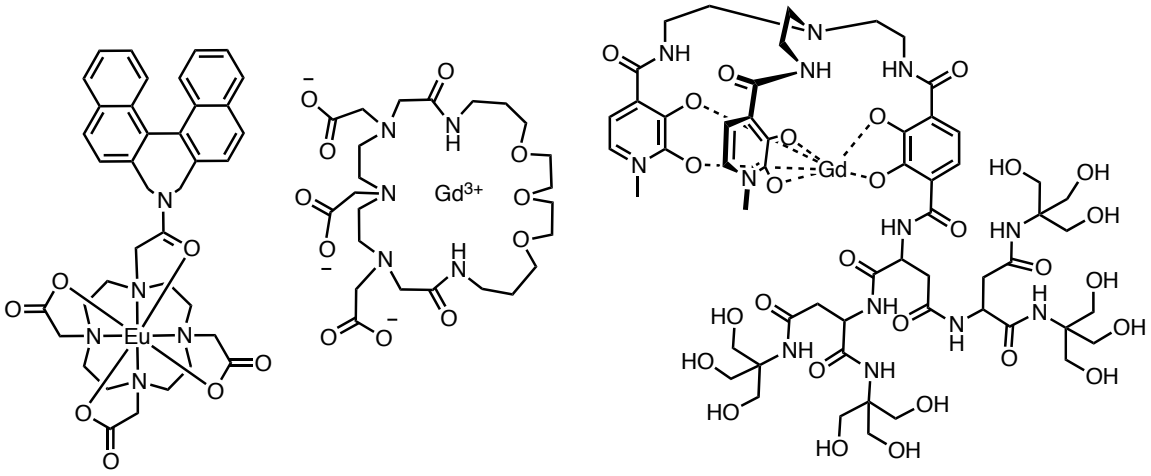

1.4 **1.5** **1.6**

Figure 1.2: Bulky T_1 agents used to slow tumbling rate

An added effect of increasing the size of the contrast agent is that they are retained in the blood for a longer period of time. For this reason these contrast agents have been termed blood pool agents. This has both benefits and problems. The longer retention time increases the chance of transmetalation before the kidneys can excrete the Gd complex. This leads to the release of the toxic Gd core (linked to NSF[10]). However, the increase in blood retention allows for the contrast agent to accumulate in tumours via the enhanced permeability and retention (EPR) effect allowing for easier tumour detection.[15]

To increase the rate at which these blood pool agents are removed, biodegradable polymer contrast agents have been developed. By attaching a stable gadolinium chelate onto a larger polymer the benefits of increased relaxivity and blood pooling are maintained. As the polymer degrades into the small Gd containing subunits, these are quickly filtered from the body by the kidneys and the risk of chelate transmetalation is avoided. Problems with toxicity have arisen after the polymer cleavage,[16] however, after polymer modification this issue has been resolved resulting in a safe, biodegradable polymeric contrast agent.[17]

1.3 ParaCEST Contrast Agents

There is a new class of contrast agent currently being developed which operates on a fundamentally different relaxation mechanism known as *chemical exchange saturation transfer* (CEST) providing a *negative contrast*, outlined in **Figure 1.3** and **Figure 1.4**. As mentioned, when a hydrogen nucleus is placed in a magnetic field the number of aligned spins and the number of spins opposing the magnetic field is slightly different (**Figure 1.3, A**). When irradiated at the resonance frequency the energy is absorbed by the nucleus causing the α spin to flip to the β state, giving rise to a detectable signal. If a presaturation pulse is applied, it will cause the spins to equalize and in turn cause the signal to disappear. When the pulse is stopped the spins will quickly equilibrate leaving no detectable change. In CEST agents there are two pools of exchangeable protons, bulk water and a secondary source (an amino or hydroxyl moiety on the contrast agent) that undergo chemical exchange. Provided chemical exchange between these two pools is slow enough that distinct resonances are observed (**Figure 1.3, B**), it is possible to irradiate at a frequency causing only the secondary pool to be saturated (**Figure 1.3, D**). If the chemical exchange is too fast the exchangeable proton signals will coalesce and eliminate the possibility of CEST enhancement (**Figure 1.4, B**). If the equilibrium return rate is quicker than the chemical exchange rate there will be no net change in the output (**Figure 1.3, E & Figure 1.4, A**). However, if the chemical exchange rate is faster between the two pools than the equilibrium return rate, the α and β spin population difference will decrease in the bulk water signal as well (**Figure 1.3, F & Figure 1.4, C**).

This will cause an overall decrease in signal intensity for the bulk water pool, which was **not** saturated (**Figure 1.3, G**).[6] Irradiating at the negative offset of the secondary pool generates a control spectrum with unenhanced contrast. By subtracting the control spectrum from the CEST enhanced spectrum a darker picture is generated in areas where the contrast agent is present in great enough concentration, this is termed *negative contrast.*

In order to maximize the effectiveness of a CEST agent it is important that the two pools are in relatively fast exchange, yet the signals need to remain separate to allow for irradiation at the secondary pool. The larger the difference in Δω, the faster the chemical exchange between the two pools can be without coalescing (**Figure 1.3, C**), allowing for more chemical exchange and a greater reduction in the bulk water signal. When only relying on an organic framework, chemical shift separation between exchangeable pools (Δω) is limited to 2-6 ppm (CEST) but when a paramagnetic metal centre is incorporated Δω can reach upwards of 100 ppm (paraCEST).[18]

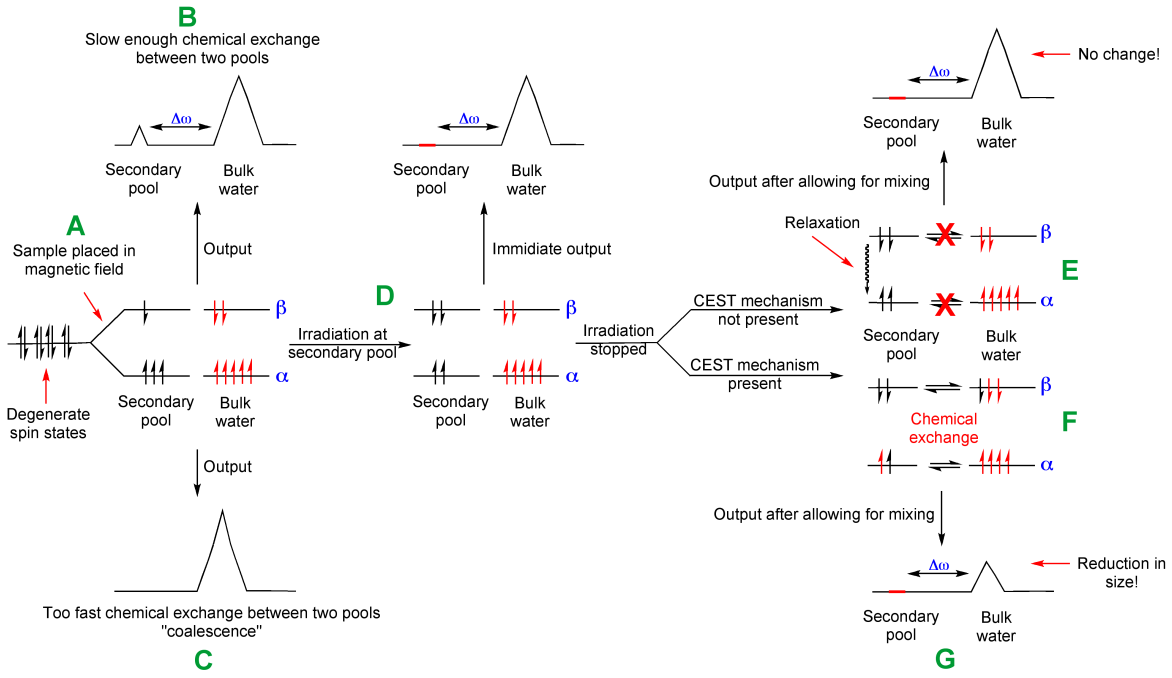

Figure 1.3: CEST effect following nuclear spin states

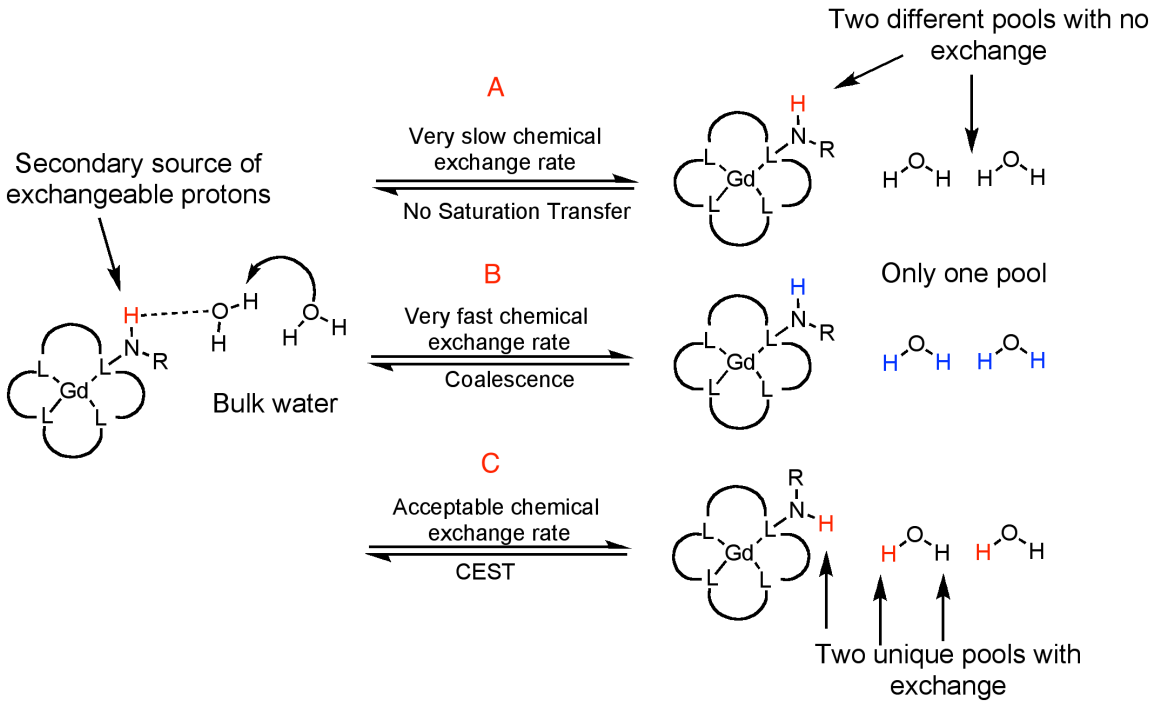

Figure 1.4: CEST effect following proton exchange

Using a gadolinium centre is not required in paraCEST agents as it is in T_1 contrast agents. Only the chemical shift location of the secondary pool and chemical exchange between the secondary pool and bulk water is important in paraCEST agents and not the spin only quantum number. Large changes in the chemical shift location can be provided by many paramagnetic metal species, however due to the similar properties of the lanthanide series, changing the metal centre has little effect on stability and biodistribution of the complex, yet the difference in magnetic moment have a profound effect on shift location allowing for a quick way to optimize potential agents.

ParaCEST agents offer many advantages over the traditional T_1 contrast agents in that they can be used not only to detect tumour growth and tissue death, they can also be used to determine temperature and pH. Since paraCEST agents are not always "on" it is possible to administer paraCEST agents with different tissue/organ affinities allowing for selective activation (provided there is a different shift location of the secondary pool) of each agent during the same procedure, which allows for a more information-rich image. Temperature and pH changes are indicative of a variety health problems (tumour growth,

carotid atherosclerotic plaques, etc.)[19] as there is a discrepancy (sometimes very small) between healthy and diseased tissue; accurately identifying these changes allows for a better diagnosis.[20] pH changes affect the efficiency of the CEST mechanism, however, as a change (reduction or increase) in *negative contrast* can also be caused by concentration differences one must either know the exact local concentration (very hard to do) or administer a second paraCEST agent with the same biodistribution but a different pH dependent CEST effect. By taking a ratio of the two CEST spectra, concentration can be neglected. It is also possible to do this using one paraCEST agent, provided two different sources of exchangeable protons are present with distinct resonances on the same complex. Temperature measurements are best done by scanning the resonance frequency until a maximum CEST effect is found, as location of the secondary pool is highly temperature dependent. Comparing the location of the secondary pool to a calibration curve one can collect accurate *in vivo* temperature.[18]

1.4 Purpose

New ligand design is paramount to addressing the rising use of lanthanides in medicine, be it for diagnostic imaging (MRI, NIR) or for therapeutic purposes (γ-emission). There is always demand for systems that can offer increased function and safety profiles while minimizing the amount of complex needed. With lanthanide complexes being the overwhelming majority of contrast agents, the list of useful ligand sets for lanthanides must be expanded in order to discover new properties. The majority of newly designed CEST contrast agents are based on the same ligand design as previous T_1 contrast agents: either ethylenediaminetetraacetic acid **1.7** (EDTA) or 1,4,7,10-tetraazacyclododecane **1.8** (cyclen), **Figure 1.5**, with incorporation of a secondary source of exchangeable protons. Our goal was to design new ligand architectures to increase relaxivity and ultimately lower the required dose of contrast agent (typically between 3-5 g per 100 kg of body weight) while still maintaining the same safety profile as commercial contrast agents.

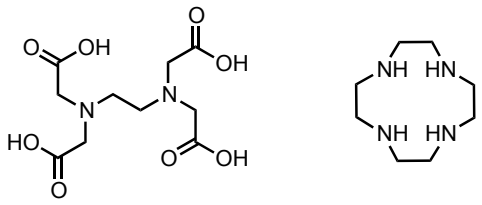

EDTA (linear) **1.7**

Cyclen (cyclic) **1.8**

Figure 1.5: Commercial contrast agent frameworks

Our plan was to focus on ligand sets that are known to bind lanthanides and remain chemically inert under physiological conditions. To account for the broad use of lanthanide complexes in the medical field we wanted to be able to easily modify the ligand in order to change some of its biological properties (via bio-molecule attachment for target delivery) while maintaining the core stability. However, the primary goal was to assess the new ligands as building blocks for future paraCEST agents. To incorporate the desired CEST mechanism we needed to make sure a source of secondary protons was present. As it is not possible to predict accurately which functional group will give a secondary source of protons in the intermediate exchange rate (not too fast or too slow) that group too had to be modifiable.

With these goals in mind, this thesis will outline the investigation of three classes of ligands for the purpose of using them as paraCEST contrast agents. Chapter 2 will examine Kläui ligands and their kinetic lability. Chapter 3 will focus on the synthesis of a novel class of pybox ligands based around analogues of the amino alcohol tyrosinol. Chapter 4 will focus on the modification of a water soluble *p*-sulfonated-calix[4]arene scaffold to incorporate lanthanide-binding elements. The final chapter will summarize these accomplishments, and set some future goals for the project

Chapter 2 – Lanthanide Complexes of the Kläui Metalloligand, $CpCo(P=O(OR)_2)_3$: An Examination of Ligand Exchange Kinetics between Isotopomers by Electrospray Mass Spectrometry

Adapted from: Kevin J. H. Allen[1], Emma C. Nicholls-Allison[1], Kevin R. D. Johnson[1], Rajinder S. Nirwan[1], David J. Berg[1], Dennis Wester[2], and Brendan Twamley[3]. *Inorg. Chem.* **2012**, *51*, 12436.

[1]Department of Chemistry, University of Victoria, Victoria, British Columbia, Canada
[2]Nordion Inc., 4004 Westbrook Mall, Vancouver, BC, Canada V6T 2A3
[3]University Research Office, 109 Morrill Hall, University of Idaho, Moscow, ID, USA 83844−3010.

KJHA designed the research, performed the syntheses, and collected and analyzed the data. ECNA helped determine the effects of water concentration on ligand exchange. RSN and KRDJ performed the first in-house synthesis of **2.1a** and **2.1b** using literature precedent.

2.1 Introduction to Kläui ligands

As stated in Chapter 1, all commercial contrast agents are based on either a EDTA or cyclen type stucture.[21, 22] It was our goal to use a radically different ligand set to see if we could make a new class of paraCEST agents. The cobalt metalloligands, $[CpCo(P=O(OR)_2)_3]^-$, developed by Kläui function as tripodal oxygen donors to a wide variety of metals.[23] The high affinity of lanthanides for oxygen donors and the exceptional stability of the Kläui metalloligands to oxidizing agents, water, and aqueous acids suggested that these ligands might provide a suitable platform to develop new contrast agents.[23, 24] A key feature of the Kläui ligand is that the phosphite substituents are modifiable. This tunability allows for alteration of the solubility of the ligand in water or polar organic solvents.

Lanthanide complexes of Kläui metalloligands, L_{CoP}, have been reported in the past. Included in this group are a number of mono(ligand) complexes such as $(L_{CoP})Ln(por)$ (Ln = Nd, Er, Yb, Y; por = various porphyrin derivatives),[25-31] $(L_{CoP})Y(H_2Bpz_2)$,[32] clusters with molybdenum oxo anions,[33] and acetate-bridged dimers $[(L_{CoP})Ln]_2(\mu\text{-}CH_3CO_2)_4$ (Ln = Nd, Y).[34, 35] Among the bis(ligand) complexes, both neutral complexes such as $(L_{CoP})_2Ln(X)$ (X = acac, Cr_2O_7, $CH_3CO_2^-$)[36] and salts such as $[(L_{CoP})_2Ln(OH_2)_n]^+X^-$ (Ln = Eu, La; n = 1, 2; X = BF_4^-, Cl^-)[37, 38] have been structurally characterized. Of these, the latter are expected to have the greatest water solubility and most potential as contrast agents, particularly since they have water molecules bound to the metal center.

In the work described here, we have developed several lanthanide complexes of the type $[(L_{CoP})_2Ln]^+Cl^-$ (Ln = Nd, Eu, Tb, Yb) that appear to be either solvent free or to contain very weakly bound water molecules. We have verified crystallographically that the complex $[(L_{CoP})_2Ln]^+$ $[CoCl_3(THF)]^-$ contains a 6-coordinate cation ***without*** bound waters (*vide infra*). Additionally, since lanthanide complexes of the Kläui metalloligand must show relatively low kinetic lability in aqueous solution to be useful as contrast agents, we have investigated the rate of intermetallic ligand exchange between isotopomers using electrospray mass spectrometry. To the best of our knowledge, this is

the first reported use of ESI MS to determine ligand exchange rates in lanthanide chemistry, although, Electrospray MS has been used to determine the rate of ligand exchange between platinum centers that form supramolecular polygons.[39] Finally, we also report our attempts to synthesize novel Kläui ligands with chelating groups on the phosphite arms in order to slow down the rate of ligand exchange.

2.2 First generation Kläui Ligands.

The Kläui ligands, $[CpCo(P{=}O(OR)_2)_3]^-$ were prepared as their sodium salts from Cp_2Co or $CpCo(CO)(I)_2$ using modified literature procedures, for **2.1a** (R = Et) and **2.1b** (R = Ph), respectively (**Scheme 2.1**).[40, 41] Paramagnetic $[CpCo(P{=}O(OR)_2)_3]_2Co$, **2.2a,** was found as a side product. This had previously been unreported as a by-product during the synthesis of **2.1b**. Conveniently, it could be cleaved through reflux with NaCN in methanol.

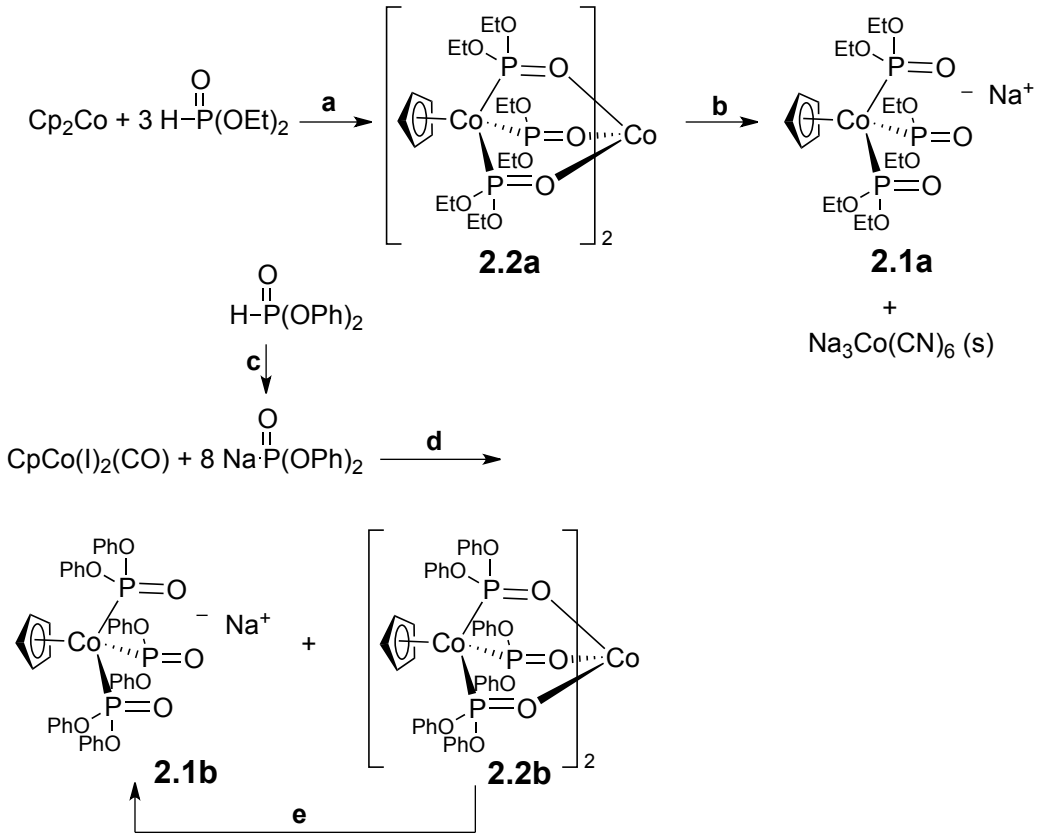

Scheme 2.1: Synthesis of ligands, $[CpCo(P{=}O(OR)_2)_3]^-Na^+$, **2.1a** (R = Et) and **2.1b** (R = Ph). Conditions: a) 130 °C, 18 h, 78% yield; b) NaCN, MeOH, reflux in air, 18 h, 95% yield; c) NaH, THF, 0 °C; d) reflux, THF, 18 h, 73% yield; e) NaCN, toluene-MeOH, reflux in air, 18 h.

Reaction of two equiv of the Na^+ salts of **2.1a** or **2.1b** with one equiv of $LnCl_3(H_2O)_n$ (n = 7, Ln = Nd; n = 6, Ln = Eu, Tb, Yb) in THF afforded the bis(ligand) complexes, $\{[CpCo(P{=}O(OR)_2)_3]_2Ln(H_2O)_x\}^+Cl^-$ (Ln = Nd, **2.3**; Eu, **2.4**; Tb, **2.5**; Yb, **2.6**; R = Et, **a**; R = Ph, **b**) as microcrystalline solids (**Scheme 2.2**). Based on the ^1H NMR of recrystallized complexes, the water content of these complexes varies from 2 to more than 20 equivalents but the average value for most complexes is about 8 equivalents of water. Most samples remain hydrated with 2-4 waters after exposure to vacuum at room temperature.

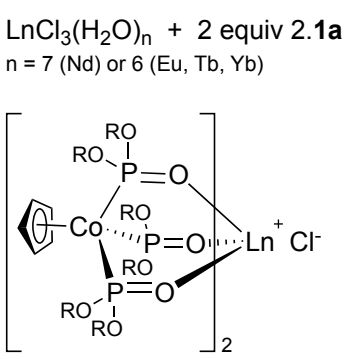

	Ln	R	Yield %
2.3a	Nd	Et	90
2.3b	Nd	Ph	91
2.4a	Eu	Et	82
2.5a	Tb	Et	73
2.5b	Tb	Ph	85
2.6a	Yb	Et	83
2.6b	Yb	Ph	93

Scheme 2.2: Synthesis of lanthanide complexes, $\{[CpCo(P{=}O(OR)_2)_3]_2Ln\}^+ Cl^-$

Thermogravimetric analysis of complex **2.3a** shows steady loss of *ca.* 4 water molecules until the anhydrous complex is reached at 65 °C, **Figure 2.1**. Anhydrous **2.3a** remains stable until about 185 °C at which point it loses mass consistent with loss of ethyl chloride (*or* ethene and HCl); steady mass loss due to further decomposition occurs beyond 210 °C. A TGA of **2.5a** (Ln = Tb) shows very similar behaviour with loss of *ca.* 2 water molecules by *ca.* 65 °C and loss of ethyl chloride beginning at only 135 °C. Presumably greater steric crowding at the smaller Tb^{3+} center in **2.5a** destabilizes the complex relative to Nd^{3+} complex **2.3a**. Interestingly, Nolan *et al* reported a neutral, dimeric complex, $\{[CpCo(P{=}O(OEt)_2)_3][\mu\text{-}CpCo(P{=}O(OEt)_2)_2(P(O)_2(OEt)]Y\}_2$ containing one bridging $[CpCo(P{=}O(OEt)_2)(PO_2(OEt)]^{2-}$ ligand.[42] The authors obtained this complex by refluxing the Na^+ salt of **2.1a** with anhydrous YCl_3 in THF and given the low temperature required for loss of ethyl chloride from **2.3a** and **2.5a** by TGA, it is reasonable to speculate that ligand fragmentation occurs after complex formation at the temperatures used.

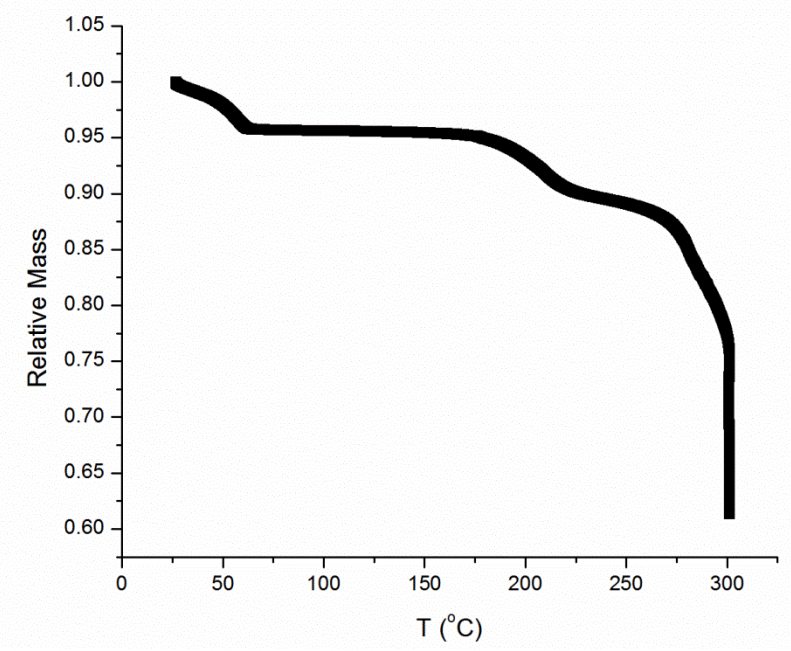

Figure 2.1: Thermogravimetric analysis of **2.3a** showing loss of water followed by EtCl or ethylene and HCl.

The phenyl-substituted complex **2.6b** (Ln = Yb) also shows low temperature loss of two water molecules (complete by 50 °C), but in this case the anhydrous complex remains stable to more than 220 °C (**Figure A11**). Above this temperature there is a clear mass loss consistent with loss of a phosphite arm ($O=P(OPh)_2$) followed by further decomposition at temperatures above 250 °C. The ease with which these complexes dehydrate on heating during TGA strongly suggests that the water molecules present are not bonded to the metal ions. This is confirmed crystallographically for $\{[CpCo(P=O(OPh)_2)_3]_2Yb\}^+ \{CoCl_3(THF)\}^- \bullet 2C_6H_6$, **2.7,** discussed below.

During the initial synthesis of yellow microcrystalline **2.6b**, a small amount of green X-ray quality crystals were obtained that correspond to the expected $\{[CpCo(P=O(OPh)_2)_3]_2Yb\}^+$ cation with a tetrahedral $\{CoCl_3(THF)\}^-$ counterion, **2.7**. Recrystallization of **2.7** from acetone containing NaCl resulted in a pale yellow solid corresponding to **2.6b**. Complex **2.7** shows absorptions at 592, 623 and 684 (ε = 22 L mol^{-1} cm^{-1}) which are consistent with the blue, distorted tetrahedral $[CoCl_3(THF)]^-$

anion;[43] pale yellow **2.6b** on the other hand shows only a peak tailing into the visible at *ca*. 400 nm.

An ORTEP3 plot[44] of **2.7** is shown in **Figure 2.2** while selected bond distance and angles are collected in **Table 2.1**. At this writing, there are 24 reports of crystallographically characterized lanthanide complexes containing Kläui ligands, although in all cases the phosphite substituents are aliphatic making this the first example of an aryl substituted Kläui lanthanide complex.[25-38] The bond lengths within the Kläui ligand of **2.7** are unremarkable; however, the Yb-O distances are at the long end of the range of distances in the previously reported complexes after adjustment for lanthanide ionic radius and coordination number (lit[25-38]: 2.10-2.24 Å, mean = 2.17 Å; **2.7**: 2.205(4)-2.227(4) Å, mean = 2.213 Å). This observation, the fact that **2.7** is the only 6-coordinate complex containing two Kläui ligands and the lack of chloride or water coordination suggests that the ytterbium center in **2.7** is relatively crowded.

Table 2.1: Selected bond lengths and angles for $\{[CpCo(P{=}O(OPh)_2)_3]_2Yb\}^+ \{CoCl_3(THF)\}^- \bullet 2C_6H_6$, **2.7** [a]

Cation					
Yb(1)-O(3)	2.227(4)	Yb(1)-O(6)	2.207(4)	Yb(1)-O(9)	2.213(4)
Yb(1)-O(12)	2.220(4)	Yb(1)-O(15)	2.205(4)	Yb(1)-O(18)	2.207(4)
P(1)-O(3)	1.512(5)	P(2)-O(6)	1.521(5)	P(3)-O(9)	1.517(5)
P(4)-O(12)	1.509(5)	P(5)-O(15)	1.506(4)	P(6)-O(18)	1.502(5)
Co(1)-P(1)	2.160(2)	Co(1)-P(2)	2.150(2)	Co(1)-P(3)	2.159(2)
Co(2)-P(4)	2.161(2)	Co(2)-P(5)	2.162(2)	Co(2)-P(6)	2.171(2)
Co(1)-Cp(1)[b]	1.694	Co(2)-Cp(2)[b]	1.736	Co(1)-C(Cp1)$_{ave}$[c]	2.075
Co(1)-C(Cp2)$_{ave}$[c]	2.110				
Yb(1)-O(3)-P(1)	128.3(3)	Yb(1)-O(6)-P(2)	131.1(3)	Yb(1)-O(9)-P(3)	128.4(3)
Yb(1)-O(12)-P(4)	132.7(3)	Yb(1)-O(15)-P(5)	132.6(2)	Yb(1)-O(18)-P(6)	133.5(3)
Co(1)-P(1)-O(3)	118.9(2)	Co(1)-P(2)-O(6)	119.2(2)	Co(1)-P(3)-O(9)	120.0(2)
Co(2)-P(4)-O(12)	119.8(2)	Co(2)-P(5)-O(15)	120.1(2)	Co(2)-P(6)-O(18)	119.3(2)
Anion					
Co(3)-Cl(1)	2.245(2)	Co(3)-Cl(2)	2.223(2)	Co(3)-Cl(3)	2.238(2)
Co(3)-O(19)	2.037(5)				
Cl(1)-Co(3)-Cl(2)	113.56(11)	Cl(1)-Co(3)-Cl(3)	117.44(11)	Cl(1)-Co(3)-O(19)	102.3(2)
Cl(2)-Co(3)-Cl(3)	113.3(10)	Cl(2)-Co(3)-O(19)	105.7(2)	Cl(3)-Co(3)-O(19)	102.4(2)

[a] estimated standard deviation in parentheses, [b] Cp designated the centroid of the cyclopentadienyl C_5 ring, [c] average distance from cobalt to the cyclopentadienyl ring carbons.

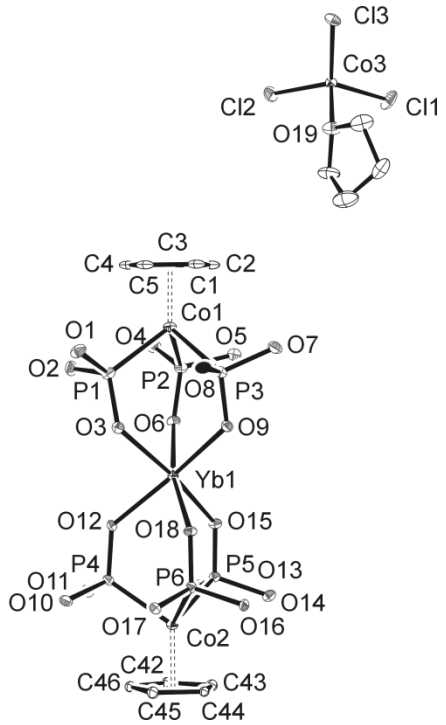

Figure 2.2: ORTEP3[44] plot of $\{[CpCo(P{=}O(OPh)_2)_3]_2Yb\}^+ \{CoCl_3(THF)\}^- \bullet 2C_6H_6$, **2.7** (50% probability ellipsoids; phosphite phenyl groups and benzenes of solvation omitted for clarity).

The solid state structure of **2.7** suggested that complexes **2.3-2.6** also exist as salts containing a $\{[CpCo(P{=}O(OR)_2)_3]_2Ln\}^+$ cation. Indeed, electrospray MS in positive ion mode from acetonitrile or a mixture of acetonitrile and water readily gave the expected isotopic pattern for the intact cation as shown, for example, for **2.3a** in **Figure 3.3**. No higher mass peaks were observed suggesting that the cations are not solvated, at least under ESI-MS conditions.

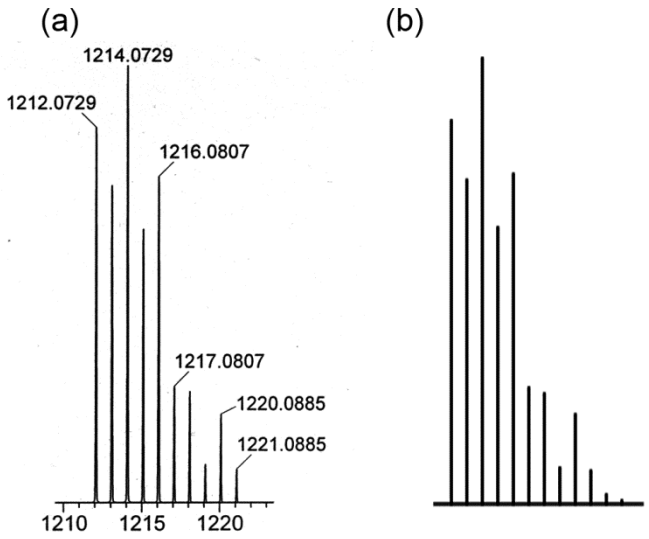

Figure 2.3: Observed (a) and simulated (b) isotopic distribution for the cation, $\{[CpCo(P{=}O(OEt)_2)_3]_2Nd\}^+$, of **2.3a**.

To examine how the Ln(Kläui)$_2$ complexes behave in solution, variable temperature ^{1}H NMR spectra were collected on **2.6b** over a 40 K range and the change in chemical shift was plotted against 1/T (**Figure 2.4)**. A straight line in this plot suggests that only one species is present. If loosely bound water (or solvents) were present and undergoing dynamic exchange we would expect to see deviation from linearity as the equilibrium constant is altered. The linear relationship and the crystal structure suggest that there are no bound water (or solvent) molecules in the Ln(Kläui)$_2$ complexes.

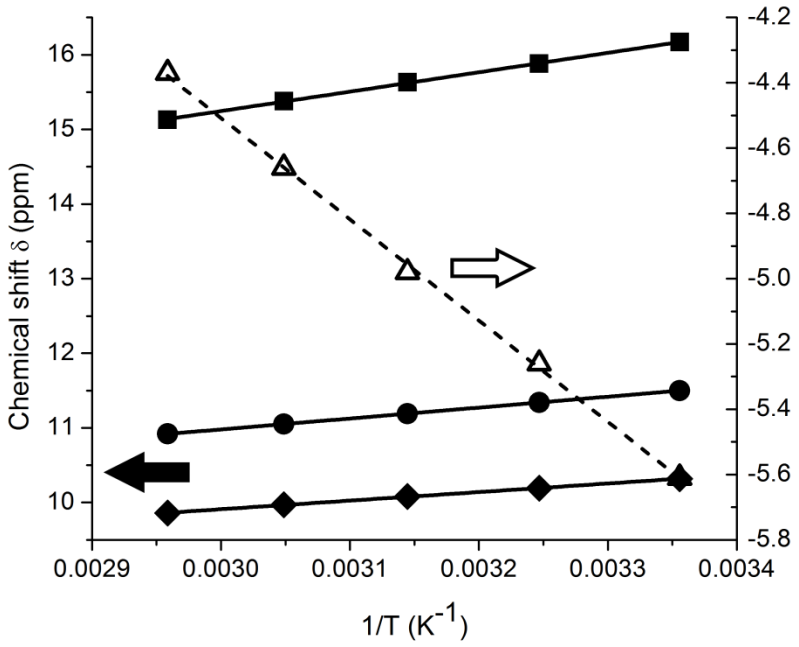

Figure 2.4: Variable temperature ^{1}H NMR data (360MHz, d_6-DMSO) of $\{[CpCo(P{=}O(OPh)_2)_3]_2Yb\}^+ Cl^-$ (**2.6b**) over the range of 298-338K. Solid lines use ppm values from axis on the left, dashed lines use ppm values from axis on the right.

The utility of complexes like **2.3-2.6** as possible MRI relaxation agents depends, in part, on the lability of the Kläui metalloligand in aqueous solution at blood pH (*ca*. 7.4).[21, 22, 45] Although we expected the unmodified Kläui ligands used here to be quite labile, there is no information available in the literature regarding the lability of a tridentate ligand set such as that presented by a Kläui ligand. Therefore to provide a baseline for any future work, we set out to determine the lability of the ligands used here as a function of metal size and ligand substituent. In addition, since these complexes are only soluble in polar solvents containing limited amounts of water, we also examined how increasing water in a polar solvent changes the rate of ligand exchange.

The ease with which we obtained a mass spectrum for the cations of **2.3-2.6** by +ESI-MS suggested a straightforward method to measure the rate of ligand exchange. The Kläui ligands were easily deuterated at every position except the cyclopentadienyl ring by using either d_6-ethanol or d_6-phenol when preparing the phosphite. In both cases this allows formation of the d_{30}-$[CpCo(P{=}O(OR)_2)_3]^-$ ligand from which the corresponding

d_{60}-{[CpCo(P=O(OR)$_2$)$_3$]$_2$Ln}$^+$ analogs of **2.3-2.6** were prepared. The ligand exchange reaction was followed by mixing equimolar amounts of d_0 -**2.3-2.6** with their d_{60} analogs in acetonitrile and following the rate of disappearance of either the d_0 or d_{60} cation or the rate of appearance of the d_{30} ligand exchange product with time as illustrated in **Figure 2.5** for {[CpCo(P=O(OEt)$_2$)$_3$]$_2$Tb}$^+$ Cl$^-$, **2.5a**. The response factor of the mass spectrometer to the d_0-, d_{30}-, d_{60}-isotopomers is assumed to be identical in all cases, with starting concentrations selected to ensure good signal-to-noise ratio without overloading the instrument.

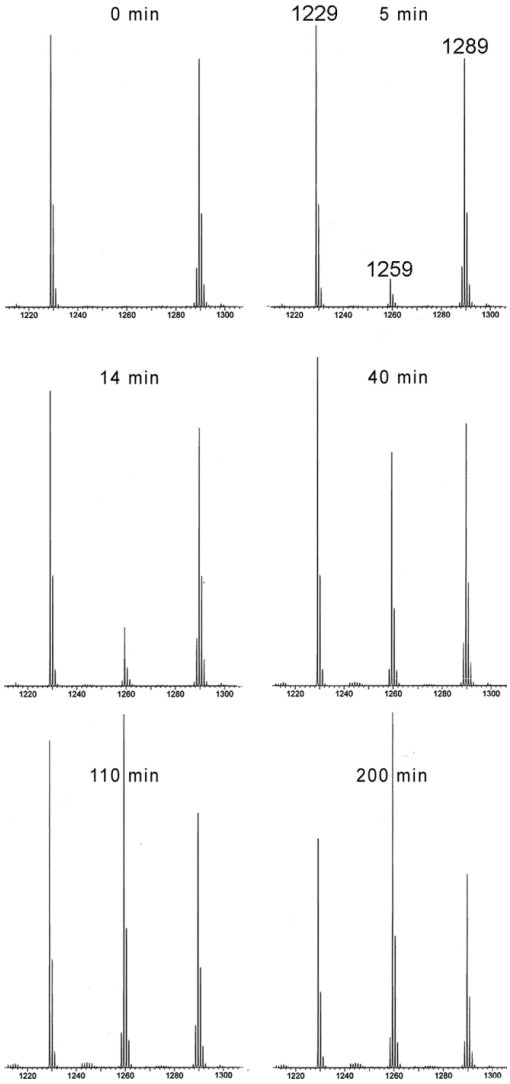

Figure 2.5: Electrospray mass spectra (positive mode, acetonitrile) showing the evolution of the d_0, d_{30} and d_{60} isotopic manifolds over time for the cation of {[CpCo(P=O(OEt)$_2$)$_3$]$_2$Tb}$^+$ Cl$^-$, **2.5a**, after mixing equimolar amounts of the d_0- and d_{60}-isotopomers (7.905 x 10^{-6} M).

The reaction between the d_0- and d_{60}-{[CpCo(P=O(OR)$_2$)$_3$]$_2$Ln}$^+$ complexes follow first order behaviour in each complex (2nd order overall) so a plot of 1/[d_{60}] or 1/[d_0] versus time initially follows a straight line of slope k. Good linear behaviour is observed until at least 25% conversion, eventually the back reaction becomes significant and the apparent rate declines (**Figure 2.6**). As expected, the reaction mixture eventually reaches a thermodynamic 1:2:1 mixture of d_0:d_{30}:d_{60} isotopomers (*c.f.* **Figure 2.5** at 200 min).

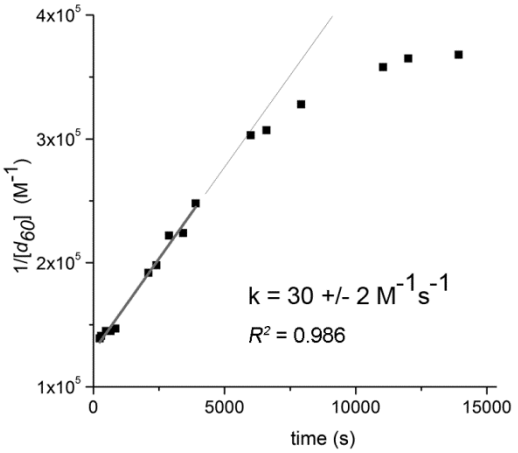

Figure 2.6: Plot of 1/[d_{60}-**2.5a**] versus time for the reaction between d_0 and d_{60}-{[CpCo(P=O(OEt)$_2$)$_3$]$_2$Tb}$^+$ Cl$^-$ (**2.5a**) in acetonitrile monitored by +ESI-MS (7.905 x 10^{-6} M each)

The observed rate constants for ligand exchange derived from electrospray MS are summarized in **Table 2.2**. We estimate an error of roughly 10% in these values based on the reproducibility between runs. Our ability to handle very fast reactions is limited by the time required to mix the d_0- and d_{60}-isotopomers and inject them into the mass spectrometer (*ca.* 1-2 min). In the case of {[CpCo(P=O(OEt)$_2$)$_3$]$_2$Nd}$^+$ Cl$^-$, **2.3a**, this meant that we could only estimate a lower limit for the rate constant k. Fortunately, in most of the cases studied here, the rate was sufficiently slow that reliable values for k could be determined.

Table 2.2: Summary of rate constant data for ligand exchange between d_0- and d_{60} $\{[CpCo(P{=}O(OR)_2)_3]_2Ln\}^+ Cl^-$

Entry	compd	Ln	R	ACN:H_2O[a]	k ($M^{-1}s^{-1}$)[b]	M
1	**2.3a**	Nd	Et	100 :0	>2500	7.905×10^{-6}
2	**2.4a**	Eu	Et	100 :0	575	7.905×10^{-6}
3	**2.4a**	Eu	Et	100 :0	>2500	1.581×10^{-4}
4	**2.5a**	Tb	Et	100 :0	30	7.905×10^{-6}
5	**2.5a**	Tb	Et	90 :10	55	7.905×10^{-6}
6	**2.5a**	Tb	Et	80 :20	67	7.905×10^{-6}
7	**2.5a**	Tb	Et	70 :30	74	7.905×10^{-6}
8	**2.5a**	Tb	Et	60 :40	166	7.905×10^{-6}
9	**2.5a**	Tb	Et	50 :50	268	7.905×10^{-6}
10	**2.5b**	Tb	Ph	100:0	34	7.905×10^{-6}
11	**2.5b**	Tb	Ph	50:50	100	7.905×10^{-6}
12	**2.6a**	Yb	Et	100:0	0.3	7.905×10^{-6}
13	**2.6a**	Yb	Et	100:0	0.3	1.581×10^{-4}
14	**2.6a**	Yb	Et	50:50	11	7.905×10^{-6}

[a] Acetonitrile:water ratio in *v/v* percentages
[b] estimated error *ca.* 10%

The rate constant for ligand exchange increases sharply as the ionic radius of the lanthanide increases (**Figure 2.7**).[46] In fact, a plot of log k vs. lanthanide ionic radius in 6-coordination is roughly linear (**Figure 2.8**). This observation is consistent with an associative mechanism where ligand exchange occurs within a dimeric aggregate through bridging interactions, **Figure 2.9**. The X-ray structure of the related neutral yttrium dimer, $\{[CpCo(P{=}O(OEt)_2)_3][\mu\text{-}CpCo(P{=}O(OEt)_2)_2(P(O)_2(OEt)]Y\}_2$, mentioned above, is noteworthy in this regard because it shows that dimer formation is feasible in a similar system.[42] Although there are no structurally characterized examples of *intact* $[CpCo(P{=}O(OEt)_2)_3]^-$ units bridging two lanthanide centers, it is reasonable to assume that such a dimer could form, particularly if one P=O arm dissociates from the lanthanide center. We would expect in an associative type mechanism to show a concentration dependence as it requires two species to come in close contact with one another. Entries 2 and 3 in **Table 2.2** show a rate increase with increasing concentration as predicted for an associative mechanism. However, when the smaller Yb centred complex (**2.6a**) was used we saw no change in rate (entries 12 and 13) which is more consistent with a dissociative mechanism. From the limited data available it appears that the type of exchange

mechanism is dependent on the size of the lanthanide centre. There is only a very limited amount of data present to base these conclusions and the experiment needs to be repeated at many more concentrations to comment on the mechanism more definitively.

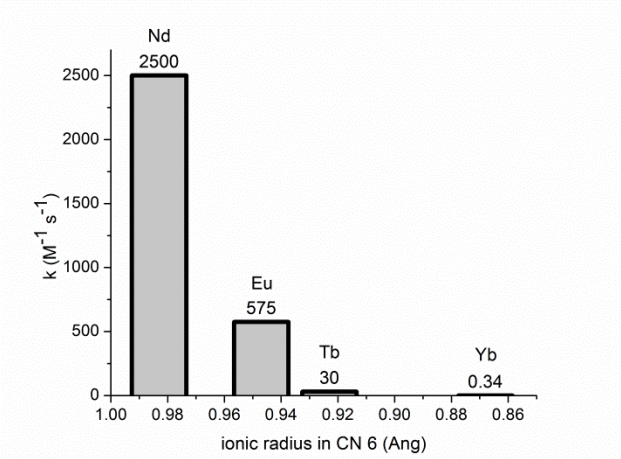

Figure 2.7: Plot of rate constant k versus ionic radius (Å) for the reaction between d_0 and d_{60}-{[CpCo(P=O(OEt)$_2$)$_3$]$_2$Ln}$^+$ Cl$^-$ (**2.3a**-**2.6a**) in acetonitrile monitored by ESI MS

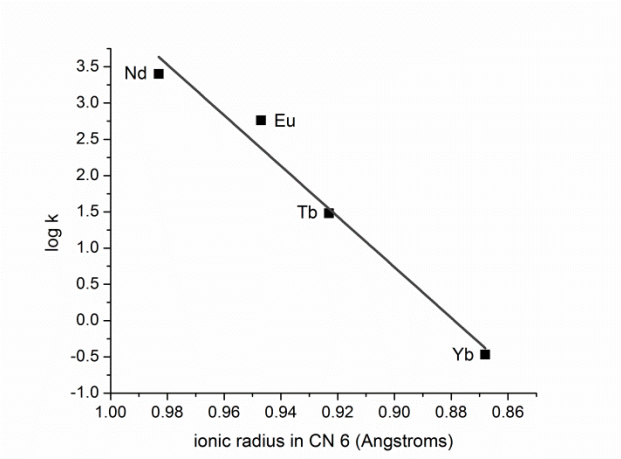

Figure 2.8: Plot of log k versus ionic radius (Å) for the reaction between d_0 and d_{60}-{[CpCo(P=O(OEt)$_2$)$_3$]$_2$Ln}$^+$ Cl$^-$ (**2.3a**-**2.6a**) in acetonitrile monitored by ESI MS

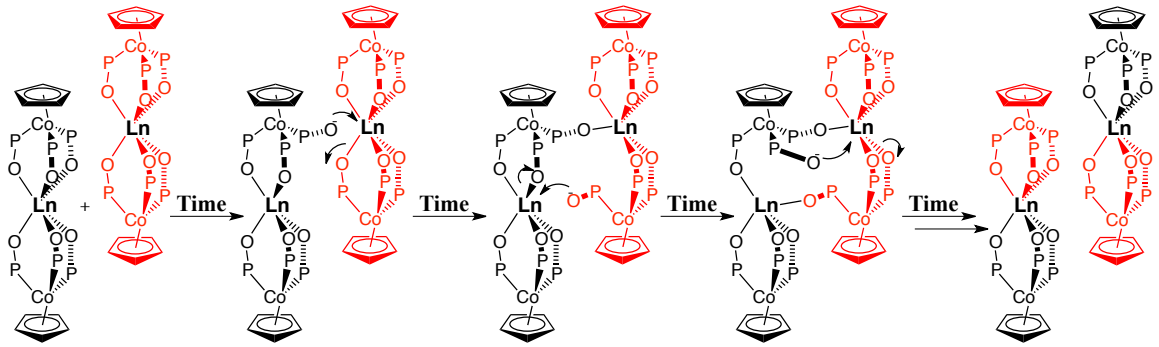

Figure 2.9: Possible associative type mechanism where one P=O dissociates to form a dimeric aggregate. Phosphorus substituents are removed for clarity.

Addition of water to the acetonitrile solvent was investigated to the limit of solubility (*ca.* 50% water) in the case of the Tb complexes **2.5a** and **2.5b**. The rate of exchange increased rapidly with increasing water content in the solvent, as illustrated for **2.5a** in **Figure 2.10**. Overall, the rate constant increased about 8-fold for the Et complex **2.5a** and about 3-fold for the Ph complex **2.5b** on going from pure acetonitrile to a 50:50 acetonitrile-water mixture. The reason for this strong water dependence is not clear but it could be that water competes with P=O binding and dissociation of one arm of the Kläui ligand facilitates bridge formation. We have not investigated the effect of changing pH on the rate of exchange but it is quite likely that labile hydroxo bridges could form at slightly basic pH and that these could facilitate dimer formation.

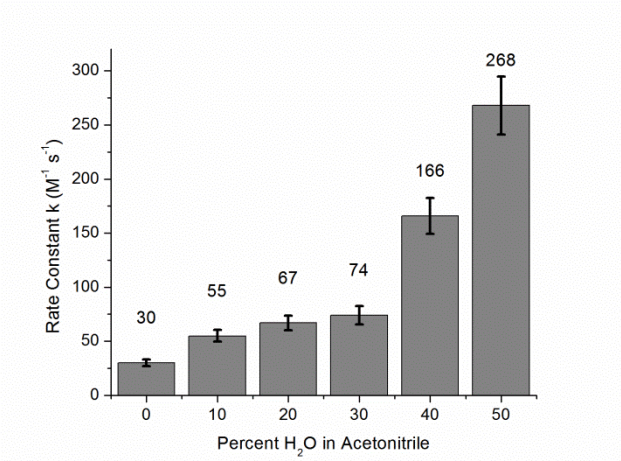

Figure 2.10: Plot of rate constant k versus water content (*v/v*) for the reaction between d_0 and d_{60}-{[CpCo(P=O(OEt)$_2$)$_3$]$_2$Tb}$^+$ Cl$^-$ (**2.5a**) in acetonitrile monitored by ESI MS

There does not appear to be a strong rate dependence on the phosphite substituent. The rate constants for the Et and Ph complexes of Tb, **2.5a** and **2.5b**, are essentially the same within experimental error in pure acetonitrile although **2.5a** is noticeably faster in 50:50 acetonitrile-water (*ca*. 2.7 times). This is not surprising if steric effects dominate the exchange process because the substituents are relatively far away from the metal center and the size differences between an Et and Ph group are not that extreme. On the other hand, Kläui and coworkers have found that changing from Et to Ph causes a change from a dimeric $[CpCo(P{=}O(OEt)_2)_3]_2Rh_2(CO)_3$ to a monomeric $[CpCo(P{=}O(OPh)_2)_3]Rh(CO)_2$.[47, 48]

2.3 Second generation Kläui Ligands.

In order to use the Kläui ligand as paraCEST contrast agent, we needed to decrease the exchange rate, increase the water solubility, and incorporate a moiety with a secondary source of exchangeable protons. To accomplish this we attempted to install chelating groups on the phosphite arms of the Kläui ligand to decrease the exchange rate.[4] These groups should also promote hydrogen bonding to increase the hydrophilicity of the complexes, as well as function as a new source of exchangeable protons for the CEST mechanism.

Using the knowledge gathered from the first generation of Kläui ligands, we decided to pursue two types of second generation ligands, one based on the $CpCo(P{=}O(OPh)_2)_3]^-Na^+$, **2.1b** and one based on $CpCo(P{=}O(OEt)_2)_3]^-Na^+$, **2.1a**, **Figure 2.11**. Incorporation of a carboxylic acid on the ortho position of diphenyl phosphite could have potentially allowed for a nine coordinate Kläui ligand **2.8**. The other option we thought possible was to incorporate an amine at then end of an alkyl chain (dialkyl phosphite). Ideally, if the chain is the correct length, the amine should chelate onto the lanthanide again, giving a potential nine coordinate ligand, **2.9**. Both methods had unique disadvantages. If the binding pocket is too small for the diphenyl phosphite analogue (**2.8**) no enhanced chelation would be seen. If the alkyl chain in the amine derivative (**2.9**) was too long it could potentially cause oligomerization or act as a tether and increase the ligand exchange rate, if in fact it is an associative type mechanism. Using these groups to

increase chelation had other advantages; they both provided a large secondary pool of exchangeable protons (O**H** on acid, N**H₂** on amine) for the CEST mechanism and both promoted hydrogen bond formation that should aid in water solubility (depending on the protonation state).

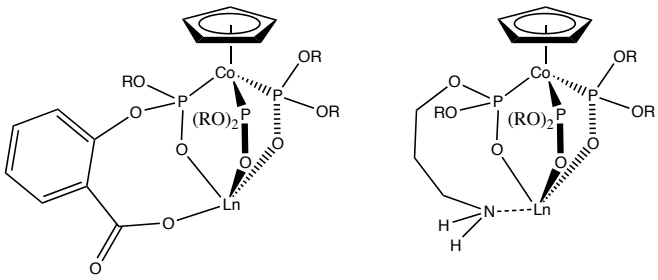

2.8 Ln **2.9 Ln**

Figure 2.11: Proposed conformations of second generation Kläui Ln complexes based a carboxylic acid (**2.8 Ln)** and an amine derivative (**2.9 Ln**)

Primary amines are known to react with phosphorous trichloride[49] requiring protection of the amine before synthesizing the phosphite. The BOC protecting group was originally chosen as it is simple to install and its removal results in carbon dioxide and isobutene, both of which are volatile. Unfortunately, the presence of strong acid (the HCl generated during phosphite synthesis) resulted in premature cleavage of the BOC group leading to very poor yields of **2.10, Scheme 2.3**. Nonetheless, synthesis of the Kläui ligand **2.11** was attempted with the isolated phosphite but failed to yield any promising results (**Scheme 2.3 A**). In order to combat early cleavage, an acid-stable protecting group, phthalimide, was used in place of BOC to generate **2.12**. Using a tertiary amine (as opposed to a secondary amine) did not seem to affect the formation of Kläui ligand **2.13**, **Scheme 2.3 A'**, however, the conditions required to remove the phthalimide were too harsh and resulted in ligand decomposition during the deprotection.

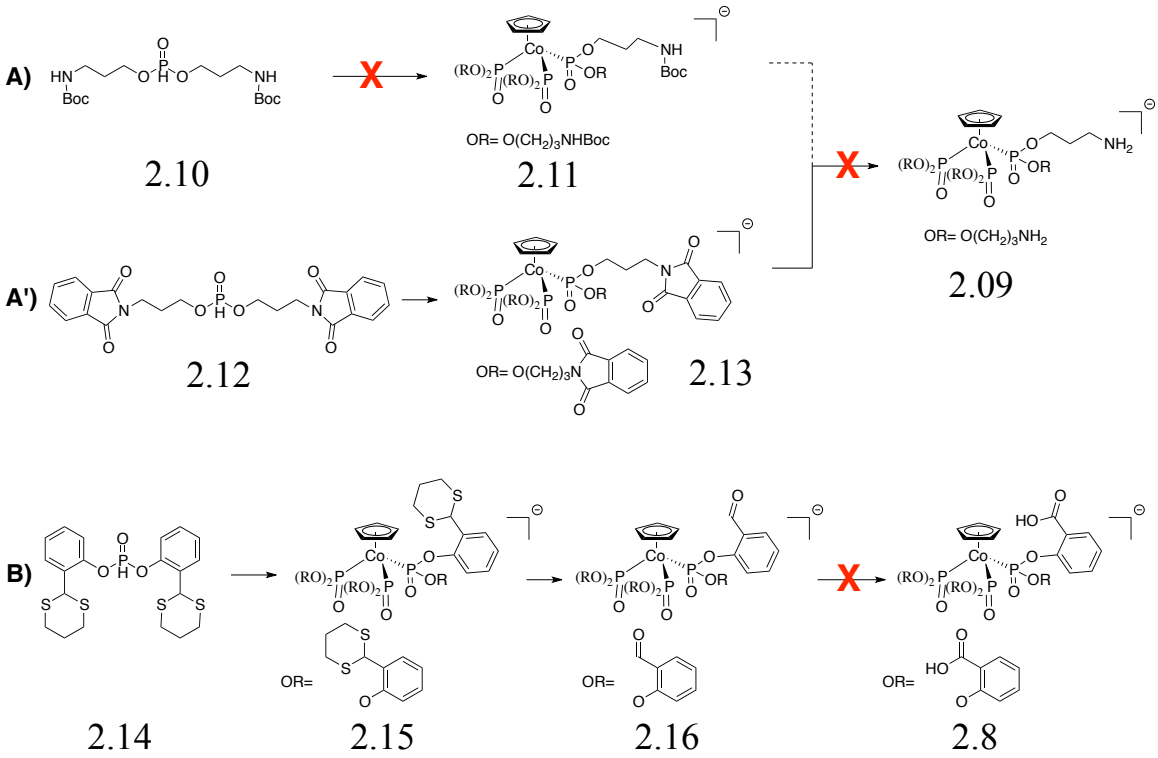

Scheme 2.3: Proposed pathway to new Kläui ligands

Unable to access the Kläui ligand with a terminal amine group we focused on incorporation of a carboxylic acid moiety. Much like before, the phosphite could not be made in the presence of a carboxylic acid so a dithiane-functionalized aromatic ring was incorporated to form phosphite **2.14** in the hope of accessing the acid through functional group manipulation, **Scheme 2.3 B**. Formation of the dithiane functionalized Kläui ligand **2.15**, as well as conversion to the aldehyde functionalized Kläui ligand **2.16,** proceeded straightforwardly**.** Unfortunately, all attempts to oxidize the aldehyde to the carboxylic acid functionalized Kläui ligand **2.8** resulted in either no change or complete ligand decomposition.

In order to incorporate chelating functionality into the Kläui ligand the functional groups needed to first be protected due to the synthetic route used for ligand formation. From the information gathered it would seem that the somewhat harsh conditions in forming the Kläui ligand or its precursors required robust protecting groups as the easily removable groups fall off during ligand synthesis. Using more robust protecting groups

allowed for formation of Kläui ligands; however, deprotection to give the desired chelating functionality (as well as a secondary pool of protons) proved to be too harsh for the ligand structure resulting in decomposition. Due to this dichotomy, coupled with the unpublished, confidential, toxicity data obtained by PNNL, we decided to abandon this ligand class in search of a more easily tunable ligand.

2.4 Concluding remarks.

We have shown that the complexes $\{[CpCo(P=O(OR)_2)_3]_2Ln\}^+ Cl^-$ (R = Et, Ph) are isolated as salts with good solubility in acetonitrile and limited solubility in water. Intramolecular ligand exchange was followed by ESI MS using the d_0 and d_{60}-isotopomers of the cation. The kinetic results are consistent with an associative process. The rate of exchange increases rapidly with increasing lanthanide ionic radius and water content but the phosphite substituents have comparatively little effect. The rate of ligand exchange is sufficiently high that lanthanide complexes of the simple $[CpCo(P=O(OR)_2)_3]^-$ ligands are not likely to be suitable for medical uses. We attempted to incorporate chelating functionality into the phosphite groups to lower the ligand exchange rate to an acceptable level, especially for complexes of the later lanthanides. However, the desired modification to the phosphite arms prevented Kläui ligand formation. These setbacks caused us to revaluate the Kläui ligand. Originally touted as "easily modifiable", this seems only to be the case if non-functionalized alkyl chains or a very limited variety of substituted aromatic rings are incorporated on the phosphite arms. Accepting this, it was decided that a new ligand design was needed for a novel contrast agent. In subsequent chapters we will explore several very different ligand scaffolds on which to build a MR contrast agent.

2.5 Experimental.

All experiments were performed under an inert argon atmosphere using standard glovebox (Braun MB150-GII) or Schlenk techniques in flame-dried glassware unless otherwise noted. THF and diethyl ether were freshly distilled from sodium/benzophenone before use; dichloromethane was distilled from calcium hydride unless stated otherwise. $CpCo(I)_2CO$ was synthesized from commercially available (Aldrich) $CpCo(CO)_2$ according to literature procedure.[50] The deuterated phosphites d_{10}-diethylphosphite and d_{10}-diphenylphosphite were prepared from PCl_3 in two steps: initial reaction of PCl_3 with *t*-butanol (1 equiv) followed by addition of commercially available d_6-ethanol or d_6-phenol (2 equiv) by a modification of a literature procedure as described below.[51] Acetonitrile for ESI MS studies was HPLC grade. All other chemicals were purchased from Sigma-Aldrich and used as is. Spectra for NMR spectroscopy were recorded on Bruker AMX-300MHz or 360MHz NMR spectrometers. FT-IR spectra were recorded on a Perkin Elmer Spectrum 1000 FT-IR spectrometer. An Omega Engineering Model 199 melting point apparatus was used for melting point data and melting points are not corrected. Kinetic +ESI-MS data was collected on a Q-TOF II spectrometer by MicroMass. Calculated and observed isotope patterns for ligands, and metal complexes are provided in the appendix.

2.5.1 Synthesis

$O=P(H)(OC_2D_5)_2$ Anhydrous t-butanol (3.5 g, 48 mmol) was dissolved in dichloromethane (10 mL) and the mixture was added to freshly distilled PCl_3 (6.59 g, 48.0 mmol) dissolved in dichloromethane (50 mL) at 0 °C. The solution was stirred 1 h, then allowed to warm to room temperature and deuterated ethanol (5.0 g, 96 mmol) was added dropwise over 0.5 h. This solution was stirred for 1.5 h at room temperature and then refluxed for 18 h. Removal of the solvent under reduced pressure and vacuum distillation afforded pure deuterated diethylphosphite as a clear and colourless oil. Yield: 5.3 g (75%). ^{1}H NMR ($CDCl_3$, 300 MHz, 22°C): δ 6.79 (d, 1H, $^1J_{PH}$ = 694 Hz). $^{31}P\{^1H\}$ NMR (121.5 MHz): δ 6.4 s.

$O=P(H)(OC_6D_5)_2$ Anhydrous t-butanol (1.85 g, 25.0 mmol) dissolved in 10 mL dichloromethane was added to freshly distilled PCl_3 (3.43 g, 25.0 mmol) dissolved in dichloromethane (30 mL) at 0 °C. The solution was stirred for 1 h, then allowed to warm to room temperature. Deuterated phenol (5.0 g, 50 mmol) dissolved in dichloromethane (30 mL) was added dropwise over 0.5 h, the solution stirred for 1.5 h at room temperature and then refluxed for 18 h. Removal of the solvent under reduced pressure left a yellow oil containing up to 5% of the mono-aryl substituted phosphite as a contaminant. The crude product was re-dissolved in dichloromethane (30 mL) and ammonia was bubbled through the solution for 10 min resulting in a milky white suspension. Filtration through Celite® and removal of the solvent under reduced pressure afforded pure deuterated diphenylphosphite as a clear colourless oil. Yield: 5.43 g (89%). ^{1}H NMR (CD_2Cl_2, 300 MHz, 22°C): δ 7.34 (d, 1H, $^1J_{PH}$ = 732 Hz). $^{31}P\{^1H\}$ NMR (CD_2Cl_2, 121.5 MHz): δ 0.9 s.

$[CpCo(P=O(OEt)_2)_3]^-$ Na^+, 2.1a Solid NaCN (0.95 g, 19 mmol) was added to a slurry of **2.2a** (3.57 g, 3.20 mmol), described below, in 30 mL methanol. The mixture was refluxed in air for 18 h, the solution cooled to room temperature, filtered through Celite® and washed with dichloromethane leaving behind insoluble $Na_3[Co(CN)_6]$. The filtrate was evaporated to dryness under reduced pressure and the residue was recrystallized from hot acetone to yield pure **2.1a**. Yield: 3.21 g (95%). Mp. 188-189 °C. IR (thin film, NaCl): 2974m, 2927w, 2894w, 1384w, 1161s, 1047s, 929s, 830w, 759m, 723m cm^{-1}. ^{1}H NMR ($CDCl_3$, 300 MHz, 22°C): δ 4.99 (s, 5H, C_5H_5), 3.98-3.89 (m, 12H, CH_2), 1.21 (t, $^3J_{HH}$ = 7.3 Hz, 18H, CH_3). $^{31}P\{^1H\}$ NMR ($CDCl_3$, 121.5 MHz): δ 105.8 s. $^{13}C\{^1H\}$($CDCl_3$, 75.5 MHz): δ 89.67 (s, C_5H_5), 58.64 (m, CH_2), 16.70 (s, CH_3).

[CpCo(P=O(OC$_2$D$_5$)$_2$)$_3$]$^-$ Na$^+$, *d$_{30}$*-2.1a The deuterated complex was prepared in the same manner as **2.1a** from NaCN and *d$_{60}$*-**2.2a**. Yield: 2.06 g (99%) Mp 188-190 °C. IR (thin film, NaCl): 2224m, 2144w, 2101w, 1426w, 1183s, 1163s, 1099m, 1061m, 1007s, 908w, 814m, 733w, 687m, 667m cm^{-1}. ^{1}H NMR ($CDCl_3$, 300 MHz, 22 °C) δ 4.96 (s, C$_5$*H$_5$*). ^{2}H NMR ($CHCl_3$, 55.3 MHz): δ 3.9 (s, 12D, C*D$_2$*), 5.5 (s, 18D, C*D$_3$*). ^{31}P{^{1}H} NMR ($CDCl_3$, 121.5 MHz): δ 105.6 s. ^{13}C{^{1}H} NMR ($CDCl_3$, 75.5 MHz): δ 89.60 (s, *C$_5$*H$_5$), 57.74 (quin, $^1J_{CD}$ = 21 Hz, *C*D$_2$), 15.62 (sept, $^1J_{CD}$ = 20 Hz, *C*D$_3$).

[CpCo(P=O(OPh)$_2$)$_3$]$^-$ Na$^+$, 2.1b A solution of diphenylphosphite (7.65 g, 32.7 mmol) in freshly distilled THF (100 mL) was added dropwise to a slurry of NaH (0.98 g, 60% dispersion in mineral oil, 24 mmol) in THF (60 mL) at 0 °C. This suspension was stirred for 0.5 h at 0 °C and then allowed to warm to room temperature. $CpCo(I)_2CO$ (1.70 g, 4.19 mmol) dissolved in THF (50 mL) was then added dropwise over 1 h resulting in an orange solution. The orange solution was allowed to stir for 1 h and then refluxed for 18 h. After cooling to room temperature, a small amount of water was added to quench the reaction and the solvent was removed under reduced pressure leaving an orange solid. The orange residue was dispersed in hexanes, filtered and the solid washed with water (50 mL), followed by cold methanol (50 mL) to leave crude **2.1b** as a yellow powder. ^{1}H NMR revealed ~5% impurity consistent with the presence of $[CpCo(P{=}O(OPh)_2)_3]_2Co$, **2.2b**. To remove this impurity, the crude product was dissolved in a mixture of toluene (50 mL) and methanol (10 mL) containing NaCN (0.05 g) and the mixture was refluxed in air overnight. After filtration through Celite® to remove any unreacted NaCN and insoluble $Na_3[Co(CN)_6]$, pure **2.1b** was recovered as a yellow solid. Yield: 3.37 g (73%). Mp. 302 °C (dec). IR(thin film, NaCl): 3065w, 1591s, 1489s, 1213s, 1193m, 1157w, 1068w, 1023w 872s, 763w, 690m cm^{-1}. ^{1}H NMR ($CDCl_3$, 300 MHz, 22 °C) δ 6.85-6.77 (m, 30H, aryl*H*), 5.59 (s, 5H, C$_5$*H$_5$*). ^{31}P{^{1}H} NMR ($CDCl_3$, 121.5 MHz): δ 103.2 s. ^{13}C{^{1}H} NMR ($CDCl_3$, 75.5 MHz): δ 152.69 (m, *ipso*-aryl*),* 128.78 (s, *m*-aryl), 122.99 (s, *p*-aryl), 121.90 (s, *o*-aryl), 90.72 (s, *C$_5$*H$_5$).

[CpCo(P=O(OC$_6$D$_5$)$_2$)$_3$]$^-$ Na$^+$, *d$_{30}$*-2.b The same procedure was used to prepare *d$_{30}$*-**2.1b** as that used to prepare **2.1b** except that *d$_{10}$*-diphenylphosphite was used in place of diphenylphosphite. Yield: 1.13 g (46%). Mp. 311 °C (dec). IR (thin film, NaCl): 2276w, 1557s, 1375s, 1204m, 1156s, 1140s, 962w, 889m, 847m, 799s, 772w, 680w cm^{-1}. ^{1}H NMR (CDCl$_3$, 300 MHz, 22 °C): δ 5.59 (s, C$_5$*H$_5$*). ^{2}H (CHCl$_3$, 55.3 MHz): δ 7.0 (s, br, 30D, aryl*D*). ^{31}P{^{1}H} NMR (CDCl$_3$, 121.5 MHz): δ 102.5 s. ^{13}C{^{1}H} NMR (CDCl$_3$, 75.5 MHz): δ 152.65 (m, *ipso*-aryl*),* 128.78 (t, $^1J_{CD}$ = 22 Hz, *m*-aryl), 122.51 (t, $^1J_{CD}$ = 20 Hz, *p*-aryl), 121.56 (t, $^1J_{CD}$ = 22 Hz, *o*-aryl), 90.72 (s, *C$_5$*H$_5$**).**

[CpCo(P=O(OEt)$_2$)$_3$]$_2$Co, 2.2a Freshly sublimed cobaltocene (2.30 g, 12.2 mmol) was added to a Schlenk tube under an inert atmosphere and diethylphosphite (4.66 mL, 36.2 mmol) was injected by syringe. The resulting mixture was heated at 130 °C for 18 h, cooled to room temperature and diluted with 25 mL of methanol. After stirring for 0.5 h, the suspension was filtered to isolate **2.2a** as a pale yellow solid. Yield: 3.57 g (78%). Mp. 254-257 °C. IR (thin film, NaCl): 2973m, 2920w, 2892w, 1422w, 1385m, 1263s, 1126s, 1039s, 922s, 833w, 748m, 719m cm^{-1}. ^{1}H NMR (CDCl$_3$, 360 MHz, 22 °C): δ 33.84 (s, 10H, C$_5$*H$_5$*, $\nu_{½}$ = 21 Hz), -12.09 (s, 36H, CH$_3$, $\nu_{½}$ = 21 Hz), -23.00 (s, 12H, C*H$_A$*H$_B$, $\nu_{½}$ = 71 Hz), -29.43 (s, 12H, CH$_A$*H$_B$*, $\nu_{½}$ = 103 Hz).

[CpCo(P=O(OC$_2$D$_5$)$_2$)$_3$]$_2$Co, *d$_{60}$*-2.2a The deuterated complex was prepared by the same procedure as for **2.2a** but with *d$_{10}$*-diethylphosphite substituted for diethylphosphite. Yield: 2.19 g (74%). Mp. 239-241 °C. IR(thin film, NaCl): 2224m, 2143w, 2101w, 1422w, 1265s, 1177s, 1135s, 1090s, 1060m, 1008s, 906w, 821m, 739s, 690w, 671w cm^{-1}. ^{1}H NMR (CDCl$_3$, 300 MHz, 22 °C): δ 33.78 (s, 10H, C$_5$*H$_5$*, $\nu_{½}$ = 20 Hz). ^{2}H NMR (CHCl$_3$, 55.3 MHz): δ -11.9 (s, 36H, C*H$_3$*, $\nu_{½}$ = 7 Hz), -22.3 (s, 12H, C*H$_A$*H$_B$, $\nu_{½}$ = 13 Hz), -28.8 (s, 12H, CH$_A$*H$_B$*, $\nu_{½}$ = 12 Hz).

{[CpCo(P=O(OEt)$_2$)$_3$]$_2$Nd}$^+$ Cl$^-$, 2.3a The ligand salt **2.1a** (0.40 g, 0.72 mmol) and $NdCl_3(H_2O)_7$ (0.139 g, 0.36 mmol) were stirred in 20 mL reagent grade THF in air for 18 h. The solution was filtered through Celite® and the solvent was removed to leave a yellow solid. The solid was re-dissolved in dichloromethane, filtered through Celite® once more and the filtrate evaporated to dryness. The residue was re-dissolved in a minimum of dichloromethane and precipitated with hexanes to afford **2.3a** as a yellow solid. Yield: 0.23 g (90%). Mp. 188-190 °C. IR(thin film, NaCl): 2976m, 2927w, 2898w, 1385w, 1125s, 1041s, 933s, 832w, 769w, 727w cm^{-1}. ^{1}H NMR ($CDCl_3$, 300 MHz, 22 °C): δ 10.40 (s, 10H, C_5H_5, $\nu_{½}$ = 8 Hz), 2.05 (s, CH_AH_B, $\nu_{½}$ = 29 Hz), 1.79 (s, 12H, CH_AH_B, $\nu_{½}$ = 28 Hz), -0.15 (s, 36H, CH_3, $\nu_{½}$ = 18 Hz), -2.54 (s, ~12equiv H_2O, $\nu_{½}$ = 19 Hz). ^{31}P{^{1}H} NMR ($CDCl_3$, 121.5 MHz): δ -189.4 (s, $\nu_{½}$ = 72 Hz).

{[CpCo(P=O(OC$_2$D$_5$)$_2$)$_3$]$_2$Nd}$^+$ Cl$^-$, *d$_{60}$*-2.3a The deuterated complex was prepared according to the same procedure as **2.3a** using *d$_{30}$*-**2.1a** instead of **2.1a**. Yield: 0.102 g (84%). Mp. 177-178 °C. IR (thin film, NaCl): 2226s, 2143m, 2102m, 1425w, 1187s, 1133s, 1086s, 1059s, 1008s, 928m, 829s, 731w, 683m, 673m cm^{-1}. ^{1}H NMR ($CDCl_3$, 300 MHz, 22°C): δ 10.44 (s, C_5H_5, $\nu_{½}$ = 7 Hz), -10.53 (s, ~4 equiv H_2O, $\nu_{½}$ = 51 Hz). ^{2}H NMR ($CHCl_3$, 55.3 MHz): δ 2.06 (s, 12D, CD_AD_B, $\nu_{½}$ = 4 Hz), 1.74 (s, 12D, CD_AD_B, $\nu_{½}$ = 5 Hz), -0.15 (s, 36D, CD_3, $\nu_{½}$ = 3 Hz). ^{31}P{^{1}H} NMR ($CDCl_3$, 121.5 MHz): δ -189.3 (s, $\nu_{½}$ = 66 Hz).

{[CpCo(P=O(OPh)$_2$)$_3$]$_2$Nd}$^+$ Cl$^-$, 2.3b Complex **2.3b** was prepared as a yellow solid using the same procedure as **2.3a** but starting from **2.1b** and $NdCl_3(H_2O)_7$. Yield: 0.356 g (91%). Mp. 291 °C (dec). IR (thin film, NaCl): 3065w, 1589s, 1488s, 1208s, 1183m, 1163m, 1134s, 1071w, 1024w, 910s, 888s, 847w, 757m, 689m cm^{-1}. ^{1}H NMR ($CDCl_3$, 300 MHz, 22 °C): δ 10.48 (s, 10H, C_5H_5, $\nu_{½}$ = 8 Hz), 5.38 (s, 12H, *p*-aryl*H*, $\nu_{½}$ = 9 Hz), 4.88 (s, 24H, *o/m*-aryl*H*, $\nu_{½}$ = 21 Hz), 3.96 (s, 24H, *o/m*-aryl*H*, $\nu_{½}$ = 20 Hz), -3.99 (s, 7 equiv H_2O, $\nu_{½}$ = 45 Hz). ^{31}P{^{1}H} NMR ($CDCl_3$, 121.5 MHz): δ 195.4 (s, $\nu_{½}$ = 55 Hz).

{[CpCo(P=O(OC$_6$D$_5$)$_2$)$_3$]$_2$Nd}$^+$ Cl$^-$, *d$_{60}$*-2.3b The deuterated complex was prepared according to the same procedure as **2.3a** using *d$_{30}$*-**2.1b** instead of **2.1a**. Yield: 0.091 g (85%). Mp. 285 °C (dec). IR (thin film, NaCl): 2277w, 1556s, 1372s, 1155s, 1132s, 964w, 898s, 853m, 804s, 770w, 703w cm^{-1}. ^{1}H NMR (CDCl$_3$, 300 MHz, 22 °C): δ 10.61 (s, C$_5$*H$_5$*, ν$_{½}$ = 8 Hz), -7.62 (s, 4 equiv H$_2$O, ν$_{½}$ = 143 Hz). ^{31}P{^{1}H} NMR (CDCl$_3$, 121.5 MHz): δ 194.7 (s, ν$_{½}$ = 56 Hz).

{[CpCo(P=O(OEt)$_2$)$_3$]$_2$Eu}$^+$ Cl$^-$, 2.4a Complex **2.4a** was isolated as a yellow solid using the same procedure as **2.3a** starting from **2.1a** and EuCl$_3$(H$_2$O)$_6$. Yield: 0.21 g (82%). Mp. 158-160 °C. IR (thin film, NaCl): 2976m, 2927w, 2899w, 1386w, 1125s 1040s, 934s, 832w, 770w, 727w cm^{-1}. ^{1}H NMR (CDCl$_3$, 300 MHz, 22 °C): δ 5.95 (s, 12H, C*H$_A$*H$_B$, ν$_{½}$ = 24 Hz), 5.64 (s, 12H, CH$_A$*H$_B$*, ν$_{½}$ = 26 Hz), 2.96 (s, ~30 equiv H$_2$O, ν$_{½}$ = 10 Hz), 2.45 (s, 36H, C*H$_3$*, ν$_{½}$ = 13 Hz), 0.72 (s, 10H, C$_5$*H$_5$*, ν$_{½}$ = 10 Hz). ^{31}P{^{1}H} NMR (121.5 MHz): δ -12.7 (s, ν$_{½}$ = 51 Hz).

{[CpCo(P=O(OC$_2$D$_5$)$_2$)$_3$]$_2$Eu}$^+$ Cl$^-$, *d$_{60}$*-2.4a Complex *d$_{60}$*-**2.4a** was prepared using the same procedure as **2.3a** starting from *d$_{30}$*-**2.1a** and EuCl$_3$(H$_2$O)$_6$. Yield: 0.091 g (74%). Mp. 161-162 °C. IR (thin film, NaCl): 2226m, 2144w, 2103w, 1424w, 1187s, 1136s, 1088s, 1060s, 1010s, 829s, 732w, 693m, 674m cm^{-1}. ^{1}H NMR (CDCl$_3$, 300 MHz, 22 °C): δ 6.05 (s, ~9 equiv H$_2$O, ν$_{½}$ = 20 Hz), 0.73(s, C$_5$*H$_5$*, ν$_{½}$ = 7 Hz). ^{2}H NMR (CHCl$_3$, 55.3 MHz): δ 5.97 (s, 12D, C*D$_A$*D$_B$, ν$_{½}$ = 5 Hz), 5.62 (s, 12D, CD$_A$*D$_B$*, ν$_{½}$ = 5 Hz), 2.42 (s, 36D, C*D$_3$*, ν$_{½}$ = 3 Hz). ^{31}P{^{1}H} NMR (121.5 MHz): δ -12.3 (s, ν$_{½}$ = 65 Hz).

{[CpCo(P=O(OEt)$_2$)$_3$]$_2$Tb}$^+$ Cl$^-$, 2.5a Complex **2.5a** was prepared as a yellow solid using the same procedure as **2.3a** starting from **2.1a** and TbCl$_3$(H$_2$O)$_6$. Yield: 0.19 g (73%). Mp. 145-147 °C. IR (thin film, NaCl): 2976m, 2927w, 2899w, 1386w, 1128s, 1042s, 935s, 834w, 770w, 729w cm^{-1}. ^{1}H NMR (CDCl$_3$, 300 MHz, 22°C): δ 146.8 (s, 10H, C$_5$*H$_5$*, ν$_{½}$ = 150 Hz), -40.4 (s, 36H, C*H$_3$*, ν$_{½}$ = 124 Hz), -58.5 (s, 12H, C*H$_A$*H$_B$, ν$_{½}$ = 418 Hz), -66.8 (s, 12H, CH$_A$*H$_B$*, ν$_{½}$ = 410 Hz), -125.4 (s, ~2 equiv H$_2$O, ν$_{½}$ = 1527 Hz).

{[CpCo(P=O(OC$_2$D$_5$)$_2$)$_3$]$_2$Tb}$^+$ Cl$^-$, *d$_{60}$*-2.5a Complex *d$_{60}$*-**2.5a** was prepared using the same procedure as **2.3a** starting from *d$_{30}$*-**2.1a** and $TbCl_3(H_2O)_6$. Yield: 0.10 g (81%). Mp. 130-131 °C. IR (thin film, NaCl): 2225s, 2144m, 2102m, 1425w, 1186s, 1136s, 1089m, 1060m, 1008s, 928m, 829m, 731w, 692m, 673m cm^{-1}. ^{1}H NMR ($CDCl_3$, 300 MHz, 22 °C): δ 141.4 (s, C$_5$*H$_5$*, $\nu_{½}$ = 1800 Hz), -84.7 (s, ~2equiv H_2O, $\nu_{½}$ = 1354 Hz).

{[CpCo(P=O(OPh)$_2$)$_3$]$_2$Tb}$^+$ Cl$^-$, 2.5b Complex **2.5b** was prepared as a yellow solid using the same procedure as **2.3b** starting from **2.1b** and $TbCl_3(H_2O)_6$. Yield: 0.083 g (85%). Mp. 281 °C (dec). IR(thin film, NaCl): 3039w, 1590s, 1488s 1207s, 1185m, 1163m, 1138s, 1111m, 1024w, 913s, 893s, 844w, 763m, 729m, 690m cm^{-1}. ^{1}H NMR ($CDCl_3$, 300MHz, 22 °C): δ 180.4 (s, 10H, C$_5$*H$_5$*, $\nu_{½}$ = 841 Hz), -44.5 (s, 12H, *p*-aryl*H*, $\nu_{½}$ = 153 Hz), -62.6 (s, 24H, *o/m*-aryl*H*, $\nu_{½}$ = 242 Hz), -112.6 (s, 24H, *o/m*-aryl*H*, $\nu_{½}$ = 1174 Hz).

{[CpCo(P=O(OC$_6$D$_5$)$_2$)$_3$]$_2$Tb}$^+$ Cl$^-$, *d$_{60}$*-2.5b Complex *d$_{60}$*-**2.5b** was prepared using the same procedure as **2.3b** starting from *d$_{30}$*-**2.1b** and $TbCl_3(H_2O)_6$. Yield: 0.067 g (68%). Mp. 284 °C (dec). IR (thin film, NaCl): 2277w, 1557m, 1373s, 1155s, 1136s, 963w, 898s, 853m, 805s, 771w cm^{-1}. ^{1}H NMR ($CDCl_3$, 300 MHz, 22°C): δ 174 (s, C$_5$*H$_5$*, $\nu_{½}$ = 2243 Hz).

{[CpCo(P=O(OEt)$_2$)$_3$]$_2$Yb}$^+$ Cl$^-$, 2.6a Complex **2.6a** was prepared as a yellow solid using the same procedure as **2.3a** starting from **2.1a** and $YbCl_3(H_2O)_6$. Yield: 0.382 g (83%). Mp. 190-191 °C. IR (thin film, NaCl): 2977m, 2928w, 2899w, 1387w, 1110s, 1038s, 937s, 835w, 772w, 728w cm^{-1}. ^{1}H NMR ($CDCl_3$, 300 MHz, 22°C): δ 9.81 (s, 24H, C*H$_2$*, $\nu_{½}$ = 42 Hz), 5.55 (s, 36H, C*H$_3$*, $\nu_{½}$ = 14 Hz), 4.06 (s, ~2 equiv H_2O, $\nu_{½}$ = 18 Hz), -4.79 (s, 10H, C$_5$*H$_5$*, $\nu_{½}$ = 7 Hz). ^{31}P{^{1}H} NMR (121.5 MHz): δ 67.7 (s, $\nu_{½}$ = 76 Hz).

{[CpCo(P=O(OC$_2$D$_5$)$_2$)$_3$]$_2$Yb}$^+$ Cl$^-$, *d$_{60}$*-2.6a Complex *d$_{60}$*-**2.6a** was prepared using the same procedure as **2.3a** starting from *d$_{30}$*-**2.1a** and $YbCl_3(H_2O)_6$. Yield: 0.174 g (76%). Mp. 199-200 °C. IR (thin film, NaCl): 2226m, 2143w, 2116w, 1423w, 1187w, 1123s, 1086m, 1055m, 1006s, 986s, 824w, 694w, 675w cm^{-1}. ^{1}H NMR ($CDCl_3$, 300 MHz, 22°C): δ 1.72 (s, ~8 equiv H_2O, $\nu_{½}$ = 7 Hz), -4.81 (s, C_5H_5, $\nu_{½}$ = 7 Hz). ^{2}H ($CHCl_3$, 55.3 MHz): δ 9.79 (s, 12D, CD_AD_B, $\nu_{½}$ = 5 Hz), 9.68 (s, 12D, CD_AD_B, $\nu_{½}$ = 5 Hz), 5.56 (s, 36D, CD_3, $\nu_{½}$ = 4 Hz). ^{31}P{^{1}H} NMR ($CDCl_3$, 121.5 MHz): δ 67.8 (s, $\nu_{½}$ = 71 Hz).

{[CpCo(P=O(OPh)$_2$)$_3$]$_2$Yb}$^+$ Cl$^-$, 2.6b Complex **2.6b** was prepared as a yellow solid using the same procedure as **2.3b** starting from **2.1b** and $YbCl_3(H_2O)_6$. Yield: 0.204 g (93%). Mp. 283 °C (dec). IR(thin film, NaCl): 3040w, 1590s, 1487s 1208s, 1185m, 1162m, 1081s, 1069m, 1024w, 913s, 888s, 847w, 770w, 757m, 689m cm^{-1}. ^{1}H NMR ($CDCl_3$, 300 MHz, 22°C): δ 15.72 (s, 24H, *o/m*-aryl*H*, $\nu_{½}$ = 20 Hz), 11.44 (s, 24H, *o/m*-aryl*H*, $\nu_{½}$ = 20 Hz), 10.30 (s, 12H, *p*-aryl*H*, $\nu_{½}$ = 14 Hz), 1.40 (s, ~9 equiv H_2O, $\nu_{½}$ = 9 Hz), -6.01 (s, 10H, C_5H_5, $\nu_{½}$ = 10 Hz). ^{31}P{^{1}H} NMR ($CDCl_3$, 121.5 MHz): δ 48.4 (s, $\nu_{½}$ = 51 Hz).

{[CpCo(P=O(OC$_6$D$_5$)$_2$)$_3$]$_2$Yb}$^+$ Cl$^-$, *d$_{60}$*-2.6b Complex *d$_{60}$*-**2.6b** was prepared using the same procedure as **2.3b** starting from *d$_{30}$*-**2.1b** and $YbCl_3(H_2O)_6$. Yield: 0.096 g (88%). Mp. 278 °C (dec). IR (thin film, NaCl): 2273w, 1556m, 1370s, 1155m, 1129m, 1080s, 960w, 905s, 856w, 807m, 770w cm^{-1}. ^{1}H NMR ($CDCl_3$, 300 MHz, 22°C): δ -5.91 (s, C_5H_5, $\nu_{½}$ = 7 Hz), 1.48 (s, ~9 equiv H_2O, $\nu_{½}$ = 10 Hz). ^{31}P{^{1}H} NMR ($CDCl_3$, 121.5 MHz): δ 47.6 (s, $\nu_{½}$ = 42 Hz).

{[CpCo(P=O(OPh)$_2$)$_3$]$_2$Yb}$^+$ {CoCl$_3$(THF)}$^-$ • 2 C$_6$H$_6$, 2.7 Complex **2.7** was isolated as a teal green crystalline solid in yields ranging from 10-65% in various trials as a byproduct in the synthesis of **2.6b** from **2.1b** and $YbCl_3(H_2O)_6$. Recrystallization of green **2.7** from acetone containing NaCl results in isolation of yellow **2.6b** in quantitative yield. Mp. 218-222 °C. IR (thin film, KBr): 2980w, 2929w, 1719w, 1590m, 1488s, 1454w, 1423w, 1204s, 1162m, 1081m, 1024m, 914s, 889s, 766m, 689m

cm^{-1}. ^1H NMR ($CDCl_3$, 300 MHz, 22 °C): δ 12.49 (s, 24H, *o/m*-aryl*H*), 10.55 (s, 24H, *o/m*-aryl*H*), 9.62 (s, 12H, *p*-aryl*H*), -3.09 (s, 10H, C_5H_5). MS (+LSIMS): 1820.1 amu.

$O=P(H)(OC_3H_6NHBOC)_2$, 2.10 The same procedure was used to prepare **2.10** as that used to prepare **$O=P(H)(OC_2D_5)_2$** except that HOC_3H_6NHBOC was used in place of HOC_2D_5. Complex **2.10** was isolated as a clear, colourless oil using the same procedure as **$O=P(H)(OC_6D_5)_2$** starting from HOC_3H_6NHBoc. Yield: 0.11 g (12%). ^1H NMR ($CDCl_3$, 300 MHz, 22°C): δ 6.81 (d, 1H, $^1J_{PH}$ = 699 Hz), 4.11 (dt, $^3J_{HH}$ = 6.0 Hz, $^3J_{HP}$ = 8.6 Hz, 4H, -CH_2CH_2OP-), 3.22 (t, $^3J_{HH}$ = 6.4Hz, 4H, BocNHCH_2CH_2-), 1.85 (p, $^3J_{HH}$ = 6.2 Hz, 4H, -$CH_2CH_2CH_2$-), 1.40 (s, 18H, $(CH_3)_3$). $^{31}P\{^1H\}$ NMR (121.5 MHz): δ 10.7 s.

$O=P(H)(OC_3H_6NHPhth)_2$, 2.12 The same procedure was used to prepare **2.12** as that used to prepare **$O=P(H)(OC_2D_5)_2$** except that $HOC_3H_6NHPhth$ was used in place of HOC_2D_5. Complex **2.12** was isolated as a white powder using the same procedure as **$O=P(H)(OC_6D_5)_2$** starting from $HOC_3H_6NHPhth$. Yield: 16.1 g (72%). ^1H NMR ($CDCl_3$, 300 MHz, 22°C): δ 6.84 (d, 1H, $^1J_{PH}$ = 700 Hz), 7.86-7.71 (m, 4H, Phth), 7.76-7.69 (m, 4H, Phth), 4.11 (dt, $^3J_{HH}$ = 6.2 Hz, $^3J_{HP}$ = 7.6 Hz, 4H, -CH_2CH_2OP-), 3.79 (t, $^3J_{HH}$ = 6.8 Hz, 4H, PhthNHCH_2CH_2-), 2.06 (p, $^3J_{HH}$ = 6.5 Hz, 4H, -$CH_2CH_2CH_2$-). $^{31}P\{^1H\}$ NMR (121.5 MHz): δ 8.5 s.

$[CpCo(P=O(OC_3H_6NHPhth)_2)_3]^-$ Na^+, 2.13 The same procedure was used to prepare **2.13** as that used to prepare **2.1b** except that **2.12** was used in place of diphenylphosphite. **2.13** was recovered as a yellow solid. Yield: 1.6 g (36%). Mp. 295 °C (dec). ^1H NMR ($CDCl_3$, 300 MHz, 22°C) δ 7.69-7.49 (m, 24H, Phth), 5.12 (s, 5H, C_5H_5), 3.96 (m, 12H, -CH_2CH_2OP-), 3.71 (m, 12H, PhthNHCH_2CH_2-), 1.86 (m, 12H, -$CH_2CH_2CH_2$-) $^{31}P\{^1H\}$ NMR ($CDCl_3$, 121.5 MHz): δ 107.50 s. $^{13}C\{^1H\}$ NMR ($CDCl_3$, 75.5 MHz): δ 168.78, 134.23, 132.77, 123.41, 90.16, 61.20, 36.03, 30.85.

$O=P(H)(OC_{10}H_{11}S_2)_2$, 2.14 The same procedure was used to prepare **2.14** as that used to prepare **$O=P(H)(OC_2D_5)_2$** except that $HOC_{10}H_{11}S_2$ was used in place of HOC_2D_5. Complex **2.14** was isolated as an off white powder using the same procedure as

O=P(H)(OC$_6$D$_5$)$_2$ starting from $HOC_{10}H_{11}S_2$. Yield: 10.4 g (91%). ^{1}H NMR (CD_2Cl_2, 300 MHz, 22 °C): δ 7.60 (d, 1H, $^1J_{PH}$ = 741 Hz), 7.68 (d, 2H, $^1J_{PH}$ = 7.5 Hz), 7.42-7.25 (m, 6H), 5.48 (s, 2H), 3.03-2.79 (m, 8H), 2.19-2.09 (m, 2H), 1.94-1.78 (m, 2H). $^{31}P\{^1H\}$ NMR (CD_2Cl_2, 121.5 MHz): δ 1.5 s.

[CpCo(P=O(OC$_{10}$H$_{11}$S$_2$)$_2$)$_3$]$^-$ Na$^+$, 2.15 The same procedure was used to prepare **2.15** as that used to prepare **2.1b** except that **2.14** was used in place of diphenylphosphite. **2.15** was recovered as a yellow solid. Yield: 0.172 g (78%). Mp. 286 °C (dec). ^{1}H NMR ($CDCl_3$, 300 MHz, 22 °C) δ 7.42 (d, 6H, $^3J_{HH}$ = 7.9 Hz), 7.34 (d, 6H, $^3J_{HH}$ = 8.5 Hz, 6.84 (t, 6H, $^3J_{HH}$ = 7.6 Hz), 6.57 (d, 6H, $^3J_{HH}$ = 7.9 Hz), 6.11 (s, 5H, C_5H_5), 4.96 (s, 6H), 2.89-2.42 (m, 24H), 2.00-1.87(m, 6H), 1.75-1.57 (m, 6H). $^{31}P\{^1H\}$ NMR ($CDCl_3$, 121.5 MHz): δ 106.68 s. $^{13}C\{^1H\}$ NMR ($CDCl_3$, 75.5 MHz): δ 148.27, 127.60, 126.14, 125.46, 121.19, 117.55, 89.47, 42.60, 29.39, 29.08, 22.51.

[CpCo(P=O(O$_2$C$_7$H$_5$)$_2$)$_3$]$^-$ Na$^+$, 2.16 12 equiv (0.31 g, 1.4 mmol) of HgO was added to a solution of THF/H_2O (15% *v/v,* 20 mL), that was purged with Ar. 12 equiv (1.4 mmol, 0.18 mL) BF_3 etherate was then added and stirred for 0.5 h. 0.182 g (0.119 mmol) of **2.15** was then added, and the solution was refluxed under Ar for 4 h. The solution was then filtered and the solvent was removed under reduced pressure to yield a yellow solid. This solid was re-dissolved in CH_2Cl_2 and filtered again. The solvent was again removed under reduced pressure and **2.16** was recovered as a yellow solid. Yield: 0.035 g (30%). Mp. 292 °C (dec). ^{1}H NMR ($CDCl_3$, 300 MHz, 22°C) δ 10.04 (s, 5H), 7.46 (d, 6H, $^3J_{HH}$ = 7.5 Hz), 7.32 (d, 6H, $^3J_{HH}$ = 8.3 Hz, 6.97 (t, 6H, $^3J_{HH}$ = 7.7 Hz), 6.88 (d, 6H, $^3J_{HH}$ = 7.3 Hz), 6.13 (s, 5H, C_5H_5). $^{31}P\{^1H\}$ NMR ($CDCl_3$, 121.5 MHz): δ 112.58 s. DEPT45 $^{13}C\{^1H\}$ NMR ($CDCl_3$, 75.5 MHz): δ 189.11, 135.03, 130.41, 124.13, 122.69, 92.18

2.5.2 Kinetic experiments.

The following procedure describes the kinetic experiment for the d_0-**2.6a** and d_{60}-**2.6a** crossover experiment; all other kinetic runs were performed in an analogous fashion using the appropriate lanthanide, ligand and solvent combination.

Solutions of d_0-**2.6a** and d_{60}-**2.6a** (10 mg of each) in HPLC grade acetonitrile (10.00 mL) were prepared separately and then diluted 100-fold to give solutions with a final concentration of 10 μg/mL. A 0.500 mL aliquot of each solution was added to a vial and mixed for 10 s and samples of this mixture were injected into the Q-TOF II mass spectrometer running in +ESI MS mode. Spectra were collected every 5 min for the first hour, followed by every 30 min for the next 6 h and then every hour for the next 18 h. For other complexes, the sampling rate was adjusted as appropriate. In all cases the reaction was followed until thermodynamic equilibrium (1:2:1 ratio of d_0:d_{30}:d_{60} isotopomers) was established. The total counts for the major mass peak of each isotopomer were used to establish the relative concentrations of each species. The mass spectrometer response was assumed to be identical for the different isotopomers of the complex in all cases. The effect of water content in the acetonitrile solvent on the exchange rate was examined for **2.5a** using solvent mixtures containing 0, 10, 20, 30 40 and 50% (*v/v*) water to acetonitrile. The maximum water content of 50% was dictated by the solubility limit of **2.5a** in the mixed solvent.

Chapter 3 – Investigations into Oxazoline Based Contrast Agents

3.1 Introduction to Oxazolines

Oxazolines were first discovered in 1884, however, it took another 5 years to properly deduce the correct structure of the heterocycle (**Figure 3.1A**).[52] Since then, many examples of oxazoline functionality have been reported in the literature, with a wide variety of uses. Oxazolines have been used as the building blocks for living polymers that show promise as drug delivery tools.[53] They have been used as ancillary ligands on a cisplatin analogue.[54] They are used as protecting groups in organic synthesis, most prevalently in carbohydrate chemistry.[55-57] Compounds containing oxazoline functionality have been isolated from a variety of natural sources such as sponges and bacterium. These compounds have shown some interesting pharmacological properties, BE-70016 (**Figure 3.1B**) for example, isolated from *Actinoplane*, has two oxazoline rings and is found to possess anti-tumour properties.[58].

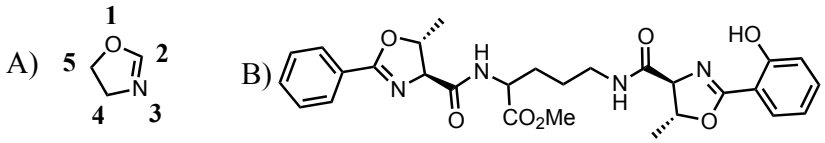

Oxazoline ring BE-70016

Figure 3.1: A) Oxazoline ring and numbering. B) BE-70016, isolated from the sponge *Actinoplane*

For the study of inorganic chemistry, the most interesting use of oxazoline rings is the incorporation into a variety of ligand systems (**Figure 3.2**). Oxazoline-derived ligands have gained popularity for several reasons: 1) The formation of an oxazoline is fairly direct starting from easily attainable chiral starting materials (an amino alcohol and an acid derivative or cyanide, *vide infra*); 2) the proximity of the metal to the chiral centre and the multitude of chiral substituents available allow these ligands to exercise effective control over the enantioselectivity of the catalyst; 3) these ligand sets are quite versatile

with different bonding geometries, including monodentate (**3.1**), bidentate (**3.2, 3.3**), and multidentate (**3.4, 3.5, 3.6**) modes (*see* **Figure 3.2**); 4) oxazoline ligands coordinate effectively to a variety of transition metals (*e.g.* Pd, Ni, Zn, Mn, Rh) for use in a wide range of asymmetric catalytic reactions.[59-62]

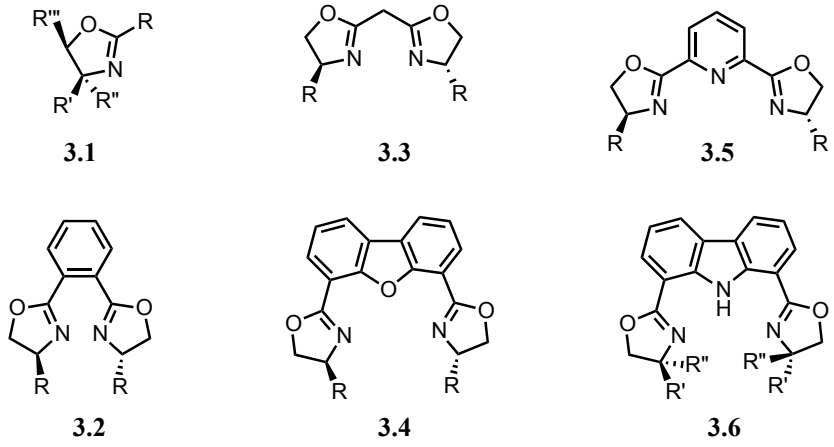

Figure 3.2: A selection of oxazoline ligands

More recently, oxazoline-lanthanide complexes have been developed. Our group has demonstrated that carbazole-based oxazoline-lanthanide complexes are very stable to ligand redistribution and thermal degradation, while supporting interesting ytterbium redox chemistry.[63] Other groups have used lanthanide-oxazoline complexes for asymmetric catalysis.[64, 65] A benefit of using a lanthanide based catalyst is that due to the similarities in bonding for the lanthanide series it is possible to tune catalytic behaviour by exchanging one lanthanide cation for another with relative ease. Desimoni *et al.* showed that by simply changing the lanthanide ion used in an oxazoline-lanthanide catalyzed Diels-Alder reaction one could effect which enantiomer was formed, while maintaining an enantiomeric excess of >95%.[66]

We were interested in designing a novel paraCEST agent using an oxazoline core because the oxazoline functionality is stable under biological conditions,[67, 68] and oxazoline-lanthanide systems are well behaved. While the advantages mentioned above were very exciting, the major drawback of current generation of oxazoline-lanthanide

complexes is ligand lability. The lability is due to the low denticity of the current ligands. Upon examination of the Cambridge Structural Database only one oxazoline-based ligand has a potential denticity >3, and it is reported to be air and water stable.[69] With this in mind we set out to design a ligand that could form a metal complex with a high coordination number to increase the thermodynamic stability and give the desired safety profile needed for contrast agents (see Chapter 1). The following chapter will outline the synthesis of several novel oxazoline based ligands, examine their stability, and ultimately rule them out as potential contrast agents.

3.2 TROX Ligand System

A recent publication by Li[70] demonstrated a simple one pot synthesis, **Scheme 3.1**, of chiral tris-oxazolines (TROX, **3.8**) from amino alcohols that would be very well suited for chelation of lanthanide ions. Following this route but using 2-hydroxyphenyl glycinol as the amino alcohol should allow us to insert another chelating group on the 4-position of the oxazoline ring (for numbering, *see* **Figure 3.1A**). With this modification, a 7-coordinate chelate, **3.8c** would be formed that should be able to strongly bind a lanthanide ion (**3.9**) and give a kinetically stable contrast agent, **Figure 3.3**.

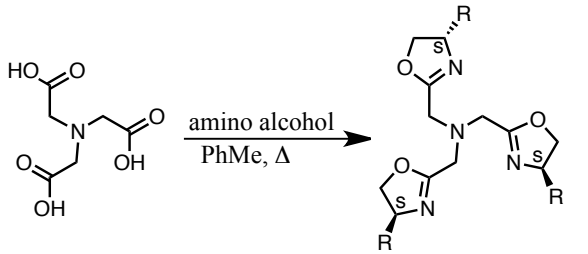

3.7

3.8a R = 2-MeOPh
3.8b R = Ph
3.8c R = 2-(OH)Ph

Scheme 3.1: Li TROX synthesis

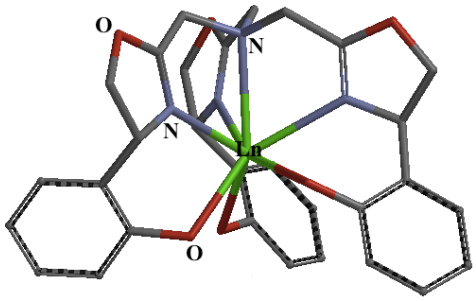

3.9

Figure 3.3: Proposed Ln TROX complex

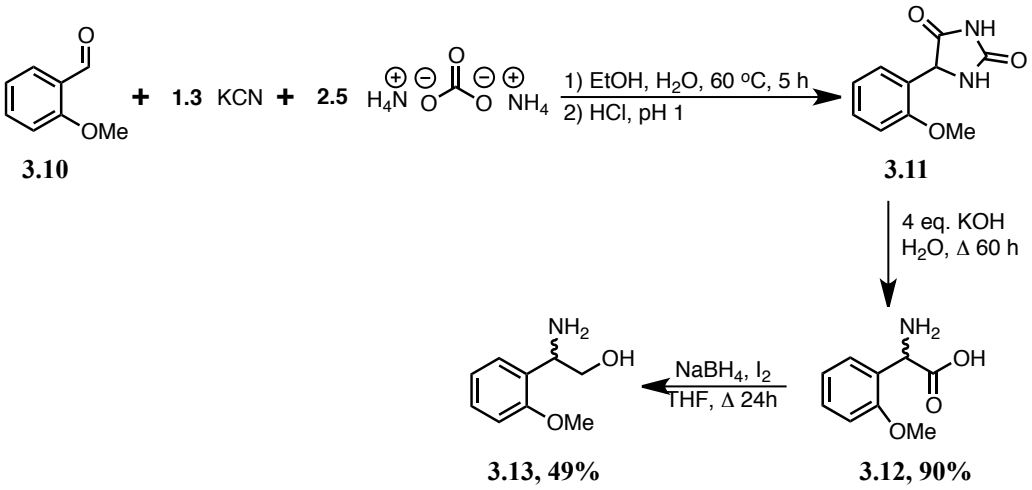

Scheme 3.2: Synthesis of 2-methoxyphenyl glycinol

We were unsure if the presence of a free hydroxyl group would hinder the oxazoline formation and decided that it should be protected until after oxazoline formation. Reduction of 2-methoxyphenyl glycine, **3.12**, a literature compound with a known synthesis,[71] with $NaBH_4$ and I_2 gave **3.13** in a 49% yield,[72] **Scheme 3.2**. Following the procedure **Scheme 3.1** using **3.13** as the amino alcohol produced a yellow solid expected to be **3.8a** in 30% yield.

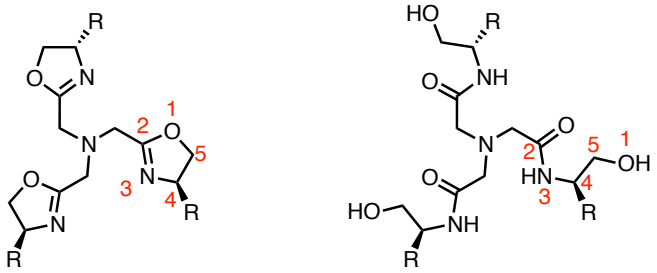

Figure 3.4: Open and closed form of the TROX ligand

The ^1H was consistent with those expected from the report by Li *et al.*;[70] however, after examining other oxazoline systems in detail some inconsistencies were noted. It is often difficult to differentiate between the closed, **3.8a**, and open, **3.14a,** form of an oxazoline

(**Figure 3.4**) without using more advanced 2D NMR techniques. A HMBC (Heteronuclear Multiple Bond Correlation) spectrum shows correlations between hydrogen and carbon nuclei that are 3 bonds apart. In the case of **3.8a** and **3.14a**, a HMBC correlation will only exist between the protons on the 5-position of the oxazoline ring and the carbon in the 2-position for **3.8a**, **Figure 3.5A**. Surprisingly, not only was this correlation not observed (**Figure 3.5A, X_1)**, the correlation between the hydrogen on the 4-position and the carbon at the 2-position was also absent (**Figure 3.5A, X_2)**, proving that neither ligand in **Figure 3.4** was formed. Analysis by chemical impact MS suggested that some form of salt was formed, however this could not be verified. To test if the methoxy group was somehow hindering oxazoline formation, the reaction in **Scheme 3.1** was repeated using commercially available (R)-phenylglycinol, in hopes of generating either **3.8b or 3.14b**. Yet again analysis of the HMBC spectrum (**Figure 3.5B**) showed the same results noted above. It is evident from our results that the Li method cannot accommodate ***any*** aryl substituents. The lack of 2D NMR (or any ^{13}C NMR) spectra in the Li report to conclusively prove the presence of oxazoline rings caused us to question the validity of their results and led us to pursue another synthetic route.

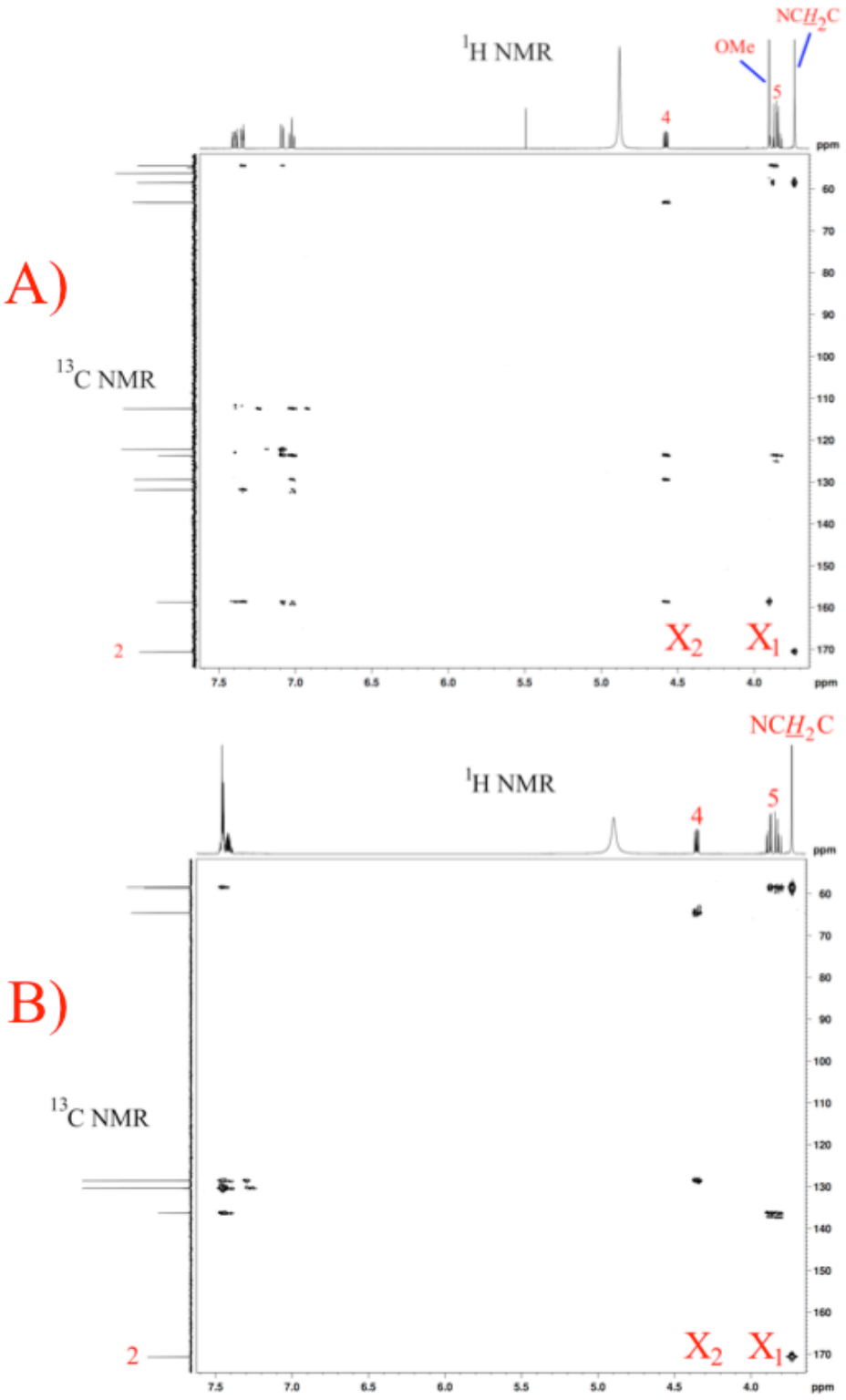

Figure 3.5: HMBC spectrum of **A) 3.8a**. and **B) 3.8b**. X_1 indicates the location of the expected correlation between the 5-position of the oxazoline ring and the carbon in the 2-position. X_2 indicates the location of the expected correlation between the 4-position of the oxazoline ring with the carbon in the 2-position.

A new synthetic pathway to the TROX ligand, **3.16a**, based on work done by Katsuki[73] was then proposed. First the amide bond is formed, followed by cyclization under Appel conditions, **Scheme 3.3**. Before proceeding with 2-methoxyphenyl glycinol, **3.14**, the literature method was verified using phenyl glycinol. Katsuki *et al.* had reported a 44% yield of **3.15b** using phenyl glycinol as the amino alcohol and our results verified the formation of **3.15b** by ^{1}H NMR and LR-ESI-MS. However, a drawback of the Appel reaction is that a stoichiometric amount of triphenylphosphine oxide is formed as a byproduct. This is a problem because **3.15b** was reported to be acid sensitive and the typical conditions for the removal of phosphine oxide by acidic silica column resulted in decomposition of the ligand. Attempts to sequester the oxide using a modified Merrifield resin,[74] or using resin-bound triphenylphosphine did not yield favourable results. Ultimately, after a very careful, quick silica column, 35 mg (from 500 mg loaded) of phosphine-free **3.15b** was isolated.

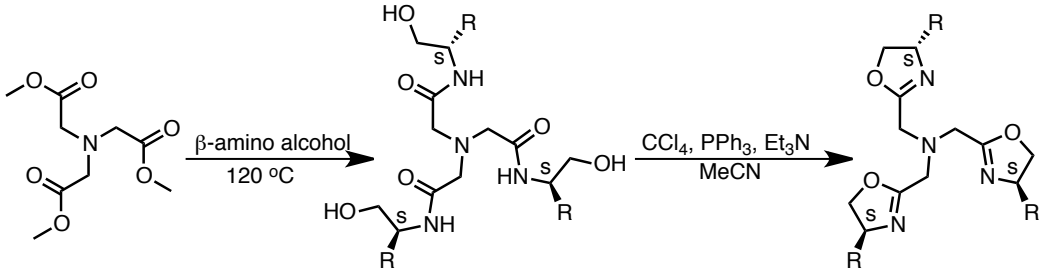

3.7b

3.16a R = 2-MeOPh
3.16b R = Ph

3.15a R = 2-MeOPh
3.15b R = Ph

Scheme 3.3: Synthesis of TROX ligands **3.15b** and **3.16b** by the Katsuki method**.**

The ^{1}H NMR was immediately collected in deuterated chloroform showing pure **3.15b**; this was then left 24 h and run again showing that it had partially ring opened to the open TROX ligand **3.16b**, presumably due to residual acid in the chloroform, **Figure 3.6**. An attempt at complexing a lanthanide ion using the open TROX ligand **3.16b** was made, however no evidence of successful chelation was observed. Having observed how sensitive this ligand is, it was decided that this class of ligand would never be viable for *in vivo* use and should be abandoned as a potential contrast agent.

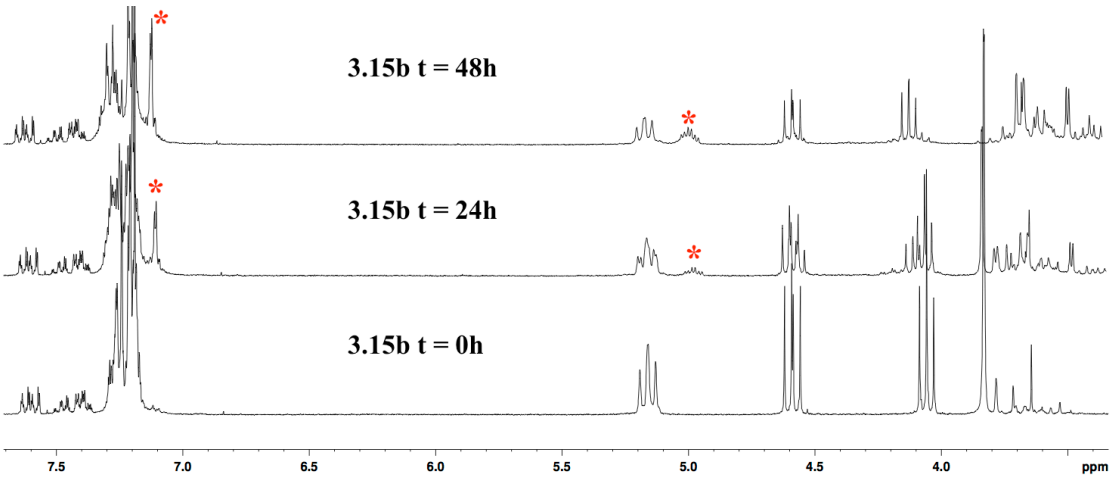

Figure 3.6: Decomposition of **3.15b** into **3.16b** over 48h; * denotes key signals of 3.16b growing in.

3.3 Pyridine Bis(Oxazoline) Ligand Systems

Though the previous attempt at using an oxazoline based ligand failed due to acid-sensitivity, the literature showed that tridentate, 2,6-bis(oxazoline)pyridine (PyBOx) systems could be made using a variety of synthetic routes with a multitude of amino alcohols that supported multi-gram scale synthesis and tolerated purification by column chromatography, indicating at least some stability towards mildly acid conditions.[75-78] The PyBOx framework has been very well studied,[79] yet we could find only one mention of a 5-coordinate lanthanide complex.[69] In this paper they used an L-serine based amino alcohol to form a ^{t}Bu-pbxa ligand, **3.17**. Using this ligand they formed a series of air and water stable ML_2 lanthanide complexes (Gd complex **3.18** shown in **Figure 3.7)**. This supported the idea that a PyBOx ligand with an increased chelation number will form a more stable complex over traditional PyBOx ligands and could be useful as a potential MR imaging agent.

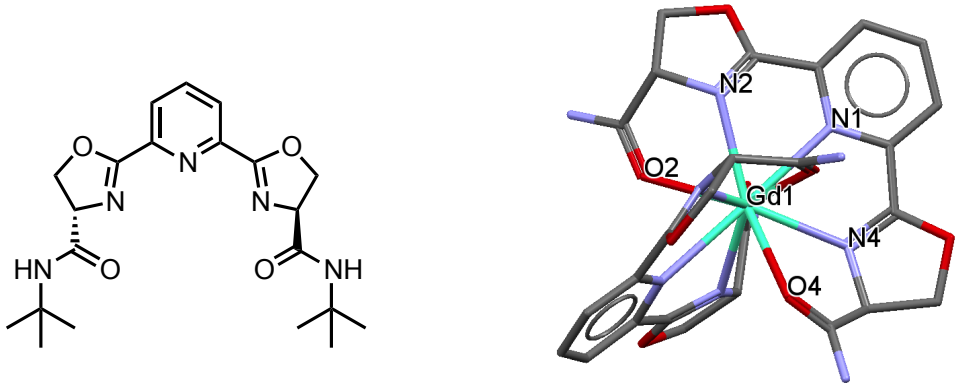

A) 3.17 **B) 3.18**

Figure 3.7: A) ^{t}Bu-pbxa ligand **3.17**. **B) 3.18**, Gd complex of **3.17** with hydrogen and t-butyl groups removed for clarity.[69]

A low-level equilibrium geometry calculation was performed to generate a model (**Figure 3.8)**, to examine if a pentadentate PyBOx ligand made from *ortho*-tyrosinol would be feasible. Examination of the bond lengths showed a reasonable correlation to that of the (^{t}Bu-pbxa)$_2$Gd crystal structure, (**Table 31)**, suggesting that *o*-TyPyBOx **3.19** would make a good candidate ligand to bind a lanthanide ion strongly for use as a contrast agent.

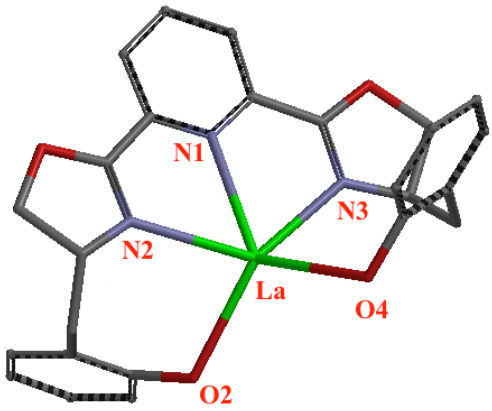

3.19b

Figure 3.8: Spartan equilibrium geometry model calculated using molecular mechanics, MMFFaq of **3.19b** o-TyPyBOx La complex

Table 3.1: Selected bond lengths and angles from (^{t}Bu-pbxa)$_2$La **3.18b** and *o*-TyPyBOx **3.19** calculated structure.

Bond	3.18b (Crystal structure)	3.19b (Spartan Structure)
N(1)-La	2.717	2.695
N(2)-La	2.637	2.643
N(3)-La	2.629	2.644
O(2)-La	2.529	2.644
O(4)-La	2.570	2.642
N(1)-La-N(2)	61.44	62.55
N(2)-La-N(3)	60.18	62.56

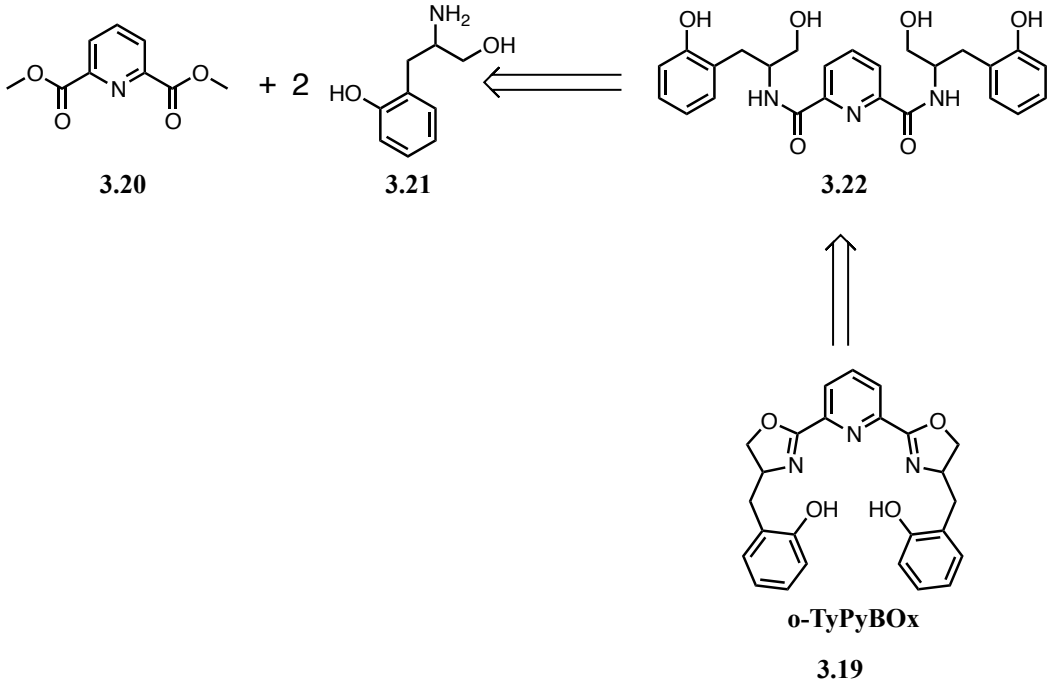

Scheme 3.4: Retrosynthesis of *o*-TyPyBOx, **3.19**

The retro-synthesis **Scheme 3.4** was proposed to make *o*-TyPyBOx, **3.19**. *o*-Tyrosinol, **3.21**, is not commercially available and must be reduced from its parent amino acid, *o*-tyrosine. *o*-Tyrosine is a non-natural amino acid and as such is expensive ($113 for 0.1g of the racemate). Synthesis of *o*-tyrosine, **3.34**, is a fairly intensive process and to arrive at the desired amino alcohol (*o*-tyrosinol, **3.41**) required 7 synthetic steps, *vide infra*, therefore it was decided that conditions should be optimized using the less exotic, natural amino acid L-tyrosine, **3.23**. With compound **3.26** being commercially available it

allowed for expedient testing of the appropriate reduction conditions, and gave sufficient amounts of **3.28** for determination of ideal conditions for formation of the oxazoline ligand **3.29**. As no tyrosine based PyBOx ligand was found in the literature it was unclear whether the incorporation of free hydroxyl groups would pose a synthetic problem. To avoid this ambiguity it was decided that the benzyl protecting group was to be left on until after the formation of the oxazoline where a final deprotection would be attempted to give the free hydroxyl groups needed for complexation of the lanthanide.

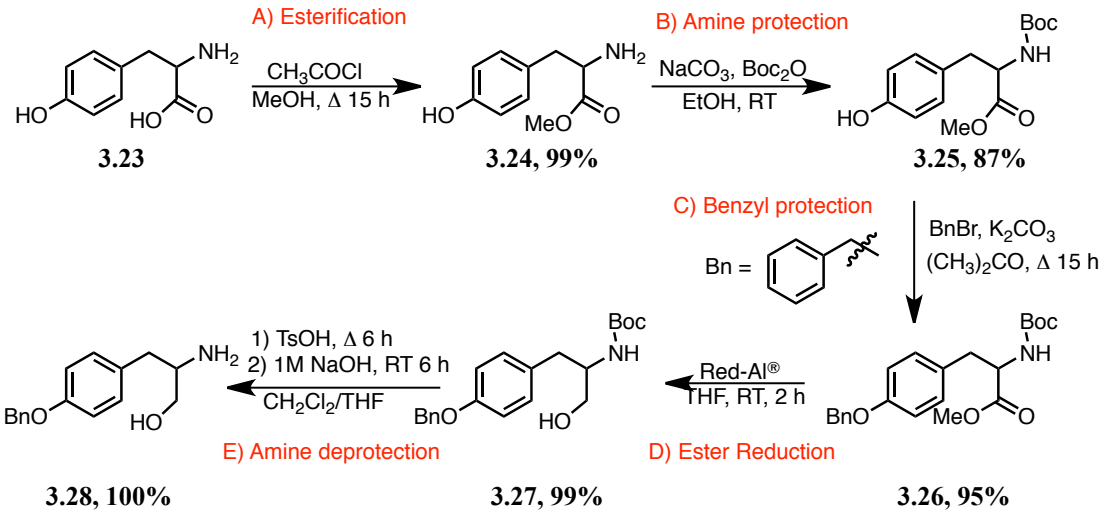

Scheme 3.5: Synthesis of benzyl protected tyrosinol, **3.28**.

To generate TyPyBOx, **3.30**, several methods of oxazoline formation were tested and it was found that a two-step one pot synthesis of **3.29** worked best to give a 55% yield upon recrystallization from ethanol, **Scheme 3.6**.[80] Examination of the HMBC shows a correlation between the -OC***H*₂**CH- (H on C5) at δ 4.34 and 4.21 ppm protons and the newly formed O***C***N carbon (C2) at δ 162.94 ppm (see **Figure 1** for numbering) confirming the formation of the oxazoline ring **(Figure 3.9)**.

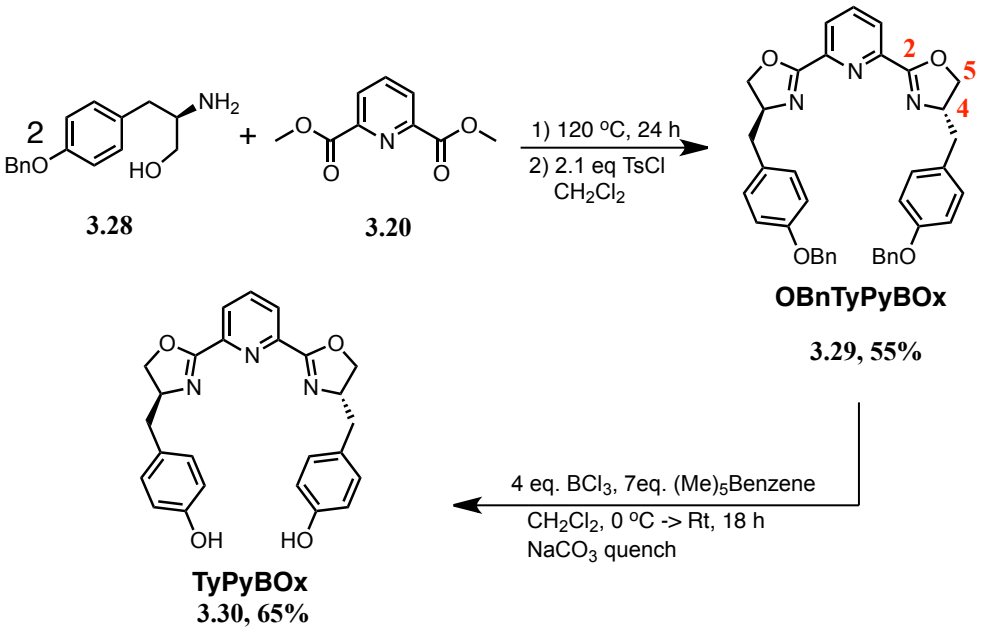

Scheme 3.6: Synthesis of the ligands OBnTyPyBOx, 3.29, and TyPyBOx, **3.30**

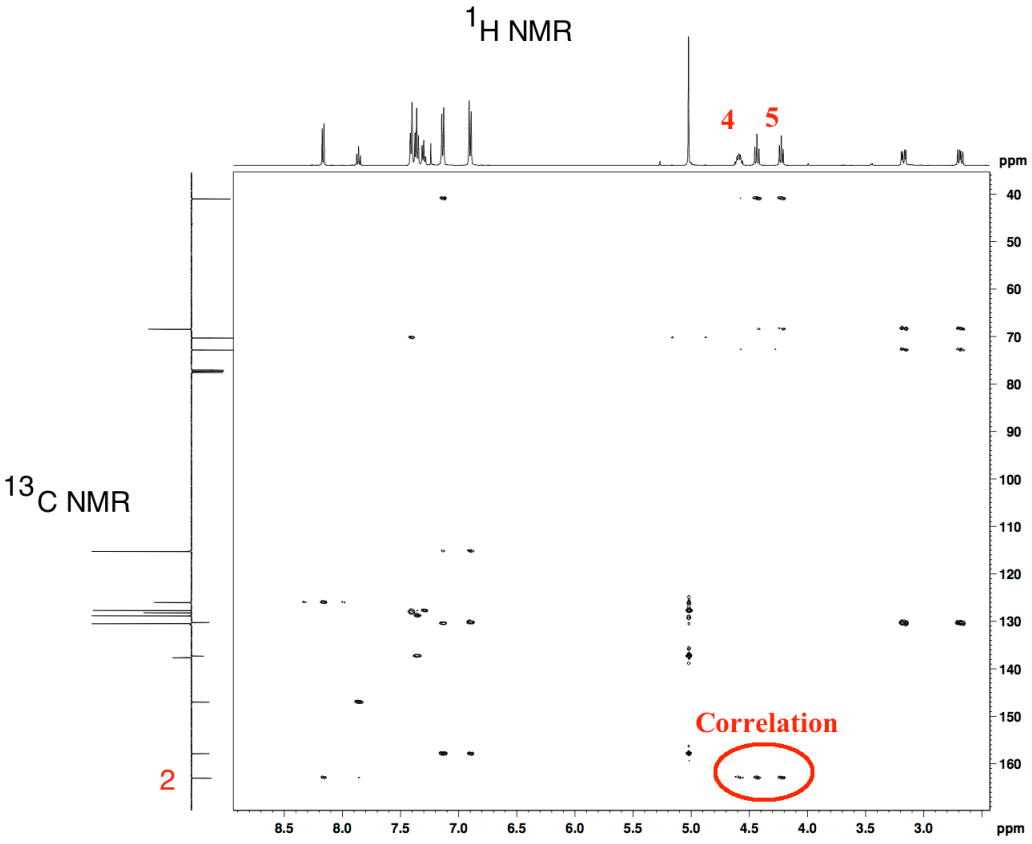

Figure 3.9: HMBC spectrum of **3.29** showing a correlation between C2 and the protons on C4 proving oxazoline formation has occurred (*see* **Scheme 3.6** for labeling).

Removal of the benzyl protecting group proved to be a challenge. Using 20 mol/% Pd/C at room temperature and atmospheric pressure or 20 atm of H_2, it was found that the benzyl groups remained intact. If the solution was heated to reflux as hydrogen was bubbled through the benzyl groups could be cleaved. However, under these conditions it was found via ESI-MS that a M+4 peak was also forming. It is believed that the imino bond in the oxazoline ring is also being reduced to form the oxazolidine ligand, **3.32, Figure 3.10**. The reaction was monitored over time via +ESI-MS for 8h at different temperatures and solvents to see if the reaction could be stopped before any formation of the oxazolidine product; selected results are summarized in **Table 3.2**. Ultimately it was found that it was not possible to remove fully the benzyl protecting groups while maintaining the oxazoline functionality using this method.

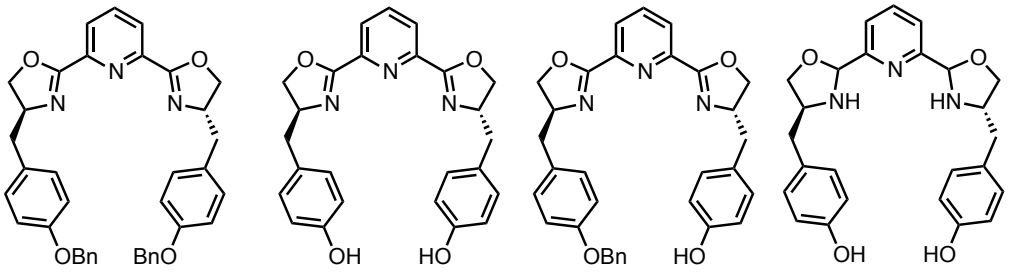

OBnTyPyBOx **TyPyBOx**

3.29 **3.30** **3.31** **3.32**

Figure 3.10: Structures of benzyl deprotection products

Table 3.2: Summary of selected benzyl deprotection results using 20 mol % Pd/C, followed by +ESI-MS.

Solvent	Pressure /atm	Temp / °C	Time /h	3.29 present	3.31 present	3.30 present	3.32 present
MeOH	1	22	1	✔	✖	✖	✖
MeOH	1	22	18	✔	✖	✖	✖
MeOH	20	22	18	✔	✖	✖	✖
PhMe	1	22	18	✔	✖	✖	✖
PhMe	20	22	18	✔	✖	✖	✖
PhMe	1	110	1	✔	✖	✖	✖
EtOH	1	22	1	✔	✖	✖	✖
EtOH	1	65	1	✔	✔	✖	✖
EtOH	1	65	3	✔	✔	✔	✖
EtOH	1	65	4	✔	✔	✔	✔
EtOH	1	65	6	✖	✔	✔	✔
EtOH	1	65	8	✖	✖	✔	✔
EtOH	1	40	1	✔	✖	✖	✖
EtOH	1	40	3	✔	✔	✖	✖
EtOH	1	40	4	✔	✔	✖	✖
EtOH	1	40	6	✔	✔	✔	✔
EtOH	1	40	8	✔	✔	✔	✔

Deprotection was finally achieved using boron trichloride (BCl_3) and pentamethylbenzene, to give a 65% yield of **3.30**, and an overall synthetic yield starting from the amino acid tyrosine of 29%. A major draw back of using this deprotection method is that upon quenching, any excess BCl_3 produces HCl that will cause the oxazoline ring to open. To compensate for this, $NaCO_3$ was added to the quench to neutralize the acid as it was formed. Again, an HMBC spectrum was used to confirm that a correlation existed between the -OC***H*****$_2$**CH- protons at δ 4.40 and 4.10 ppm and the O***C***N carbon at δ 161.67 ppm showing the oxazoline ring was unaffected by the deprotection process.

Using the information gathered from the synthesis of **3.30**, an analogous synthesis was done starting with the previously mentioned *ortho*-tyrosine amino acid, **3.34**. To avoid the unreasonable cost *o*-tyrosine was synthesized in house, **Scheme 3.7.**[81] Comparable yields were found for all steps leading to the benzyl protected *ortho*-tyrosinol, **3.39**. Formation of the desired *o*-OBnTyPyBOx ligand **3.40** was confirmed by HR-ESI-MS, however this reaction produced a complex mixture of additional byproducts as seen in the

^{1}H NMR (**Figure 3.11B**). Comparison between the ^{1}H NMR of crude *o*-OBnTyPyBOx **3.40** and of OBnTyPyBOx **3.29** allowed us to identify which peaks correspond to the desired product (**Figure 3.11 A & B)**. Movement of the hydroxyl group from the *para* position to the *ortho* position altered the solubility of the complex, making the *ortho*-tyrosine PyBOx analogue (**3.40**) soluble in alcohols (MeOH, EtOH, IPA, ^{t}BuOH, Hexanol). Due to this increase in solubility new conditions for purification were required; unfortunately, none of the tested conditions offered any noticeable improvements in purity giving a near identical complex mixture. As a mixture of the D/L amino alcohol, **3.39**, was used during the synthesis, it was thought that a mixture of the enantiomeric R,R and S,S PyBOx ligand was formed, along with the meso (R,S and S,R) compound. However, examination of the ^{13}C NMR spectrum (**Figure 3.12**) suggested that it was not a mixture of diastereomers as only one set of peaks are present. Surprisingly, any attempt at column chromatography resulted in decomposition of the ligand, presumably due to acid sensitivity. This was unexpected as other PyBOx systems were purified using column chromatography. This would seem to suggest that placement of the hydroxyl group somehow alters the stability of the complex. Attempted removal of the benzyl protecting groups on the crude product did not yield any promising results in the NMR or the LR-ESI-MS.

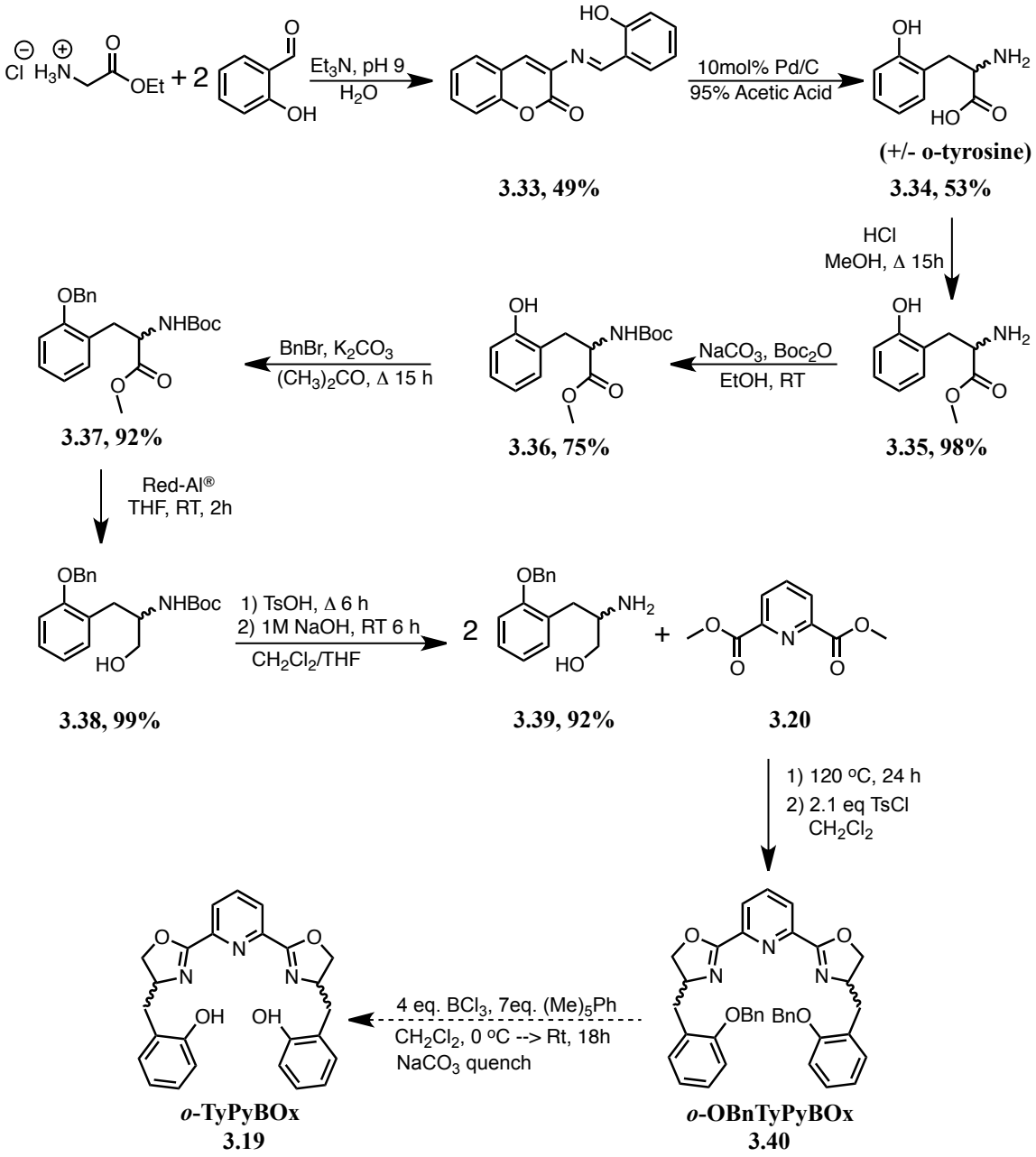

Scheme 3.7: Synthesis of *o*-TyPyBOx, **3.19**

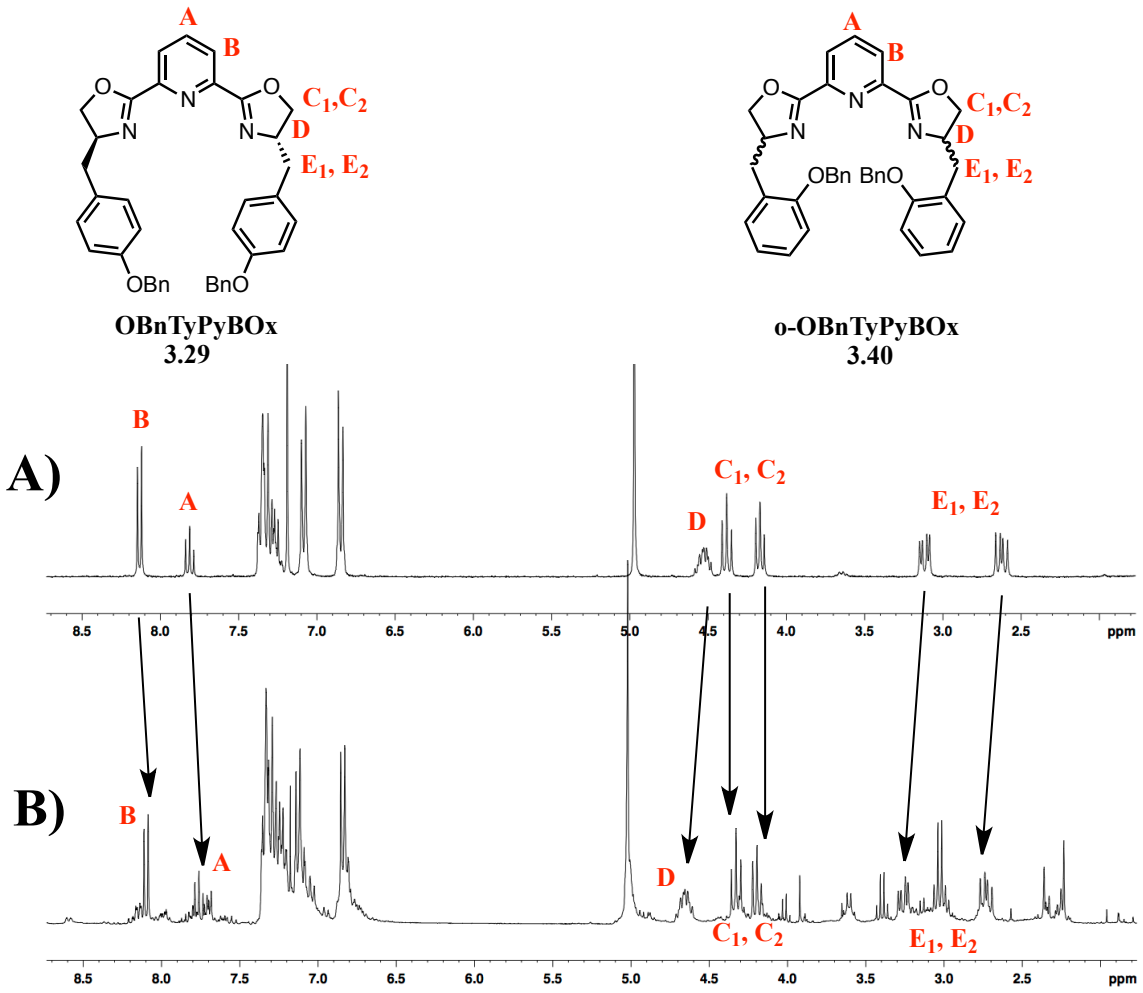

Figure 3.11: Comparison of the ^{1}H NMR spectra of the novel PyBOx ligands, **3.29** (A) and **3.40** (B)

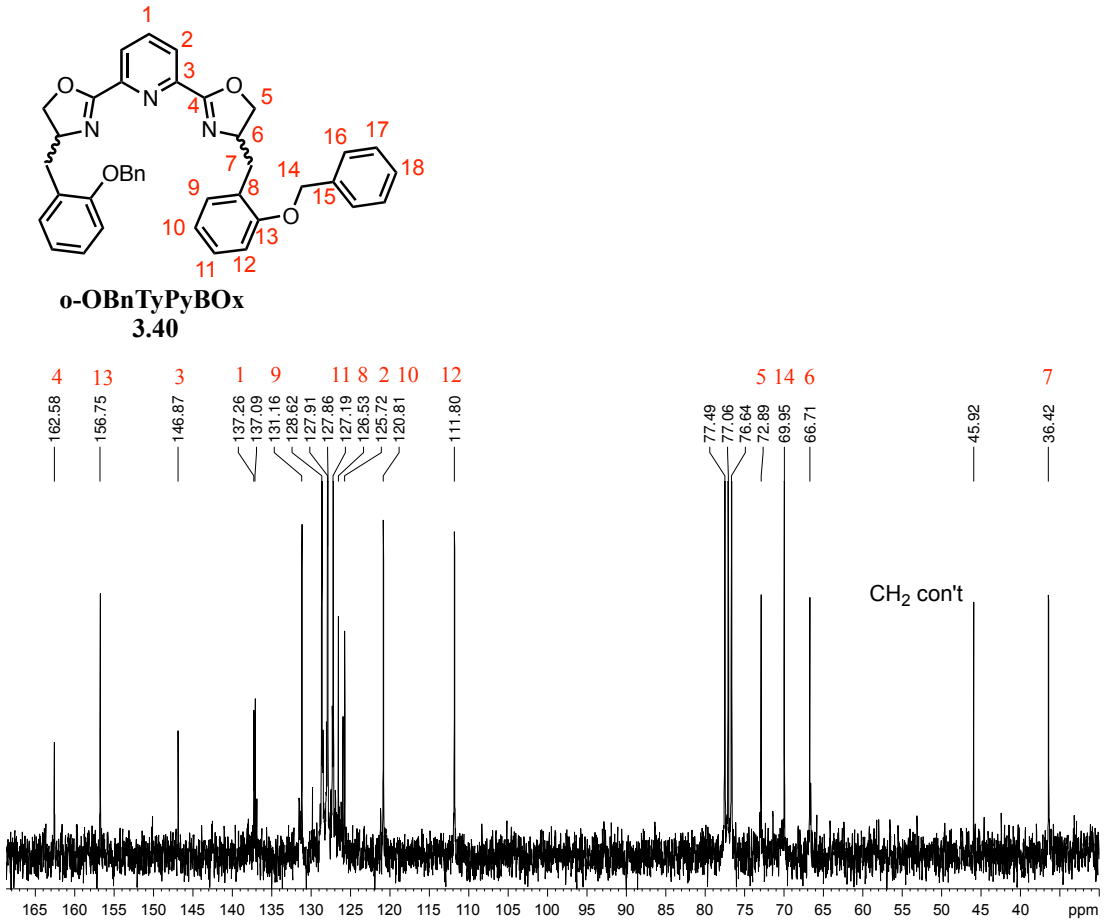

Figure 3.12: The ^{13}C NMR spectrum of *o*-OBnTyPyBOx, **3.40**, indicating that no diastereomeric compounds are present. Benzyl aromatic carbons were not labelled, * indicates $–CH_2-$ contaminant, $-CH_3$ contaminant at 8.62 ppm was removed for clarity.

The removal of the benzyl protecting groups on the tyrosine based PyBOx ligand **3.30** was the most synthetically challenging step in the synthesis, therefore, it was desirable to see if incorporation of the benzyl protecting group was indeed necessary. To test this, the benzyl groups were removed from the amino alcohol **3.39** prior to oxazoline formation to give an unprotected *o*-tyrosinol **3.21**. No product was observed. The synthesis of **3.19** was attempted using a known method of oxazoline formation that accommodates free hydroxyl groups on the amino alcohol, **Scheme 3.8**,[82] however no product was isolated.

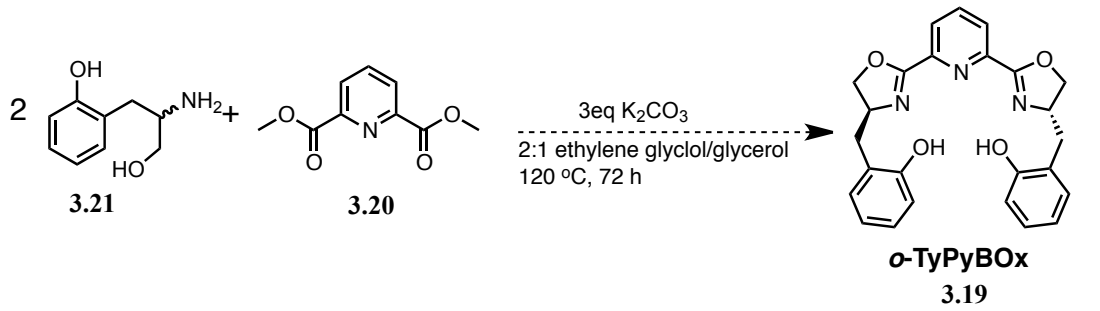

Scheme 3.8: Synthesis of *o*-TyPyBOx **3.19** using unprotected *o*-tyrosinol **3.21**.

To investigate if it was the pyridine backbone or the free hydroxyl on the phenyl ring of the *o*-tyrosinol that was hindering the formation of the *o*-TyPyBOx ligand **3.19**, an analogous reaction to **Scheme 3.8** was carried out using a carbazole backbone, **Scheme 3.9**. The carbazole backbone was selected because the chemistry behind carbazole bis-oxazoline formation is well understood by the Berg group as they have used this backbone with great success.[63] Upon purification, the +HR-ESI-MS supported a fully cyclized product **3.42**, however analysis of the ^{1}H showed an additional multiplet from δ 6.67-6.61 ppm that equated to 2 protons. Combining this information with a peak in ^{13}C NMR at δ 167.3 ppm rather then the standard location of δ 162 ppm seen in the previously published carbazole bis-oxazoline systems[63] suggested that the bis-oxazoline **3.42**, was not formed, but rather an open form of the oxazoline, **3.43**. An HMBC spectrum was again used to verify that no correlation between CH***C*H$_2$O (H on C8) and the N***C***O (C7) was found. An unexpected correlation between the proton on carbon 8 and carbon 16 was also seen (**Figure 3.13**). The only way for this correlation to exist would be by the formation of cyclic chroman product **3.44**. This product has the same chemical formula as **3.42** and fully complies with all the NRM and HR-+ESI MS data. This result shows that the phenolic oxygen must be protected during the formation of the oxazoline ring when the hydroxyl group is in the *ortho* position; without this protection, a dehydration to form a chroman ring will occur. This reaction was also carried out using a racemic mixture of *o*-tyrosinol but since only one set of peaks was observed in the ^{1}H and ^{13}C NMR spectrum, either a racemic mixture (R,R and S,S) or a meso compound (R,S and S,R) was formed.

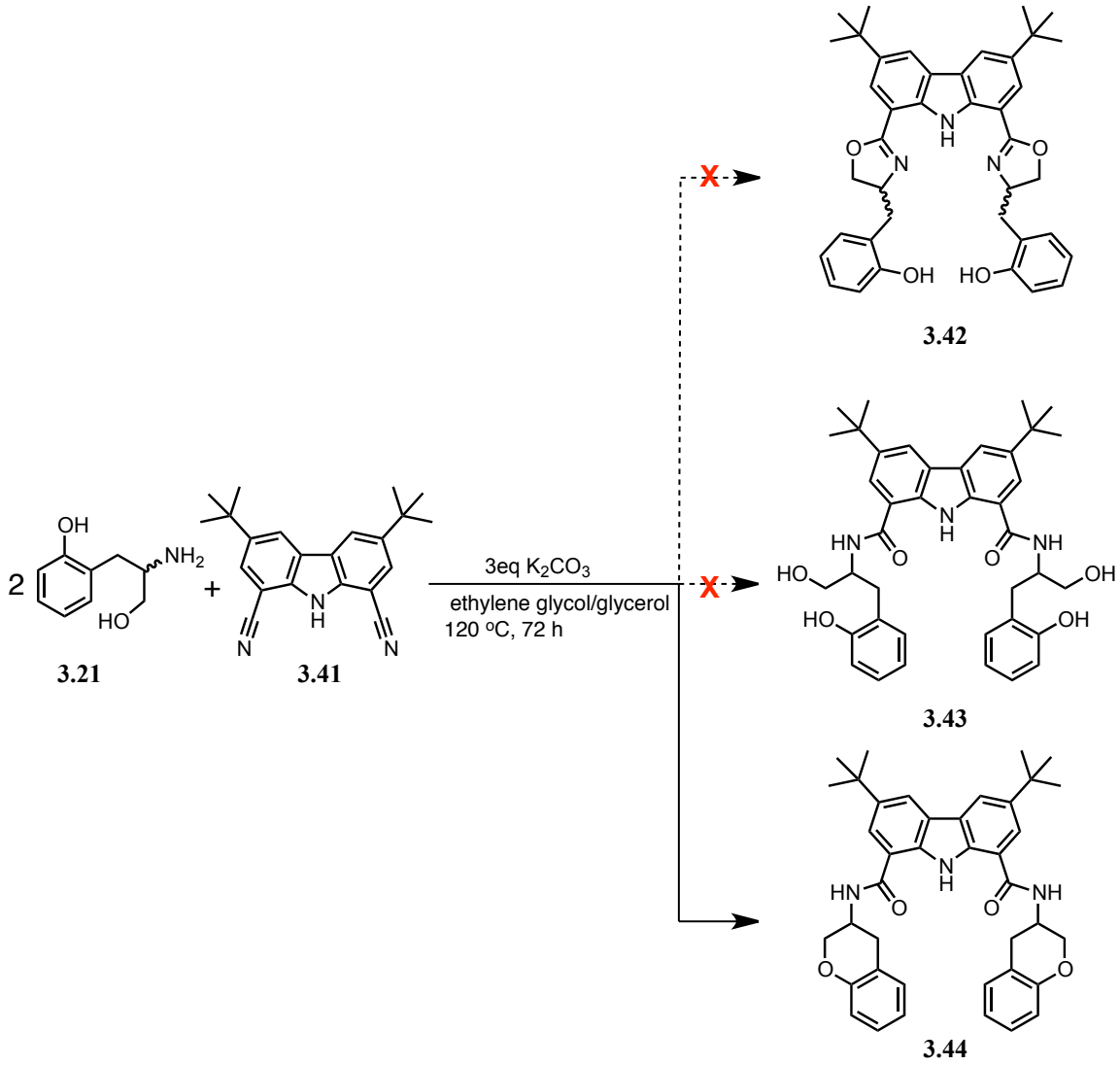

3.21 **3.41** **3.42** **3.43** **3.44**

Scheme 3.9: Proposed synthetic route to the carbazole backbone bis-oxazoline.

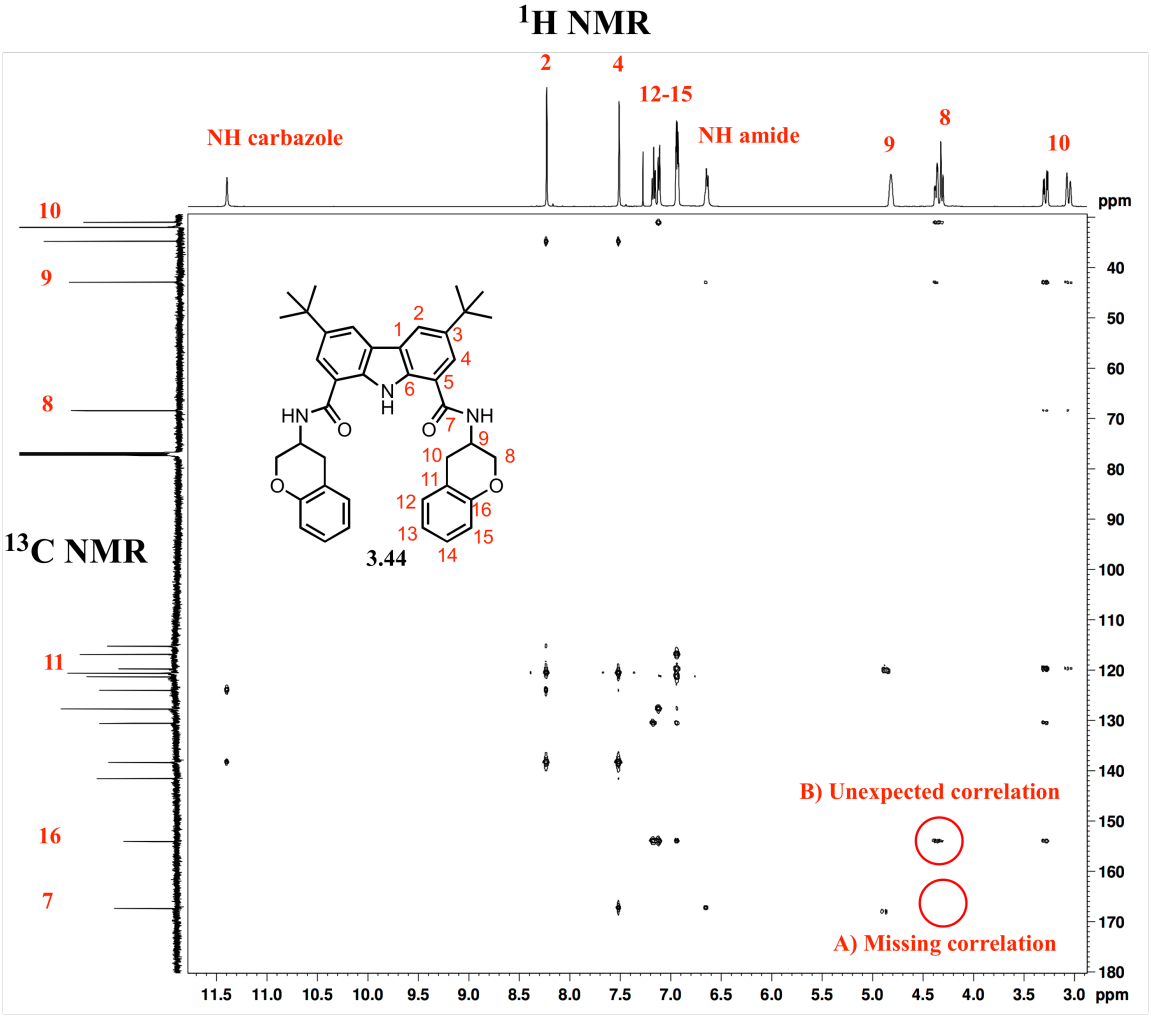

Figure 3.13: HMBC spectrum of **3.44** showing **A)** the missing correlation confirming no oxazoline functionality and **B)** the unexpected correlation confirming ether formation. (Only significant carbons were labelled and t-butyl correlations were removed for clarity).

3.3 Concluding remarks.

Novel oxazoline ligands **3.29, 3.30, 3.40** were formed including the first known examples of PyBOx ligand based on tyrosine. The TROX based ligand **3.15b** was found to decompose under very mild acidic conditions. A tyrosine based PyBOx ligand (**3.29**) was synthesized in order to determine the best route to form an *ortho*-tyrosine based ligand (**3.19**), as it would be well suited to form a penta-coordinated lanthanide complex, that may have enough kinetic stability for use as MR imaging agents. Unfortunately, the

o-OBnTyPyBOx (**3.40**) ligand was unable to be purified via recrystallization and any attempt at column chromatography caused the ligand to decompose. To see if purification would be possible if the benzyl protecting groups were removed prior to oxazoline formation, the unprotected amino alcohol (*o*-tyrosinol, **3.21**) was used but no product was observed in this case. To determine if this was due to the pyridine backbone, a carbazole backbone was used in its place. It was found that the protection of the phenolic hydroxyl group was vital. If left unprotected, a chroman ring forms via a dehydration reaction, preventing the formation of an oxazoline and forming compound **3.44**. The difficulty in purification and apparent instability led us to conclude that physiological conditions would be too harsh which negates the use of oxazoline ligand **3.19** as a possible MRI contrast agent**.** With the difficulties encountered using an oxazoline system, we set out to investigate a different ligand class as discussed in the next chapter.

3.4 Experimental

All experiments were performed under an inert argon atmosphere using standard Schlenk techniques in flame-dried glassware unless otherwise noted. THF was freshly distilled from sodium/benzophenone before use. CH_2Cl_2 was used as is unless specified; dry CH_2Cl_2 was distilled from calcium hydride. **3.26** was purchased from Chem-Impex. All other chemicals were purchased from Sigma-Aldrich and used as is. **3.12** (90%),[71] **3.24** (99%),[80] **3.25** (87%),[80] **3.26** (95%),[83] **3.27** (99%),[84] **3.28** (100%),[80] **3.33** (49%),[81] **3.34** (53%)[81] were synthesized by literature methods. Spectra for NMR spectroscopy were recorded on Bruker AMX-300 MHz or 500 MHz NMR spectrometers. LR-ESI-MS data was collected on a Finnigan Mat LCQ mass spectrometer. HR-ESI-MS data was collected using a ThermoFisher Orbitrap Executive mass spectrometer.

3.4.1 Synthesis

2-methoxyphenyl glycinol, **3.13** $NaBH_4$ (0.83 g, 22 mmol) was added to THF (100 mL). **3.12** (2.0 g, 11 mmol) was added in one portion and the temperature was reduced to 0 °C. I_2 (2.8 g, 11 mmol) in THF (50 mL) was then added over 0.5 h. The solution was stirred at 0 °C for 2 h and then refluxed for 18 h. MeOH was added to quench the reaction, the solvent was removed under reduced pressure and 20% KOH water solution was added. The suspension was stirred for 4 h. The aqueous solution was then extracted with CH_2Cl_2 (3 x 100 mL) and the organic layers were then extracted with 1M HCl solution and discarded. The aqueous product layer was then made basic to pH 14 with KOH and extracted with CH_2Cl_2 (3 x 100 mL) to give a colourless organic product layer. The solvent was removed under reduced pressure to give a colourless oil that solidified upon standing to a white powder. Yield 0.90 g (49%). ^{1}H NMR matched literature values.[85]

OMe TROX, **3.8a** Synthesis of **3.8a** was attempted by an adaptation of a literature procedure[70] using **3.14** as the amino alcohol. Yield: 1.3 g (30%, using OMe TROX mw) ^{1}H NMR (MeOD, 500MHz, 22 °C): δ 7.41-7.38 (m, 3H), 7.35 (dd, $^3J_{HH}$ = 7.8Hz, $^4J_{HH}$ = 1.8Hz, 3H), 7.09 (dd, $^3J_{HH}$ = 8.3Hz, $^4J_{HH}$ = 1.0Hz, 3H), 7.02 (td, $^3J_{HH}$ = 7.5Hz, $^4J_{HH}$ = 1.8Hz, 2H), 4.58 (dd, $^3J_{HH}$ = 8.4Hz, $^3J_{HH}$ = 4.9Hz, 3H), 3.90 (s, 9H), 3.88-3.82 (m, 6H), 3.74 (s, 6H). ^{13}C{^{1}H} NMR (MeOD, 125MHz): δ 170.56, 158.67, 131.83, 129.42, 123.68, 122.23, 112.53, 63.23, 58.50, 56.24, 54.44.

Ph TROX, **3.8b** Synthesis of **3.8b** was attempted by an adaptation of a literature procedure[70] using phenyl glycinol as the amino alcohol. ^{1}H NMR (MeOD, 500MHz, 22 °C): δ 7.47-7.39 (m, 15H), 4.35 (dd, $^3J_{HH}$ = 8.3Hz, $^3J_{HH}$ = 4.2Hz, 3H), 3.90 (s, 9H), 3.90-3.80 (m, 6H), 3.74 (s, 6H). ^{13}C{^{1}H} NMR (MeOD, 125MHz): δ 170.64, 136.30, 130.40, 130.45, 128.56, 164.58, 58.56, 58.43.

Ph TROX, 3.15b The synthesis of **3.15b** was done via a literature procedure.[73] ^{1}H NMR matched literature values.[73] ^{1}H NMR ($CDCl_3$, 300MHz, 22 °C): δ 7.30-7.16 (m, 15H), 5.16 (t, $^3J_{HH}$ = 9.1Hz, 3H), 4.59 (dd, $^3J_{HH}$ = 10.2Hz $^3J_{HH}$ = 8.5Hz, 3H, Ha/Hb of C*H*$_2$O), 4.06 (t, $^3J_{HH}$ = 8.5 Hz, 3H, Ha/Hb of C*H*$_2$O), 3.83 (s, 6H).

OBnTyPyBOx, **3.29** **3.28** (1.0 g, 3.9 mmol) was added to dimethyl 2,6-pyridinedicarboxylate, **3.20**, (0.37 g, 1.9 mmol) and the neat mixture heated to 120 °C for 24h. The reaction product was cooled and a solution of 4-toluenesulfonyl chloride (0.78 g, 4.1 mmol) and 1.5 mL triethylamine in 30 mL dry CH_2Cl_2 was added. The reaction mixture was refluxed overnight, cooled and extracted (2 x 20 mL H_2O followed by 2 x 20 mL brine) and dried over anhydrous $MgSO_4$. After filtration to remove the $MgSO_4$, the solvent was removed under reduced pressure to give a brown solid. The brown solid was recrystallized from warm EtOH to yield a white powder. Yield: 0.63 g (55%). ^{1}H NMR ($CDCl_3$, 500MHz, 22 °C): δ 8.16 (d, $^3J_{HH}$ = 7.2Hz, 2H, py *meta*-CH), 7.86 (t, $^3J_{HH}$ = 7.2Hz, 1H, py *para*-CH), 7.42-7.28 (m, 10H, Bn PhH), 7.14 (d, $^3J_{HH}$ = 8.3Hz, 4H, Ph *ortho*-CH), 6.90 (d, $^3J_{HH}$ = 8.6Hz, 4H, Ph *meta*-CH), 5.02 (s, 4H, Bn-CH_2), 4.64-4.55 (m, 2H, C*H*N), 4.43 (t, $^3J_{HH}$ = 9.1Hz, 2H, Ha/Hb of C*H*$_2$O), 4.22 (t, $^3J_{HH}$ = 8.2 Hz, 2H, Ha/Hb of C*H*$_2$O), 3.17 (dd, *J* = 5.5 Hz, 14.0 Hz, 2H, Hb/Ha of C*H*$_2$Ph-4-OBn), 2.68 (dd, *J* = 8.7 Hz, 14.0 Hz, 2H, Hb/Ha of C*H*$_2$Ph-4-OBn). ^{13}C{^{1}H} NMR ($CDCl_3$, 125MHz): δ 162.94, 157.85, 147.00, 137.64, 137.31, 130.48, 130.22, 128.82, 128.18, 127.70, 126.02, 115.24, 72.82, 70.28, 68.45, 40.98. HR-ESI-MS: 610.2702 ($[M+H]^+$, $C_{39}H_{36}N_3O_4$; calcd: 610.2701).

TyPyBOx, **3.30** **3.29** (0.25 g, 0.41 mmol) was dissolved in 10 mL dry CH_2Cl_2. Pentamethylbenzene (0.182 g, 1.24 mmol) was added and the solution cooled to -78 °C. 1M BCl_3 in hexane (1.65 mmol, 1.64 μL) was added and the reaction was stirred for 2 h and warmed to RT and filtered through an 80/20 mixture of Celite/$NaCO_3$, rinsing with MeOH, into a flask containing powdered $NaCO_3$ and Na_2SO_4 under Ar. The solution was filtered in air and the solvent was removed under reduced pressure. The resulting white powder was then rinsed with water to remove any boric acid and centrifuged. The remaining powder was dissolved in MeOH and dried over anhydrous $MgSO_4$ for 24 h to

give a hygroscopic white solid. Yield: 0.114 g (65%). ^{1}H NMR (D_6-DMSO, 500MHz, 22 °C): δ 8.10 (d, $^{3}J_{HH}$ = 7.8Hz, 2H, py *meta*-CH), 7.86 (dd, $^{3}J_{HH}$ = 7.0Hz, $^{3}J_{HH}$ = 8.4Hz 1H, py *para*-CH), 7.14 (d, $^{3}J_{HH}$ = 8.3Hz, 4H, Ph *ortho*-CH), 6.60 (d, $^{3}J_{HH}$ = 8.3Hz, 4H, Ph *meta*-CH), 4.55-4.47 (m, 2H, C*H*N), 4.40 (t, $^{3}J_{HH}$ = 8.8Hz, 2H, Ha/Hb of CH_2O), 4.10 (t, $^{3}J_{HH}$ = 8.1 Hz, 2H, Ha/Hb of CH_2O), 2.88 (dd, $^{3}J_{HH}$ = 5.8 Hz, 14.0 Hz, 2H, Hb/Ha of CH_2Ph-4-OH), 2.64 (dd, *J* = 7.7 Hz, 14.0 Hz, 2H, Hb/Ha of CH_2Ph-4-OH). ^{13}C{^{1}H} NMR ($CDCl_3$, 125MHz): δ 161.67, 157.20, 146.41, 138.07, 130.14, 126.60, 125.65, 115.37, 71.71, 67.61, 39.98. LR-ESI-MS: 430.47 ($[M+H]^+$, $C_{25}H_{24}N_3O_4$; calcd: 430.18).

DL-*o*-Tyr-OMe, **3.35** A modified literature procedure[80] using **3.34** as the amino acid was used. Yield: 5.27 g (98%). NMR matched literature values.[86]

N-BOC-DL-*o*-Tyr-OMe, **3.36** A modified literature procedure[80] using **3.35** as the amino ester was used. Yield: 5.97 g (75%). NMR matched literature values.[87]

N-BOC-DL-*o*-Tyr(Bn)-OMe, **3.37** A modified literature procedure[83] using **3.36** as the amino ester was used. Yield: 0.628 g (95%). NMR matched literature values.[88]

N-BOC-DL-*o*-Tyr(Bn)-OH, **3.38** Red-Al (13.3 mL, 65+ wt%) in PhMe was added to THF (60 mL) and cooled to 0 °C. **3.37** (4.41 g, 11.4 mmol) was dissolved in 40 mL THF and added drop-wise over 2 h. The reaction was then allowed to warm to RT with stirring overnight. The solution was cooled to 0 °C and MeOH was added to quench the reaction. A saturated solution of Rochelle's salt was added (40 mL) and the reaction mixture was extracted (2 x 60 mL) with EtOAc. The organic layers were combined and washed (2 x H_2O, 2 x $NaHCO_3$, and 2 x brine). The organic layer was evaporated to dryness under reduced pressure to give a white solid. Yield: 4.03 g (99%). ^{1}H NMR ($CDCl_3$, 300MHz, 22 °C): δ 7.42-7.30 (m, 5H, Bn PhH), 7.24-7.13 (m, 2H, PhCH), 6.98-6.90 (m, 2H, PhCH), 5.11-5.02 (m, 2H, Bn-CH_2), 3.84-3.71 (m, 1H, C*H*N), 3.52-3.48 (m, 2H, CH_2O), 2.93-2.77 (m, 2H, CH_2Ph-*o*-OBn), 1.39 (s, 9H, $(CH_3)_3$ of BOC), 1.83 (br s, <1H, OH/NH).

DL-*o*-Tyr(Bn)-OH, **3.39** **3.38** (4.00 g, 11.2 mmol) was dissolved in a 50/50 mixture of CH_2Cl_2/PhMe (300 mL). p-Toluenesulfonic acid (7.51 g, 43.6 mmol) was added and the solution was refluxed for 8 h. The reaction mixture was let cool, a 1M NaOH solution in water (150 mL) was added and the resulting biphasic solution was allowed to stir overnight. The reaction mixture was then extracted (3 x 150 mL) with EtOAc, the organic layers were combined and washed (2 x 100 mL) with brine. The organic layer was dried over anhydrous $MgSO_4$ and stripped to give a yellow oil. The oil was dissolved in hot hexanes and upon cooling gave a white solid. Yield: 2.66 g (92%). ^{1}H NMR ($CDCl_3$, 300MHz, 22 °C): δ 7.42-7.28 (m, 5H, Bn PhH), 7.22-7.15 (m, 2H, PhCH), 6.94-6.88 (m, 2H, PhCH), 5.00 (s, 2H, Bn-CH_2), 3.52 (dd, *J* = 4.1 Hz, 11.0 Hz, 1H, Hb/Ha of C*H*$_2$O), 3.3 (dd, *J* = 6.9 Hz, 11.0 Hz, 1H, Hb/Ha of C*H*$_2$O), 3.18-3.06 (m, 1H, C*H*N), 2.83 (dd, *J* = 5.9 Hz, 13.5 Hz, 1H, Hb/Ha of C*H*$_2$Ph-*o*-OBn), 2.61 (dd, *J* = 7.5 Hz, 13.3 Hz, 1H, Hb/Ha of C*H*$_2$Ph-*o*-OBn), 1.83 (s, 3H, OH/NH_2). ^{13}C{^{1}H} NMR ($CDCl_3$, 75MHz): δ 156.75, 136.93, 131.27, 128.67, 128.03, 127.74, 127.39, 127.27, 120.94, 111.85, 70.14, 66.28, 53.14, 35.55.

***o*-OBnTyPyBOx**, **3.40** **3.40** was synthesized following the same procedure as OBnTyPyBOx, **3.29**, starting with amino alcohol **3.39**. It proved difficult to purify this compound and an impure pale yellow oil was obtained. Integration values given vary from the structure due to multiple overlapping products. Selected peaks in ^{1}H NMR of crude product ($CDCl_3$, 300MHz, 22 °C): δ 8.11 (d, $^3J_{HH}$ = 7.8Hz, 2H, py *meta*-CH), 7.77 (t, $^3J_{HH}$ = 7.6Hz, 1H, py *para*-CH), 7.39-7.28 (m, 13H (10H), Bn PhH), 7.16-6.78 (m, 12H (8H), PhCH), 5.04 (s, 4H, Bn-CH_2), 4.72-4.61 (m, 2H, C*H*N), 4.34 (t, $^3J_{HH}$ = 9.4Hz, 2H, Ha/Hb of C*H*$_2$O), 4.21 (t, $^3J_{HH}$ = 8.2 Hz, 2H, Ha/Hb of C*H*$_2$O), 3.27 (dd, *J* = 5.2 Hz, 13.7 Hz, 2H, Hb/Ha of C*H*$_2$Ph-2-OBn), 2.74 (dd, *J* = 9.0 Hz, 13.7 Hz, 2H, Hb/Ha of C*H*$_2$Ph-2-OBn). ^{13}C{^{1}H} NMR ($CDCl_3$, 75MHz): δ 162.53, 156.75, 146.87, 137.26, 137.09, 131.16, 128.27, 127.91, 127.86, 127.19, 126.53, 125.72, 120.81, 111.80, 72.89, 69.95, 66.71, 36.42. (Also, CH_2 & CH_3 impurity 45.92, 8.62). HR-ESI-MS: 610.2702 ($[M+H]^+$, $C_{39}H_{36}N_3O_4$; calcd: 610.2706).

3,6-di-^{t}butyl-N^{1},N^{8}-di(chroman-3-yl)-9*H*-carbazole-1,8-dicarboxamide, 3.44

Compounds **3.21** (0.050 g, 0.30 mmol) and **3.41** (0.050 g, 0.15 mmol) were added to a 2:1 (*v/v*) solution of ethylene glycol and glycerol (6 mL) and heated to 120 °C for 72 h. The solution was diluted with water and extracted with CH_2Cl_2 (3 x 20 mL). The organic layer was separated and the solvent was removed under reduced pressure to give a crude yellow oil. The crude oil was purified by column chromatography to give a pale yellow oil. Yield: 0.022 g (23%). See **Figure 3.13** for labelled diagram. ^{1}H NMR ($CDCl_3$, 300MHz, 22 °C): δ 11.40 (s, 1H, N*H*), 8.23 (s, 2H, C(2)*H*), 7.51 (s, 2H, C(4)*H*), 7.17 (t, $^{3}J_{HH}$ = 7.8Hz, 2H, C(14)*H*), 7.12 (d, $^{3}J_{HH}$ = 7.8Hz, 2H, C(12)*H*), 6.96-6.91 (m, 2H, C(15)H&C(13)H), 6.67-6.62 (m, 2H, Carbazole N*H*), 4.85-4.79 (m, 2H, C(9)H), 4.39-4.29 (m, 4H, Ha/Hb of $C(8)H_2$), 3.29 (dd, $^{3}J_{HH}$ = 16.7Hz, $^{3}J_{HH}$ = 5.1Hz, 2H, *Ha*/Hb of $C(10)H_2$), 3.06 (app. d, $^{3}J_{HH}$ = 16.7Hz, Ha/*Hb* of $C(10)H_2$), 1.43 (s, 18H, $C(CH_3)_3$). $^{13}C\{^{1}H\}$ NMR ($CDCl_3$, 75MHz): δ 167.48 (7), 154.06 (16), 141.54 (3), 138.35 (6), 130.58 (12), 127.71 (14), 123.97 (1), 121.30 (13), 120.60 & 120.57 (2 &4), 119.73 (11), 116.86 (15), 115.22 (5), 68.40 (8), 42.88 (9), 34.72 (($\underline{\mathbf{C}}(CH_3)_3$), 31.96 ($C(\underline{\mathbf{C}}H_3)_3$), 30.97 (10). HR-ESI-MS: 652.3145 ($[M+Na]^+$, $C_{40}H_{43}N_3NaO_4$; calcd: 652.3151).

Chapter 4 – Investigation of Upper Rim Modified Calix[4]arenes as Potential MR Contrast Agents

A portion of this work — the synthesis of compound **4.34** — was previously published in a paper in which this compound found uses distinct from those discussed here.

Sara Tabet, Sarah F. Douglas, Kevin D. Daze, Graham A.E. Garnett, Kevin J. H. Allen, Emma M. M. Abrioux, Jeremy E. Wulff, Fraser Hof*. *Bioorganic & Medicinal Chemistry* **2013,** *21* (22), 7004-7010.

*Department of Chemistry, University of Victoria, Victoria, British Columbia, Canada

My contributions to this paper were the design, synthesis, and characterization of 5-(2,3-dimethoxyphenyl)-25, 26, 27, 28-tetrahydroxy-11-17-23-trisulfonatocalix[4]arene (**4.34**).

All work in this Chapter was conceived of and carried out by me, with the exception of some contributions from undergraduate Derek Reay who helped design and run the dye-displacement assay for EDTA and compound **4.39**.

4.1 Introduction to Calix[4]arenes

Calix[n]arenes are macrocycles formed through a condensation between "n" copies of a phenol and formaldehyde. Through careful temperature control the number of repeating phenol units can be controlled, **Figure 4.1**. Calix[4]arene presents a very interesting scaffold for contrast agent design as it offers two regions, the "upper rim" and the "lower rim" (**Figure 4.1**) which can be synthetically manipulated.[89-91] A wide variety of well-developed synthetic strategies allows for many types of symmetric and dissymmetric modifications to both the lower and upper rim of the calix[4]arene. The range of modifications possible was very attractive for contrast agent development as it would allow us a large variety of ways to tune the ligand in order to maximize the stability and relaxivity of a potential contrast agent.

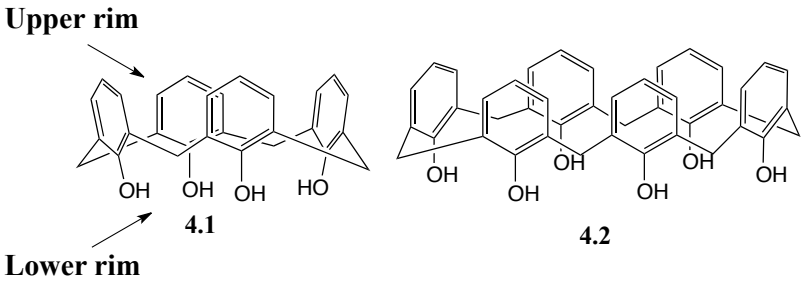

Figure 4.1: Examples of some different sizes of calixarene scaffolds; calix[4]arene (**4.1**), and calix[6]arene (**4.2**). Arrows show the naming convention for upper and lower rims

There has been some interest in using calix[4]arenes as MRI contrast agents, **Figure 4.2**. Roundhill *et al* attached acetamides to the lower rim of a *t*-butylcalix[4]arene (**4.3**), formed a complex with gadolinium, and investigated the relaxivity of the resulting complex; they concluded that the relaxivity was in the correct range for an MR contrast agent, however, it lacked water solubility and had a stability constant ($\log K_{ML}$) of only 3, which is far too low ever to be useful clinically (*see* Chapter 1).[92] Both Bryant *et al* and Botta *et al* found that a calix[4]arene modified on the lower rim to bind Gd would also non-covalently bind to the protein human serum albumin, giving a large increase in relaxivity due to the slow tumbling rate (*see* Chapter 1). However, both the Bryant compound **4.4**, and the Botta compound **4.5** also had $\log K_{ML}$ values too low (5.3 and 13, respectively) to be used in a clinical setting.[93, 94] Peters *et al* were able to ensure the

formation of a high stability Gd complex by adding 4 DOTA ligands (*see* Chapter 1) to the upper rim of a calix[4]arene via an amide bond **4.6**. Complex **4.6** does show promise as a potential contrast agent, however further optimization of the water exchange rate must be addressed to ensure maximal efficiency.[95]

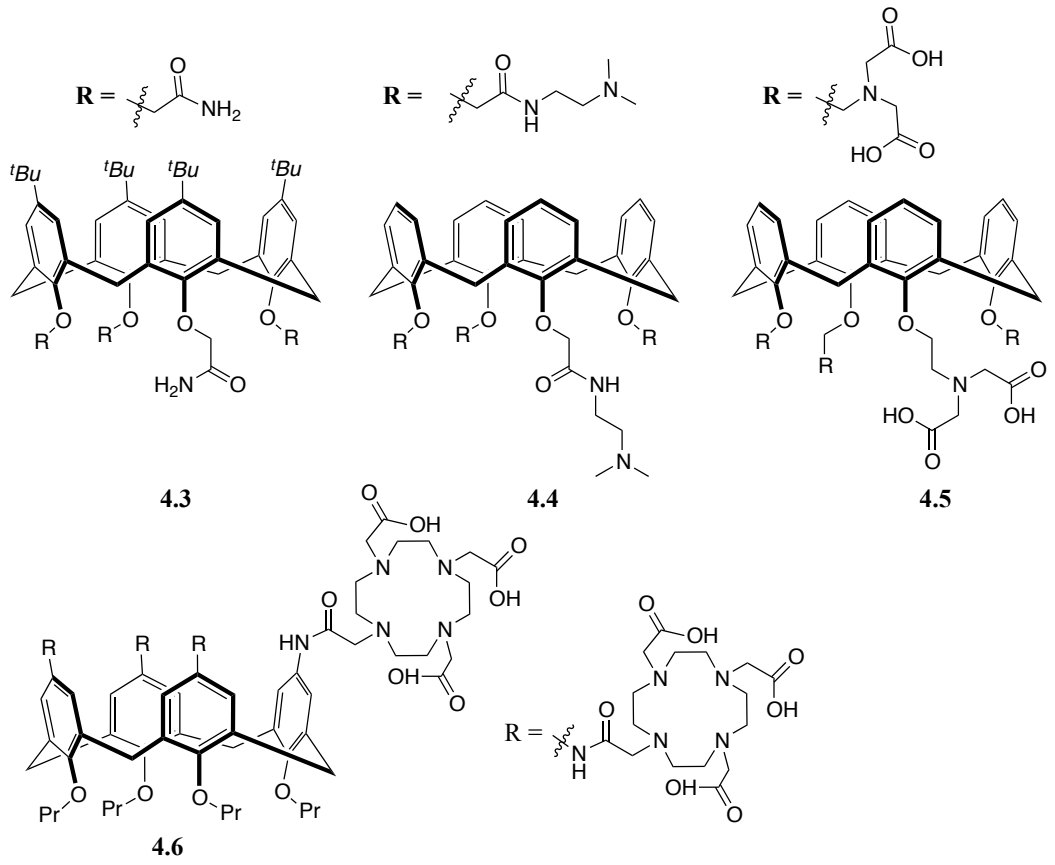

Figure 4.2: Examples of calix[4]arenes tested as MR contrast agents.

The main issues with using **4.3**, **4.4**, and **4.5** calix[4]arene gadolinium complexes as contrast agents is either their low stability constant K_{ML}, their low water solubility or both. Sulfonation of the upper rim of a calix[4]arene creates the water soluble complex *p*-sulfonatocalix[4]arene (PSC), **4.7**. PSC is a well-studied supramolecular host capable of binding a variety of organic and inorganic guests.[90, 96-99] In order for a contrast agent to be of use *in vivo* it is important that the ligand has a high LD_{50} as contrast agents are administered at high dosage (*see* Chapter 1). The LD_{50} of PSC is reported to >200 mg/kg making it very safe for *in vivo* studies.[100, 101] However, the $\log K_{ML}$ for PSC-Ln complexes

range from a low of 3.8 for Yb to a high of only 4.23 for La at pH = 2.[90] At physiological pH (pH = 7.4), the stability constant of the La complex increases to 5.3 but this is still too low for use as a contrast agent. Work by our group has shown that it is possible to modify the upper rim to include mono-, di-, or trisubstituted *p*-sulfonate groups to promote water solubility while installing a synthetic handle for functional group manipulation on the non-sulfonated phenolic rings, **Figure 4.3**. Through the use of the Suzuki coupling reaction, our group was then able to install a large variety of functional groups, in order to make a diverse library of water soluble calix[4]arene hosts capable of selective recognition of the different methylation states of lysine.[102, 103]

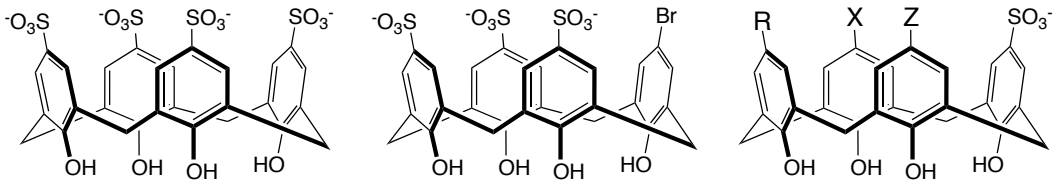

Figure 4.3: Structures of sulfonated calix[4]arenes.

None of these sulfonated hosts were designed to provide the strong chelation of a lanthanide ion that is required for a MR contrast agent. I was interested in using the pre-organized calix[4]arene scaffold to append multiple lanthanide chelates to the upper rim where they could function cooperatively to form a highly stable Ln-calix[4]arene complex. By leaving the lower rim unmodified we hoped to exploit the exchangeable phenolic protons as a secondary pool of protons in a CEST mechanism (*see* Chapter 1). The following chapter will discuss the synthesis of several novel calix[4]arenes and examine their K_{ML} either by NMR titration or through a dye-displacement assay, to determine their viability as MR contrast agents.

4.2 Catechol Functionalized Calix[4]arenes

Catechol containing compounds can be found throughout the literature and have a wide range of uses. Catecholamines are biosynthesized from amino acid precursors (either L-phenyl alanine or L-tyrosine) via a series of enzymatic processes. The most abundant in the human body are L-DOPA (**4.11**), dopamine (**4.12**), L-adrenaline (**4.13**), and L-noradrenaline (**4.14**), **Figure 4.4**.[104] These small molecules act as neurotransmitters and play vital roles in biological processes. Vanillin (**4.15**) is used as a cheaper, synthetic, alternative to natural vanilla (which contains vanillin as well as many other compounds). Eugenol (**4.16**), safrole (**4.17**), and piperonal (**4.18**) are heavily used fragrances in the perfume industry.[105] These are just a few of the naturally occurring compounds containing catechol functionality that have found significant uses in everyday life.

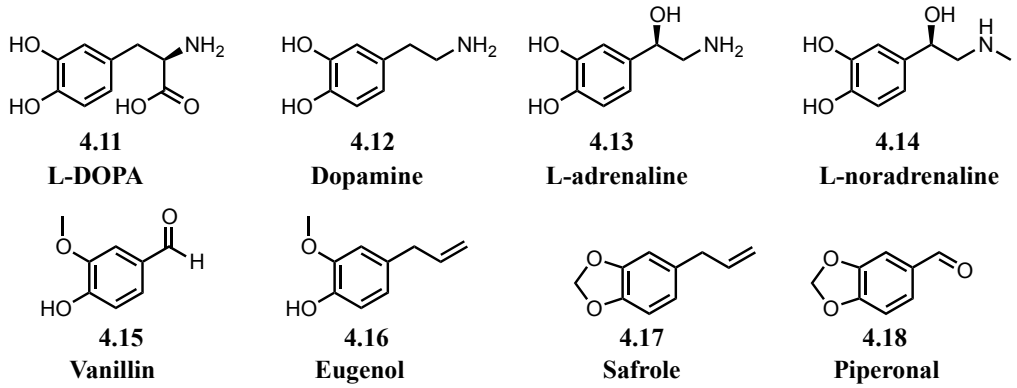

Figure 4.4: Catechol containing compounds

Another facet of catechol chemistry is their use in metal chelation. Catechol itself is a bidentate ligand capable of complexing a wide range of metals.[106, 107] However, by designing a ligand with multiple catechol moieties, more thermodynamically stable tetra (**4.19**) and hexa-coordinate (**4.20**) ligands can be formed, **Figure 4.5**.[108, 109] Catechol based ligands have shown a good affinity for binding transition metals, as well as lanthanides and actinides.[107] Haino *et al* attached catechols to the upper rim of a calix[4]arene via an amide bond to form **4.21** that showed formation of clathrates with various solvents.[110] Compound **4.21** lacked any water solubilizing functionalities and the catechol groups were not in an ideal position to bind lanthanide ions cooperatively.

Lemaire *et al* showed that attaching two catechol containing moieties to the lower rim of a *p*-sulfonatocalix[4]arene, **4.22,** afforded a water soluble calix[4]arene capable of strongly binding UO_2^{2+}.[109] These authors found a $\log K_{ML}$ of 16.3 and 20.2 at pH 7.4 and 9.0, respectively, for **4.22**. These $\log K_{ML}$ values are near what is needed for a contrast agent (*see* Chapter 1). With this in mind we wanted to probe how appending multiple catechol groups to the upper rim of a water soluble calix[4]arene scaffold would affect lanthanide binding in hopes of creating a highly stable, water soluble, calix[4]arene contrast agent. Existing methodology allows for de-symmetrisation of the upper rim of a calix[4]arene, incorporating varying numbers of sulfonate groups that allow for water solubility, while including aryl-bromide groups that facilitate Suzuki coupling with aryl boronic acids and esters, **Scheme 4.1**.[102]

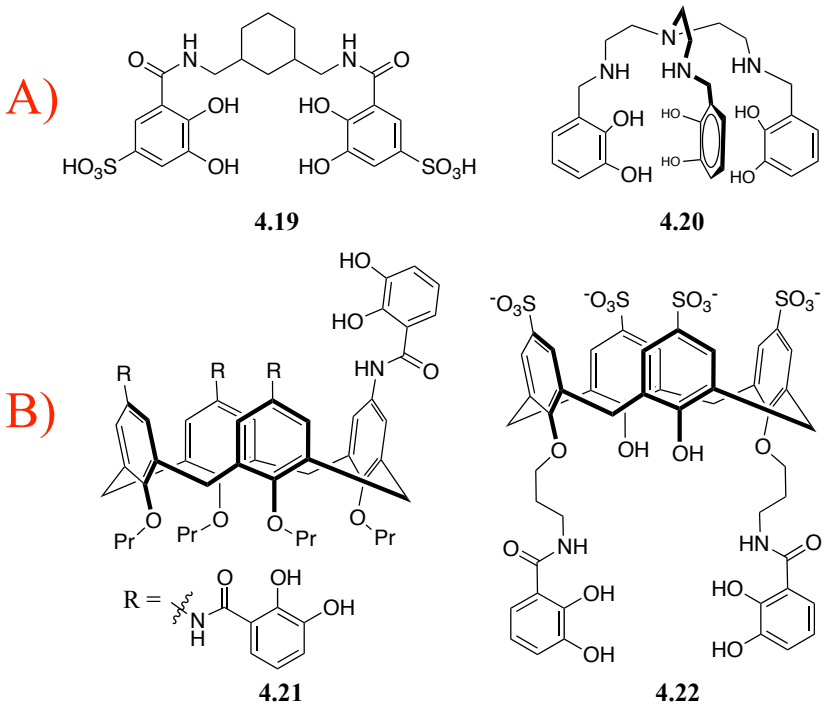

Figure 4.5: A) Examples of catechol based ligands used for lanthanide and actinide complexation. **B)** Calix[4]arenes containing catechol moieties.

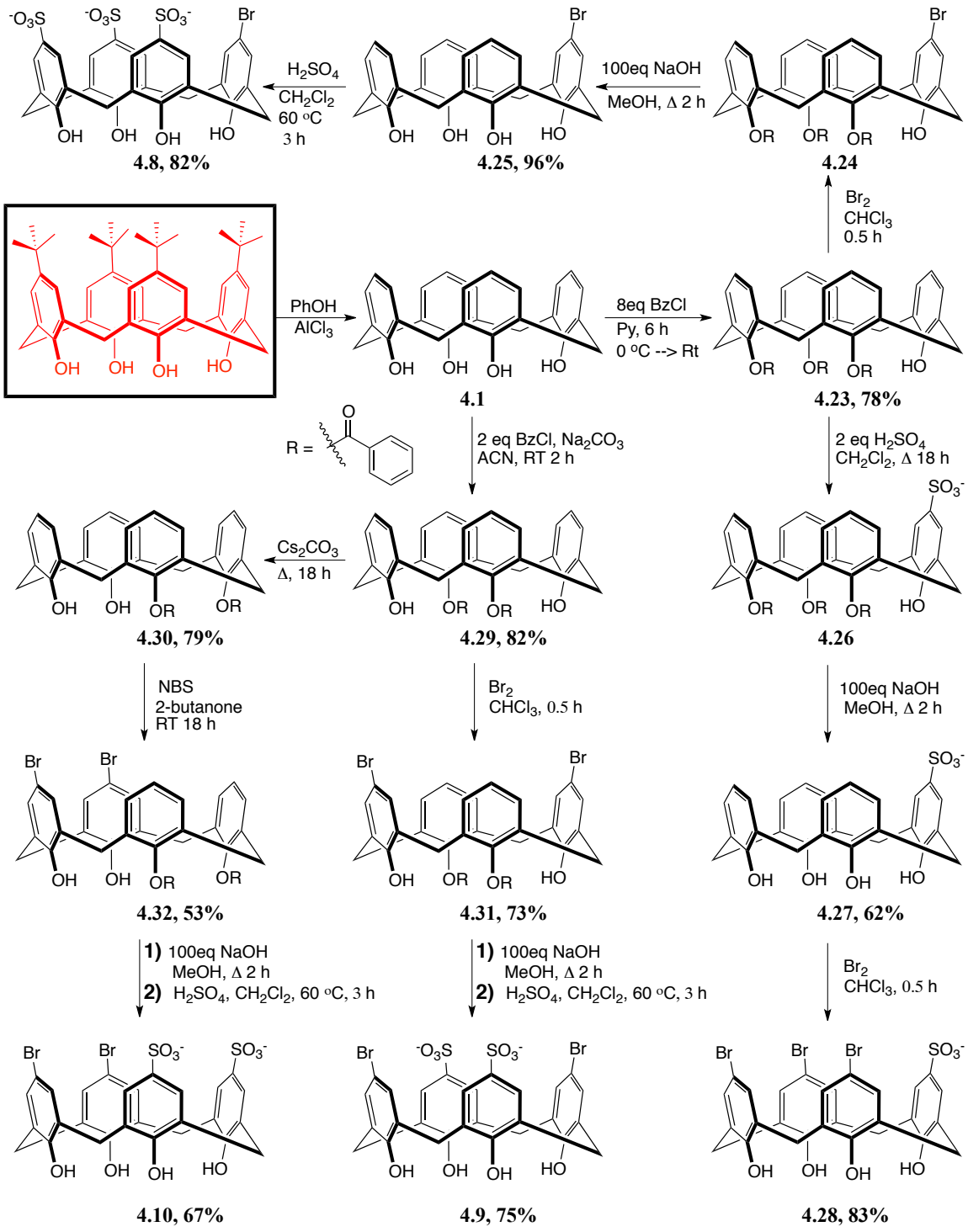

Scheme 4.1: Synthesis of various brominated, sulfonated calix[4]arenes. Calix[4]arenes **4.9**, **4.10**, and **4.28** and precursors were synthesized by Kevin Daze.

A condensation reaction between *t*-butyl phenol and formaldehyde followed by a Friedel-Crafts dealkylation to remove the *t*-butyl group from *t*-butylcalix[4]arene gave

4.1 on a 50 g scale.[111, 112] Esterification of the lower rim in the presence of 8 equivalents of benzoyl chloride yielded the tri-esterified calix[4]arene **4.23** in high yield.[113] Only three of the phenolic groups were protected due to the steric bulk of the benzoyl protecting group. The aromatic rings of the esterified phenol are deactivated relative to the non-esterified ring, allowing for selective functionalization of the upper rim of the calix[4]arene. Treating **4.23** with bromine (**4.24**),[114] followed by deprotection of the ester groups (**4.25**),[115] and sulfonation[102] allowed for the formation of **4.8** on multi-gram scale. Alternatively, if **4.23** is sulfonated first (**4.26**), followed by ester deprotection (**4.27**) and bromination, **4.28** can be made, allowing for three simultaneous Suzuki couplings. If only two equivalents of benzoyl chloride are added during the esterification step, calix[4]arene **4.29** is formed. Either by scrambling the ester groups (**4.30**) or proceeding via the chemistry outlined above, compounds **4.9** and **4.10** were accessible.

Using established calixarene-Suzuki chemistry[102] it was then possible react (2,3-dimethoxyphenyl)boronic acid with **4.8** to form compound **4.33**, suspending this compound overnight in 1 M BBr_3 (CH_2Cl_2 solution) allowed for removal of the methyl groups to give an unprotected, catechol-functionalized, calix[4]arene, **4.34**, in a 30% yield after HPLC purification, **Scheme 4.2**. Using this method we hoped to generate a series of catechol complexes starting from **4.9, 4.10,** and **4.28** to generate **4.35, 4.36,** and **4.37**, in order to determine how each additional catechol unit would affect the stability constant, **Figure 4.6.**

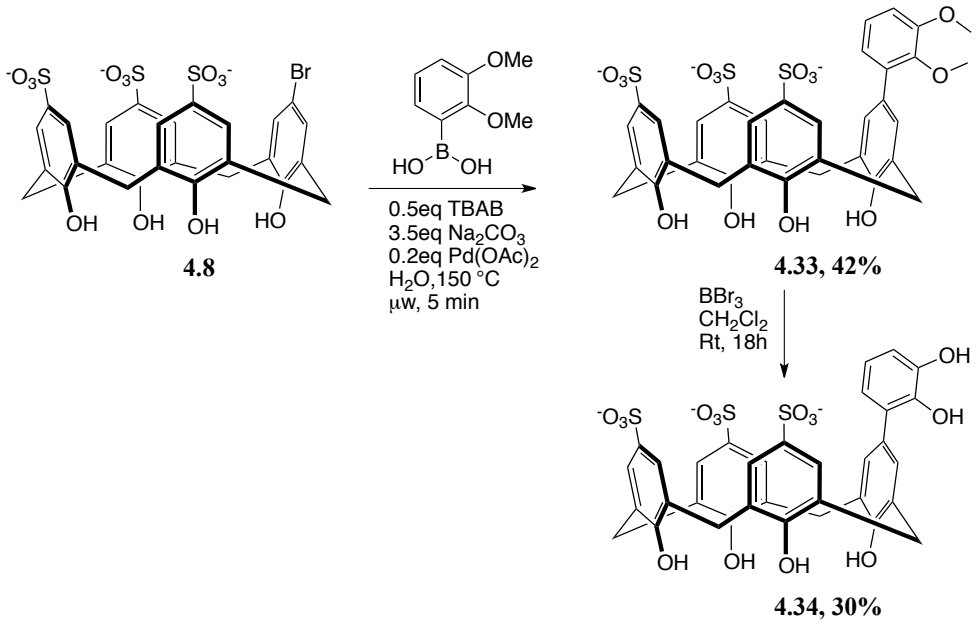

Scheme 4.2: Synthesis of 5-(2,3-dihydroxyphenyl)-25, 26, 27, 28-tetrahydroxy-11-17-23-trisulfonatocalix[4]arene, **4.34**.

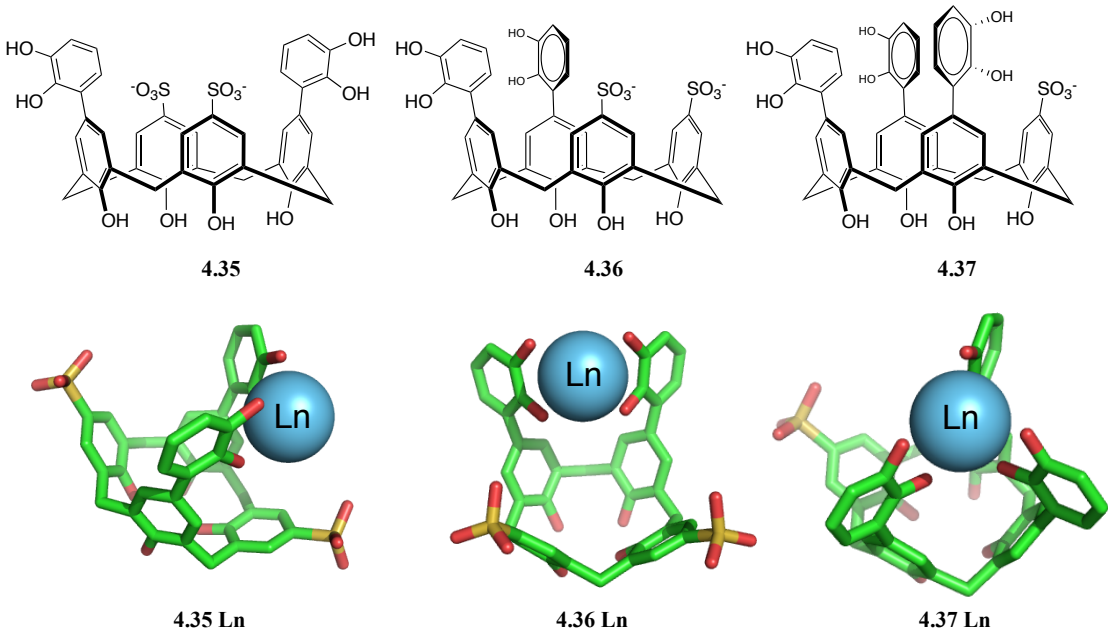

Figure 4.6: Catechol-based calix[4]arenes with Spartan equilibrium geometry models calculated using molecular mechanics, MMFFaq.

4.2.1 NMR Titration of 4.34

Binding constants can be determined in a number of ways. Potentiometric titrations, isothermal titrations, dye displacement assays, and NMR titrations are some of the more common methods. NMR titrations are an effective way to determine binding constants of intermediate strength. If the binding is too strong a square curve is generated by the NMR method preventing meaningful numbers from being extracted. As we did not expect extremely high binding from the incorporation of one catechol unit, we thought this would be a good method to establish a starting point for the K_{ML} values of our catechol functionalized calix[4]arenes.

To determine a meaningful K_{ML} value from an NMR titration, the ligand concentration and pH must remain constant as the metal is added. A stock ligand (**4.34**) solution was made using a 50 mM sodium acetate buffered D_2O solution (pD 7.8). A portion of this was placed in a NMR tube and a portion was added to a known amount of $YCl_3 \bullet 6H_2O$ (**8** equivalents). The metal containing solution was slowly titrated into the NMR tube and the effects of metal chelation were observed, **Figure 4.7**. It was noted that as the titration proceeded the solution changed from colourless to green to black and the intensity of the ^1H NMR peaks slowly decreased. It appears that **4.34** decomposes as it remains in solution. No additional signals were observed in the ^1H NMR as the decomposition proceeded suggesting that the decomposition product is insoluble. The NMR tube was observed 1 week later and a brown-black precipitate was present on the bottom with a colourless solution above. The same decomposition effect was noted when **4.34** was dissolved in distilled water and buffered water, both with and without the metal present, although decomposition occurred more slowly without the metal ion present. Catechols are known to undergo oxidation to benzosemiquinone radicals.[116] A possible explanation for the loss of signal strength is that this radical species undergoes decomposition to form an insoluble product. Since the concentration was changing during the titration, it was not possible to calculate a meaningful stability constant. Based on how **4.34** behaved in solution we decided to forgo making any further catechol-based calix[4]arenes and moved on to other functionalized calix[4]arenes.

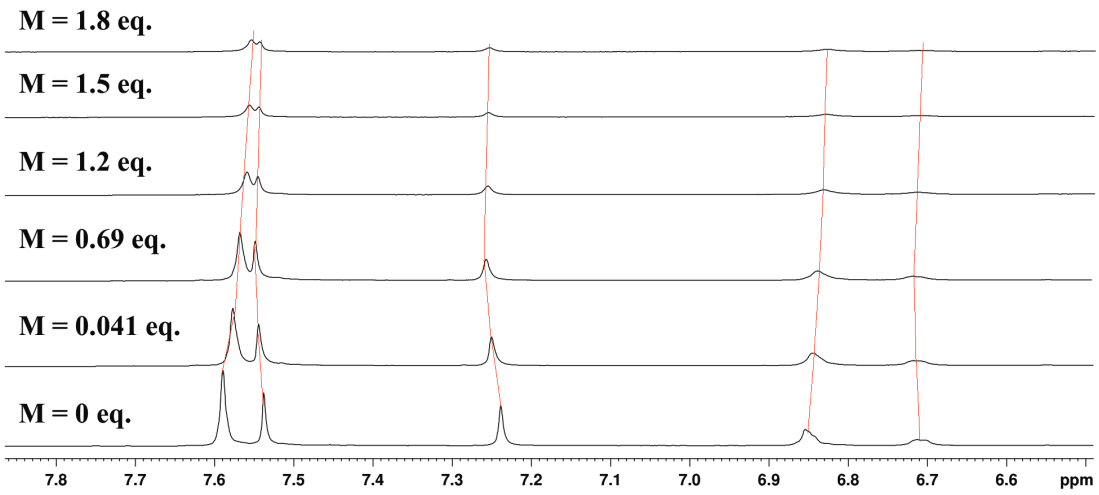

Figure 4.7: Titration data for **4.34** showing the change in peak location upon addition of various equivalents of metal, M = $YCl_3 \bullet 6H_2O$

4.3 Iminodiacetic Acid Functionalized Calix[4]arenes

Iminodiacetic acid (IDA), **4.38**, like nitrilotriacetic acid, **3.7** (used to form compound **3.15b**) is an effective metal chelator incorporating an amine with carboxylic acid appendages. However, with only two carboxyl groups present it can only form a tridentate ligand as opposed to a pentadentate ligand as seen with **3.7**. The benefit of using a secondary amine (**4.38**) over the tertiary amine (**3.7**) is that the nitrogen is still open for functionalization. IDA has been attached to many different supports (silica gel, AN-DVB, PBA, GMA, etc.) and has shown effective sequestration of many different metals (Cd, Co, Cr, Cu, Hg, Ni, Pb, and Zn) from wastewater.[117, 118] An interesting use of IDA lanthanide chelation, given by Swarbrick *et al*, demonstrates how a thiol-modified IDA can be attached to a protein through a disulfide bond with an exposed cysteine residue and used as a tag in paramagnetic NMR exchange spectroscopy.[119] For this technique the issue with previous lanthanide tags was that they bound the ions too strongly and did not allow for observation between the bound and unbound state (which is required); the weaker binding of the IDA ligand allowed for the faster exchange needed. This weaker binding is expected from IDA ligands as they are only tridentate, however, we believed that if multiple IDA groups were incorporated onto an appropriate scaffold, the IDA appendages could function together to strongly bind lanthanide ions

and be potentially useful as an MR imaging agent. We proposed that the calix[4]arene scaffold would be ideally suited for IDA incorporation and should generate a highly chelating ligand which can be used to strongly bind lanthanide ion, **Ln-4.39**, **Figure 4.8**.

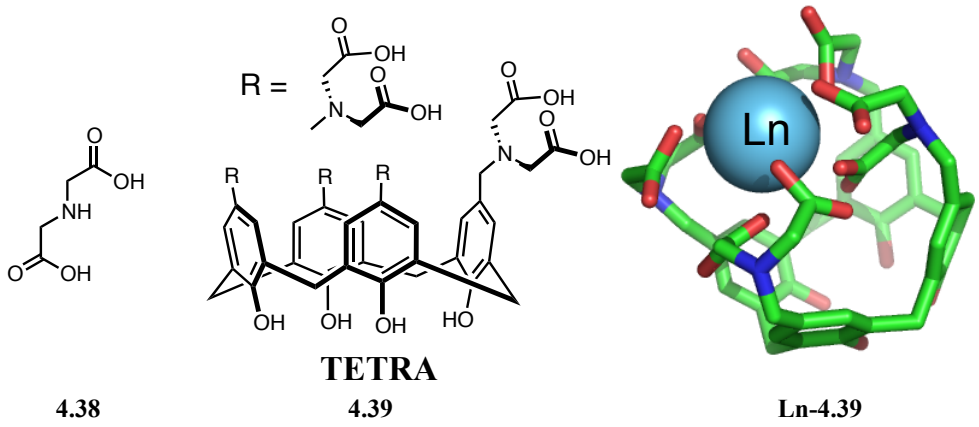

Figure 4.8: Proposed IDA-Calix[4]arene **4.39** and its lanthanide complex **Ln-4.39**.

Amine functionality can be installed on the upper rim of a calix[4]arene by a number of synthetic routes,[102, 120-122] however no examples exist of an upper rim IDA functionalized calix[4]arene. The most direct route to inserting the IDA group is using a Mannich reaction. This involves formation of an iminium ion that then reacts at the *para* position of the phenol ring of the calix[4]arene to form a aryl-carbon bond. Unfortunately, due to the limited solubility of IDA in organic solvents it was not possible to form the IDA iminium ion directly. Diethyl iminodiacetate, **4.40**, an esterified analogue of IDA, which is soluble in organic solvents was used to form the iminium ion, **4.41**. This ion could then react with the calix[4]arene **4.1** and form compound **4.42**. In order to ensure complete substitution it was found that the reaction had to be carried out in a sealed vessel, at least 20 equivalents of the iminium ion had to be used, and the ion had to be allowed to form prior to addition of calix[4]arene **4.1**. To remove the excess iminium ion, it was first hydrolyzed back to **4.40** and formaldehyde (by acid/base extraction). Compound **4.40** could then be removed via distillation under reduced pressure to give **4.42** as a viscous yellow oil. Cleavage of the ester groups under basic conditions, followed by precipitation with TFA gave the tetra substituted calix[4]arene (**TETRA**) **4.39** in a 17% yield, **Scheme 4.3**.

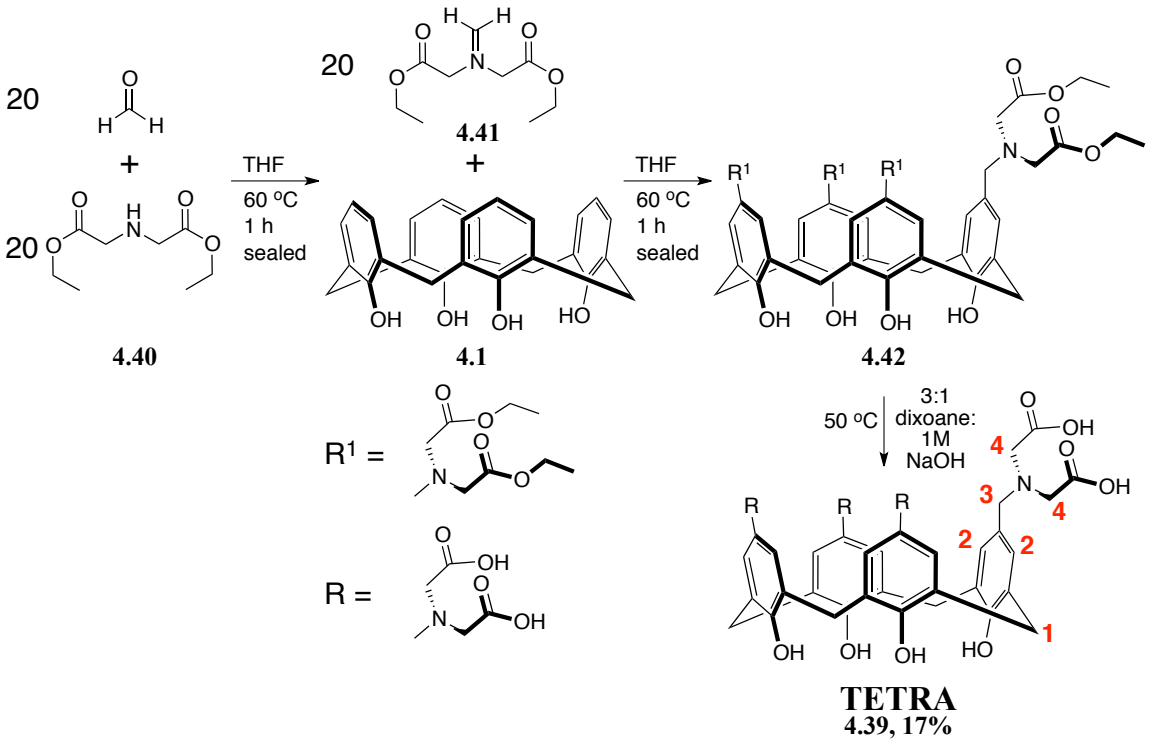

Scheme 4.3: Synthesis of tetra-substituted IDA calix[4]arene, **4.39**, **TETRA**

4.3.1 NMR Titration of 4.39

In order to determine the stability constant of **4.39**, ^{1}H NMR titrations were performed in a similar fashion to the catechol functionalized calix[4]arene, **4.34**, described above. An 11.5 mM ligand solution was prepared in 100 mM ammonium acetate buffer (pD 8.35). A portion of this was separated and 10 equivalents of $LaCl_3 \bullet 6H_2O$ were added; upon addition of the metal a white precipitate formed. Initially, it was thought that this was $La(OH)_3$ which is highly insoluble in water, however, when the $LaCl_3 \bullet 6H_2O$ was added to a solution only containing the buffered solution no precipitate formed. We suspected that addition of the metal salt may have altered the pD to a level where the ligand was no longer soluble, however, no change in pD was detected by glass electrode pH/pD measurements. To see if any binding could be observed qualitatively, a buffered solution containing only $LaCl_3 \bullet 6H_2O$ (and no ligand) was added to a buffered ligand solution. After 0.1 equivalents of metal was added (1 aliquot) the solution became cloudy and no changes in chemical shifts were observed in the ^{1}H NMR spectrum. We suspect that a coordination polymer is forming when the metal is added, although we would

expect the 1:1 complex to be more thermodynamically favoured. In an attempt to convert the suspected polymer to the 1:1 complex (**4.39**), we heated the precipitate to 60 °C for 72 h in D_2O but the ^1H NMR spectrum failed to show any changes, **Figure 4.9 A & B**. We could not heat the solution beyond 60 °C as VT ^1H NMR showed that at higher temperature compound **4.39** began to decompose (**Figure 4.9 C, D, & E)**. The difficulty encountered in using NMR titrations for the determination of the stability constant led us to use a dye displacement assay developed by Sherry *et al*,[123] the results of which will be discussed in **Section 4.5**.

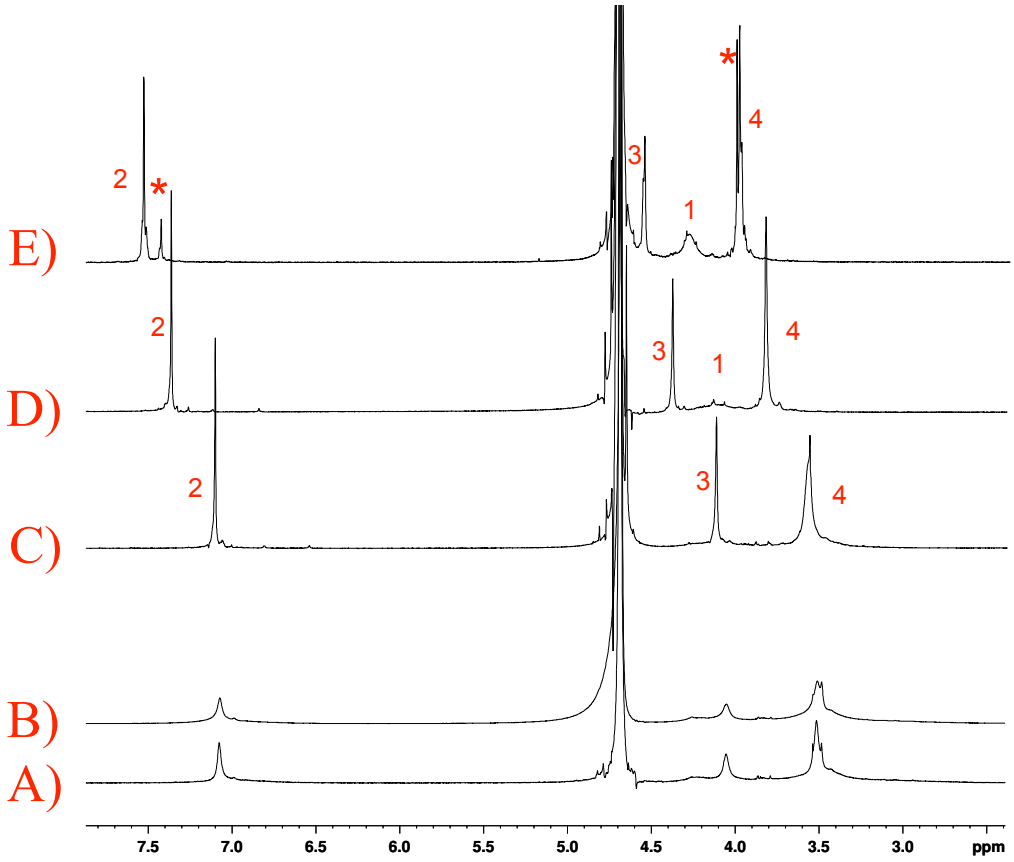

Figure 4.9: ^1H NMR spectrum of **4.39**: **A)** in 100 mM ammonium acetate buffered D_2O before addition of $LaCl_3 \bullet 6H_2O$ **B)** after addition of 0.1 equiv. $LaCl_3 \bullet 6H_2O$. **C)** RT NMR of **4.39** in D_2O (pH ≈ 10) due to the highly fluxional behaviour of 4.39 the methylene protons are not visible at RT. **D)** VT ^1H NMR at 57 °C revealed a broad signal at corresponding to the methylene proton peaks (1). **E)** Heating above 70 sharpened the broad signal (1), however, a decomposition product was observed (*). See **Scheme 4.3** for labelling. Spectra **A** and **B** were run on a 300 MHz NMR spectrometer, **C**, **D**, and **E** were run on a 500 MHz NMR spectrometer.

4.4 Cyclen Functionalized Calix[4]arenes

Cyclen (**1.8**) based, gadolinium-centered, contrast agents (**Figure 4.10A**) are among the most popular commercially available agents. The sales of Dotarem, **4.43**, for example, were over $200 million in 2011. The reason for their popularity is that cyclen-based MRI contrast agents have a very good safety profile due to their high thermodynamic stability constants that arises from the more rigid macrocyclic core (*see* **Table 1.1**). There has been a large amount of interest in modification of the nitrogen appendages attached to the cyclen ring to generate novel MR contrast agents some examples of which are given in **Figure 4.10B**.[124-127]

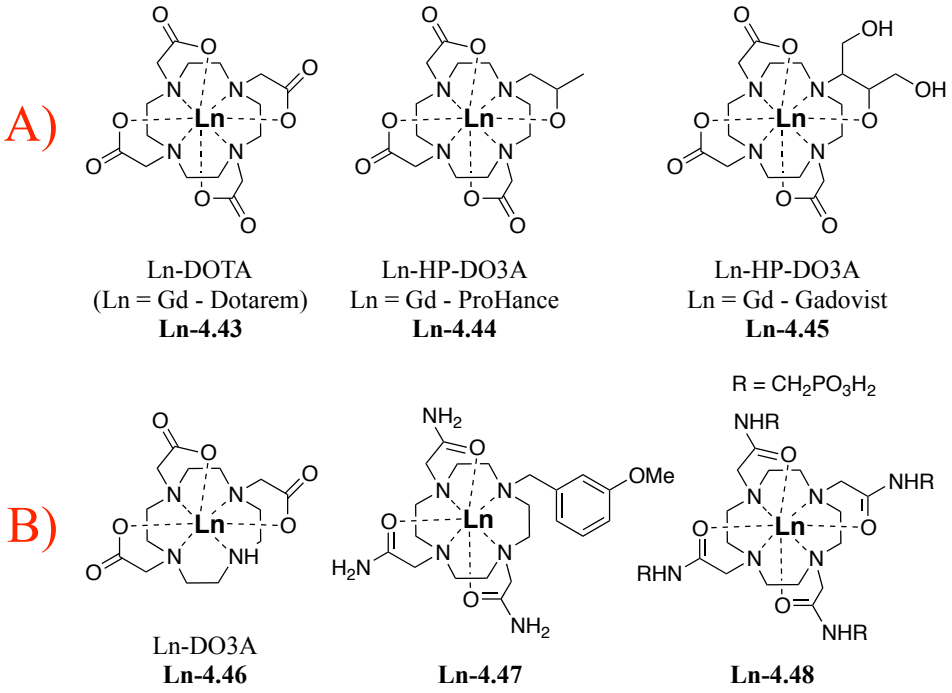

Figure 4.10: **A)** Commercially available cyclen-based MR contrast agents. **B)** Modified cyclen-based potential contrast agents.

Altering the functional groups attached to the cyclen amines can have a wide range of effects but it is of vital importance that these groups remain strong lanthanide chelators in order to maintain a high stability constant. Incorporation of amide groups onto the cyclen ring (**4.47, 4.48**) has allowed for the creation of a cyclen-based, thermodynamically stable, paraCEST contrast agent (*see* Chapter 1 for paraCEST explanation).[6] A popular

method for modification of the cyclen ring is sacrificing one of the chelate arms to give DO3A, **4.46**. DO3A has high stability constant ($\log K_{ML} = 21.0$)[125] and the free secondary amine allows for simple incorporation of a wide variety of functional groups that allow tuning of the potential contrast agents as desired, while still maintaining the high stability associated with the cyclen core.[125, 126, 128, 129]

We were interested in attaching a DO3A type ligand to the *p*-sulfonatocalix[4]arene scaffold to see if we could make a highly water soluble, strongly chelating, MR imaging agent. Using a sulfonated calix[4]arene to gain water solubility would allow us to leave the lower rim phenols unfunctionalized in the hope that the phenolic protons could serve as the secondary pool of protons in a paraCEST mechanism. Several examples of cyclen functionalized calix[4]arenes exist in the literature, **Figure 4.11**. König *et al* used Buchwald-Hartwig amination to attach a BOC protected cyclen ligand to a calix[4]arene, **4.49**.[130] The calix[4]arene they used was completely protected on the lower rim and the upper rim contained no other water solubilizing functionalities. Previous attempts in our group to use the Buchwald-Hartwig amination on calix[4]arenes **4.8** proved unsuccessful indicating that a different synthetic route would be required for installation of the DO3A appendage. The previously mentioned Peters ligand (**4.6**) attached 4 DOTA ligands to the upper rim of calix[4]arene by an amide bond.[95] Amide formation on a trisulfonated calix[4]arene was not known when this this project began but Kevin Daze has recently shown that by using **4.51** and an acid chloride (**4.52**) it is possible to form an amide bond, **4.53 (Scheme 4.4).** Unfortunately there are no literature examples of a DOTA type ligand with one appendage as the acid chloride (**4.50**).

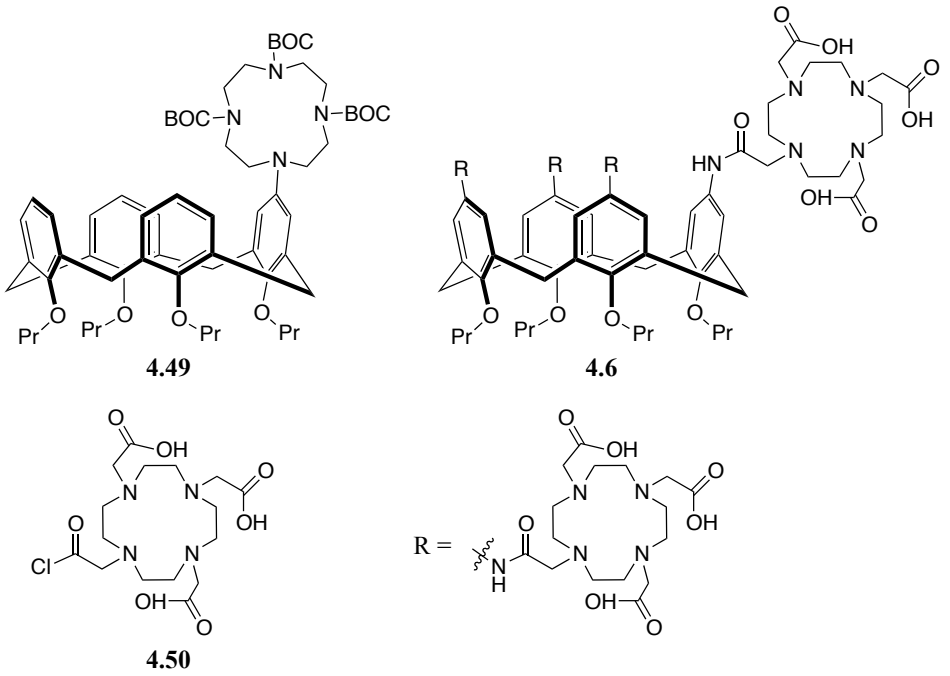

Figure 4.11: Cyclen functionalized calix[4]arene **4.49** and **4.6**

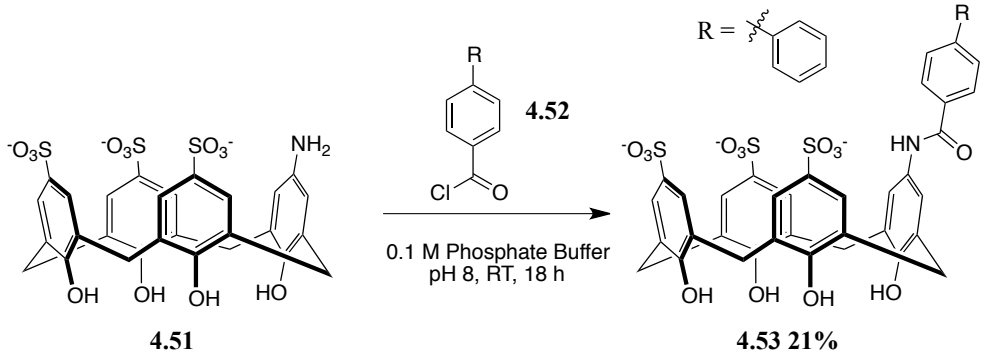

Scheme 4.4: Synthesis of amide-containing trisulfonated calix[4]arene, **4.53**, prepared by Kevin Daze

To attach the cyclen ligand to a trisulfonated calix[4]arene we envisioned using a cyclen functionalized aryl boronic acid and coupling it to **4.8** using the established calix[4]arene-Suzuki chemistry.[102] Using literature precedent, DO3A t-butyl ester **4.54** was alkylated using 4-bromomethylphenylboronic acid pinacol ester, **4.55,** to form the boronic acid pinacol ester **4.56** (Scheme 4.5). Removal of the *t*-butyl groups under acidic condition, gave the desired compound **4.57** in a 65% yield.[131] In a successful calix[4]arene-Suzuki coupling, the reaction mixture typically changes from a light orange

to a dark black colour whereas unsuccessful couplings usually remain orange. Mixing **4.8** and **4.57** in water while using the previously mentioned calix[4]arene-Suzuki coupling conditions (*see* **Scheme 4.2**) showed no colour change suggesting the reaction failed. Purification of this mixture by HPLC/MS showed no desired product mass, however, 8 mg of a UV-active compound containing a palladium isotope pattern was isolated, HR-ESI-MS revealed this compound to be **4.58**. As the reaction occurs the DO3A portion of the ligand acts as a palladium scavenger removing the catalyst causing the catalytic cycle to terminate. This was unexpected, it had been previously shown that resin bound DOTA does not bind palladium and is a very ineffective as a scavenger ligand.[132] The MS isotope pattern revealed that it was a 1:1 ratio of Pd to complex, to compensate for the loss of Pd during the reaction 1.3 equivalents of $Pd(OAc)_2$ catalyst was added to exclusively form the palladium containing complex **4.58**. It was found that by adding 10 equiv. of thiourea to the finished reaction and heating the mixture to 60 °C overnight, the thiourea would bind the Pd and the resulting complex precipitated from the solution. Filtration of the soluble portion and HPLC purification gave the desired DO3A-calix[4]arene complex (**PCC**) **4.59** in a 24% yield, **Scheme 4.5**.

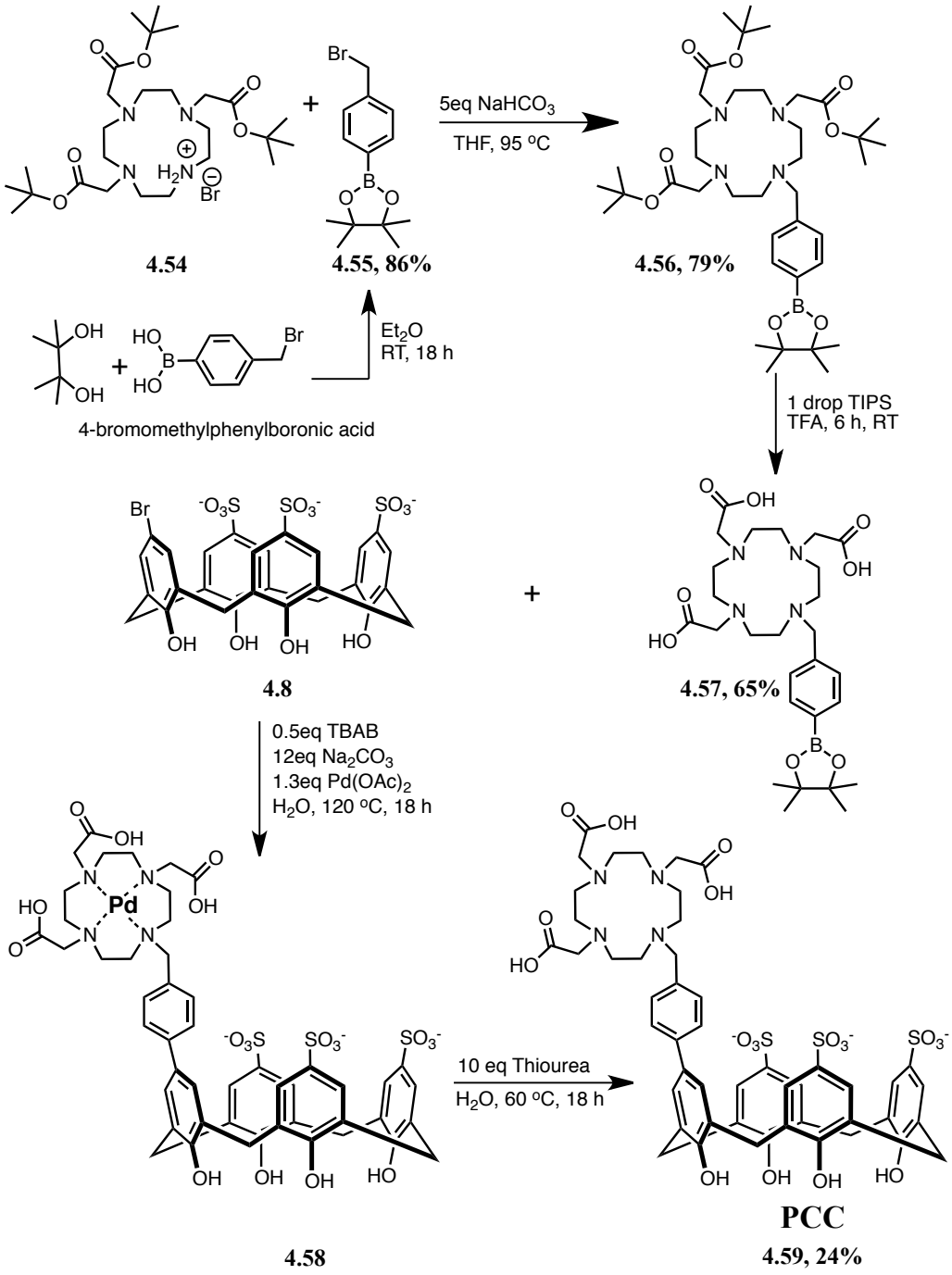

Scheme 4.5: Synthesis of DO3A functionalized trisulfonated calix[4]arene, **4.59**.

We were interested in probing how placement of the DO3A ring would affect the strength of metal binding. Movement of the cyclen moiety may dictate whether the sulfonate groups on the calix[4]arene scaffold play a role in metal chelation. Using 3-bromomethylphenylboronic acid in place of 4-bromomethylphenylboronic acid and

following the chemistry outlined in **Scheme 4.6** we were able to generate a *meta*-substituted analogue of **4.59**, **4.60** (**MCC**) in a 20% yield, **Figure 4.12**. Compounds **4.59** and **4.60** were soluble under basic conditions, however, their solubility decreased substantially around pH 5. Synthesis of this ligand class was confirmed by HR-ESI-MS coupled with ^{1}H NMR. Much like the IDA-based calix[4]arene (**4.39**) previously discussed, **PCC** and **MCC** are highly fluxional in solution. VT ^{1}H NMR at 95 °C was required to collect a meaningful spectrum, **Figure 4.13**. The purity was determined to be >97% by reinjection of a 50 µM solution of the compound onto a HPLC/MS equipped with Phenomenex Luna C18 analytical column.

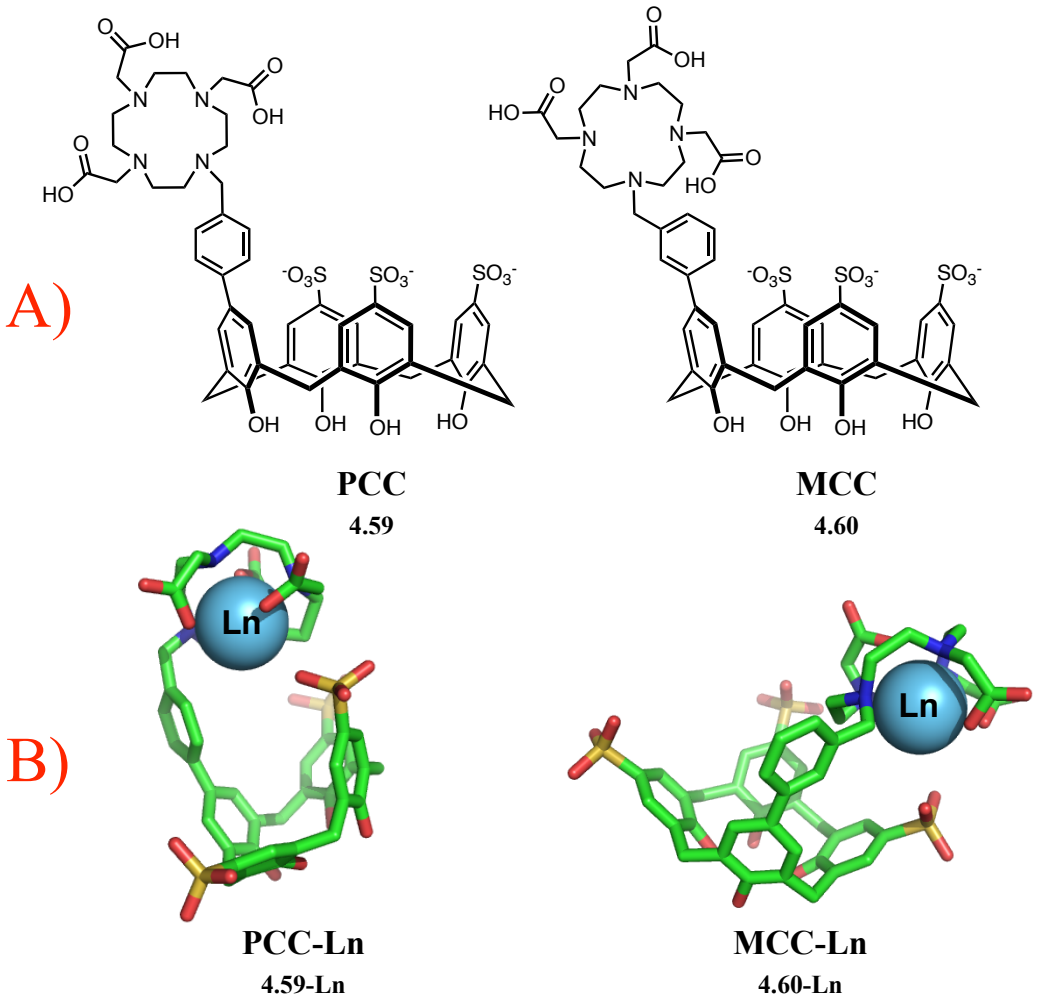

Figure 4.12: A) DO3A base calix[4]arenes **PCC** (**4.59**) and **MCC** (**4.60**) **B)** Spartan equilibrium geometry models calculated using molecular mechanics, MMFFaq of **4.59-Ln** and **4.60-Ln**

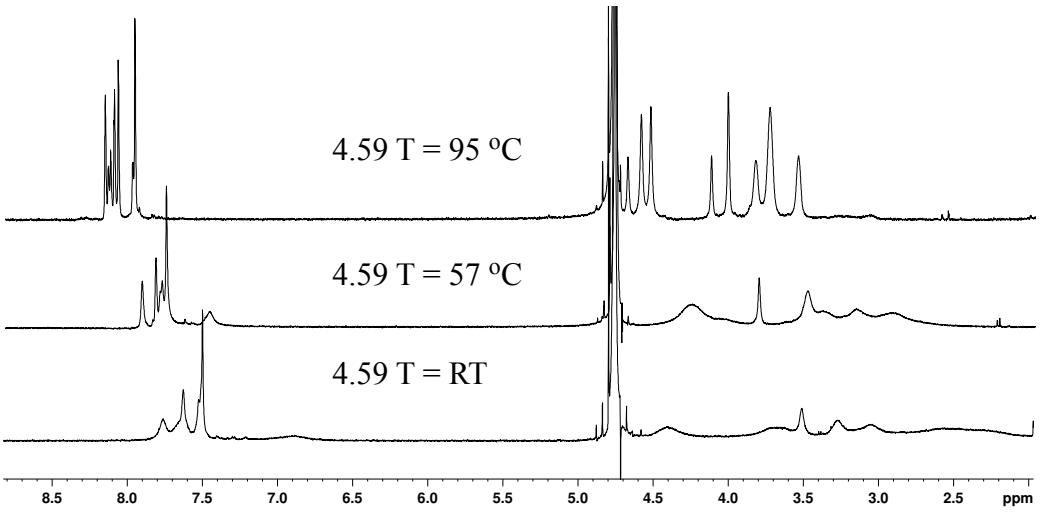

Figure 4.13: ^{1}H NMR spectrum of **4.59**

To determine if metal binding could be observed by ^{1}H NMR, $LaCl_3 \bullet 6H_2O$ was added portion-wise in 0.1 equivalent aliquots to ligand solutions of **4.59**, and **4.60** in 100 mM ammonium acetate D_2O buffer at pD 8.4 and pD 4.0. Both cases resulted in a cloudy solution after about 0.3 equivalents of $LaCl_3 \bullet 6H_2O$ had been added. As the addition proceeded the white precipitate became more prevalent. The same result was also observed for $GdCl_3 \bullet 6H_2O$. Both metals were tested in a buffer solution containing no ligand to determine if a precipitate formed but none was observed. It was suspected that a similar coordination polymer as that seen in the case of ligand **4.39** (TETRA) was forming. To see if the suspected polymer could be driven to the more thermodynamically stable 1:1 complex, the solution containing the white precipitate was heated at 90 °C for 72 h but unfortunately no change was seen. To test if Gd was bound by the DO3A ring at physiological pH, **4.59** (PCC) was added to water and the pH was adjusted to 7.4. 1 equivalent of $GdCl_3 \bullet 6H_2O$ was then added and again a white precipitate formed. The pH was readjusted to 7.4 and the suspension allowed to stir for 3 days to equilibrate. After 3 days the precipitate remained so several drops of DMSO were added to solubilize the white precipitate and the solution was allowed to stir for 3 more days. A LR-ESI-MS confirmed the presence of Gd-**4.59**. This result confirmed that it is possible to bind a lanthanide ion with ligand **4.59**; however the difficulties with the NMR titration made it clear that the stability constant had to be determined by a different method. It was

decided that a dye displacement assay, used by Sherry *et al*[123] would be ideal for the determination of the stability constant of **4.59** and **4.60**.

4.5 Binding Constant Determination by Dye Displacement

Due to the relatively high concentration needed for NMR titrations, the large binding constants expected, and the desire to test ligand binding with paramagnetic lanthanide ions that could broaden the NMR signals into the baseline, this method was not ideal for the determination of stability constants. Sherry *et al* demonstrated that an Arsenazo III (**4.61**, **Figure 4.14**) dye displacement assay allowed for the determination of large stability constants of lanthanide complexes.[123] There are several benefits to this method: 1) The dye-lanthanide complex has a large molar extinction coefficient for the 1:1 and the 2:1 species (35,000 and 50,000 $M^{-1}cm^{-1}$) meaning that stability constants can be determined at very low concentrations which should help eliminate polymer formation observed with NMR titrations; 2) There is no magnetic field required to collect a UV-VIS spectrum so there will be no complications from paramagnetic lanthanide ions as seen in NMR; 3) Incorporation of a plate reader allows for a more efficient, high throughput method for determination of stability constants.

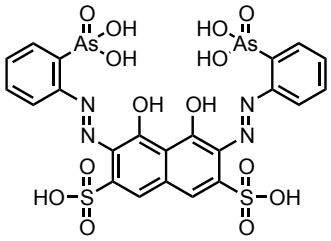

4.61

Figure 4.14: Arsenazo III dye (D) used for dye displacement assay.

By having a ligand with an unknown stability constant compete for lanthanide complexation with the dye-lanthanide complex (**Figure 4.15A**), the resulting UV-VIS spectrum can then be fit to a competitive binding model to give a pH dependent stability constant, K^{c}_{ML}, provided that K^{c}_{MD} of the dye-lanthanide complex is known. K^{c}_{ML} can then be converted to the pH independent stability constant K_{ML} if the stepwise protonation

constants (K_n) of the ligand are known, **Equation 4.1**. The UV response of Arsenazo III is known to be pH and ionic strength sensitive,[133, 134] as such it is very important that there is no change during the assay and the dye must be placed in a buffered water solution (100 mM ammonium acetate). The dye-metal complex exists in solution as an equilibrium between the free dye, a 1:1 dye-metal complex, and a 2:1 dye-metal complex, each with their own unique absorbance and stability constants, **Figure 4.15B**. Literature conditional stability constants were reported for pH = 4, however, due to ligand solubility concerns we decided to run our assay at pH = 8.35. To determine the conditional stability constants of the 1:1 ((K_{11}^c) and 2:1 (K_{12}^c) dye-metal complex, a direct metal titration was performed by adding varying equivalents of lanthanide ions (0-3 equivalents, 0-30 µM, 100 mM ammonium acetate buffer) to a stock dye solution (10 µM) and recording their absorbance spectrum over a 350 nm – 750 nm range, **Figure 4.16**.

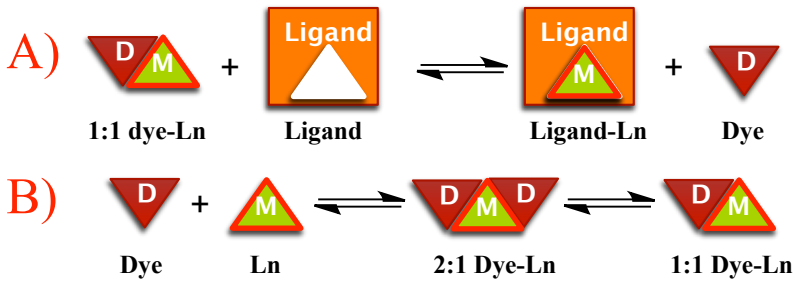

Figure 4.15: Cartoon depicting **A)** Dye displacement by a ligand. **B)** Equilibrium between Arsenazo III (**D**) and lanthanide (**M**).

$$K_{ML} = K_{ML}^{c}\alpha_H$$

$$\alpha_H = 1 + K_1[H^+] + K_1K_2[H^+]^2 + \ldots + K_1K_2\ldots K_n[H^+]^n \qquad \textbf{(4.1)}$$

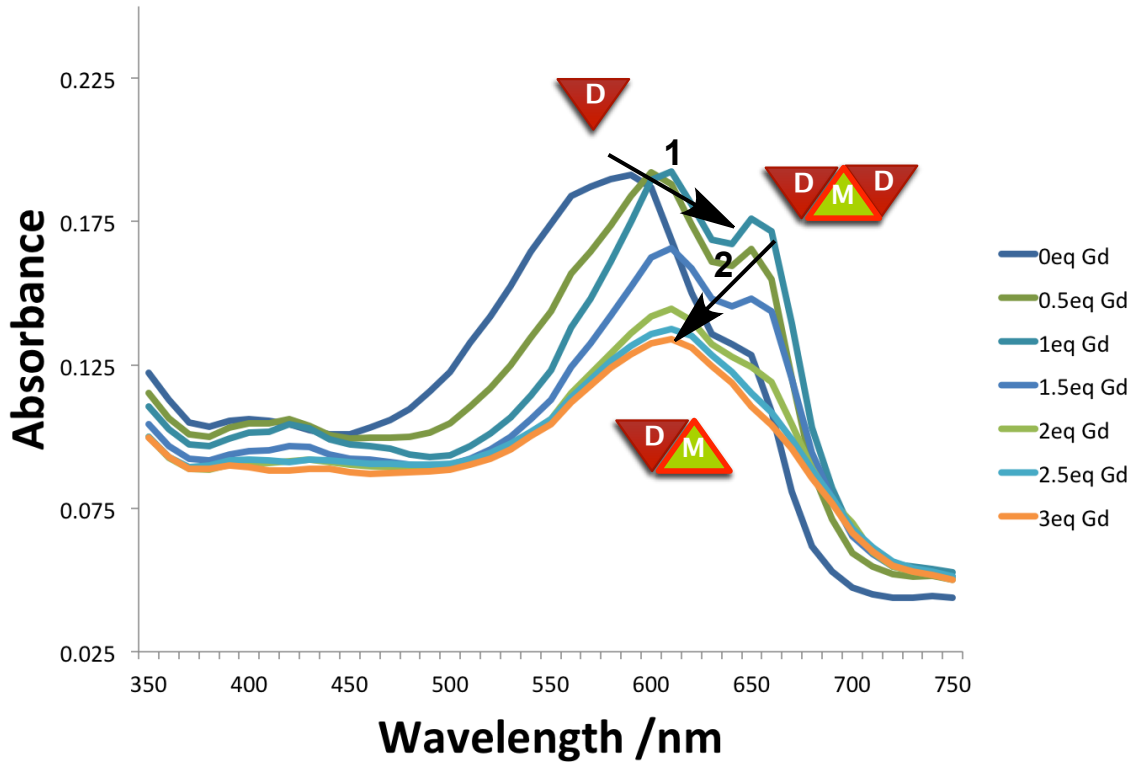

Figure 4.16: Direct titration of **4.61** with $GdCl_3$ at pH 8.35 showing the absorbance shifting from the free dye at 580 nm to the 2:1 dye-metal complex at 650 nm (**1**) followed by a shift to the 1:1 dye-metal complex at 610 nm (**2**).

Examination of **Figure 4.16** showed that a maximum response occurred between 0 and 2 equivalents of gadolinium added, as such, we decided to make our stock dye-lanthanide aqueous solution containing a ratio of 2:1 lanthanide to **4.61** (20 µM **4.61**, 40 µM $GdCl_3 \bullet 6H_2O$). 125 µL of this stock was then added to several sealable tubes and various equivalents of ligand in buffer (0-3 equiv., 200 mM ammonium acetate buffer) were then added, additional buffer solution was added so the final volume was 250 µL and the tubes were sealed and heated to 60 °C. It has been reported that macrocyclic ligands at low concentrations can take several days to reach equilibrium at RT, however, the equilibrium can be achieved in 24 h by heating the solutions to 60 °C for 18h and allowing solution to equilibrate at room temperature for 6 h. Due to the concentration dependence of absorbance readings, before any of the vials were opened they were extensively mixed to ensure that the concentration remained unchanged after the heating process. 200 µL of each solution was then pipetted into each well of NUNC 96 black-well plate, and the absorbance values from 350 – 750 nm were collected, **Figure 4.17**.

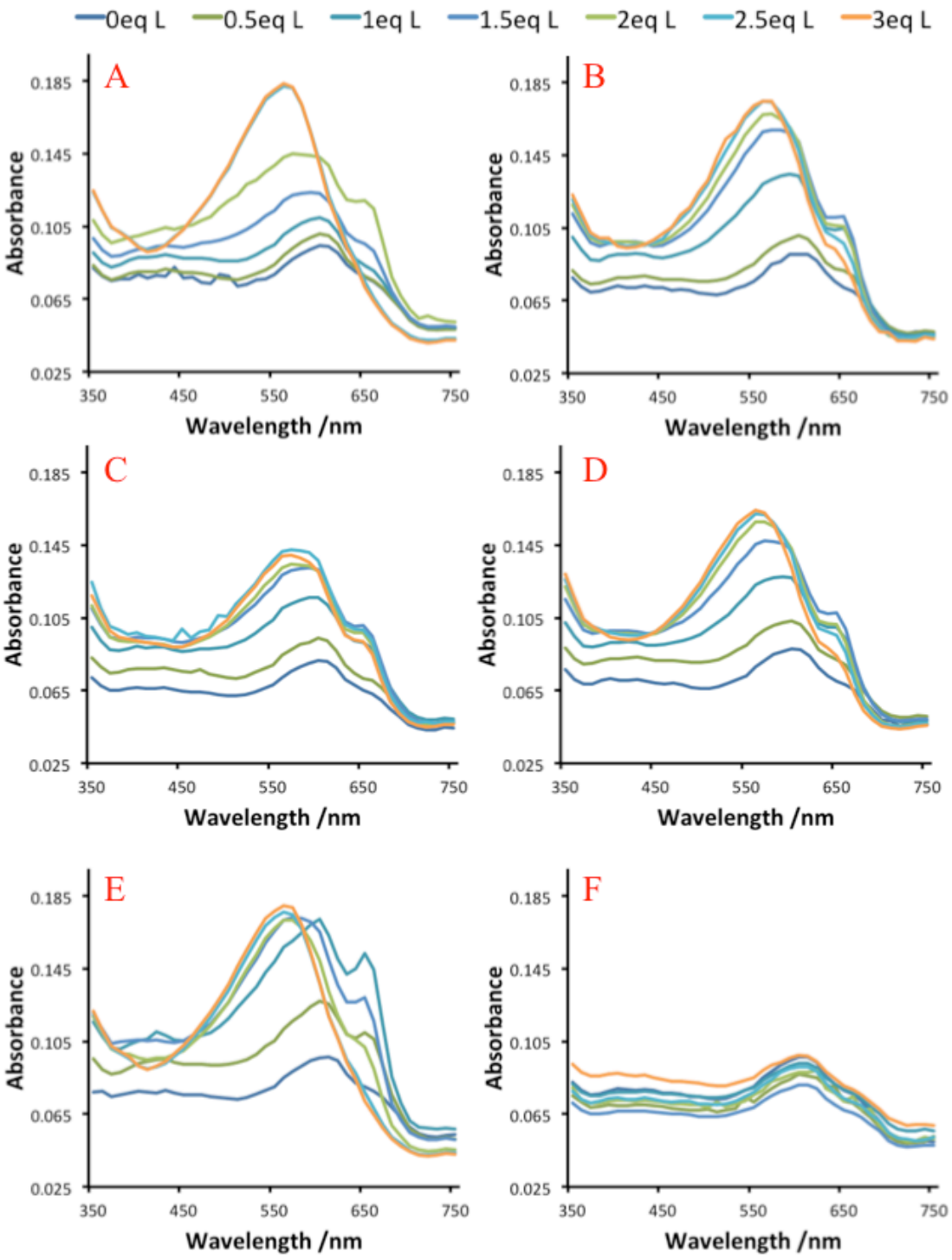

Figure 4.17: Spectrophotometric data (pH 8.35) from M = Gd dye-displacement assay of **A)** L = **DOTA** (**4.43**) **B)** L = **DO3A** (**4.46**) **C)** L = **PCC** (**4.59**) **D**) L = **MCC** (**4.60**) **E)** L = **EDTA** (**1.7**) **F)** L = **TETRA** (**4.39**)

Due to the convoluted nature of the absorbance data, attempts to fit the direct titration to an D, D_2M (D = dye, M = Ln) binding expression using HypSpec 2006 software to extract K_{11}^{c} and 2:1 K_{12}^{c} would not refine. It appears that at pH 8.35 a more complex equilibrium exists between the dye and metal. Qualitative examination of the peak shape gives us some information on K_{ML}^{c}. When 2 equivalents of the DOTA ligand are added the absorbance spectrum has completely reverted back to that of the free dye with no evidence of Gd-dye species, **Figure 4.17A**. The DO3A ligand class all appear to have a similar shape indicating a similar stability constant assuming that the stepwise protonation constants are not substantially different. This would be consistent with no increase in bonding from the sulfonate groups on the calix[4]arene, **Figure 4.17 B**, **C**, & **D**. Direct comparison between linear and cyclic ligands are not ideal due to the substantially different pKa values used to convert K_{ML}^{c} to K_{ML}. We suspected that the TETRA ligand might act more like a linear chelate due to the high flexibility of the chelate arms. To qualitatively test the TETRA ligand (**4.39**), it was compared to EDTA (**1.7**) a well-known linear chelate, **Figure 4.17 E** & **F**. It can be seen that at this pH, **4.39** is not able to out compete the dye for the metal indicating a lower K_{ML}^{c} than EDTA.

Due to the difficulty in obtaining K_{11}^{c} and 2:1 K_{12}^{c} for the dye-Gd complex at pH 8.35 the assay was redone at pH 3.99 to replicate literature conditions as closely as possible, **Figure 4.18**. At this pH the dye-Gd spectrophotometric data was well behaved with clear isosbestic points. Fitting this data to a DM, D_2L model system gave K_{11}^{c} and K_{12}^{c} consistent with literature,[135] **Table 4.1**. The iminodiacetic acid based calix[4]arene **4.39** was the only ligand shown to have no affinity for lanthanide ion chelation at pH 8.35, in order to determine if this was due to the lanthanide ion size we wanted to test for dye-displacement with different lanthanides that span the series. As K_{11}^{c} and K_{12}^{c} is different for each lanthanide the direct metal titration was repeated with La, Eu, and Yb at pH 3.99. The corresponding spectrophotometric data was then fit to DM, D_2M model and refined to give K_{11}^{c} and K_{12}^{c}.

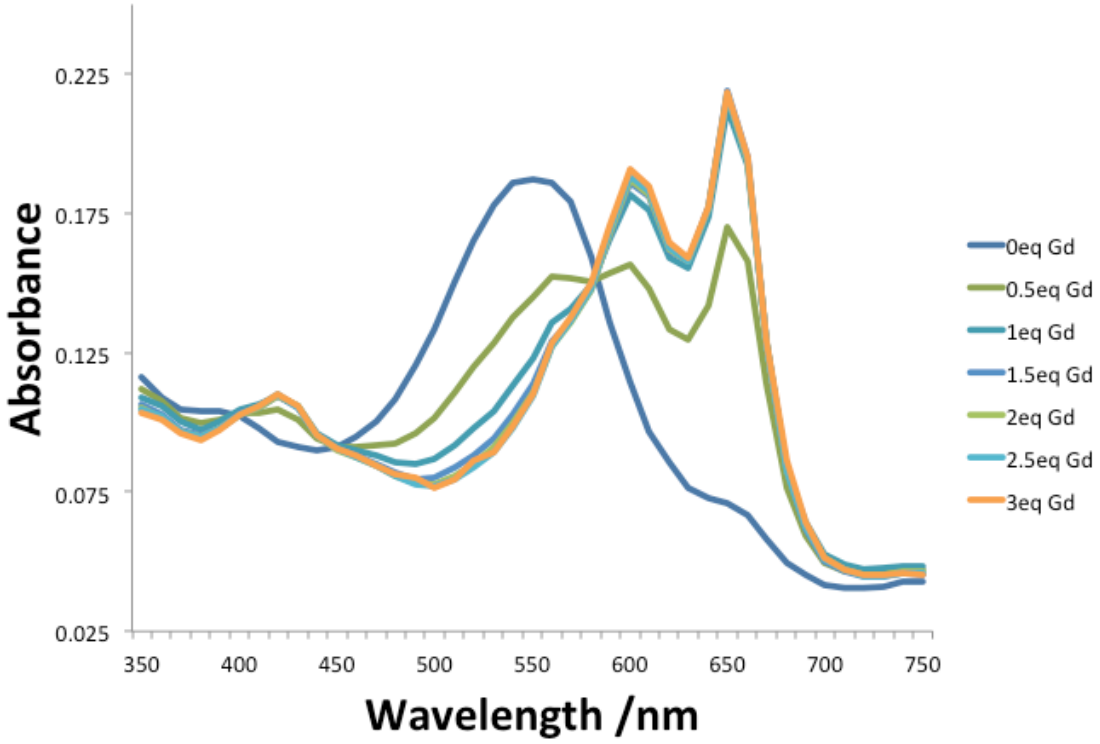

Figure 4.18: Direct titration of **4.61** with $GdCl_3$ at pH 3.99

Table 4.1: Log $\mathbf{K_{11}^c}$ and Log $\mathbf{K_{12}^c}$ values for dye-Ln complexes determined by refinement of a AB, A_2B model using spectrophotometric data at 550 nm, 600 nm, 630 nm, 650 nm.

Metal	Ionic radius /Å	Log K_{11}^c	Log K_{12}^c	Wavelengths used for refinement /nm			
La	1.032	6.6	12.1	550	600	630	650
Eu	0.947	7.4	13.4	550	600	630	650
Gd	0.938	6.5	11.8	550	600	630	650
Yb	0.868	5.4	10.4	550	600	630	650

Examination of **Figure 4.18** showed that a maximal shift in the visible spectrum occurred between 0 - 1.5 equivalents of metal added. Our stock dye-lanthanide solution was made using this ratio to generate the most information from the displacement experiment. Despite the solubility issues with ligands **4.39, 4.59**, and **4.60** at lower pH, they were sufficiently soluble to create a 20 μM stock solution at pH 4, in a 200 mM ammonium acetate buffer, all other ligand solutions were made to the same concentration. As before, various ligand equivalents (0-3equiv.) were titrated into a NUNC 96 black-well plate containing the stock dye-lanthanide complex, the spectrophotometric data from 350 – 750 nm is shown in **Figure 4.19**.

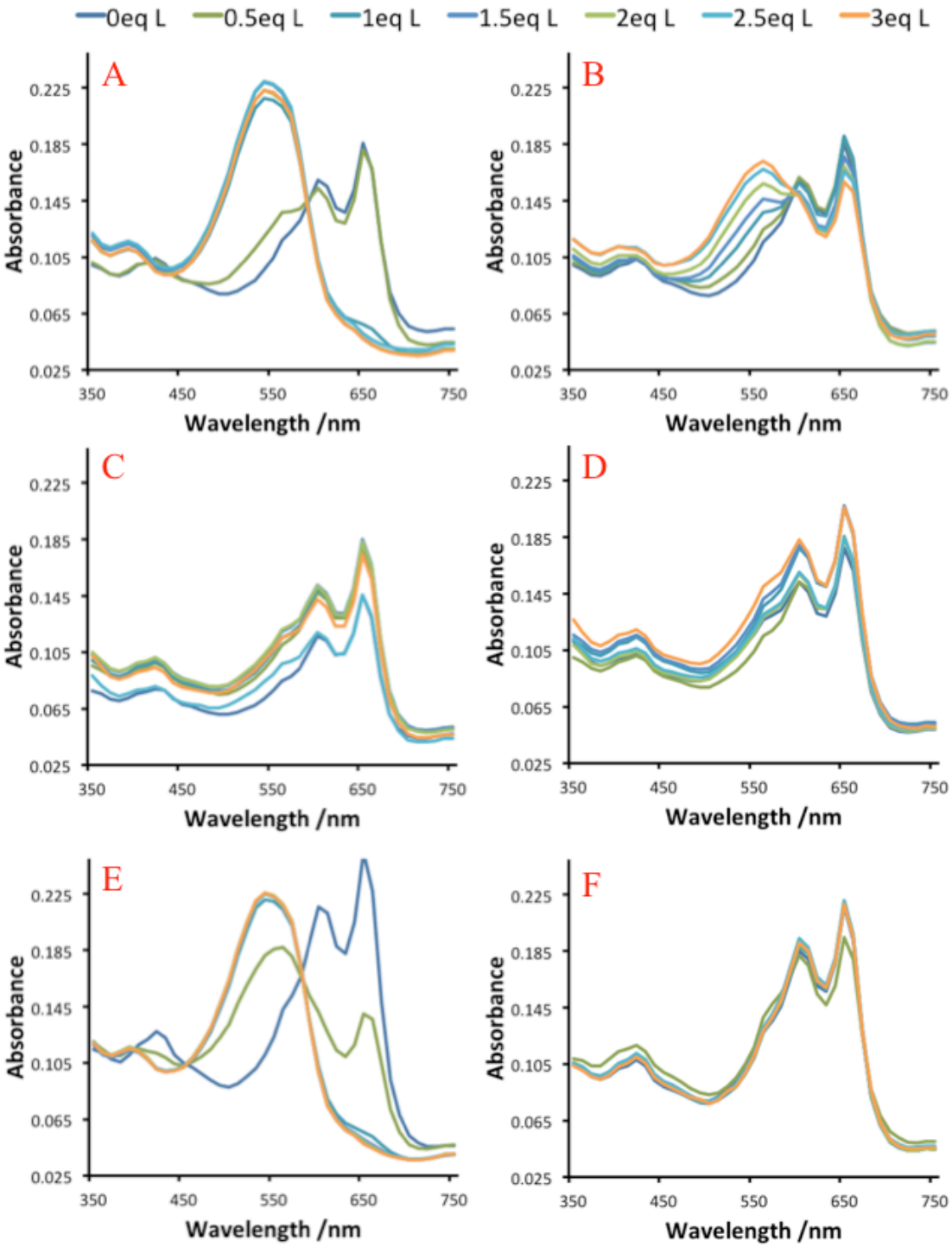

Figure 4.19: Spectrophotometric data (pH 3.99) from M = Gd dye-displacement assay of **A)** L = **DOTA** (**4.43**) **B)** L = **DO3A** (**4.46**) **C)** L = **PCC** (**4.59**) **D)** L = **MCC** (**4.60**) **E)** L = **EDTA** (**1.7**) **F)** L = **TETRA** (**4.39**)

Examination of the spectrophotometric data showed that DOTA (**4.43)**, DO3A (**4.46)**, and EDTA (**1.7**) were able to displace the dye from the metal whereas **PCC** (**4.59**), **MCC** (**4.60**), and **TETRA** (**4.39**) were not at this pH. Additionally, **TETRA** (**4.39**) was not able to out compete the dye for any of the other lanthanide ions tested (La, Eu, Yb). The change in absorbance of **4.43**, **4.46**, and **1.7** were then fit to a DM, D_2M, ML model (L = ligand used) using HypSpec 2006 to give their K^c_{ML} values. The K^c_{ML} values were then converted to K_{ML} by **Equation 4.1**, **Table 4.2**. A good agreement between the experimental and literature values of K_{ML} for the **1.7-Ln** complexes were seen for all but the Ln = La complex. The K_{ML} of DO3A and DOTA did differ from accepted literature values but this is most likely due to no NaCl being added to maintain the ionic strength of the solution.

Table 4.2: K^c_{ML} and K_{ML} values for **4.43**, **4.46**, and **1.7** obtained from the dye-displacement assay.

Ligand	Lanthanide	Log K^c_{ML}	Log K_{ML}	Literature Log K_{ML}
DOTA (**4.43**)	Gd	8.1[a]	22.4	25.3-24.0[136]
DO3A (**4.46**)	Gd	6.5[a]	20.0	21.0[136]
EDTA (**1.7**)	Gd	9.8[b]	17.5	17.4[137]
EDTA (**1.7**)	La	6.1[b]	13.8	15.5[137]
EDTA (**1.7**)	Eu	9.0[b]	16.7	17.3[137]
EDTA (**1.7**)	Yb	11.6[b]	19.3	19.6[137]

[a] 100 mM ammonium acetate buffer, [b] 100 mM ammonium acetate buffer with 100 mM NaCl.

The lack of response from the addition of **4.39** could indicate several possibilities. The lack of solubility of **4.39** at this pH could cause it to precipitate out of solution and at the very low concentrations we were working with it is possible that the precipitate would be too small to notice. However, examination of the 96-well plate under a microscope did not support this. More likely, the orientation of the IDA groups on the calix[4]arene scaffold would not allow for cooperative binding, in turn making the IDA groups function as a di- or tridentate ligand (with or without coordination of the amine) that was incapable of out competing the dye for the lanthanide ion.

The lack of dye-displacement at pH 3.99 by **4.59** and **4.60** was surprising; we expected to see a similar response to **4.46** as was observed at pH 8.35. Macrocyclic metal complexes are known to form much slower than their linear counterparts due to the mechanism by which the metal complex is formed. The carboxylate groups are all positioned above the macrocycle, they create a negative charge drawing the positively charged lanthanide towards the cavity to form a weakly bound adduct, this adduct then undergoes a rearrangement to form a highly stable complex.[5] In our case at pH 3.9 the carboxylic acids may be protonated and thus capable of forming a hydrogen bond with the negatively charged sulfonate groups on the calix[4]arene backbone. With the carboxylates unable to draw the metal into the macrocyclic cavity it may not be possible for **4.59**, and **4.60** to out compete **4.61** for metal chelation. When the assay is run under basic conditions, the carboxylic acids are deprotonated and are then repelled by the negatively charged sulfonate groups. Now unbound, they are capable of sequestering the metal and bringing it towards the macrocyclic cavity, forming a highly stable complex. An equilibrium geometry model of **4.59** was calculated using molecular mechanics (MMFFaq force field) with the carboxylic acid protonated (**A**) and deprotonated (**B**) that supports this possibility, **Figure 4.20**.

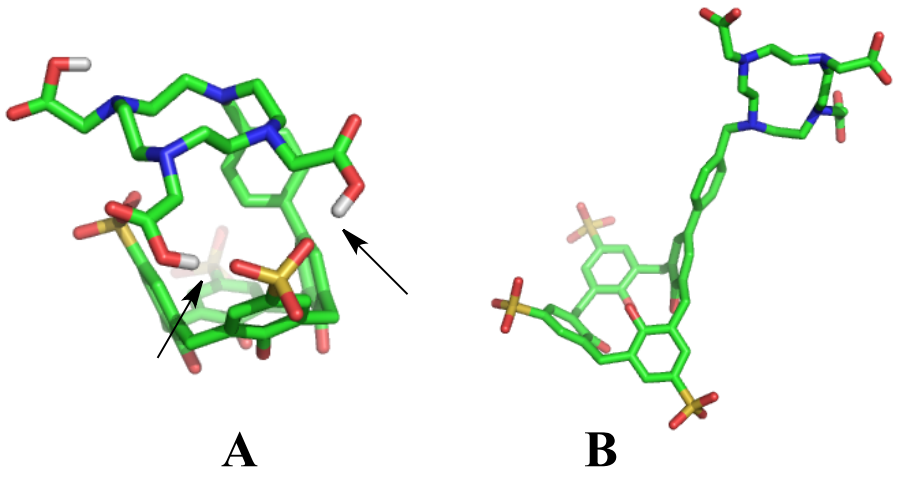

Figure 4.20: Spartan equilibrium geometry model calculated using molecular mechanics, MMFFaq of **4.59** with the carboxylic acid protonated (**A**) and deprotonated (**B**). Arrows indicate location of intramolecular hydrogen bond. Only the protons on the carboxylic acid are shown for clarity.

4.6 Concluding Remarks

Novel calix[4]arene ligands **4.34**, **4.39**, **4.59**, and **4.60** were formed and a literature dye-displacement assay was modified for high throughput determination of stability constants by incorporation of a plate reader. The catechol functionalized ligand **4.34** was found to be unstable in solution, most likely forming an insoluble decomposition product. Four IDA groups were attached to a calix[4]arene scaffold to form ligand **4.39** in hopes that the IDA groups would cooperatively coordinate to a lanthanide ion forming a highly stable chelate. When lanthanide ions were added to a solution of **4.39** a white precipitate formed, most likely a coordination polymer. A dye-displacement assay (Ln = Gd) was performed at pH 3.99 and pH 8.35. We hoped that under the dilute conditions of the displacement assay, polymer formation could be avoided. No change in absorbance was observed for **4.39** indicating that the IDA groups were not cooperatively binding the lanthanide to out complete **3.61** for metal coordination. To determine if metal binding for **4.39** was size dependent the dye-displacement assay was conducted (pH = 3.99) with a group of lanthanide ions that span the series (La, Eu, Gd, and Yb). There was no change in absorbance and it was concluded that **4.39** could not outcompete the dye for metal chelation no matter what size of lanthanide ion was present. Calix[4]arene **4.59** and **4.60** were synthesized using a Suzuki coupling reaction. To the best of my knowledge this is the first example of a DO3A based ligand being used in a Suzuki reaction. Surprisingly the cyclen based ligands bound palladium, however, it was possible to remove the Pd using thiourea. The dye-displacement assay at pH 8.35 showed qualitatively that **4.59** and **4.60** had a similar K_{ML}^{c} to DO3A, however due to the convoluted spectrophotometric data of the dye-displacement assay at pH 8.35, it was not possible to fit K_{ML}^{c} to an A, A_2B, BC model and obtain a value for K_{ML}^{c}. The dye-displacement assay at pH = 3.99 fit to A, A_2B, BC model. The method was validated by comparison of K_{ML} values of EDTA (**1.7**), DOTA (**4.43**), and DO3A (**4.46**) to literature results. Good agreement was seen for most EDTA-Ln complexes, and a reasonable agreement for the DOTA-Gd, and DO3A-Gd complexes. No observable binding for **4.59** and **4.60** was found at this pH. I postulate that a possible explanation for the lack of dye-displacement at acidic pH could be due to protonation of the carboxylic acid and formation of an intramolecular hydrogen bond

between the negatively charged sulfonate groups of the calix[4]arene scaffold that prevents formation of a stable coordination complex. At physiological pH of 7.4 however, the carboxylic acids would be deprotonated and behave in a similar fashion to that seen at pH 8.35. We believe that compounds show **4.59** and **4.60** promise as potential MR contrast agents and merit relaxivity studies.

4.7 Experimental

THF was freshly distilled from sodium/benzophenone before use. CH_2Cl_2 was used as is unless specified; dry CH_2Cl_2 was distilled from calcium hydride . **4.40**, **4.43**, and **1.8** were purchased from Strem Chemicals, 2,3-dimethoxyphenylboronic acid was purchased from Frontier Scientific. All other chemicals were purchased from Sigma-Aldrich and used as is. **4.22**,[111] **4.1**,[112] **4.23**,[113] **4.24**,[114] **4.25**,[115] **4.54**,[138] **4.56**,[131] and **4.57**[112] were synthesized by literature methods. Samples for NMR spectroscopy were recorded on Bruker AMX-300 MHz or 500 MHz NMR spectrometers. LR-ESI-MS data was collected on a Finnigan Mat LCQ mass spectrometer. HR-ESI-MS data was collected using a ThermoFisher Orbitrap Executive mass spectrometer. HPLC purification was done using a Shimadzu HPLC or a Thermo-Dionex HPLC/MS on a preparative Apollo C18 column (Alltech, 5 μm, 22 x 250 mm) or preparative Luna C-18 column (Phenomenex, 5 μm, 21.2 x 250 mm), detecting at 280 nm. Compounds were purified by running a gradient from 90:10 H_2O:MeCN to 10:90 H_2O:MeCN (all solvents containing 0.1% TFA) over 35 minutes. Analytical traces were collected using a Phenomenex Luna C18 column (5 μm, 4.6 x 250 mm) with UV-Vis detection at 280 nm. All absorbance spectra were collected on a Molecular Devices SpectraMax M5 plate reader.

4.7.1 Synthesis

5-(2,3-dimethoxyphenyl)-25, 26, 27, 28-tetrahydroxy-11-17-23-trisulfonatocalix[4]arene, **4.33** **4.8** (0.041 g, 0.055 mmol), 2,3-dimethoxyphenylboronic acid (0.010 g, 1 equiv., 0.055 mmol), tetrabutylammonium bromide (0.0089 g, 0.5 equiv., 0.028 mmol), $Pd(OAc)_2$ (0.0025 g, 20 mol%) and sodium carbonate (0.026 g, 3.8 equiv., 0.21 mmol) were dissolved in 5 mL of deionized water inside a microwave vial and irradiated at 150 °C for 5 minutes with cooling air and stirring on. The aqueous solution was washed with CH_2Cl_2 (2 x 20 mL) followed by EtOAc (1 x 25 mL) and concentrated. HPLC purification and evaporation of product fractions *in vacuo* afforded a white powder. Yield 0.018 g (42%). Mp: 245 °C (dec). IR (KBr pellet): 3366br, 1465s, 1261w, 1213s, 1160s, 1118s, 1042s, 889w, 784m, 661m, 625m, 559m. ^{1}H NMR (500MHz, D_2O, 22 °C): δ 7.64 (d, $^3J_{HH}$ = 2.1 Hz, 2H), 7.62 (d, $^3J_{HH}$ = 2.0 Hz, 2H), 7.37 (s, 2H), 7.10 (s, 2H), 6.96 (t, $^3J_{HH}$ = 7.8 Hz, 1H), 6.82 (d, $^3J_{HH}$ = 7.8Hz, 1H), 6.76 (d, $^3J_{HH}$ = 6.9Hz, 1H), 3.99 (m, br, 8H), 3.70 (s, 3H), 2.48 (s, 3H). ^{13}C NMR (125MHz, D_2O, 22 °C): δ 153.3, 152.3 150.9, 147.8, 145.2, 135.4, 135.3, 134.4, 131.4, 130.0, 129.1, 128.5, 128.2, 128.0, 126.6, 126.5, 126.4, 124.9, 122.3, 112.1, 59.6, 56.0, 30.7, 30.5. HR-ESI-MS: 799.0793 ($[M-H]^-$, $C_{36}H_{31}O_{15}S_3^-$; calcd: 799.0830).

5-(2,3-dihydroxyphenyl)-25, 26, 27, 28-tetrahydroxy-11-17-23-trisulfonatocalix[4]arene, 4.34 Compound **4.33** (0.018 g, 0.053 mmol), was suspended in dry CH_2Cl_2 and cooled to -78 °C. 1 M BCl_3 in CH_2Cl_2 (0.3 mL) was added and the reaction mixture was allowed to warm to RT while stirring overnight. The solvent was then removed under reduced pressure and dissolved in 0.1% TFA water (2 mL). HPLC purification and evaporation of product fractions *in vacuo* afforded a white powder. Yield 0.005 g (30%). Mp: >250 °C (dec). IR (KBr pellet): 3381br, 1473s, 1266w, 1212s, 1158s, 1115s, 1040s, 892w, 809w, 781m, 658m, 622m, 561w, 551w. ^{1}H NMR (500MHz, D_2O, 22 °C): δ 7.66 (s, 2H), 7.64 (s, 2H), 7.57 (s, 2H), 7.25 (s, 2H), 6.77 (d, $^3J_{HH}$ = 7.2 Hz, 1H), 6.73 (d, $^3J_{HH}$ = 7.5Hz, 1H), 6.63 (d, $^3J_{HH}$ = 7.0Hz, 1H), 4.03 (m, 8H). ^{13}C NMR (125MHz, D_2O, 22 °C): δ 152.2, 151.2, 147.6, 144.6, 140.8, 136.2, 135.7,

131.9, 130.0, 129.3, 128.8, 128.4, 128.2, 127.9, 126.7, 126.6, 126.5, 122.0, 120.9, 115.0, 30.7, 30.6. HR-ESI-MS: 771.0517 ([M-H]$^-$, $C_{34}H_{27}O_{15}S_3^-$; calcd: 771.0507).

5-11-17-23-methyl(diethyl iminodiacetate)-25, 26, 27, 28-tetrahydroxy-calix[4]arene, 4.42 Diethyl iminodiacetate, **4.40**, (4.8 mL, 24 mmol) and formaldehyde (37%, 1.8 mL, 24 mmol) were added to THF (10 mL) and heated to 60 °C in a sealed vessel for 1 h. The vessel was removed from heat and let cool for ~0.3 h. **4.1** (0.50 g, 1.2 mmol) was then added to the reaction mixture and heated to 60 °C for 18 h. The solvent was removed under reduced pressure to give a colourless oil. This oil was then dissolved in CH_2Cl_2 and extracted with 1 M HCl (3 x 20 mL). The organic layer was discarded and the aqueous product layer was made basic to pH 10 with ammonium hydroxide and extracted with CH_2Cl_2 (3 x 20 mL). The organic product layers were combined and dried over anhydrous $MgSO_4$. The organic product layer was then filtered to remove the $MgSO_4$ and the solvent was removed under reduced pressure to give a colourless oil consisting of the product, **4.39**, and diethyl iminodiacetate, **4.40**. The diethyl iminodiacetate was then distilled under reduced pressure to give a pale yellow viscous oil consisting of **4.39** and a variable % of **4.40**. This mixture was then dissolved in 1,4-dioxane and redistilled under reduced pressure to remove the remaining **4.40**. This step was repeated 3-5 times until the purity of **4.39** was > 90% (via NMR) giving a viscous yellow oil. ^{1}H NMR (500 MHz, D_2O, 22 °C): δ 10.16 (s, 4H, OH), 7.02 (s, 8H, calix-Ph-H), 4.22-4.14 (m, 4H, Ha/Hb of Ar-C*H*$_2$-Ar), 4.10 (q, $^3J_{HH}$ = 7.0 Hz, 16H), 3.66 (s, 8H, Ar-C*H*$_2$-N), 3.51-3.47 (m, 4H, Ha/Hb of Ar-C*H*$_2$-Ar), 3.46 (s, 16H, NC*H*$_2$C), 1.20 (t, $^3J_{HH}$ = 7.2 Hz, 24H). ^{13}C NMR (75 MHz, D_2O, 22 °C): δ 171.1, 148.0, 131.7, 129.7, 128.1, 60.3, 57.4, 54.0, 31.7, 14.2. LR-ESI-MS: 1227.80 ([M-H]$^-$, $C_{64}H_{83}N_4O_{20}$; calcd: 1227.56).

5-11-17-23-tetramethyl(iminodiacetic acid)-25, 26, 27, 28-tetrahydroxy-calix[4]arene, 4.39 A 1 M NaOH water solution (5 mL) was added to 1,4-dioxane solution (2 mL) containing **4.42** (0.2 g, 0.2 mmol) and vigorously stirred at 50 °C overnight. The solvent was removed under reduced pressure to give a yellow oil. This oil was dissolved in water and the product was precipitated with TFA to give a white

powder. This powder was only soluble under basic conditions (pH >8). After dissolving the powder in 100 mM ammonium acetate buffer (pH 3.99) and HPLC purification, evaporation of product fractions gave a white powder that was partially soluble under acidic conditions (pH = 3.9). ^{1}H NMR (500 MHz, D_2O/NaOD, 57 °C): δ 7.42 (s, 8H, calix-Ph-H), 4.44 (s, 8H, Ar-C*H*$_2$-N), 4.16 (s, br, 8H, Ar-C*H*$_2$-Ar), 3.88 (s, 16H, NC*H*$_2$C). ^{13}C NMR (75 MHz, D_2O, 22 °C): δ 179.6, 151.8, 130.8, 130.2, 128.4, 57.4, 57.0, 31.8. LR-ESI-MS: 1005.00 ([M+H]$^+$, $C_{48}H_{53}N_4O_{20}^+$; calcd: 1005.33).

1,4,7,10-tetraazacyclododecane-1,4,7-tris(*t*-butyl acetate)-10-(methylphenyl-4-boronic acid pinacol ester), 4.56 Compound **4.56** was synthesized by a literature method,[131] however, the ^{1}H NMR did not agree. Examination of the ^{1}H NMR data provided in the literature was inconsistent with the molecular formula reported. Yield 0.63 g (79 %). ^{1}H NMR (300 MHz, $CDCl_3$, 22 °C): δ 7.72 (d, $^{3}J_{HH}$ = 8.2 Hz, 2H), 7.43 (d, $^{3}J_{HH}$ = 7.43 Hz, 2H), 3.47 (d, J_{HH} = 4 Hz, 2H), 3.28-2.13 (m, 22H), 1.44 (s, 27H), 1.31 (s, 12H). LR-ESI-MS: 753.27 ([M+Na]$^+$, $C_{39}H_{67}BN_4NaO_8^+$; calcd: 753.38).

1,4,7,10-tetraazacyclododecane-1,4,7-tris(*t*-butyl acetate)-10-(methylphenyl-3-boronic acid pinacol ester), (*meta* analogue of 4.56) A modified literature procedure was used,[131] starting from 3-bromomethylphenylboronic acid pinacol ester instead of 4-bromomethylphenylboronic acid pinacol ester to give **1,4,7,10-tetraazacyclododecane-1,4,7-tris(*t*-butyl acetate)-10-(methylphenyl-3-boronic acid pinacol ester)**, the *meta* analogue of **4.56**, as a colourless oil that solidified upon standing. Yield 0.31 g (84 %). ^{1}H NMR (300 MHz, $CDCl_3$, 22 °C): δ 7.73-7.67 (m, 2H), 7.63 (dt, $^{3}J_{HH}$ = 7.6 Hz, $^{4}J_{HH}$ = 1.5 Hz, 1H), 7.27 (t, $^{3}J_{HH}$ = 7.4 Hz, 1H), 3.51-2.11 (m, 24H), 1.44 (m, 27H), 1.33 (s, 12H). LR-ESI-MS: 753.64 ([M+Na]$^+$, $C_{39}H_{67}BN_4NaO_8^+$; calcd: 753.49).

1,4,7,10-tetraazacyclododecane-1,4,7-tris(acetic acid)-10-(methylphenyl-3-boronic acid pinacol ester), (*meta* analogue of 4.57) A modified literature procedure was used[113] starting from the ***meta* analogue of 4.56** instead of **4.56** to give **1,4,7,10-tetraazacyclododecane-1,4,7-tris(acetic acid)-10-(methylphenyl-3-boronic**

acid pinacol ester), the ***meta*** **analogue of 4.57**, as a yellow oil that solidified upon standing. Yield 0.16 g (69 %). ^{1}H NMR (300 MHz, D_2O, 22 °C): δ 7.88-7.79 (m, 2H), 7.63 (d, $^{3}J_{HH}$ = 7.9 Hz, 1H), 7.52 (t, $^{3}J_{HH}$ = 7.4 Hz, 1H), 3.46 (s, br, 2H) 3.46-3.06 (m, 22H), 1.23 (s, 12H). ^{13}C NMR (75 MHz, D_2O, 22 °C): δ 173.23 (br), 169.0 (br), 136.3, 135.4 (br), 133.9 (br), 133.0, 129.3, 85.6, 75.6, 57.9, 54,6, 52.9, 51.3 (br), 49.6 (br), 48.3 (br), 23.8, the carbon on the aromatic ring attached to the boron was too weak to be observed**.** LR-ESI-MS: 563.27 ($[M+H]^+$, $C_{27}H_{44}BN_4O_8^+$; calcd: 563.33).

5-(1,4,7,10-tetraazacyclododecane-1,4,7-tris(acetic acid)-10-(methylphenyl-4-boronic acid pinacol ester))-25, 26, 27, 28-tetrahydroxy-11-17-23-trisulfonatocalix[4]arene Pd, 4.58 Compounds **4.8** (0.066 g, 0.089 mmol), **4.57** (0.050 g, 0.089 mmol), tetrabutylammonium bromide (0.014 g, 0.5 equiv., 0.043 mmol), $Pd(OAc)_2$ (0.0040 g, 20 mol%) and sodium carbonate (0.042 g, 3.8 equiv., 0.34 mmol) were dissolved in 5 mL of deionized water inside a sealed vessel and heated at 150 °C for 2 h. The aqueous solution was washed with CH_2Cl_2 (2 x 20 mL) followed by EtOAc (1 x 25 mL) and concentrated. HPLC purification and evaporation of product fractions *in vacuo* afforded an off white powder. Yield 0.008 g (8%) yield. HR-ESI-MS: 600.0640 ($[M-2H]^{-2}$, $C_{49}H_{50}N_4O_{19}S_3Pd(II)^{-2}$; calcd: 600.0628).

5-(1,4,7,10-tetraazacyclododecane-1,4,7-tris(acetic acid)-10-(methylphenyl-4-boronic acid pinacol ester))-25, 26, 27, 28-tetrahydroxy-11-17-23-trisulfonatocalix[4]arene, 4.59 Compounds **4.8** (0.066 g, 0.089 mmol), **4.57** (0.050 g, 0.089 mmol), tetrabutylammonium bromide (0.014 g, 0.5 equiv., 0.043 mmol), $Pd(OAc)_2$ (0.024 g, 1.2 equiv., 0.11 mmol) and sodium carbonate (0.13 g, 12 equiv., 1.04 mmol) were dissolved in 5 mL of deionized water inside a sealed vessel and heated at 150 °C for 2 h. The solution was cooled, 2 mL of an aqueous solution of thiourea was added (0.068 g, 10 equiv., 0.89 mmol) and the mixture was left to stir overnight at 60 °C. The solution was then centrifuged to remove the majority of the insoluble Pd-thiourea complex followed by filtration through Celite®. The aqueous solution was washed with CH_2Cl_2 (2 x 20 mL), followed by EtOAc (1 x 25 mL) and concentrated. HPLC purification and evaporation of product fractions *in vacuo* afforded a white powder. Yield

0.023 g (24%) yield. A purity of >97% was determined by reinjection of a 50 μM solution of the compound onto a Thermo-Dionex HPLC/MS equipped with a Phenomenex Luna C18 column (5 μm, 4.6 x 250 mm) detecting at 280 nm. Mp: >250 °C (dec). ^{1}H NMR (500 MHz, D_2O/NaOD, 95 °C): δ 8.16 (s, 2H), 8.13 (app. d, J_{HH} = 7.3 Hz, 2H), 8.10 (app. d, J_{HH} = 1.9 Hz, 2H), 8.08 (app. d, J_{HH} = 1.4 Hz, 2H), 7.99-7.95 (m, 4H), 4.68 (s, 2H), 4.59 (s, 4H), 4.53 (s, 4H), 4.12 (s, 2H), 4.01 (s, 4H), 4.83 (s, 4H), 3.73 (s, 8H), 3.55 (s, 4H). HR-ESI-MS: 1097.2451 ([M-H]$^-$, $C_{49}H_{53}N_4O_{19}S_3^-$; calcd: 1097.2471).

5-(1,4,7,10-tetraazacyclododecane-1,4,7-tris(acetic acid)-10-(methylphenyl-3-boronic acid pinacol ester))-25, 26, 27, 28-tetrahydroxy-11-17-23-trisulfonatocalix[4]arene, 4.60 Compound **4.60** was prepared according to the same procedure as **4.59** except using 1,4,7,10-tetraazacyclododecane-1,4,7-tris(acetic acid)-10-(methylphenyl-3-boronic acid pinacol ester) to give **4.60** as a white powder. Yield 0.019 g (20%) yield. A purity of >97% was determined by reinjection of a 50 μM solution of the compound onto a Thermo-Dionex HPLC/MS equipped with a Phenomenex Luna C18 column (5 μm, 4.6 x 250 mm) detecting at 280 nm. Mp: >250 °C (dec). ^{1}H NMR (500 MHz, D_2O/NaOD, 87 °C): δ 8.43-8.01 (m, 10H), 7.97-7.8 (m, 2H), 4.76-4.67 (m, 8H), 4.48-2.84 (m, 24H). HR-ESI-MS: 1097.2450 ([M-H]$^-$, $C_{49}H_{53}N_4O_{19}S_3^-$; calcd: 1097.2471).

4.7.2 NMR titration experimental

A stock ligand solution of **4.34** (0.0076 g, 4.9 mM) was made using a 50 mM sodium acetate buffered D_2O solution (pD 7.8). 0.5 mL of this solution was placed in a NMR tube and a 1 mL portion was added to YCl_3•$6H_2O$ (0.0122 g, 40.0 mM). The metal containing solution was titrated into the NMR tube solution in 5 μL aliquots, collecting a ^{1}H NMR spectrum after every addition. The volume of metal solution was increased to 10 μL, followed by 35 μL, until a final volume of 345 μL was added (2.8 equiv. M). The addition continued well past the point where no more peak shifts occurred in the ^{1}H NMR spectrum to ensure saturation. Upon observation of decomposition of **4.34** no further NMR titrations were performed.

4.7.3 General direct metal titration

A stock ligand solution of **4.61** (20 μM) were made up in deionized water with 200 mM NaCl for ionic strength control. Stock lanthanide solutions (30 μM) of La(III), Eu(III), Gd(III), and Yb(III) were made in 200 mM ammonium acetate buffer (pH = 3.99). 100 μL was added into each well of a NUNC 96 black-well plate. The lanthanide solutions were then added in various volumes to ensure a range of 0-3 equivalents of lanthanide to dye. The wells were then diluted with the appropriate amount of buffered solution so that the final volume of each well was 200 μL. The absorbance spectrum of each well was then collected. Each trial was run in duplicate to ensure reproducibility.

4.7.4 General dye-displacement assay

A stock solution of lanthanide and **4.61** was made up in deionized water to ensure 1.5:1 Ln to dye ratio (30 μM Ln, 20 μM **4.61**). This ratio was chosen based on analysis of the direct titration graph in order to gain a maximal response in absorbance. Ligands **4.39, 4.43**, **4.46**, **4.59**, and **4.60** were made up in 200 mM ammonium acetate (90 μM, pH = 3.99). Ligand **1.7** was made up in 200 mM ammonium acetate buffer (90 μM, pH = 3.99) with 200 mM NaCl for ionic strength control. 125 μL of the Ln-dye solution was added to a sealable tube. The ligand solutions were then added in various volumes to ensure a range of 0-3 equivalents of ligand to metal. The tubes were then diluted with the appropriate amount of buffered solution so that the final volume of each tube was 250 μL, sealed and heated to 60 °C for 18 h, then left to equilibrate at RT for 6 h. They were then shaken well to ensure that no change in concentration occurred during the heating process. 200 μL was added to each to each well of NUNC 96 black-well plate and the absorbance spectrum of each well was then collected. Each trial was run in duplicate to ensure reproducibility.

4.7.5 Determination of conditional stability constants

The conditional stability constants of **4.61-Ln** complexes were determined using an DM, D_2M model and fitting the absorbance values at 550, 600, 630, and 650 nm using HypSpec 2006 software.

The conditional stability constants of **Ln-4.43**, **Ln-4.46**, and **Ln-1.7** complexes were determined using an DM, D_2M, ML model and fitting the absorbance values at 550, 600, 630, and 650 nm using HypSpec 2006 software.

Chapter 5 – Concluding Remarks and Future Directions

5.1 Concluding Remarks

New ligand design is critically important to meet the ever growing demand for MR contrast agents with increased function (higher relaxivity, exchangeable protons for paraCEST, blood pool characteristics, etc.) that maintain the high safety profile of the current commercial agents. This thesis focused on the synthesis and stability of several ligand classes (Kläui ligands, oxazoline-based ligands, and calix[4]arene derived ligands) to determine their viability as strong lanthanide chelators for potential use as MRI contrast agents.

Literature reports of Kläui ($CpCo(P{=}O(OR)_2)_3$) lanthanide complexes described them as air and water stable, however, there was no mention of their ligand lability. In order for lanthanide Kläui complexes to be useful as MR contrast agents they must be resistant to transmetallation, as free lanthanide ions are inherently toxic. We determined that the rate of ligand exchange for the series of cationic $Ln(Kläui)_2^+$ complexes (R = Et, Ph. Ln = Nd, Eu, Tb, Yb) ranged from > 2500 $M^{-1}s^{-1}$ (Ln = Nd) to 0.3 $M^{-1}s^{-1}$ (Ln = Yb) and was roughly linear in relation to the size of the lanthanide ion. We also observed a 10-fold increase in ligand exchange rate as the water concentration was increased from 0 to 50% in acetonitrile. From this we concluded that the traditional alkyl and phenyl Kläui ligands were not well suited for MR contrast agents.

Through incorporation of additional functional groups we hoped to: slow down the rate of ligand exchange, increase water solubility, and include a secondary source of exchangeable protons to facilitate a CEST mechanism. We attempted to install a range of functional groups on the phosphite arms, however, synthetic difficulties ultimately showed that the “easily modifiable” phosphite arms were really only amenable to non-functionalized alkyl chains. It was possible to incorporate some functionality on the aryl

rings but the extent of functionalization was limited to only a thioacetal, or an aldehyde group.

From our experience with the Kläui ligand we learned that we must have a ligand with a coordination number to the lanthanide ion of greater than 3 in order to limit ligand exchange and prevent transmetallation. Bis and tris-oxazoline ligands are known to form stable complexes with lanthanide ions and are accessible from a wide range of amino alcohol starting materials. We used this knowledge to develop several novel ligands that incorporate multiple oxazolines that were functionalized with additional chelating groups, including, to the best of my knowledge, the first PyBOx ligand based on a tyrosine amino acid with a free hydroxyl group (**3.30**). Unfortunately, we discovered that our ligands were sensitive to very mildly acid conditions causing ligand decomposition. We concluded that in a physiological environment the apparent instability of our ligands discounted them for use as lanthanide chelators for the purpose of MR imaging agents.

Using what we learned from the modification of the Kläui scaffold, we knew we needed a robust, and easily functionalizable skeleton, while our oxazoline based ligands showed us the importance of choosing a chemically inert moiety for chelation of the lanthanide ion. By using a calix[4]arenes scaffold, that is very stable under physiological conditions, and appending groups (catechol, IDA, and DO3A) that are typically chemically inert we were able to create four novel, water soluble, calix[4]arene ligands. While performing a ^{1}H NMR titration to determine the K_{ML} of the mono-substituted catechol calix[4]arene **4.34** we discovered that it was not stable in solution. As such we decided to not pursue the catechol moiety and focused instead on the IDA and DO3A based calix[4]arenes.

We needed to ascertain the K_{ML} of our ligands in order to determine their viability as potential contrast agents. Through creation of a plate reader-based assay we were able to adapt an existing dye-displacement assay for high throughput use. We found that our TETRA (**4.39**) ligand was not able to out-compete the dye for lanthanide chelation at pH 8.35 or pH 3.99. At pH 8.35 our **PCC** (**4.59**) and **MCC** (**4.60**) ligands displaced the dye

from the metal, however, due to the convoluted nature of the dye-metal equilibrium at this pH we were not able to derive a K_{ML}^{c}. By comparison of the spectrophotometric response of **PCC** (**4.59**) and **MCC** (**4.60**) to that of DOTA (**4.43**) and DO3A (**4.46**) we are able to say that the strength of our ligand chelation is close to that of DO3A ($\log K_{ML}^{c}$ = 21). At pH = 3.99 no displacement of the dye by our ligands (**4.59**, **4.60**) was observed. It is likely that the carboxylic acids on the DO3A appendage are protonated forming hydrogen bonds with the negatively charged sulfonate groups on the calix[4]arene skeleton. This prevents carboxylic acids from drawing the lanthanide ion into the cyclen macrocycle where it would rearrange to form a highly stable complex. The lack of dye displaced under acidic pH does not discount **PCC** (**4.59**) and **MCC** (**4.60**) as potential contrast agents. Under physiological pH the carboxylic acids will be deprotonated and behave similarly to what was seen when the dye-displacement assay was conducted at pH = 8.35.

5.2 Future Directions

5.2.1 Calix[4]arene Based Ligands

My ultimate goal was to design ligands that offered improvement over commercial contrast agents. Both **PCC** (**4.59**) and **MCC** (**4.60**) have shown that they have a similar stability constant to DO3A. The next logical step will be to determine their relaxivity. NMRD experiments will need to be performed and compared to current MR contrast agents. The relaxivity should also be determined in the presence of the blood protein HSA. Sulfonated calix[4]arenes have been shown to associate with HSA in aqueous solution.[97] Interactions between contrast agent and proteins have been shown to greatly enhance their relaxivity, while decreasing the rate at which the contrast agent is excreted by the kidneys allowing for longer imaging time and signal enhancement.[139] The high affinity of sulfonated calix[4]arenes for HSA binding, coupled with the high stability constant garnered from the DO3A chelating group makes **4.59** and **4.60** ideally suited for

improved relaxivity while maintaining the high safety profile needed for new MR imaging agents.

It will also need to be determined if a **PCC** and **MCC** complex can function as a paraCEST agent. The phenolic protons are in exchange with water, however, it is not known if they are in the correct exchange regime required for a CEST mechanism (see Chapter 1). A CEST NMR experiment, scanning a wide chemical shift range to locate the phenolic protons, would answer this question. Assuming they are not exchanging too fast (coalesced) or too slow (no exchange), a CEST response would be measured by irradiating at their chemical shift location (the secondary pool) to evaluate their possibility as potential paraCEST contrast agents.

5.2.2 Lanthanide Kläui Complexes

We postulated that the mechanism for ligand exchange between the Kläui isotopomers is an associative type mechanism for the larger lanthanides (Nd) and dissociative for the smaller lanthanides (Yb). However, the limited data available needs to be expanded to probe this further. In order to elucidate the mechanism fully, multiple ligand exchange experiments will need to be run at various concentrations on the same lanthanide ion. If a change in the rate is observed it would indicate that an associative mechanism is present, however, if the rate remains constant we know that a dissociative mechanism is active. By repeating this experiment with various sizes of the lanthanide ions it should be possible to determine where (or if) in the lanthanide series a change in mechanism occurs. With a more concrete knowledge of the type of mechanism present we should be able to use rational ligand design to create ligands that better regulate the exchange process.

Compound **2.16** is the only known example of a Kläui ligand with a functionalized phenyl ring. We were unable to oxidize the phenolic aldehyde to the desired carboxylic acid, however, there was never an attempt to convert it to an imine. Imine formation using a primary amine (**5.1**), followed by reduction to the secondary amine (**5.2**) may

allow for a facile method of installing a moiety well suited for lanthanide chelation, **Figure 5.1**. By selecting a variety of primary amines a wide range of R groups can be selected that could aid in chelation, promote water solubility, or incorporate a CEST mechanism.

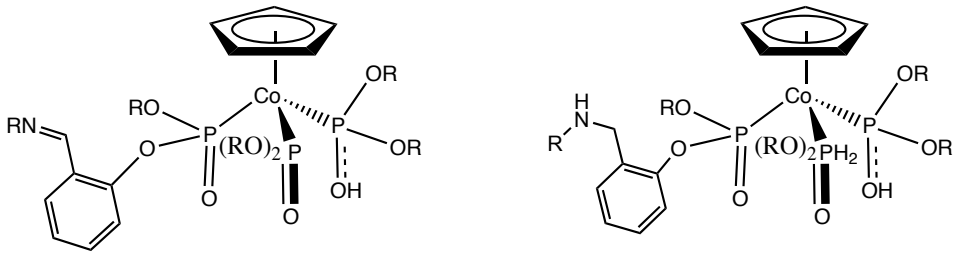

OR = O(2-C=NR)Ph
5.1

OR = O(2-CNHR)Ph
5.2

Figure 5.1: Imine Kläui ligand **5.1** formed through a condensation between a primary amine and **2.16**. An aryl amine containing Kläui ligand, **5.2**

Advances in contrast agent development has mainly focused on the same small class of ligands. It was my goal to explore different classes of ligands in hopes to expand the types of complexes that would be suitable for contrast agent development. My results have highlighted the difficulty in moving from the well established MR agent scaffolds into new territories, however, I was able to discern some fundamentally new knowledge on ligand lability and stability that was not known prior to my work. Ultimately, the insight we gained from the exploration of multiple ligand systems enabled us to develop a water-soluble lanthanide chelate that shows promise as a potential MR imaging agent.

References

1. Lauterbur, P. C., Image Formation By Induced Local Interactions: Examples Employing Nuclear Magnetic Resonance. *Nature* **1973,** *242*, 190-191.
2. America, R. S. o. N. http://www.radiologyinfo.org (accessed October 26, 2013).
3. Nelson, J. H., *Nuclear Magnetic Resonance Spectroscopy*. Pearson Education, Inc.: New Jersey, 2003.
4. Caravan, P., Strategies for increasing the sensitivity of gadolinium based MRI contrast agents. *Chemical Society Reviews* **2006,** *35* (6), 512-523.
5. Merbach, A. E.; Tóth, É., *The Chemistry of Contrast Agents in Medical Magnetic Resonance Imaging*. John Wiley & Sons, Ltd: 2001.
6. Woods, M.; Woessner, D. E.; Sherry, A. D., Paramagnetic lanthanide complexes as PARACEST agents for medical imaging. *Chemical Society Reviews* **2006,** *35* (6), 500-511.
7. Zhou, Z.; Lu, Z.-R., Gadolinium-based contrast agents for magnetic resonance cancer imaging. *Wiley Interdisciplinary Reviews: Nanomedicine and Nanobiotechnology* **2013,** *5* (1), 1-18.
8. Woods, M.; Zhang, S.; Sherry, A. D., Toward the Design of MR Agents for Imaging β-Cell Function. *Current Medicinal Chemistry - Immunology, Endocrine & Metabolic Agents* **2004,** *4* (4), 349-369.
9. Rocklage, S. M.; Worah, D.; Kim, S.-H., Metal ion release from paramagnetic chelates: What is tolerable? *Magnetic Resonance in Medicine* **1991,** *22* (2), 216-221.
10. Neuman, H. U.S. Food and Drug Administration Joint Meeting of the Cardiovascular and Renal Drugs and Drug Safety and Risk Management Advisory Committees. http://www.fda.gov/AdvisoryCommittees/CommitteesMeetingMaterials/Drugs/CardiovascularandRenalDrugsAdvisoryCommittee/default.htm (accessed November 10, 2013).
11. Caravan, P.; Farrar, C. T.; Frullano, L.; Uppal, R., Influence of molecular parameters and increasing magnetic field strength on relaxivity of gadolinium- and manganese-based T1 contrast agents. *Contrast Media & Molecular Imaging* **2009,** *4* (2), 89-100.
12. Hamblin, J.; Abboyi, N.; Lowe, M. P., A binaphthyl-containing Eu(iii) complex and its interaction with human serum albumin: a luminescence study. *Chemical Communications* **2005,** (5), 657-659.
13. Pierre, V. r. C.; Botta, M.; Raymond, K. N., Dendrimeric Gadolinium Chelate with Fast Water Exchange and High Relaxivity at High Magnetic Field Strength. *Journal of the American Chemical Society* **2004,** *127* (2), 504-505.
14. Wai-Yan Chan, K.; Barra, S.; Botta, M.; Wong, W.-T., Novel gadolinium(III) polyaminocarboxylate macrocyclic complexes as potential magnetic resonance imaging contrast agents. *Journal of Inorganic Biochemistry* **2004,** *98* (5), 677-682.

15. Daldrup, H.; Shames, D. M.; Wendland, M.; Okuhata, Y.; Link, T. M.; Rosenau, W.; Lu, Y.; Brasch, R. C., Correlation of dynamic contrast-enhanced magnetic resonance imaging with histologic tumor grade: comparison of macromolecular and small-molecular contrast media. *Pediatric Radiology* **1998,** *28* (2), 67-78.
16. Xu, R.; Wang, Y.; Wang, X.; Jeong, E.-K.; Parker, D. L.; Lu, Z.-R., In Vivo Evaluation of a PAMAM-Cystamine-(Gd-DO3A) Conjugate as a Biodegradable Macromolecular MRI Contrast Agent. *Experimental Biology and Medicine* **2007,** *232* (8), 1081-1089.
17. Ye, Z.; Wu, X.; Tan, M.; Jesberger, J.; Grisworld, M.; Lu, Z.-R., Synthesis and evaluation of a polydisulfide with Gd–DOTA monoamide side chains as a biodegradable macromolecular contrast agent for MR blood pool imaging. *Contrast Media & Molecular Imaging* **2013,** *8* (3), 220-228.
18. Viswanathan, S.; Kovacs, Z.; Green, K. N.; Ratnakar, S. J.; Sherry, A. D., Alternatives to Gadolinium-Based Metal Chelates for Magnetic Resonance Imaging‚Ä†. *Chemical Reviews* **2010,** *110* (5), 2960-3018.
19. Zhang, S.; Malloy, C. R.; Sherry, A. D., MRI Thermometry Based on PARACEST Agents. *Journal of the American Chemical Society* **2005,** *127* (50), 17572-17573.
20. Tóth, É.; Burai, L.; Merbach, A. E., Similarities and differences between the isoelectronic GdIII and EuII complexes with regard to MRI contrast agent applications. *Coordination Chemistry Reviews* **2001,** *216-217* (0), 363-382.
21. Aime, S.; Crich, S. G.; Gianolio, E.; Giovenzana, G. B.; Tei, L.; Terreno, E., High sensitivity lanthanide(III) based probes for MR-medical imaging. *Coordination Chemistry Reviews* **2006,** *250* (11‚Äì12), 1562-1579.
22. Strijkers, G. J.; Mulder, W. J. M.; van Tilborg, G. A. F.; Nicolay, K., MRI contrast agents: current status and future perspectives. *Anti-Cancer Agents In Medicinal Chemistry* **2007,** *7* (3), 291-305.
23. Kläui, W., The Coordination Chemistry and Organometallic Chemistry of Tridentate Oxygen Ligands with π-Donor Properties. *Angewandte Chemie International Edition in English* **1990,** *29* (6), 627-637.
24. Kläui, W.; Kunz, P. C.; Seidel, S. N.; Gladysz, J. A., *Inorganic Syntheses* **2010,** *35*, 125.
25. Zhu, X.-J.; Wang, P.; Leung, H. W. C.; Wong, W.-K.; Wong, W.-Y.; Kwong, D. W. J., Synthesis, Characterization, and DNA-Binding and -Photocleavage Properties of Water-Soluble Lanthanide Porphyrinate Complexes. *Chemistry – A European Journal* **2011,** *17* (25), 7041-7052.
26. Ke, H.; Wong, W.-K.; Wong, W.-Y.; Tam, H.-L.; Poon, C.-T.; Jiang, F., Synthesis, Crystal Structure, and Photophysical Properties of Novel (Monophthalocyaninato)lanthanide Complexes Stabilized by an Organometallic Tripodal Ligand. *European Journal of Inorganic Chemistry* **2009,** *2009* (9), 1243-1247.
27. Zhu, X.-J.; Jiang, F.-L.; Poon, C.-T.; Wong, W.-K.; Wong, W.-Y., Synthesis, Structure and Spectroscopic Properties of Lanthanide Complexes of N-Confused Porphyrins. *European Journal of Inorganic Chemistry* **2008,** *2008* (20), 3151-3162.

28. Jiang, F.-L.; Wong, W.-K.; Zhu, X.-J.; Zhou, G.-J.; Wong, W.-Y.; Wu, P.-L.; Tam, H.-L.; Cheah, K.-W.; Ye, C.; Liu, Y., Synthesis, Characterization, and Photophysical Properties of Some Heterodimetallic Bisporphyrins of Ytterbium and Transition Metals – Enhancement and Lifetime Extension of Yb3+ Emission by Transition-Metal Porphyrin Sensitization. *European Journal of Inorganic Chemistry* **2007,** *2007* (21), 3365-3374.
29. Zhu, X.; Wong, W.-K.; Lo, W.-K.; Wong, W.-Y., Synthesis and crystal structure of the first lanthanide complex of N-confused porphyrin with an [small eta]2 agostic C-H interaction. *Chemical Communications* **2005,** *0* (8), 1022-1024.
30. He, H.; Wong, W.-K.; Guo, J.; Li, K.-F.; Wong, W.-Y.; Lo, W.-K.; Cheah, K.-W., Monoporphyrinate neodymium (III) complexes stabilized by tripodal ligand: synthesis, characterization and luminescence. *Inorganica Chimica Acta* **2004,** *357* (15), 4379-4388.
31. Wong, W.-K.; Hou, A.; Guo, J.; He, H.; Zhang, L.; Wong, W.-Y.; Li, K.-F.; Cheah, K.-W.; Xue, F.; Mak, T. C. W., Synthesis, structure and near-infrared luminescence of neutral 3d-4f bi-metallic monoporphyrinate complexes. *Journal of the Chemical Society, Dalton Transactions* **2001,** *0* (20), 3092-3098.
32. Sang, H. H.; Park, S.; Jeong, J. H., *Bulletin of the Korean Chemical Society* **1999,** *20*, 741.
33. Yi, X.-Y.; Y. Sung, H. H.; Williams, I. D.; Leung, W.-H., Cerium(iv)-containing oxomolybdenum cluster with a unique Ce6Mo9O38 core structure. *Chemical Communications* **2008,** *0* (28), 3269-3271.
34. Roh, S.-G.; Jeong, J. H., Di-[mu]-acetato-O:O'-di-[mu]-acetato-O,O':O'-bis{[(cyclopentadienyl)tris(dimethylphosphito-P)cobalt-O,O',O"]neodymium(III)}. *Acta Crystallographica Section C* **2000,** *56* (4), e120-e121.
35. Han, S. H.; Roh, S.-G.; Jeong, J. H., Synthesis and crystal structure of bis[(μ-κO:μ-κO'-acetato)(μ-κO:κ^2O′-acetato)][(η5-Cp)tris(dimethylphosphito-P)cobalt-O,O′,O″]yttrium(III). *Polyhedron* **1999,** *18* (23), 3027-3030.
36. Kim, K. C.; Park, Y. C.; Jeong, J. H., *Bulletin of the Korean Chemical Society* **1997,** *18*, 670.
37. Englert, U.; Ganter, B.; Wagner, T.; Kläui, W., Reversible Topotactic Hydration and Dehydration of an Europium Complex [1]. *Zeitschrift fur Anorganische und Allgemeine Chemie* **1998,** *624* (6), 970-974.
38. Cho, I. Y.; Yeo, H. J.; Jeong, J. H.; Song, C. E., Di(aqua)bis[([eta]5-cyclopentadienyl)tris(dimethylphosphito-P)cobalt-O,O',O"]lanthanum(III) Chloride. *Acta Crystallographica Section C* **1995,** *51* (10), 2035-2037.
39. Zheng, Y.-R.; Stang, P. J., Direct and Quantitative Characterization of Dynamic Ligand Exchange between Coordination-Driven Self-Assembled Supramolecular Polygons. *Journal of the American Chemical Society* **2009,** *131* (10), 3487-3489.
40. Kläui, W.; Neukomm, H.; Werner, H.; Huttner, G., [π-C_5H_5Co{$P(OR)_2O$}$_3$BF]BF_4: Synthese, Struktur und Reaktivität von (Cyclopentadienyl)kobalt-Komplexen mit neuartigen käfigbildenden Phosphit-Chelatliganden. *Chemische Berichte* **1977,** *110* (6), 2283-2289.
41. Kläui, W. N., B, *Anorganische Chemie, Organische Chemie* **1979,** *34B*, 1403.

42. Liang, L.; Stevens, E. D.; Nolan, S. P., Synthesis and characterization of an organoyttrium dimer produced via an Arbuzov dealkylation reaction. *Organometallics* **1992,** *11* (10), 3459-3462.
43. Solari, E.; Corazza, F.; Floriani, C.; Chiesi-Villa, A.; Guastini, C., Polydentate ligand exchange via formation of a dimetallic complex. Crystal structures of [(thf)Fe(acen)MCl2](M = Fe or Zn), [ClFe(salphen)FeCl(thf)2], [Ti(acen)(thf)2][CoCl3(thf)], and [Ti(acen)(thf)2]2[Fe3Cl8(thf)2][acen =N,N'-ethylenebis(acetylacetoneiminate), salphen =N,N'-o-phenylenebis(salicylideneiminate), and thf = tetrahydrofuran]. *Journal of the Chemical Society, Dalton Transactions* **1990,** (4), 1345-1355.
44. Farrugia, L., ORTEP-3 for Windows - a version of ORTEP-III with a Graphical User Interface (GUI). *Journal of Applied Crystallography* **1997,** *30* (5 Part 1), 565.
45. Weinmann, H. J.; Mühler, A.; Radüchel, B., *Biomedical Magnetic Resonance Imaging and Spectroscopy*. John Wiley and Sons Ltd: Chichester, 2000; p 705.
46. Shannon, R., Revised effective ionic radii and systematic studies of interatomic distances in halides and chalcogenides. *Acta Crystallographica Section A* **1976,** *32* (5), 751-767.
47. Kläui, W.; Schramm, G.; Asbahr, H.-O.; Englert, U., Tris-Chelating Oxygen Ligands: New Synthetic Routes to Sterically Demanding Ligands. *Chemische Berichte* **1997,** *130* (9), 1223-1229.
48. Kläui, W.; Scotti, M.; Valderrama, M.; Rojas, S.; Sheldrick, G. M.; Jones, P. G.; Schroeder, T., Dreizähnige Sauerstoff-Liganden als Cyclopentadienyl-Äquivalente: Struktur und Eigenschaften von [LRh(μ-CO)3RhL], L−□[(C5H5) Co{P(O)R2}3]−. *Angewandte Chemie* **1985,** *97* (8), 697-698.
49. A quick SciFinder search of primary amines reacting with phosphorus trichloride yielded over 800 results
50. King, R. B., *Inorganic Chemistry* **1966,** *5*, 83.
51. Ludewig, D.; Eiserbeck, W.; Feike, E. Z., Preparation of diester and monoester salts of phosphorous acid from phosphorus(III) oxide and secondary, tertiary and aromatic alcohols. *Zeitschrift fuer Chemie* **1984,** *24* (8), 290.
52. Makino, A.; Kobayashi, S., Chemistry of 2-oxazolines: A crossing of cationic ring-opening polymerization and enzymatic ring-opening polyaddition. *Journal of Polymer Science Part A: Polymer Chemistry* **2010,** *48* (6), 1251-1270.
53. Hoogenboom, R., Poly(2-oxazoline)s: A Polymer Class with Numerous Potential Applications. *Angewandte Chemie International Edition* **2009,** *48* (43), 7978-7994.
54. Yadav, P. N.; Beveridge, R. E.; Blay, J.; Boyd, A. R.; Chojnacka, M. W.; Decken, A.; Deshpande, A. A.; Gardiner, M. G.; Hambley, T. W.; Hughes, M. J.; Jolly, L.; Lavangie, J. A.; MacInnis, T. D.; McFarland, S. A.; New, E. J.; Gossage, R. A., Platinum-oxazoline complexes as anti-cancer agents: syntheses, characterisation and initial biological studies. *MedChemComm* **2011,** *2* (4), 274-277.
55. Meyers, A. I.; Temple, D. L.; Haidukewych, D.; Mihelich, E. D., Oxazolines. XI. Synthesis of functionalized aromatic and aliphatic acids. Useful protecting group for carboxylic acids against Grignard and hydride reagents. *The Journal of Organic Chemistry* **1974,** *39* (18), 2787-2793.
56. Jarowicki, K.; Kocienski, P., Protecting groups. *Journal of the Chemical Society, Perkin Transactions 1* **2001,** (18), 2109-2135.

57. Koeller, K. M.; Wong, C.-H., Synthesis of Complex Carbohydrates and Glycoconjugates: Enzyme-Based and Programmable One-Pot Strategies. *Chemical Reviews* **2000,** *100* (12), 4465-4494.
58. Sakakura, A.; Umemura, S.; Kondo, R.; Ishihara, K., Dehydrative Cyclization Catalyzed by the Combination of Molybdenum(VI) Oxides and Benzoic Acids: First Synthesis of the Antitumour Substance BE-70016. *Advanced Synthesis & Catalysis* **2007,** *349* (4-5), 551-555.
59. El Hatimi, A.; Gomez, M.; Jansat, S.; Muller, G.; Font-Bardia, M.; Solans, X., Chiral bis(oxazoline) ligands. Synthesis of mono- and bi-metallic complexes of nickel and palladium. *Journal of the Chemical Society, Dalton Transactions* **1998,** (24), 4229-4236.
60. Kanemasa, S.; Oderaotoshi, Y.; Yamamoto, H.; Tanaka, J.; Wada, E.; Curran, D. P., Cationic Aqua Complexes of the C2-Symmetric trans-Chelating Ligand (R,R)-4,6-Dibenzofurandiyl-2,2‘-bis(4- phenyloxazoline). Absolute Chiral Induction in Diels−Alder Reactions Catalyzed by Water-Tolerant Enantiopure Lewis Acids. *The Journal of Organic Chemistry* **1997,** *62* (19), 6454-6455.
61. Lee, S.-g.; Lim, C. W.; Song, C. E.; Kim, I. O.; Jun, C.-H., Synthesis of new C2-symmetric bioxazoles and application as chiral ligands in asymmetric hydrosilylation. *Tetrahedron: Asymmetry* **1997,** *8* (17), 2927-2932.
62. McManus, H. A.; Guiry, P. J., Recent Developments in the Application of Oxazoline-Containing Ligands in Asymmetric Catalysis. *Chemical Reviews* **2004,** *104* (9), 4151-4202.
63. Zou, J.; Berg, D. J.; Oliver, A.; Twamley, B., Unusual Redox Chemistry of Ytterbium Carbazole–Bis(oxazoline) Compounds: Oxidative Coupling of Primary Phosphines by an Ytterbium Carbazole–Bis(oxazoline) Dialkyl. *Organometallics* **2013,** *32* (21), 6532-6540.
64. Qian, C.; Wang, L., Asymmetric hetero-Diels–Alder reaction of glyoxylate esters and Danishefsky’s diene catalyzed by chiral bis(oxazoline)–lanthanide complexes. *Tetrahedron Letters* **2000,** *41* (13), 2203-2206.
65. Qian, C.; Wang, L., Asymmetric glyoxylate-ene reaction catalyzed by C2-symmetric chiral bis(oxazoline)–lanthanide complexes. *Tetrahedron: Asymmetry* **2000,** *11* (11), 2347-2357.
66. Desimoni, G.; Faita, G.; Guala, M.; Laurenti, A.; Mella, M., A New Pyridine-2,6-bis(oxazoline) for Efficient and Flexible Lanthanide-Based Catalysts of Enantioselective Reactions with 3-Alkenoyl-2-oxazolidinones. *Chemistry – A European Journal* **2005,** *11* (13), 3816-3824.
67. Wijtmans, M.; Celanire, S.; Snip, E.; Gillard, M. R.; Gelens, E.; Collart, P. P.; Venhuis, B. J.; Christophe, B.; Hulscher, S.; Goot, H. v. d.; Lebon, F.; Timmerman, H.; Bakker, R. A.; Lallemand, B. n. d. I. L. F.; Leurs, R.; Talaga, P. E.; Esch, I. J. P. d., 4-Benzyl-1H-imidazoles with Oxazoline Termini as Histamine H3 Receptor Agonists. *Journal of Medicinal Chemistry* **2008,** *51* (10), 2944-2953.
68. Wijtmans, M.; Denonne, F.; Celanire, S.; Gillard, M.; Hulscher, S.; Delaunoy, C.; Van houtvin, N.; Bakker, R. A.; Defays, S.; Gerard, J.; Grooters, L.; Hubert, D.; Timmerman, H.; Leurs, R.; Talaga, P.; de Esch, I. J. P.; Provins, L., Histamine H3 receptor ligands with a 3-cyclobutoxy motif: a novel and versatile constraint of the classical 3-propoxy linker. *MedChemComm* **2010,** *1* (1), 39-44.

69. Matsumoto, K.; Suzuki, K.; Tsukuda, T.; Tsubomura, T., A Chiral 2,6-Bis(Oxazolinyl)Pyridine Ligand with Amide Groups to Form Isomorphous Complexes through All the Lanthanoid Series. *Inorganic Chemistry* **2010,** *49* (11), 4717-4719.
70. Li, W. J.; Xu, Z. L.; Qiu, S. X., Concise methods for the synthesis of chiral polyoxazolines and their application in asymmetric hydrosilylation. *Beilstein Journal of Organic Chemistry* **2010,** *6*, 29.
71. Itagaki, M.; Masumoto, K.; Yamamoto, Y., Asymmetric Cyclopropanation of 2,5-Dimethyl-2,4-hexadiene by Copper Catalysts Bearing New Bisoxazoline Ligands. *The Journal of Organic Chemistry* **2005,** *70* (8), 3292-3295.
72. McKennon, M. J.; Meyers, A. I.; Drauz, K.; Schwarm, M., A convenient reduction of amino acids and their derivatives. *The Journal of Organic Chemistry* **1993,** *58* (13), 3568-3571.
73. Kawasaki, K.-i.; Katsuki, T., Enantioselective allylic oxidation of cycloalkenes by using Cu(II)-tris(oxazoline) complex as a catalyst. *Tetrahedron* **1997,** *53* (18), 6337-6350.
74. Lipshutz, B. H.; Blomgren, P. A., Efficient Scavenging of Ph3P and Ph3PO with High-Loading Merrifield Resin. *Organic Letters* **2001,** *3* (12), 1869-1871.
75. Meng, J.-c.; Fokin, V. V.; Finn, M. G., Kinetic resolution by copper-catalyzed azide–alkyne cycloaddition. *Tetrahedron Letters* **2005,** *46* (27), 4543-4546.
76. Blay, G.; Incerti, C.; Muñoz, M. C.; Pedro, J. R., Enantioselective LaIII-pyBOX-Catalyzed Nitro-Michael Addition to (E)-2-Azachalcones. *European Journal of Organic Chemistry* **2013,** *2013* (9), 1696-1705.
77. Ward, B. D.; Gade, L. H., Rare earth metal oxazoline complexes in asymmetric catalysis. *Chemical Communications* **2012,** *48* (86), 10587-10599.
78. Tse, M. K.; Bhor, S.; Klawonn, M.; Anilkumar, G.; Jiao, H.; Döbler, C.; Spannenberg, A.; Mägerlein, W.; Hugl, H.; Beller, M., Ruthenium-Catalyzed Asymmetric Epoxidation of Olefins Using H2O2, Part I: Synthesis of New Chiral N,N,N-Tridentate Pybox and Pyboxazine Ligands and Their Ruthenium Complexes. *Chemistry – A European Journal* **2006,** *12* (7), 1855-1874.
79. A SciFinder seach yielded over 300 results
80. Richter, J. M.; Whitefield, B. W.; Maimone, T. J.; Lin, D. W.; Castroviejo, M. P.; Baran, P. S., Scope and Mechanism of Direct Indole and Pyrrole Couplings Adjacent to Carbonyl Compounds: Total Synthesis of Acremoauxin A and Oxazinin 3. *Journal of the American Chemical Society* **2007,** *129* (42), 12857-12869.
81. Tzougraki, C.; Kokotos, G., Synthesis and study of Substituted Coumarins. A Facile Preparation of D,L-o-Tyrosine. *Journal of Heterocyclic Chemistry* **1986,** *23*, 87-91.
82. Seitz, M.; Kaiser, A.; Tereshchenko, A.; Geiger, C.; Uematsu, Y.; Reiser, O., Modular synthesis of chiral pentadentate bis(oxazoline) ligands. *Tetrahedron* **2006,** *62* (42), 9973-9980.
83. Hanazawa, S.; Arai, M. A.; Li, X.; Ishibashi, M., Determination of absolute stereochemistry, total synthesis, and evaluation of peptides from the myxomycete Physarum melleum. *Bioorganic & Medicinal Chemistry Letters* **2008,** *18* (1), 95-98.

84. Juszczyk, P.; Kasprzykowska, R.; Kołodziejczyk, A., Simple and efficient synthesis of chiral amino alcohols with an amino acid-based skeleton. *Letters in Peptide Science* **2003,** *10* (2), 79-82.
85. Williams, R. M.; Ehrlich, P. P.; Zhai, W.; Hendrix, J., A new synthetic approach to 1-(hydroxymethyl)-8-methoxy-1,2,3,4-tetrahydroisoquinolin-4-one. *The Journal of Organic Chemistry* **1987,** *52* (12), 2615-2617.
86. Descôteaux, C.; Brasseur, K.; Leblanc, V.; Parent, S.; Asselin, É.; Bérubé, G., SAR study of tyrosine–chlorambucil hybrid regioisomers; synthesis and biological evaluation against breast cancer cell lines. *Amino Acids* **2012,** *43* (2), 923-935.
87. Ross, A. J.; Lang, H. L.; Jackson, R. F. W., Much Improved Conditions for the Negishi Cross-Coupling of Iodoalanine Derived Zinc Reagents with Aryl Halides. *The Journal of Organic Chemistry* **2009,** *75* (1), 245-248.
88. Deaton, D. N.; Graham, K. P.; Gross, J. W.; Miller, A. B., Thiol-based angiotensin-converting enzyme 2 inhibitors: P1′ modifications for the exploration of the S1′ subsite. *Bioorganic & Medicinal Chemistry Letters* **2008,** *18* (5), 1681-1687.
89. Joseph, R.; Rao, C. P., Ion and Molecular Recognition by Lower Rim 1,3-Di-conjugates of Calix[4]arene as Receptors. *Chemical Reviews* **2011,** *111* (8), 4658-4702.
90. Dong-Sheng Guo, K. W., Yu Liu, Selective binding behaviors of p-sulfonatocalixarenes in aqueous solution. *Journal of Inclusion Phenomena and Macrocyclic Chemistry* **2008,** *62* (1-2), 1-21.
91. Daze, K. D.; Pinter, T.; Beshara, C. S.; Ibraheem, A.; Minaker, S. A.; Ma, M. C. F.; Courtemanche, R. J. M.; Campbell, R. E.; Hof, F., Supramolecular hosts that recognize methyllysines and disrupt the interaction between a modified histone tail and its epigenetic reader protein. *Chemical Science* **2012,** *3* (9), 2695-2699.
92. Georgiev, E. M.; Roundhill, D. M., An assessment of calixarene amides as potential magnetic resonance imaging enhancement agents for gadolinium(III). *Inorganica Chimica Acta* **1997,** *258* (1), 93-96.
93. Bryant, J. L. H.; Yordanov, A. T.; Linnoila, J. J.; Brechbiel, M. W.; Frank, J. A., First Noncovalently Bound Calix[4]arene–GdIII–Albumin Complex. *Angewandte Chemie International Edition* **2000,** *39* (9), 1641-1643.
94. Aime, S.; Barge, A.; Botta, M.; Casnati, A.; Fragai, M.; Luchinat, C.; Ungaro, R., A Calix[4]arene GdIII Complex Endowed with High Stability, Relaxivity, and Binding Affinity to Serum Albumin. *Angewandte Chemie International Edition* **2001,** *40* (24), 4737-4739.
95. Schühle, D. T.; Schatz, J.; Laurent, S.; Vander Elst, L.; Muller, R. N.; Stuart, M. C. A.; Peters, J. A., Calix[4]arenes as Molecular Platforms for Magnetic Resonance Imaging (MRI) Contrast Agents. *Chemistry – A European Journal* **2009,** *15* (13), 3290-3296.
96. Perret, F.; Lazar, A. N.; Coleman, A. W., Biochemistry of the para-sulfonato-calix[n]arenes. *Chemical Communications* **2006,** (23), 2425-2438.
97. Perret, F.; Coleman, A. W., Biochemistry of anionic calix[n]arenes. *Chemical Communications* **2011,** *47* (26), 7303-7319.
98. Bakirci, H.; Koner, A. L.; Nau, W. M., Binding of inorganic cations by p-sulfonatocalix[4]arene monitored through competitive fluorophore displacement in aqueous solution. *Chemical Communications* **2005,** (43), 5411-5413.

99. Beshara, C. S.; Jones, C. E.; Daze, K. D.; Lilgert, B. J.; Hof, F., A Simple Calixarene Recognizes Post-translationally Methylated Lysine. *ChemBioChem* **2010,** *11* (1), 63-66.
100. Coleman, A. W.; Jebors, S.; Cecillon, S.; Perret, P.; Garin, D.; Marti-Battle, D.; Moulin, M., Toxicity and biodistribution of para-sulfonato-calix[4]arene in mice. *New Journal of Chemistry* **2008,** *32* (5), 780-782.
101. Wang, K.; Guo, D.-S.; Zhang, H.-Q.; Li, D.; Zheng, X.-L.; Liu, Y., Highly Effective Binding of Viologens by p-Sulfonatocalixarenes for the Treatment of Viologen Poisoning. *Journal of Medicinal Chemistry* **2009,** *52* (20), 6402-6412.
102. Daze, K. D.; Ma, M. C. F.; Pineux, F.; Hof, F., Synthesis of New Trisulfonated Calix[4]arenes Functionalized at the Upper Rim, and Their Complexation with the Trimethyllysine Epigenetic Mark. *Organic Letters* **2012,** *14* (6), 1512-1515.
103. Tabet, S.; Douglas, S. F.; Daze, K. D.; Garnett, G. A. E.; Allen, K. J. H.; Abrioux, E. M. M.; Quon, T. T. H.; Wulff, J. E.; Hof, F., Synthetic trimethyllysine receptors that bind histone 3, trimethyllysine 27 (H3K27me3) and disrupt its interaction with the epigenetic reader protein CBX7. *Bioorganic & Medicinal Chemistry* **2013,** *21* (22), 7004-7010.
104. Flatmark, Catecholamine biosynthesis and physiological regulation in neuroendocrine cells. *Acta Physiologica Scandinavica* **2000,** *168* (1), 1-17.
105. Fiege, H.; Voges, H.-W.; Hamamoto, T.; Umemura, S.; Iwata, T.; Miki, H.; Fujita, Y.; Buysch, H.-J.; Garbe, D.; Paulus, W., Phenol Derivatives. In *Ullmann's Encyclopedia of Industrial Chemistry*, Wiley-VCH Verlag GmbH & Co. KGaA: 2000.
106. Pierpont, C. G.; Lange, C. W., The Chemistry of Transition Metal Complexes Containing Catechol and Semiquinone Ligands. In *Progress in Inorganic Chemistry*, John Wiley & Sons, Inc.: 2007; pp 331-442.
107. Zhu, D.-H.; Kappel, M. J.; Raymond, K. N., Coordination chemistry of lanthanide catecholates. *Inorganica Chimica Acta* **1988,** *147* (1), 115-121.
108. Di Bernardo, P.; Zanonato, P. L.; Bismondo, A.; Melchior, A.; Tolazzi, M., Protonation and lanthanide(iii) complexation equilibria of a new tripodal polyaza-polycatechol-amine. *Dalton Transactions* **2009,** (21), 4236-4244.
109. Leydier, A.; Lecerclé, D.; Pellet-Rostaing, S.; Favre-Réguillon, A.; Taran, F.; Lemaire, M., Sequestering agents for uranyl chelation: new calixarene ligands. *Tetrahedron* **2008,** *64* (49), 11319-11324.
110. Sekiya, R.; Yamasaki, Y.; Katayama, S.; Shio, H.; Haino, T., Head-to-tail polymeric columnar structure of calix[4]arene possessing catechol arms in the solid state. *CrystEngComm* **2013,** *15* (42), 8404-8407.
111. Gutsche, C. D.; Iqbal, M., p-tert-butylcalix[4]arene. *Organic Syntheses* **1990,** *68*, 234.
112. Gutsche, C. D.; Lin, L.-G., Calixarenes 12 : The synthesis of functionalized calixarenes. *Tetrahedron* **1986,** *42* (6), 1633-1640.
113. Chun, N. K.; Soon, K. D., Selective Nitration of Calix[4]arene. *Bulletin of the Korean Chemical Society* **1994,** *15* (4), 284-286.
114. Vézina, M.; Gagnon, J.; Villeneuve, K.; Drouin, M.; Harvey, P. D., (η5-Pentamethylcyclopentadienyl)rhodium Complexes of Upper-Rim Monophosphinated Calix[4]arene. *Organometallics* **2000,** *20* (2), 273-281.

115. Berthalon, S.; deVains, J.-B. R.; Lamartine, R., Selective Mono-Dealkylation of Tetra-p-tert-butyl-calix[4]arene at the Upper Rim. *Synthetic Communications* **1996,** *26* (16), 3103-3108.
116. Hider, R. C.; Mohd-Nor, A. R.; Silver, J.; Morrison, I. E. G.; Rees, L. V. C., Model compounds for microbial iron-transport compounds. Part 1. Solution chemistry and Mossbauer study of iron(II) and iron(III) complexes from phenolic and catecholic systems. *Journal of the Chemical Society, Dalton Transactions* **1981,** (2), 609-622.
117. Repo, E.; Warchoł, J. K.; Bhatnagar, A.; Mudhoo, A.; Sillanpää, M., Aminopolycarboxylic acid functionalized adsorbents for heavy metals removal from water. *Water Research* **2013,** *47* (14), 4812-4832.
118. Fu, F.; Xie, L.; Tang, B.; Wang, Q.; Jiang, S., Application of a novel strategy—Advanced Fenton-chemical precipitation to the treatment of strong stability chelated heavy metal containing wastewater. *Chemical Engineering Journal* **2012,** *189–190* (0), 283-287.
119. Swarbrick, J. D.; Ung, P.; Chhabra, S.; Graham, B., An Iminodiacetic Acid Based Lanthanide Binding Tag for Paramagnetic Exchange NMR Spectroscopy. *Angewandte Chemie International Edition* **2011,** *50* (19), 4403-4406.
120. Van Loon, J. D.; Arduini, A.; Coppi, L.; Verboom, W.; Pochini, A.; Ungaro, R.; Harkema, S.; Reinhoudt, D. N., Selective functionalization of calix[4]arenes at the upper rim. *The Journal of Organic Chemistry* **1990,** *55* (21), 5639-5646.
121. Berthalon, S.; Regnouf-de-Vains, J.-B.; Lamartine, R., Mono-functionalization of the tris-(p-tert-butyl)calix[4]arene. *Tetrahedron Letters* **1997,** *38* (49), 8527-8528.
122. Hobzova, R.; Sysel, P.; Duskova-Smrckova, M., Synthesis and characterization of calix[4]arene-containing polyimides. *Polymer International* **2011,** *60* (3), 405-413.
123. Cacheris, W. P.; Nickle, S. K.; Sherry, A. D., Thermodynamic study of lanthanide complexes of 1,4,7-triazacyclononane-N,N',N''-triacetic acid and 1,4,7,10-tetraazacyclododecane-N,N',N'',N'''-tetraacetic acid. *Inorganic Chemistry* **1987,** *26* (6), 958-960.
124. Aime, S.; Delli Castelli, D.; Fedeli, F.; Terreno, E., A Paramagnetic MRI-CEST Agent Responsive to Lactate Concentration. *Journal of the American Chemical Society* **2002,** *124* (32), 9364-9365.
125. Caravan, P.; Ellison, J. J.; McMurry, T. J.; Lauffer, R. B., Gadolinium(III) Chelates as MRI Contrast Agents: Structure, Dynamics, and Applications. *Chemical Reviews* **1999,** *99* (9), 2293-2352.
126. Takács, A.; Napolitano, R.; Purgel, M.; Bényei, A. C.; Zékány, L.; Brücher, E.; Tóth, I.; Baranyai, Z.; Aime, S., Solution Structures, Stabilities, Kinetics, and Dynamics of DO3A and DO3A–Sulphonamide Complexes. *Inorganic Chemistry* **2014,** *53* (6), 2858-2872.
127. Kálmán, F. K.; Woods, M.; Caravan, P.; Jurek, P.; Spiller, M.; Tircsó, G.; Király, R.; Brücher, E.; Sherry, A. D., Potentiometric and Relaxometric Properties of a Gadolinium-Based MRI Contrast Agent for Sensing Tissue pH. *Inorganic Chemistry* **2007,** *46* (13), 5260-5270.
128. Yoo, B.; Pagel, M. D., A PARACEST MRI Contrast Agent To Detect Enzyme Activity. *Journal of the American Chemical Society* **2006,** *128* (43), 14032-14033.

129. Tianyi Ke, E.-K. J., Xuli Wang, Yi Feng, Dennis L Parker, Zheng-Rong Lu, RGD targeted poly(L-glutamic acid)-cystamine- (Gd-DO3A) conjugate for detecting angiogenesis biomarker $\alpha_v\beta_3$ integrin with MR T1 mapping. *International Journal of Nanomedicine* **2007,** *2* (2), 191-199.
130. Stastny, V.; Lhoták, P.; Stibor, I.; König, B., Synthesis of calix[4]arene–cyclen conjugates. *Tetrahedron* **2006,** *62* (24), 5748-5755.
131. Lippert, A. R.; Gschneidtner, T.; Chang, C. J., Lanthanide-based luminescent probes for selective time-gated detection of hydrogen peroxide in water and in living cells. *Chemical Communications* **2010,** *46* (40), 7510-7512.
132. Barbaras, D.; Brozio, J.; Johannsen, I.; Allmendinger, T., Removal of Heavy Metals from Organic Reaction Mixtures: Preparation and Application of Functionalized Resins(1). *Organic Process Research & Development* **2009,** *13* (6), 1068-1079.
133. Russell, J. T.; Martonosi, A. N., The influence of pH on the absorption spectrum of arsenazo III. *Biochimica et Biophysica Acta (BBA) - General Subjects* **1978,** *544* (2), 418-429.
134. Ogan, K.; Simons, E. R., The influence of pH on arsenazo III. *Analytical Biochemistry* **1979,** *96* (1), 70-76.
135. Kumar, K.; Chang, C. A.; Tweedle, M. F., Equilibrium and kinetic studies of lanthanide complexes of macrocyclic polyamino carboxylates. *Inorganic Chemistry* **1993,** *32* (5), 587-593.
136. Kumar, K.; Chang, C. A.; Francesconi, L. C.; Dischino, D. D.; Malley, M. F.; Gougoutas, J. Z.; Tweedle, M. F., Synthesis, Stability, and Structure of Gadolinium(III) and Yttrium(III) Macrocyclic Poly(amino carboxylates). *Inorganic Chemistry* **1994,** *33* (16), 3567-3575.
137. Smith, R. M.; Martell, A. E., Critical stability constants, enthalpies and entropies for the formation of metal complexes of aminopolycarboxylic acids and carboxylic acids. *Science of the Total Environment* **1987,** *64* (1–2), 125-147.
138. Gu, S.; Kim, H.-K.; Lee, G. H.; Kang, B.-S.; Chang, Y.; Kim, T.-J., Gd-Complexes of 1,4,7,10-Tetraazacyclododecane-N,N′,N″,N‴-1,4,7,10-tetraacetic Acid (DOTA) Conjugates of Tranexamates as a New Class of Blood-Pool Magnetic Resonance Imaging Contrast Agents. *Journal of Medicinal Chemistry* **2010,** *54* (1), 143-152.
139. Caravan, P.; Cloutier, N. J.; Greenfield, M. T.; McDermid, S. A.; Dunham, S. U.; Bulte, J. W. M.; Amedio, J. C.; Looby, R. J.; Supkowski, R. M.; Horrocks, W. D.; McMurry, T. J.; Lauffer, R. B., The Interaction of MS-325 with Human Serum Albumin and Its Effect on Proton Relaxation Rates. *Journal of the American Chemical Society* **2002,** *124* (12), 3152-3162.

Appendix

7.1 Plots for determination of *k* for Kläui ligands

Figure A1 Plot of 1/[d_{60}-**2.4a**] vs. time for **2.4a** in CH_3CN

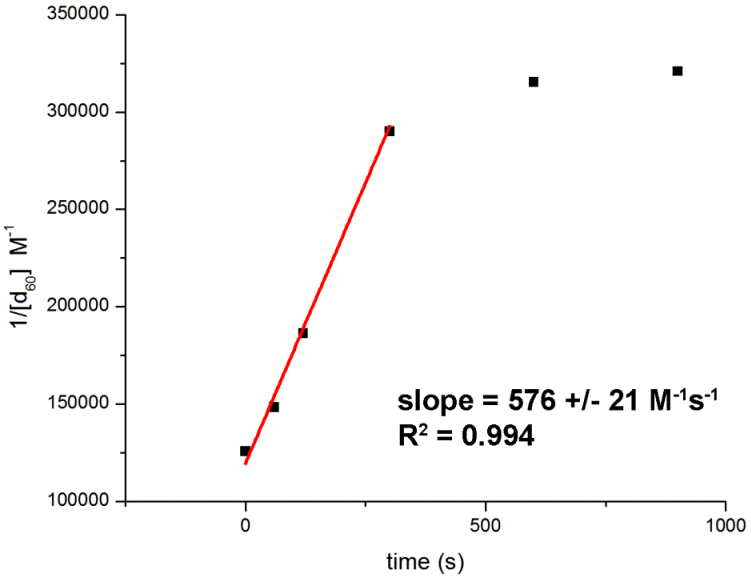

Figure A2 Plot of 1/[d_{60}-**2.5a**] vs. time for **2.5a** in 90:10 (v/v) CH_3CN:H_2O

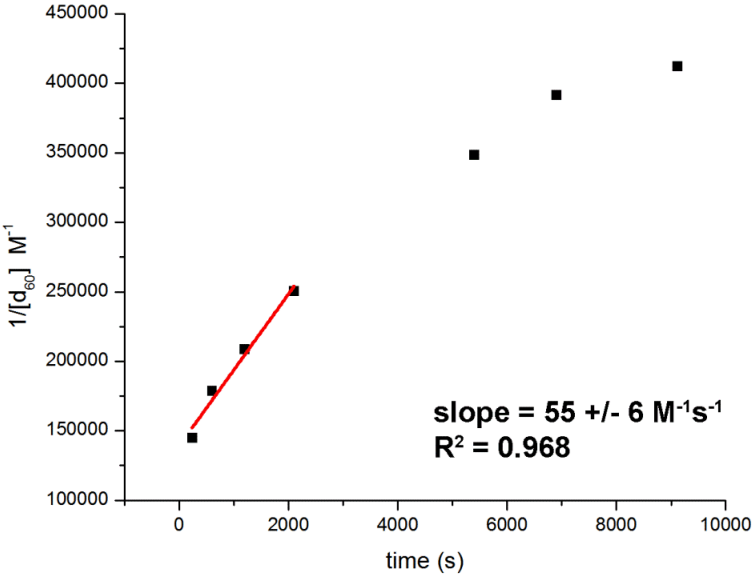

Figure A3 Plot of 1/[d_{60}-**2.5a**] vs. time for **2.5a** in 80:20 (v/v) $CH_3CN:H_2O$

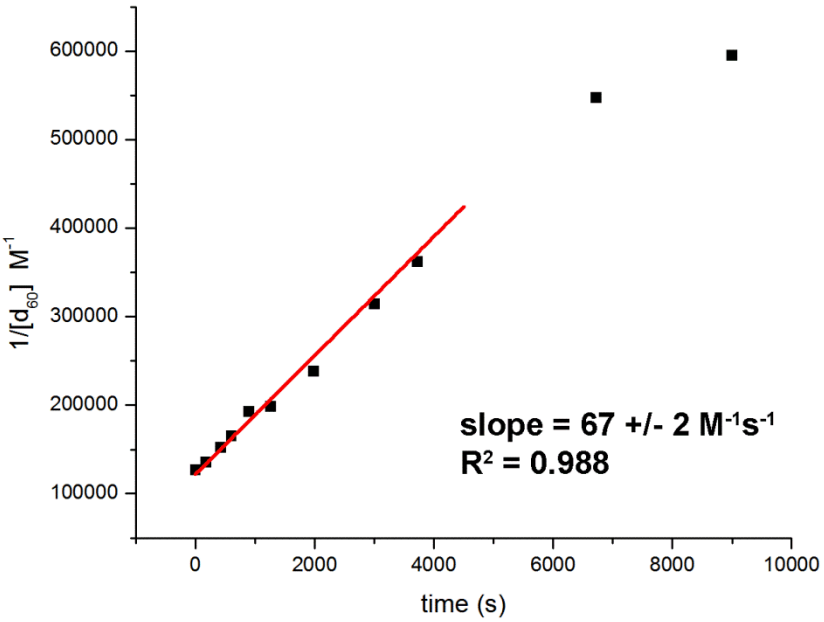

Figure A4 Plot of 1/[d_{60}-**2.5a**] vs. time for **2.5a** in 70:30 (v/v) $CH_3CN:H_2O$

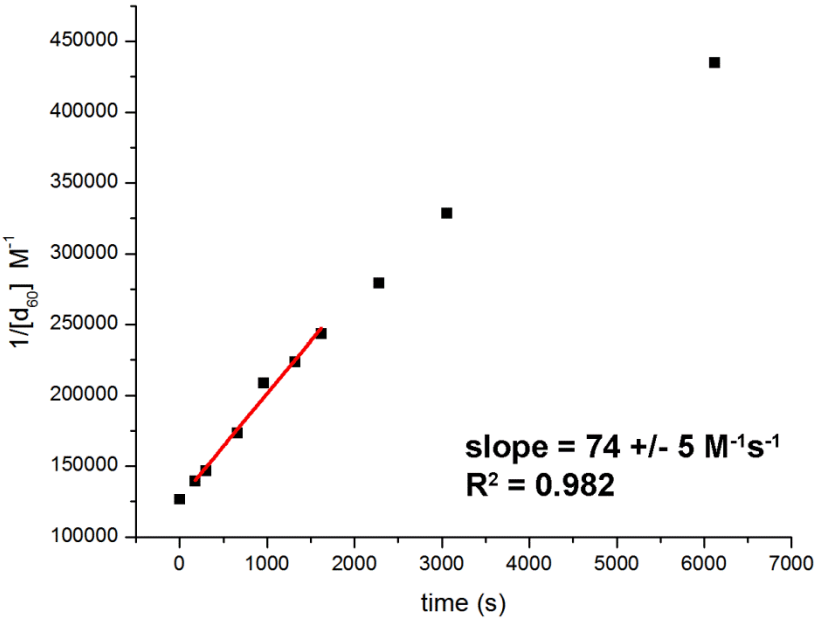

Figure A5 Plot of 1/[d_{60}-**2.5a**] vs. time for **2.5a** in 60:40 (v/v) $CH_3CN:H_2O$

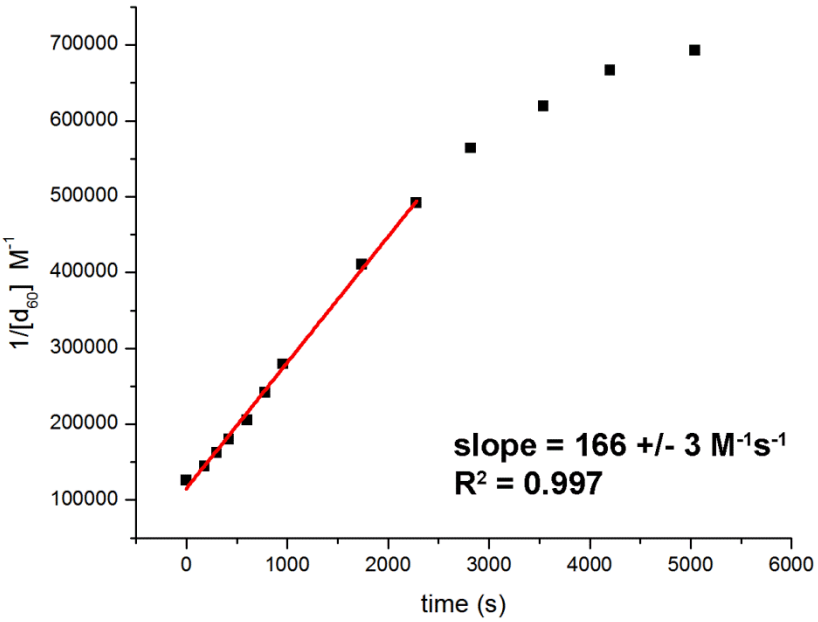

Figure A6 Plot of 1/[d_{60}-**2.5a**] vs. time for **2.5a** in 50:50 (v/v) $CH_3CN:H_2O$

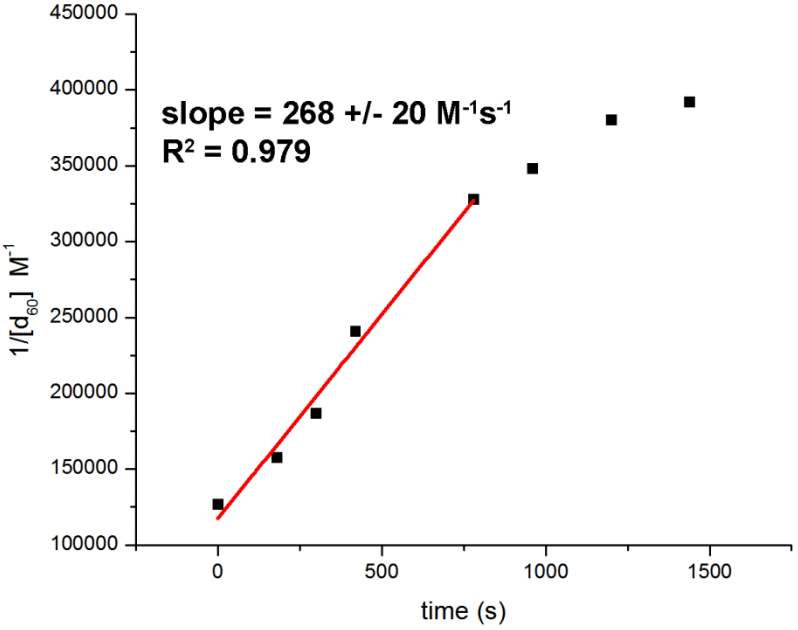

Figure A7 Plot of 1/[d_{60}-**2.5b**] vs. time for **2.5b** in CH_3CN

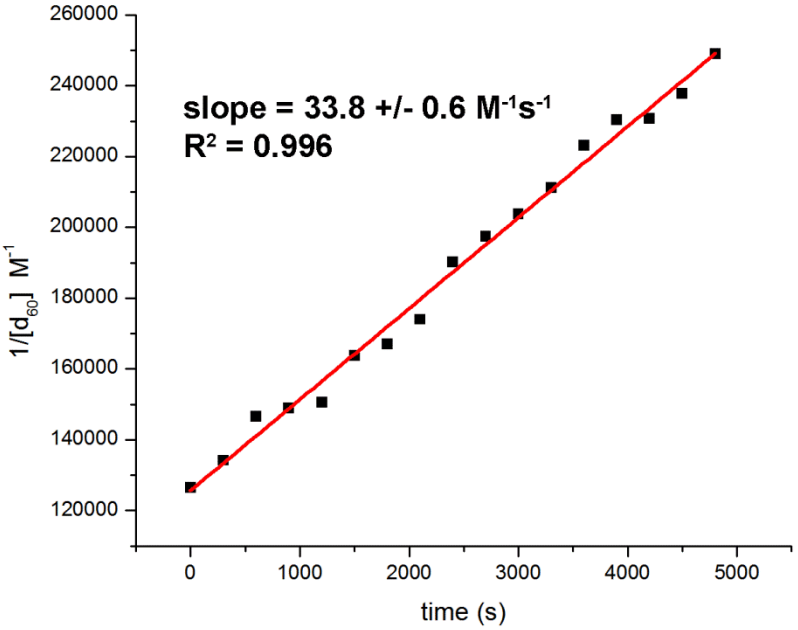

Figure A8 Plot of 1/[d_{60}-**2.5b**] vs. time for **2.5b** in 50:50 (v/v) $CH_3CN:H_2O$

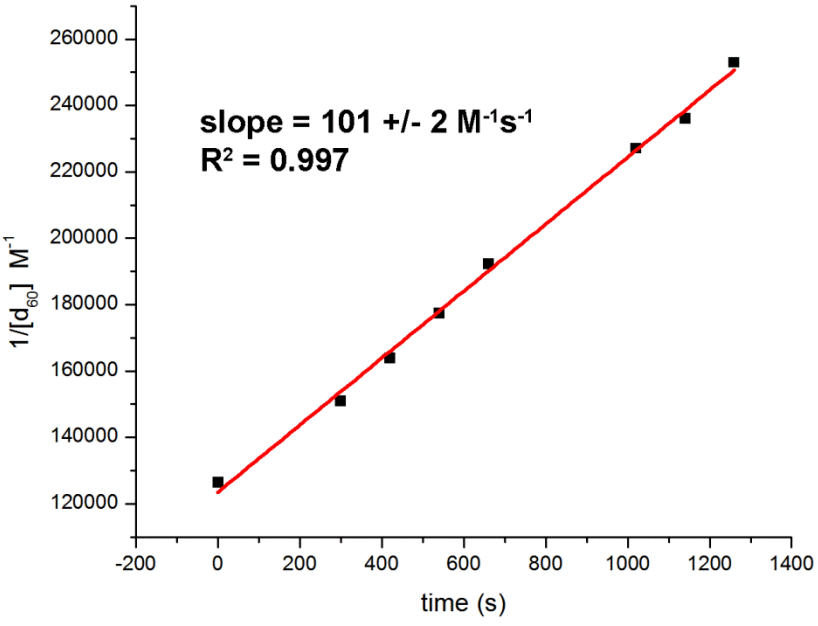

Figure A9 Plot of 1/[d_{60}-**2.6a**] vs. time for **2.6a** in CH_3CN

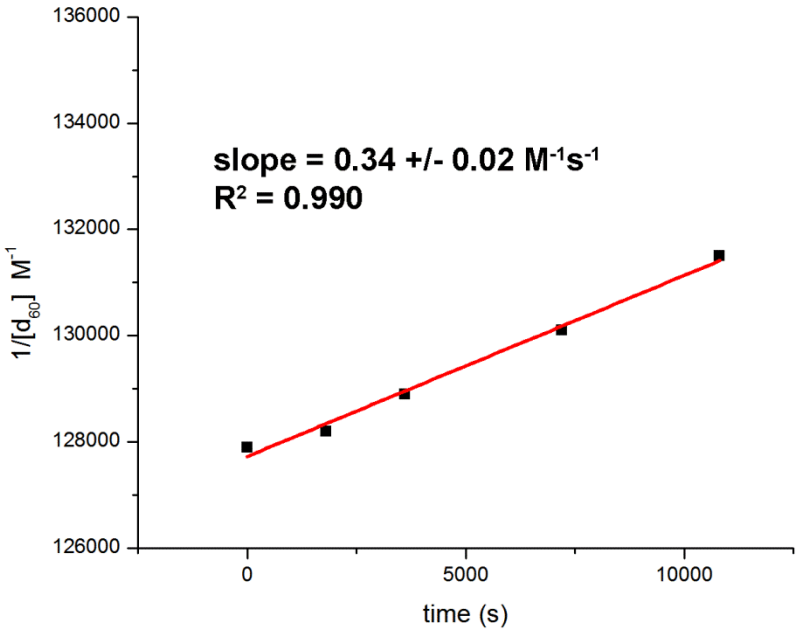

Figure A10 Plot of 1/[d_{60}-**2.6a**] vs. time for **2.6a** in 50:50 (v/v) CH_3CN:H_2O

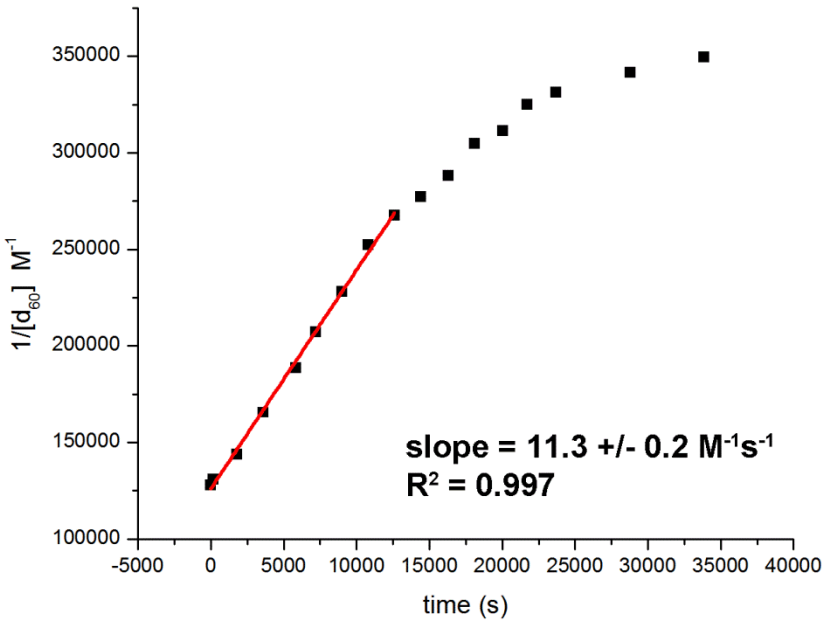

7.2 Thermogravimetric analysis of Kläui ligands

Figure A11. Thermogravimetric analysis trace for **2.5a**

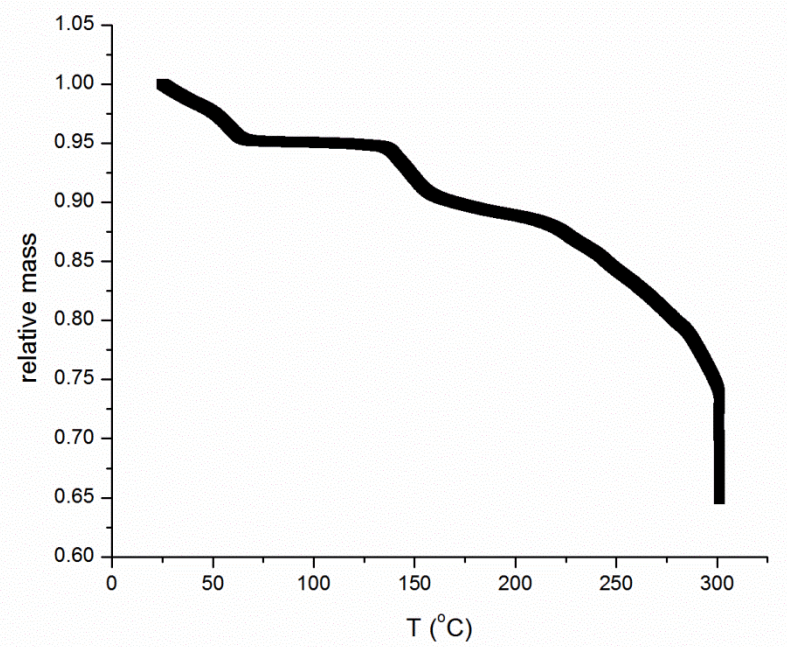

Figure A12. Thermogravimetric analysis trace for **2.6b**

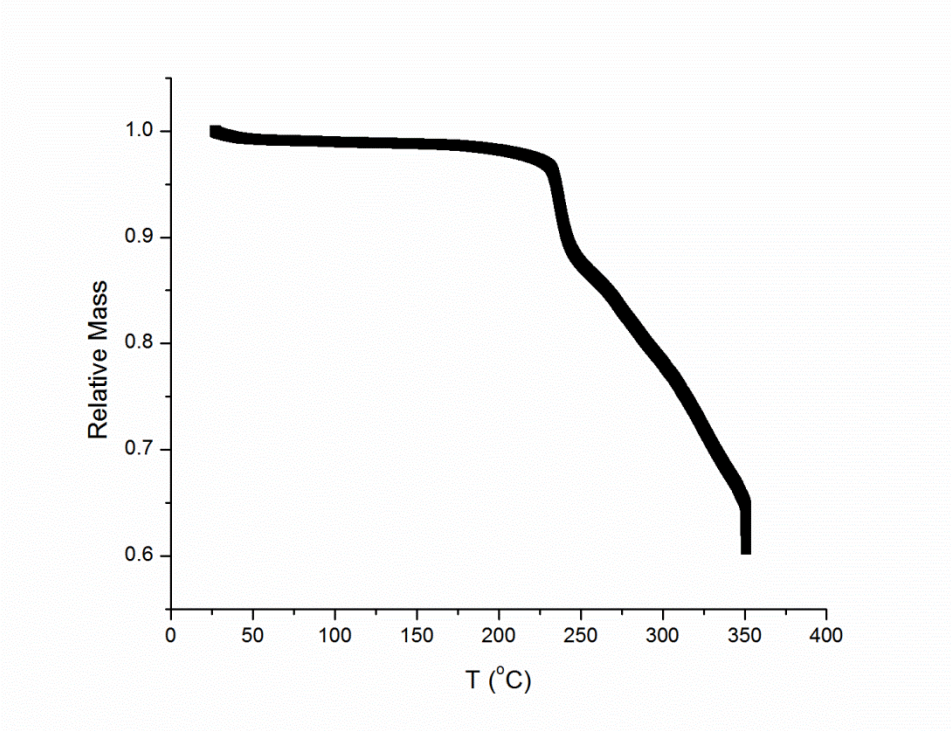

7.3 Isotope Patterns for Kläui Ligands

Figure A13 Calculated and observed isotope pattern for the molecular ion of the cation of d_{60}-**2.3a**

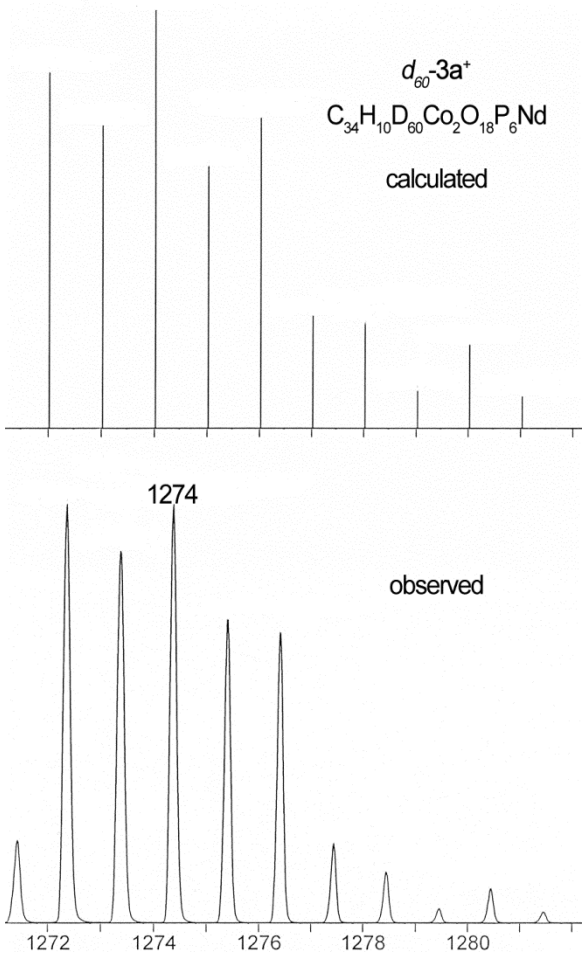

Figure A14 Calculated and observed isotope pattern for the molecular ion of the cation of **2.4a**

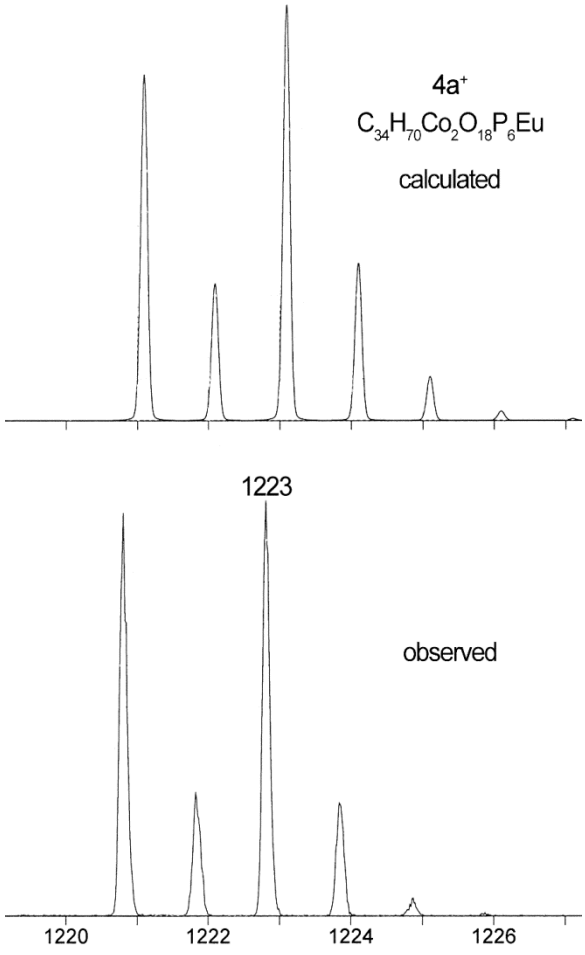

Figure A15 Calculated and observed isotope pattern for the molecular ion of the cation of d_{60}-**2.4a**

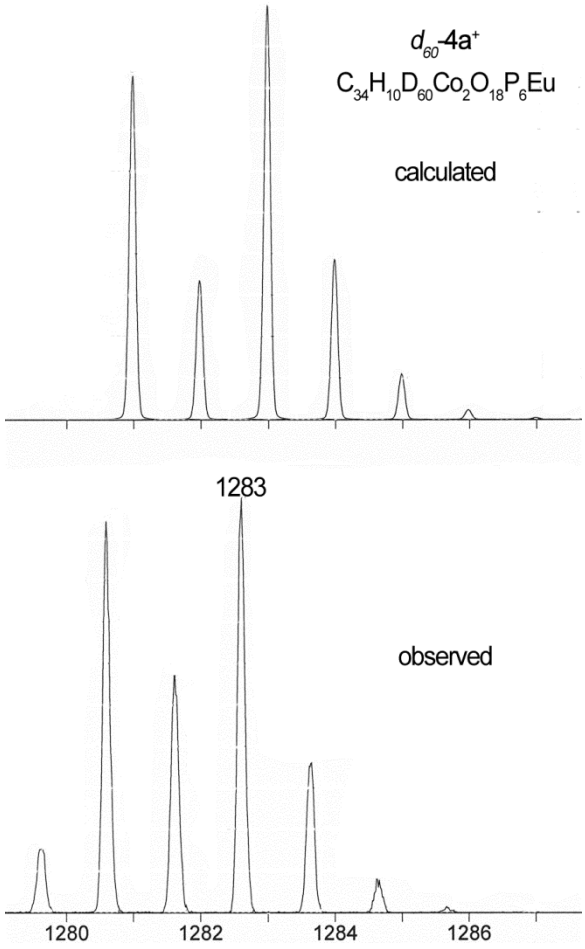

Figure A16 Calculated and observed isotope pattern for the molecular ion of the cation of **2.5a**

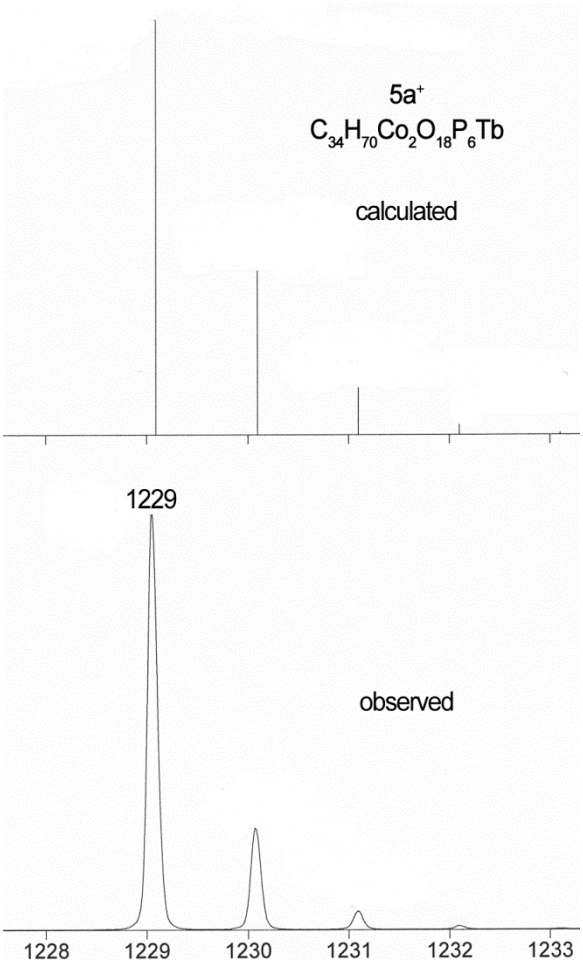

Figure A17 Calculated and observed isotope pattern for the molecular ion of the cation of d_{60}-**2.5a**

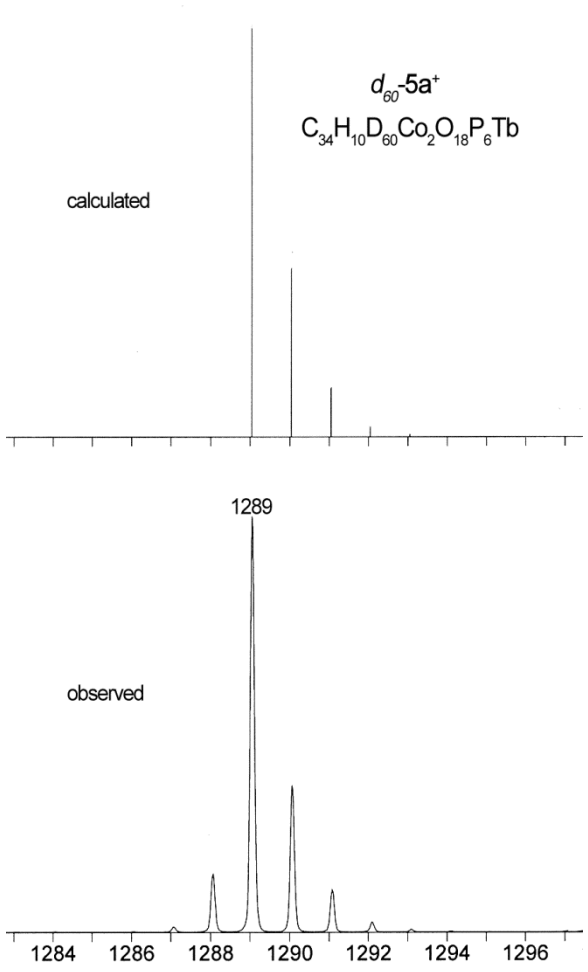

Figure A18 Calculated and observed isotope pattern for the molecular ion of the cation of **2.6a**

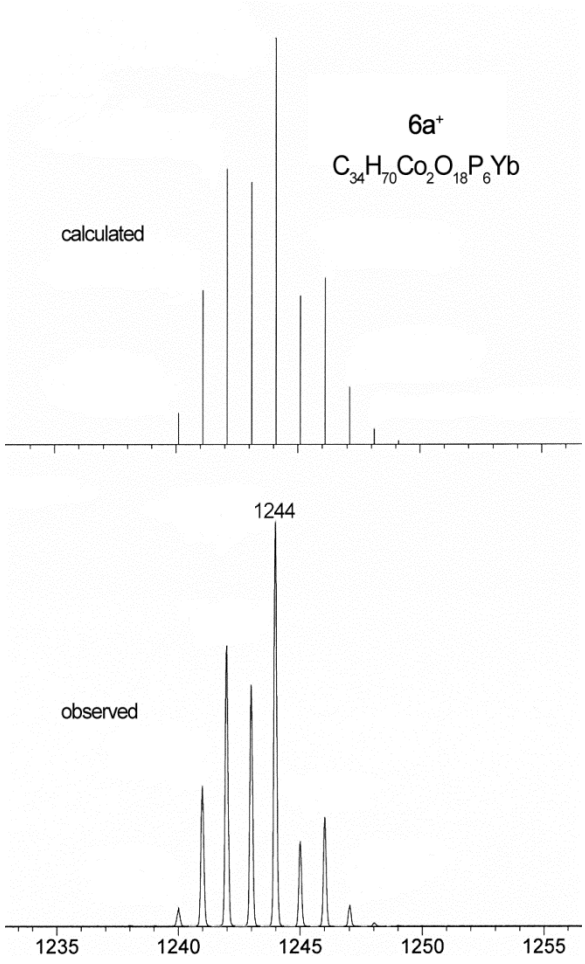

Figure A19 Calculated and observed isotope pattern for the molecular ion of the cation of d_{60}-**2.6a**

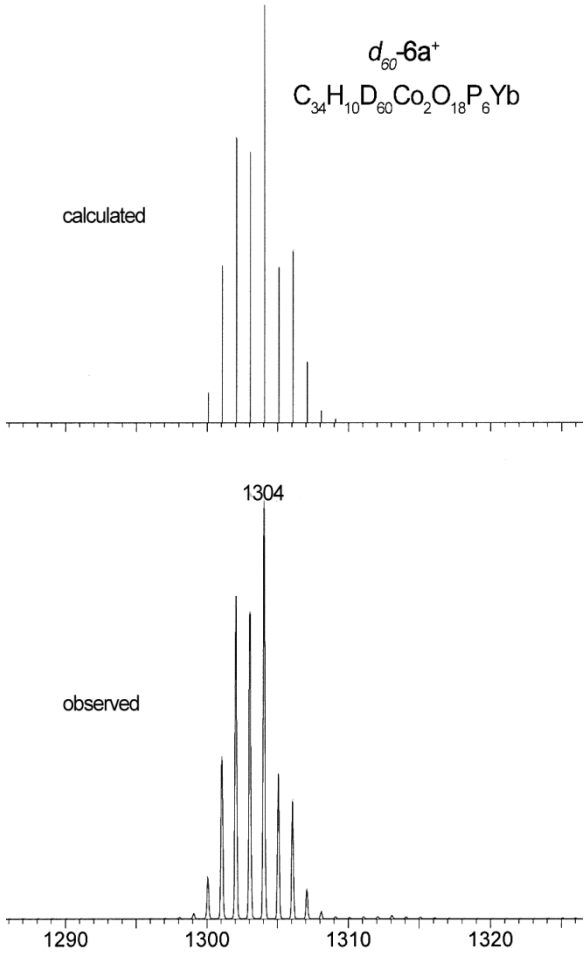

7.4 X-ray crystallography Data

Crystals of compound **2.7** were grown from benzene. Crystal structure was solved by Brendan Twamley

Table A1 Summary of Crystallographic Data for **2.7**

formula	$C_{98}H_{90}Cl_3Co_3O_{19}P_6Yb$
fw	2213.70
cryst syst	orthorhombic
space group	$P2_12_12_1$ (No. 19)
a (Å)	19.6632(7)
b (Å)	19.7358(7)
c (Å)	24.5563(9)
V (Å^3)	9529.5(6)
Z	4
ρ_{calc} (g cm^{-3})	1.543
μ (mm^{-1})	1.739
$2\theta_{max}$ (deg)	50.5
meas. refl.	123863
unique refl.	17278
R^a, $R_w{}^b$	0.048, 0.101
GOF	1.023

[a] $R = \Sigma(|F_o|-|F_c|)/\Sigma|F_o|$

[b] $R_w = [\Sigma w(|F_o|-|F_c|^2)/\Sigma w(|F_o|)^2]^{1/2}$